Author:
Liu, Zhen

Title:
Seismic analysis of low-rise masonry structures with openings in China

SEISMIC ANALYSIS OF LOW-RISE MASONRY STRUCTURES WITH OPENINGS IN CHINA

A Dissertation

Submitted to

The Academic Faulty

by

ZHEN LIU

In Accordance with

the Requirements for the Degree

Doctor of Philosophy in

Civil and Environmental Engineering

University of Bristol

July 2020

LIST OF PUBLICATIONS

The following publications are based on the work presented in this thesis:

Liu, Z., & Crewe, A. (2020). **Effects of size and position of openings on in-plane capacity of unreinforced masonry walls**. *Bulletin of Earthquake Engineering*. https://doi.org/10.1007/s10518-020-00894-0

This paper formally publishes much of the work described in Chapters 3 and 4 of this thesis.

Liu, Z., & Crewe, A. (2018). **Effect of position and size of openings on the seismic performance of masonry structures**. In Proceedings of the 16th European Conference on Earthquake Engineering (16ECEE) European Association for Earthquake Engineering (EAEE).

Dihoru, L., Crewe, A., Liu, Z., & Taylor, C. (2018**). Shaking table studies of FRP-reinforced masonry: experimental and numerical results**. In Proceedings of the 16th European Conference on Earthquake Engineering European Association for Earthquake Engineering (EAEE).

AUTHOR’S DECLARATION

I declare that the work in this dissertation was carried out in accordance with the requirements of the University's Regulations and Code of Practice for Research Degree Programmes and that it has not been submitted for any other academic award. Except where indicated by specific reference in the text, the work is the candidate's own work. Work done in collaboration with, or with the assistance of, others, is indicated as such. Any views expressed in the dissertation are those of the author.

SIGNED: ..... DATE: .....

ACKNOWLEDGMENTS

I would express my sincere gratitude to Dr Adam Crewe for initiating and supporting me in analytical research on masonry structures. His guidance has given me the chance to develop the research output about seismic analysis of URM buildings considering opening effects. Also, I would like to thank Prof. Paulo Lourenco for sharing the experimental data to make me calibrate the numerical results and Dr Francisco Galvez for sharing the knowledge of 3DEC software so that I can run the numerical analysis successfully.

I wish to acknowledge the contribution of Itasca support team to share useful information about 3DEC code and explain some questions about the operating mechanism of the software. I am also grateful to my colleagues and friends in the Department of Civil and Environmental Engineering for communicating about some topics which are very useful for me and making me feel like home.

Finally, I am particularly grateful to all my family for their love, patience and support every day during my PhD studies.

CONTENTS

LIST OF FIGURES

LIST OF TABLES

NOTATION

A	the cross-sectional area of shear walls, or the area of bearing walls
A_c	the area of the sub-contact
A_n	the area of net mortared, or grouted section
A_i	the sum of cross-section area of every seismic resistant cross wall at storey i
A_{im}	the cross-section area of storey i and piece m of walls
b	the pier aspect ratio
C_{dop}	the estimated design capacity of building with openings
C_{op}	the predicted capacity of building with openings
C_{np}	design capacity of building with solid wall
D	width of pier, or width of masonry wall
E	the Young's modulus of the material
E_b	modulus of elastic of brick
E_{ip}	design earthquake loading
E_m	modulus of elastic of masonry
e_{Ed}	eccentricity of load
F_{Ek}	seismic action force
F_b	seismic base shear force
F_C	load factor
F_{Ekb}	standard value of horizontal earthquake force
F_{out}	relationship between opening positions and out-of-plane performance capacity

F_{in} relationship between in-plane capacity and opening effects

F_i horizontal force acting on storey i

F_R strength reduction factor

f_a upper bound of vertical axial compressive stress

f_b normalised compressive strength of the masonry units

f'_{dt} lower bound of masonry diagonal tension strength

f_m compressive strength of the masonry

f_{mt} flexural tensile strength of masonry perpendicular to bed joints

f_{sw} compressive strength due to self-weight

f_{tu} conventional tensile strength of masonry

f_{tm} design value of bending tensile strength

f'_t flexural tensile strength

$f_{v,m}$ mean of shear resistance for masonry without seismic design

f_v design value of hearing resistant for masonry structures

f_{vd} design value of the shear strength of masonry

f_{vdu} ultimate shear strength

f_{vE} seismic design value of shear resistant for masonry

f_{VE} design masonry shear strength for diagonal tension

$f_{v,k}$ standard value of shear resistant for masonry without seismic design

f_{vk0} characteristic initial shear strength

f_{xd} design flexural strength appropriate to the plane of bending

G representative value of gravity load, or shear modulus of material

G_{eq} equivalent gravity load of the structure

G_m shear modulus of masonry

G_{im} shear modulus of storey i and piece m of walls

g	acceleration of gravity
H	horizontal force/ width of pier
h	height of bearing walls
h_{eff}	effective height of wall or pier
h_s	spandrel height
h_{im}	height of walls for storey i and piece m
h_u	height of the brick unit
I	horizontal second moment of area
K	stiffness in general
K_{bs}	lateral stiffness of wall
K_n	normal stiffness of joint
K_s	shear stiffness of joint
k	seismic coefficient that means the ratio of PGA to g
k_{1d}	slenderness of the pier
k_{1r}	a coefficient taking into account the slenderness and the boundary conditions of the pier
k_{2r}	a coefficient, which takes into account the assumed normal stress distribution at the compressed toe
k_{1s}	a coefficient that takes into account the actual compressed part of the reference section under the situation of ratios between uncracked and total height
L	length of the wall or pier
L_{ver}	Vertical load of wall
l	length of the wall or brick
l_c	length of the compressed part of the wall
l_u	length of the brick unit
M	moment design value

M_{Ed}	design value of the moment applied to the masonry wall
m	total mass of the building
m_i, m_j	storey masses
N	axial compression force
N_{Ed}	vertical load of masonry wall
O	superimposed load (take concrete slab for instance)
OS	opening size of masonry wall
OP	opening position of masonry wall
P	vertical compressive load
P_{CE}	expected vertical axial compressive force per load combination
P_{CL}	lower bound of vertical compressive force from load combination
q	behaviour factor
R	reaction force
r_{bE}	adjustment coefficient of ultimate seismic bearing capacity
S	soil factor, or design acceleration spectrum
$S_d(T)$	design spectrum
T	vibration period of a linear single-degree-of-freedom system
T_B	lower limit of the period of the constant spectral acceleration branch
T_C	upper limit of the period of the constant spectral acceleration branch
T_D	value defining the beginning of the constant displacement response range of the spectrum
T_1	fundamental period of vibration of the building for lateral motion in the direction considered
T_g	characteristic period
t	thickness of the wall

t_b	thickness of the brick unit
t_m	thickness of mortar joint
V	design value of shear resistance force for masonry wall
V_b	standard value of masonry wall shear strength under primary seismic intensity
V_{bjs}	lateral strength of wall or pier based on bed-joint shear strength
V_d	diagonal tension
V_{dt}	lateral strength limited by diagonal tension stress
V_R	seismic shear strength for each storey
V_r	lateral rocking strength of wall or pier component
V_{tc}	lateral strength limited by toe compressive stress
V_u	ultimate shear resistance of structure
v_{me}	expected bed-joint sliding shear strength
W	self-weight of the URM wall
W	section modulus
W_{Ed}	design lateral load per unit area
w	earthquake inertia load
x	opening proportion
y	in-plane capacity of URM wall
x_1, y_1	coordinates of central point of opening
Z	elastic section modulus of unit height or length of the wall
z_i, z_j	heights of masses
α	factor equal to 0.5 for fixed-free cantilever wall, or equal 1.0 for the fixed-fixed pier / the mass-proportional damping constant
α_{max}	peak value of horizontal earthquake effect factor coefficient
α_{maxb}	maximum value of the horizontal earthquake influence coefficient

a_g	design ground acceleration on type A ground
a_m	acceleration of the wall at mid-height
$\alpha_1\alpha_2$	bending moment coefficient taking account of the degree of fixity at the edges of the walls, the height to length ratios of the walls
β	lower bound factor for the horizontal design spectrum and recommended value is 0.2, or the stiffness-proportional damping constant
c	cohesion strength
γ	specific weight of the URM wall, or the reduction factor
Δ	displacement of the wall
ΔF^n	normal force vector increment
ΔF_i^s	shear force vector increment
ΔU^n	normal displacement vector increment
ΔU_i^s	shear displacement vector increment
δ	storey drift of building
μ	coefficient of friction, or the orthogonal ratio of the design flexural strengths of the masonry
ρ	unit weight
σ	normal stress
σ_0	average stress of masonry corresponding to the representative value of gravity load
σ_d	design compressive stress perpendicular to the shear in the member at the level under consideration
σ^t	tensile strength
σ_{v}	vertical compressive stress
$\bar{\sigma}_y$	mean vertical stress acting on the section
τ	shear stress

τ_b	ultimate shear stress of bed joint
τ_{max}	maximum shear stress
τ_p	shear stress of perpend joint
τ_u	ultimate shear strength
v_m	Poisson´s ratio of masonry
v_b	Poisson´s ratio of brick
ξ	damping ratio, or non-even coefficient of distribution of shear stress
ξ_n	an impact factor of normal stress for the masonry shear strength
λ	correction factor, the value of which is equal to $\lambda = 0{,}85$
η_1	decline slope adjustment factor
η_2	adjustment factor of damping
κ	ratio between the horizontal force and vertical force applied
$\emptyset$	friction angle
ω	dilation angle
ψ	dilation angle
δ_f	variable coefficient of masonry strength, for all types of masonry

ABSTRACT

Masonry is traditionally used in the construction of low-rise buildings all over the world. Masonry construction comprises a heterogeneous material formed from a regular or irregular repetition of blocks with or without the presence of mortar between the blocks. In recent earthquakes, unreinforced masonry (URM) structures built of masonry walls containing openings such as doors and windows have been shown to have poor seismic capacity. The poor seismic capacity of doors and windows for URM buildings can lead to significant damage or even collapse, which could threat the life of people and cause huge economic loss. Thus, it is vital to identify the structural behaviour of opening effects of URM housing and figure out solutions to reduce the seismic damage. However, although different sizes and positions of openings are known to reduce the stiffness and strength of URM walls, the relationships between the size and position of openings and the seismic capacity of the walls are not transparent. Therefore, in this thesis, a series of numerical analyses have explored many possible opening sizes and opening positions under simulated seismic loading (both static and dynamic). This work identifies the impact of openings on both the in-plane and out-of-plane behaviours of URM walls and a quick assessment procedure for the seismic capacity of URM structures based on opening situations is proposed.

To investigate the impact of openings in URM walls, this thesis introduces numerical models which were built using the code “3DEC” which is based on the Discrete Element Method (DEM). The key feature of the DEM is that it allows the development of large displacements between elements with contacts being recognized automatically during the analysis. Thus, this numerical method can capture the whole degradation progress from the initial cracking of the masonry walls right through to collapse, with the bricks being modelled as rigid or deformable blocks and the mortar as Coulomb-slip joints with zero thickness. The modelling methodology and the calibration of the numerical models are described.

For in-plane behaviour, both load-based and displacement-based quasi-static pushover analysis procedures have been studied and the results from the analyses, the crack patterns and collapse mechanisms of the masonry walls are identified and discussed, and a key output from this work is the characterization of the relationships between the sizes and positions of openings and the in-plane performance of URM walls. For out-of-plane behaviour, a series of quasi-static out-of-plane procedures under different boundary conditions and different shapes of walls have been studied. The

relationships between the openings and out-of-plane performance and the crack patterns and the collapse mechanisms of masonry walls are identified and discussed.

Dynamic analyses of URM walls are also considered. Dynamic analysis (time-history analysis) is essential for URM structures because this type of analysis can replicate the real behaviour of URM buildings in earthquakes. To look at the dynamic issues associated with URM walls, six artificial earthquake input motions based on Eurocode 8 were generated and the numerical analytical procedure using 3DEC was applied, the results are compared with static analyses for both in-plane and out-of-plane behaviours.

Using the data based on the static and dynamic analyses, relationships defining capacity reduction factors for different opening sizes and positions are proposed. Finally, a quick assessment procedure for the seismic capacity of URM structures with various opening situations is suggested. To validate the assessment procedure, a real URM building in China is modelled in 3DEC and the seismic capacity is predicted according to the proposed assessment approach. The results of the predictions, proposed procedure and numerical analysis in 3DEC are compared and a possible implementation is also introduced.

Keywords: *URM structures · Opening effects · Discrete element method · 3DEC · In-plane behaviour · Out-of-plane behaviour · Quick assessment procedure*

Chapter 1 INTRODUCTION

1.1 The motivation for the research

1.1.1 Background

Masonry is traditionally used in the construction of low-rise buildings all over the world. Masonry construction comprises a heterogeneous material comprised of regular or irregular repetition of blocks with or without the presence of mortar between the blocks. Lots of evidence from recent earthquake events has shown that this type of structure is poor at resisting earthquake loads and this has driven researchers and engineers to develop procedures to assess to what extent masonry structures can sustain earthquake loads without threatening human lives. Take the Wenchuan Earthquake, for example, a great earthquake with peak acceleration over 0.4g and a Richter magnitude of 8.0 by CENC (Epicentral intensity up to 11 degrees) which happened in Wenchuan County, China. Over 6 million dwellings collapsed or were severely damaged, and more critically, 69185 people were killed in the earthquake (Sun and Zhang, 2011, Wang et al., 2011, Xiao et al., 2012). Of all the failed buildings, masonry structures, which are built widely in many rural residential areas and some small towns in China, have shown the poorest seismic performance, based on many statistical studies. According to (Sun and Zhang, 2011), building data for 4539 buildings over an area of about 5737000 m² have been statistically analysed in Figure 1.1.

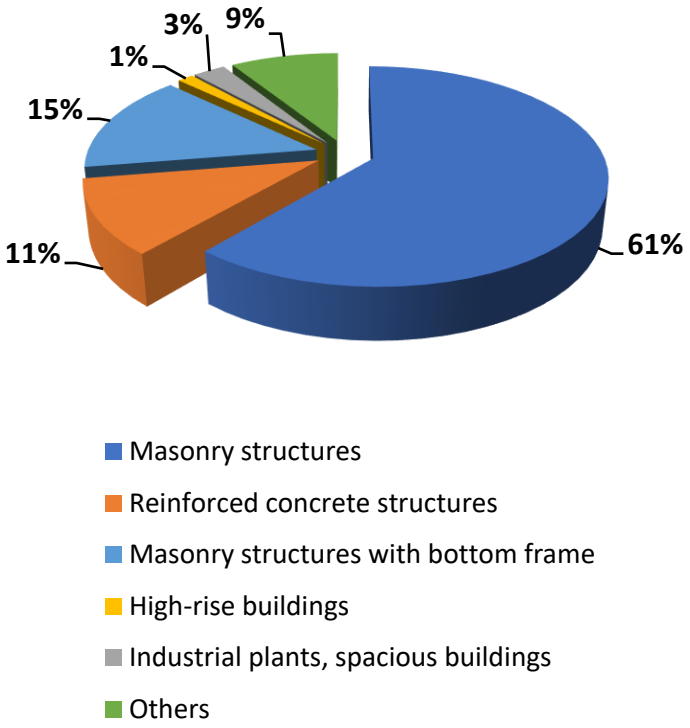

Figure 1.1 The number percentage of different types of buildings [Adapted by (Sun and Zhang, 2011)]

It can be seen that masonry structures comprise more than half (61%) of all building samples in this area. Masonry structures with bottom frame and reinforced concrete structures comprise another 15% and 11%, respectively. These three types therefore account for a total of 87% of all the building types in rural areas and small towns. Considering seismic damage to structures, a statistic study from (Lieping et al., 2008) has presented the damage degrees for these three types of buildings including masonry structures, masonry structures with bottom frame and RC frame structures. The damage degrees are divided into four levels comprising; slight damage, moderate damage, severe damage and collapse. This detailed information is shown in Figure 1.2.

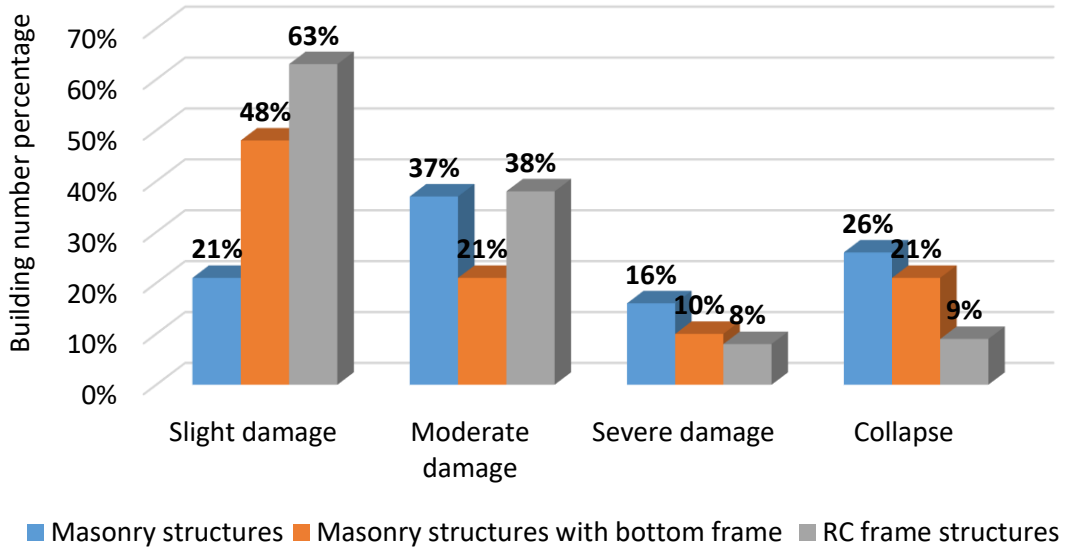

Figure 1.2 Comparison of seismic damage for masonry structures, masonry structures with bottom frame and frame structures [Adapted from (Lieping et al., 2008)]

Figure 1.2 illustrates the different damage levels for the three types of structures. The results show that masonry structures display more significant percentages of severe damage and collapse than the other two types of structures, while the rate of slight damage is lowest. In other words, the results show that masonry structures have the worst seismic performance among all the three types of structures. The sensitivity of masonry structures to damage is also illustrated by another statistical study by (Wu et al., 2010), that shows that the proportion of damage to masonry structures including severe damage and moderate damage is 70%. These and other studies consistently show that masonry structures have high fragility in earthquakes.

Due to their low-cost and limitations related to the environment, such as access to materials and undeveloped construction techniques, large numbers of masonry structures, and in particular low-rise confined masonry and unconfined masonry buildings, have been built in rural areas of China. In many areas there are plenty of low-rise masonry structures which have poor seismic performance, and typically current design codes and guidelines do not address this problem, which leads to high seismic risk to the lives of those who live in the villages and small towns (Wang, 2008). Thus, this thesis looks at typical low-rise masonry structures in rural areas of China and attempts to analyse the main factors which have a significant effect on the seismic capacity of low-rise of typical masonry structures.

1.1.2 Typical housing in the rural area of China

To identify the main characteristics of typical housing in a rural area in China, using Shandong Province as an example, some detailed information is illustrated below. Firstly, rural houses can be divided, based on roof types, into those with concrete or timber roofs (Figure 1.3). A timber roof is usually built as a pitched roof, timber roof trusses are placed above the masonry wall, and tiles are arranged on the surfaces supported by the roof trusses and beams (Figure 1.4). Usually, timber roofs are built on one-storey unreinforced masonry structures or old masonry buildings. However, for most new-built housing or for structures with two or more storeys, the timber components of the roof are replaced by concrete slabs to increase the stiffness of structures. The concrete roof is the second common roof type used in masonry housing. This type of roof is usually built as a terrace roof on one and two-storey masonry structures. This type of building often also contains other concrete members such as concrete lintels and ring beams (Figure 1.5).

(a) Typical housing with timber roof (b) Typical housing with concrete roof

Figure 1.3 Typical housing with different types of roofs [From (Wang and Hao, 2014)]

(a) The timber roof trusses (b) The layout of timer roof

Figure 1.4 The detail information about timber roof [From (Wang and Hao, 2014)]

(a) The concrete slab (b) The layout of concrete roof

Figure 1.5 The detail information of the concrete roof [From (Wang and Hao, 2014)]

Another critical aspect of masonry buildings in rural areas is the date of construction. Most older masonry buildings are usually single storey timber-roof masonry structures. This type of building has large openings and the outer walls are pure clay bricks. For more recently built dwellings, the building facades of the structures are often covered by cement, lacquer or ceramic tiles. Typical old and modern masonry buildings are shown in Figure 1.6.

(a) Typical old masonry building (b) Typical modern two-storey housing with ceramic tiles

Figure 1.6 Typical old masonry buildings and new-built masonry buildings [From (Wang and Hao, 2014)]

Alternatively, confined masonry is adopted for some more recently built structures, especially for two-storey masonry housing. This type of structure is confined by concrete ring beams and columns and concrete slabs and roofs are also employed to increase the integrity of a whole building. Confined masonry structures are mainly located in the areas close to towns and some developed regions. It is notable that, even though confined masonry structures have been proved to have better seismic performance than unconfined masonry structures, many local confined masonry structures have not shown such improved performance because of the poor construction quality of the masonry walls.

Overall, examples of the rural housing in Shandong Province show that masonry structures in rural areas can be classified according to the types of roofs, the coating of the outer walls and the existence of any confining components. This information was used to create appropriate numerical models of masonry housing in the next chapters.

1.1.3 Problem statements for the damage of low-rise masonry buildings in China

1.1.3.1 Opening effects

Both researchers and engineers face many issues when analysing the seismic capacity of masonry structures. In particular, openings can reduce the stiffness and seismic capacity of masonry structures and even change the failure mechanisms. Again taking the Wenchuan Earthquake as an example, it can be seen in Figure 1.7(a) that overlarge openings in the masonry walls divide the load-bearing wall into several pieces with an aspect ratio less than 1, and results in small walls which exhibit negative behaviours like short column effects, which leads to shear failure at both ends of the small walls. The results also showed collapsed unreinforced masonry buildings with load-bearing walls. It can be seen that the fracture patterns occurred on both sides of the door and window openings. At the right side of the door, diagonal cracks can be seen clearly, which means that the masonry walls are starting to collapse in an in-plane direction. For the window, out-of-plane failure is starting to occur around the opening.

(a) The classroom of Hongbai middle school

(b) Residential buildings in Yangcha village

Figure 1.7 Damage situation of unreinforced masonry structures [Adapted from (Lieping et al., 2008) and (Zhang and Jin, 2008)]

Another problem that occurs is irregularities in buildings due to the layout of openings. In this case the arrangement of openings affects the distribution of stiffness of the structure in an earthquake. Torsional effects will be generated if the horizontal openings are not uniformly distributed around the structure. For the vertical irregularity, the creation of openings at different floor levels can lead to soft storey effects, these being one of the most common issues causing failure. Figure 1.7(b) gives an example from Yangcha village, China of a very poor opening layout for a building. In the first floor, the

number of openings is bigger and their size is larger than the second floor, which will result in an unbalanced distribution of stiffness and then the generation of torsion. The openings in the second-floor are also located in a bad position, and once the building experiences earthquake loading, the housing is likely to show poor seismic performance due to high irregularities. Thus, it is crucial to explore the impact of openings, including opening size and position on the seismic performance of structures and develop methods to predict the strength of masonry walls with openings.

1.3.1.2 Construction quality and variety of material properties

Construction quality is another issue that cannot be completely avoided. Low construction quality can lead to a weaker connection between blocks, resulting in mortar joints with much lower compressive strength or shear strength than for high-quality construction techniques. When an earthquake occurs, the load-bearing masonry walls would then easily crack and are likely to fail, even under a low number of seismic cycles. Take the masonry structures in a typical village of China; for example. The progress of construction and the quality of the construction can be seen in Figure 1.8(a). The figure illustrates that the construction quality is not good, and there are no simple construction guidelines the builder can follow. The mortar joints and the connections between the blocks are fragile and increase the likelihood that the buildings will collapse under seismic loading.

(a) The construction progress of masonry housing (b) The detailed material information of bricks and mortars

Figure 1.8 The construction progress and detailed material information of self-built masonry building in Shandong Province of China [From (Wang, 2015)]

The material properties of the masonry structures are also an important aspect of the seismic capacity. The choice of materials such as the strength of the blocks or mortars can determine the stiffness and seismic resistant strength of the structure. According to (Wang, 2015), because of the high cost of cement, many people would prefer to use lime as a cement replacement or to use a composite mortar

including both cement and lime. Because there is less use of cement and local contractors or builders usually determine the proportions of materials in the cement mortar themselves, this leads to rather variable properties for the mortar, and about 20% of the mortars are so weak that they can fall out when a coin is used to scratch the mortar surface [Figure 1.8(b)]. Thus, it is necessary to analyse the effects of variable material properties on the seismic capacity of masonry structures.

1.3.1.3 Structural layout of roofs, lintels and cantilevers

Many structural components such as roofs, lintels and cantilevers are also essential for resisting seismic loads, but poor layout or construction can also lead to undesirable consequences. For roofs, there usually are two options; timber roofs and concrete roofs. Timber roofs were generally built in older buildings and are flexible roofs. While this type of roof can naturally tolerate some deformation, they also have low stiffness which can result in roof damage under seismic loading. For concrete roofs, these can be divided into poured concrete slabs and hollow prefabricated concrete slabs, with the latter being more common. Concrete roofs increase the stiffness of the buildings and can help resist the horizontal forces in an earthquake. However, this type of roof often has a poor connection to the masonry walls, and some oblique cracks can be generated at the connections as a result of the effects of temperature stress.

Concrete lintels are the most common lintels in low-rise masonry structures in China, although there are also other types of lintels, such as steel lintels and reinforced bricks. Lintels bear the loads from the upper masonry walls and move these loads to the sides of the windows or doors, which increases the stiffness and capacity of the masonry walls around the openings. Typical details of roofs and lintels can be seen in Figure 1.9(a). Due to poor construction quality or limitations of materials, some lintels do not have enough strength and stiffness, and this can cause buildings to fail at lower loads than expected.

To enlarge the living area of housing, extra balconies or corridors are often added to the outside of buildings. There are two types of construction methods for the cantilever members. One way is to run one end of the cantilever members along the inside of walls, leaving the other end to run outside the building to bear the loads from upper walls and slabs. Due to the low tensile strength of masonry walls and poor quality of mortar joints, cracks are often generated at the connections between the cantilever members and walls, resulting in dangerous structures. Another way to create balconies is to use simply-supported beams, with brick columns or confined concrete columns for the support components, and then concrete core slabs or cast-in-situ concrete slabs are built between them

[shown in Figure 1.9(b)]. For this construction type, there is generally no reinforcement of connections between the beams and columns so that the slabs are highly likely to collapse during an earthquake.

Figure 1.9 (a)The concrete roof and concrete lintel [From (Wang, 2015)] (b) Common cantilever members of the one-storey building

1.3.1.4 The problem targeted in the thesis and significance of the problem to be solved

Based on the contents above, there are lots of issues with the low-rise masonry structures located in China. However, the construction quality and poor material properties are highly dependent on the quality of local engineers and the construction companies, neither of which are easily controlled, and the issues with construction quality cannot be solved via analysis. Many researchers have also worked on the issues and have suggested ways to improve these aspects of construction. The structural layout of the roofs, lintels and cantilevers is a vital aspect in the design procedure for masonry buildings, but these components usually generate local failures, and it is hard to develop general guidelines for reflecting the global response of structures.

Opening effects are vital for URM masonry structures because they are not only commonly built-in to buildings but also because they have a significant impact on seismic behaviour. If the relationship between opening effects and seismic performance of URM structures are identified in detail, some equivalent relationship can be developed and it is helpful to offer theoretical support for the design code and propose a simple assessment procedure for URM buildings especially in rural area. Therefore, the large amounts of URM housing in rural area can be assessed quickly and reduce the seismic damage.

However, the current design codes and standards have few information about the clear relationship between opening effects and seismic performance of URM structures and also no simple assessment method targeting for opening effects. Thus, the thesis focuses on the opening effects and it is

important to investigate the detailed relationship between openings include size and position and seismic behaviour for URM structures.

1.1.4 Key challenges for identifying opening impacts on seismic performance and damage reduction of low-rise masonry structures

To consider strategies for identifying opening impacts on the seismic performance of low-rise masonry building, we need detailed seismic capacity analysis methods and appropriate numerical models. According to (Morandi and Magenes, 2008), two seismic design methods, including linear methods and nonlinear methods, are viable. The linear procedure can be further divided into linear static and linear dynamic analyses; the nonlinear procedure can be considered as nonlinear static (pushover) or nonlinear dynamic. Generally, when checking the seismic capacity of structures, nonlinear methods, including pushover analysis and dynamic analysis, are applied.

When URM masonry structures are subjected to seismic load, most of the walls display both in-plane and out-of-plane responses (described in Figure 1.10). One key challenge is to evaluate the seismic response of URM structures considering both in-plane and out-of-plane behaviours accurately and adequately. Another key challenge is developing accurate numerical modelling. There are two traditional ways to develop numerical models i.e. equivalent continuum and discontinuous idealisations, which equate to macro-models and micro-models (Lourenco, 1996). Both these models are based on the Finite Element (FE) method, but it is hard for FE method to reflect the interactions (such as large deformations) between every single element in detail and cannot predict, in detail, the crack patterns in masonry walls.

However, an alternative modelling approach called the discrete element method (DEM) has recently become more well-known. The development of DE (Discrete Element) models has enriched the set of tools available, especially for the analysis of masonry structures. Computational developments in the field of DEM have allowed these techniques to be progressively applied in the failure analysis of structural components and larger structures under both static and dynamic loading. However, validation of DE modelling using experimental data and the relevant experimental research is still very limited. Therefore, when considering the modelling of masonry walls it is worth considering all analytical modelling techniques such as FE modelling and DE modelling.

In addition to numerical modelling, seismic assessment procedures for URM buildings are an important method for the prevention of structural damage and for maintaining life safety in an

earthquake. Most assessment methods for masonry structures usually assess conformance to design codes, but there are always some old buildings or self-built buildings which do not satisfy the requirements of current codes, and these buildings generally experience severe damage in earthquakes.

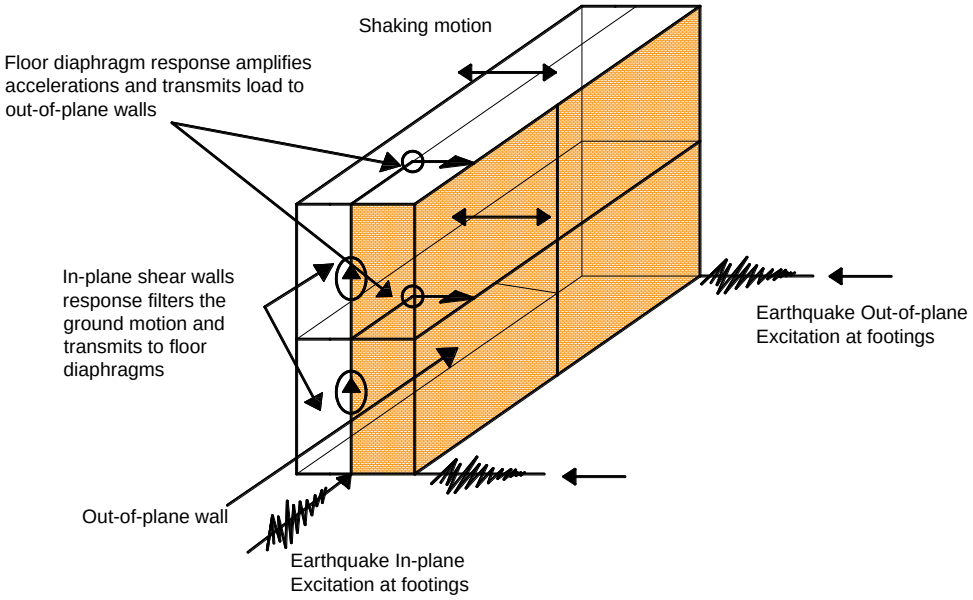

Figure 1.10 Seismic load path in URM [Adapted from (Doherty, 2000)]

According to (Jain et al., 2010), most seismic assessment methods focus on three different levels of performance, level one is rapid visual screening, level two is a preliminary assessment and level three is detailed evaluation. Of the three ways, rapid visual screening (RVS) is a simple and quick procedure to evaluate buildings and may only require 15-30 minutes to complete a survey. There is no need to calculate the specific seismic response data and the rapid visual screening method can be applied when the number of buildings to be assessed is large. (FEMA-154, 1988) was first published for RVS method and revised in 2002 with (FEMA-154, 2002), the current edition is the third edition which came out in 2015 as (FEMA-154, 2015). The FEMA P-154 report is a comprehensive score evaluation system based on parameters such as the seismic ground motion parameter zonation, structural type, stories of housing, plan and vertical irregularities, soil type etc. The method mainly considers the lateral force-resisting system of buildings and at the end of the process, a score is assigned according to the assessed outcomes of a basic score combined with vulnerability.

However, one challenge is that rapid assessment methods typically aim to assess all kinds of structures, and there are not targeted at low-rise masonry structures. Besides, a lot of factors like soil condition, size of the structure and layout of structural components still need to be considered and these factors have not been presented as simple formulas or rules, which can result in a low efficiency or poor

quality of assessment. Thus, based in a series of accurate analyses, some targeted capacity indexes, particularly for low-rise masonry buildings, need to be developed along with some rapid assessment procedures for these structures.

In summary, combining the current issues of low-rise masonry structures and key challenges for dealing with these problems, the context of the thesis is presented in Figure 1.11.

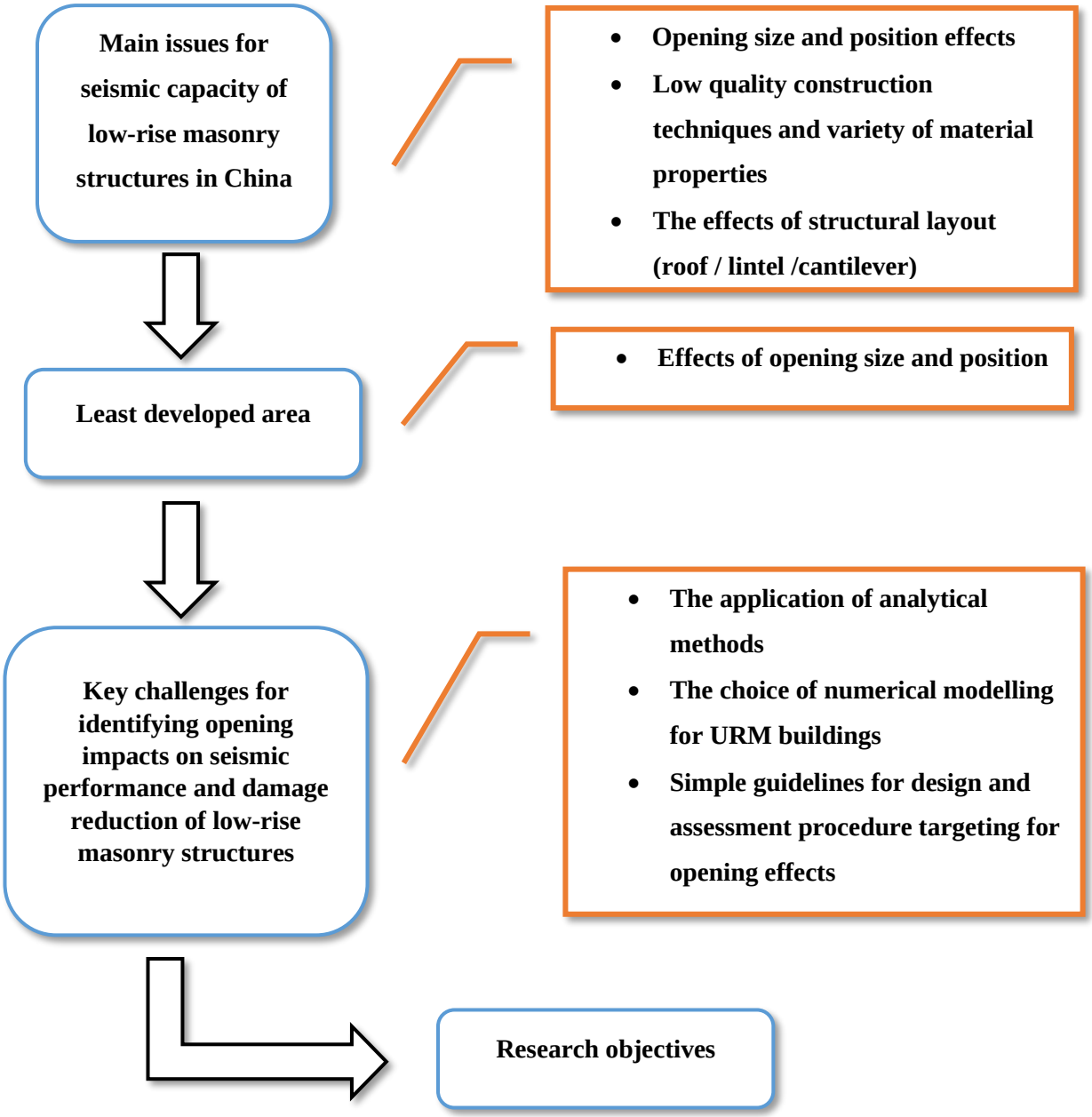

Figure 1.11 Context for the thesis

Based on Figure 1.11, the context for the thesis is presented. The main issues for seismic capacity of URM housing in China such as openings, materials and structural layout are shown, then the least developed area opening effects is introduced. To solve the problem of opening effects, some typical challenges are mentioned such as accurate numerical model, reasonable analysis method for URM structures and proposing simple assessment procedure targeting for opening effects. All these challenges are presented by the research objectives of the thesis.

1.2 Research objectives and scope

In order to deal with the key challenges relating typical low-rise masonry structures in China, the primary objectives of the research are presented below:

1) To present literature review about dealing with the key challenges and determine the numerical model method, analytical method for URM structures and assessment procedure.
2) To develop a methodology about using the Discrete Element Code 3DEC to model URM walls and buildings. The sensitivity study about the software and calibration are also needed to be applied.
3) To identify the effects of openings including opening sizes and positions under in-plane behaviour and to run quasi-static analyses and investigate the relationships between static performance and opening effects.
4) To identify the effects of openings including opening sizes and positions under out-of-plane behaviour and investigate the comparison between three-side boundary condition and four-side boundary condition.
5) To run the dynamic analysis of masonry walls and compare the static and dynamic results, then to develop realistic 3D models for masonry structures and validate their structural behaviour considering the opening effects.
6) To develop a seismic capacity index based on the comprehensive summaries of the analysed models and propose some simple guidelines for design and quick assessment procedure and to verify the proposal via a specific example and in the future to apply this assessment method to low-rise masonry buildings in China to reduce seismic damage.

1.3 Outline of the thesis

To achieve the aforementioned objectives, the content of the thesis is divided into four parts. Part I (Chapters 1 and 2) reports the problems and provides a literature review of previous research. Part II (Chapters 3, 4, 5 and 6) presents the analytical methodologies, calibration and implementation of numerical analysis procedures for openings in masonry walls. Part III (Chapter 7) summarises the outcomes of the analyses and proposes a new assessment method. Finally, part IV (Chapter 8) concludes the research. The outline of the thesis is as follows:

- **Chapter 2** In this chapter, a literature review of the state-of-the-art in research on masonry structures, modelling methods for masonry structures and modern design methods from different codes is provided.

- **Chapter 3** In this chapter, the Discrete Element Method (DEM) and 3DEC software are introduced and methodologies for the modelling of masonry with the DEM and 3DEC are illustrated.

- **Chapter 4** This chapter develops 3DEC masonry models with different opening percentages and opening positions, runs push-over analyses and builds up the relationships between in-plane performance and opening effects.

- **Chapter 5** This chapter develops 3DEC masonry models with different opening percentages and opening positions, applies static analysis procedures, then evaluates the relationship between out-of-plane capacity and opening effects.

- **Chapter 6** This chapter continues with dynamic analyses of opening impacts on masonry walls and compares the results with static analyses. Realistic 3D numerical models are created and dynamic analyses are run considering opening effects. Comparison is made between dynamic and static analyses.

- **Chapter 7** In this chapter, based on the analytical outcomes of both static and dynamic procedure, seismic fragility curves of buildings with different opening cases are developed and a relevant index for simple seismic assessment methods is proposed. A case study is developed to calibrate the proposed assessment method.

- **Chapter 8** This chapter concludes the thesis, discusses the limitations of the research, and finally proposes some ideas for future research.

Chapter 2 LITERATURE REVIEW

2.1 Introduction

Masonry structures are a widely used form of construction throughout the world. They are composed of bricks bonded with or without mortar and have a simple construction procedure compared to other types of structures such as concrete or steel. However, it is still difficult to evaluate the mechanical behaviour of masonry due to the complexity of materials. Masonry is a heterogeneous anisotropic material, and the mortar joints play the role of a weakness plane. The failure mechanisms in unreinforced masonry structures usually include in-plane failure, out-of-plane failure, connection failure, etc. As loads increase, cracks occur and structural behaviour changes from linear to non-linear. Once reaching the ultimate load, the strength capacity of the structure will drop significantly, which indicates that it is necessary to consider both linear and nonlinear analysis procedures. A number of seismic assessment procedures for URM structures have been developed by researchers and several are given in current design standards. In addition, simple rapid assessment methods are also worth consideration. Therefore, this chapter reviews opening effects for masonry structures and refer to the further investigation, modelling methods for masonry, seismic analysis procedures for URM structures, seismic performance of URM structures and general seismic assessment methods. Suitable numerical modelling methods, analysis methods and critical performance of URM buildings are also outlined in this chapter. In particular, the assessment of opening issues for URM buildings in different codes and in research papers is covered and the limitations of current methods are discussed.

2.2 Opening effects of unreinforced masonry structures

Unreinforced masonry structures (URM) are built widely around the world but have performed badly in recent earthquakes (Zhang and Jin, 2008, Ingham and Griffith, 2010, Parisi and Augenti, 2013, Kappos et al., 2002). Opening effects that include opening sizes and opening positions have been demonstrated to affect the extent of damage and modes of failure of URM walls. Openings reduce the stiffness of masonry walls and can even change the failure mechanisms of masonry walls. Many studies have been done looking at the impacts of openings on the masonry infilled walls e.g. (Al-Chaar et al., 2003, Asteris, 2003, Kakaletsis and Karayannis, 2007, Kakaletsis and Karayannis, 2008, Mohammadi and Nikfar, 2012, Asteris et al., 2016, Penava et al., 2018, Bui et al., 2019). These researchers have identified the relationships between stiffness reduction and opening percentage for masonry infilled walls through numerical and experimental investigation, and some equations have been proposed to describe the influence of openings directly. Also, for the opening effects, once the position of openings creates irregularities due to unreasonable opening positions or large opening sizes, a non-uniform distribution of gravity loads could develop among the masonry walls loading to a concentration of strength and displacement demand in local parts of a building, which could result in local failure and an increase in the seismic vulnerability of the entire structure (Parisi and Augenti, 2013). However, most research identified the opening effects for masonry infilled structures while none of them focused on the detail information about how the openings of URM structures affect the structural behaviour under both in-plane and out-of-plane loading. The equivalent relationships between opening effects and URM are not clear and not developed in further.

Besides, lots of codes and standards did not offer sufficient information about the relationship between openings effects and URM structures. EN1998-1 (2004) mentions the simplification of masonry walls divided by openings but does not give suggestions for how to deal with the effects of openings. Similarly, FEMA 273, 274, 356 (ATC, 1997a, ATC, 1997b, ATC, 2000) only consider that enlarged openings in URM walls will increase the height-to-length aspect ratio of piers and so the limit state may swap from shear to flexure. A restriction of opening length of less than 40% of overall wall length is therefore mentioned to limit any poor performance in new masonry. (GB50011, 2010) proposes a relationship between opening percentage and effects factor for unreinforced masonry structures (as described in Table 2.1). However, only three indicators are considered and no more detail information can be found.

Table 2.1 The opening effects factor [From (GB50011, 2010)]

Opening percentage	0.10	0.20	0.30
Effects factor	0.98	0.94	0.88

Based on the review, no matter the opening sizes or opening positions, the codes have few information about the equivalent relationships between opening percentages or positions and URM structural behaviour. Therefore, the opening effects for URM structures are not investigated sufficiently by researchers and codes and depending on previous study mentioned by 2.2, the opening effects play an important role in structural performance and thus it is necessary to have more analytical work and develop integrated models to identify the opening effects of URM buildings. The thesis focused on this issue and developed lots of analysis about opening effects include opening sizes and positions for URM structures and proposed the equivalent relationship.

2.3 Numerical modelling for masonry buildings

2.3.1 Challenges and strategies for masonry modelling

For numerical models, it is necessary to reflect the real response of structures by applying the proper material properties and constitutive models. However, most masonry models are sensitive to even a small change in input data which can result in an apparent difference between the deformability and strength of masonry structures. The main challenges of masonry modelling are summarised below:

- It is hard to capture the actual boundary stress for every single brick in a complete masonry structure and imagine that the strength of every mortar joint can be identified accurately. For linear tests or non-linear tests with minor cracking or small displacement, it is possible to obtain useful physical data for a wall and build a reasonably accurate numerical model, but if the numerical model is to be taken to collapse, it is hard to provide enough local detail for the material properties to be sure that the numerical model reflects reality.
- In the analysis of masonry structures, it is challenging to generate the correct, rather than an idealised, loading level and distribution (Lemos, 2004). The direction of gravity and other

expected loading direction may not represent the correct load paths and distribution. Lots of issues such as contact problems, eccentric loading, and friction could occur due to load transferring and distribution.

- Numerical models are generally developed by researchers and then the developed theories are applied by the engineering community. However, the complexity and sophistication of numerical models it is not easily understood it is hard for engineering community to support the theoretical development of masonry modelling.

Overall, it is vital to work out the dominant failure mechanisms of a numerical model which have an impact on the masonry response for a variety of material properties and different loading cases. Once the behaviour of numerical models can be identified and verified by experimental tests, simplified methods can be developed to reflect the correct masonry behaviour and predict an accurate response for a masonry structure.

According to (Milani, 2016), to develop accurate or validated numerical model, some features are considered as essential for simulating the accurate response. Firstly, opening, closing and shear sliding of joints must be considered when determining the strength and stiffness changes in the structure. A precise description of tensile failure, debonding and shear slip for the brick-mortar interface should be included, and the mechanical components must also reflect the specific behaviour of the brick-mortar interface consisting of bonding, frictional and cohesive resistance. Moreover, it should be possible to implement different material properties in the numerical model at a variety of locations. The crack propagation, post-cracking and collapse must be captured clearly. Finally, the relationship between load-capacity and displacement of whole structures should be identified.

Generally, there are two main methods for analysing masonry models: micro-models and macro-models. For micro-models, all types of representative elements such as bricks, mortar, interface of brick-mortar are modelled in detail, and the response of structures can be described accurately. Additionally, micro-models can be divided into detailed micro-models and simplified micro-models. Both have the same aim of representing masonry, based on a knowledge of the properties of all the materials and their interfaces, but for detailed micro-modelling, the brick-mortar interface is represented by discontinuum elements while for simplified micro-modelling the mortar and mortar-brick interface are combined into a single discontinuum line interface element (Lourenco, 1996, Oliveira, 2003). The macro-model deals with the interaction between the bricks and mortars as equal to the behaviour of a prism which includes the bricks and mortars. Additionally, the unit material is developed as a composite of the bricks and mortars. Therefore, the modelling methods of masonry

can be classified by detailed micro-modelling, simplified micro-modelling and macro-modelling (Lourenco and Rots, 1994) (described in Figure 2.1).

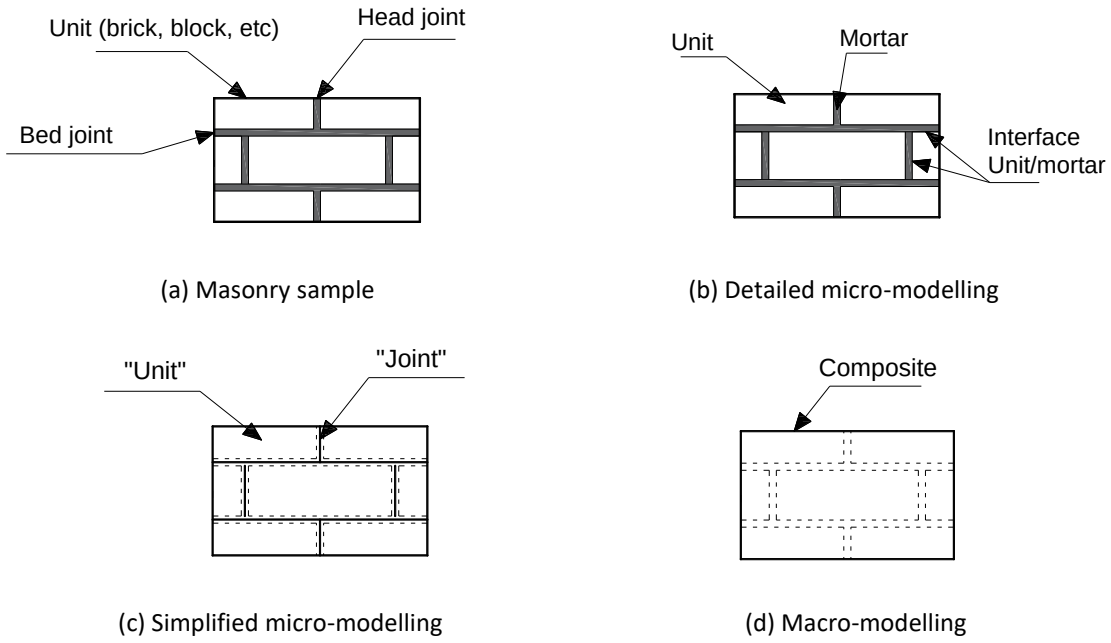

Figure 2.1 Modelling of masonry structure [Adapted from (Lourenco and Rots, 1994)]

2.3.2 Detailed micro-models for masonry structures

Detailed micro-modelling uses continuum elements for both the masonry units and the joints and interface elements are taken as discontinuous. This method can be regarded as the most accurate model to represent all possible behaviours of masonry structures (described in Figure 2.2). Both masonry units and mortar joints can be given realistic material properties and constitutive models can be applied to all elements, including interfaces. However, this approach is not suitable for modelling large structures due to the number of parameters that need to be defined and the analysis is also very time-consuming (Akhaveissy and Milani, 2013). However many researchers have used this method although they have focused on small specimens to obtain accurate results (Lourenço et al., 2006, Papa and Blockwork Structures", 2001, Zucchini et al., 2007).

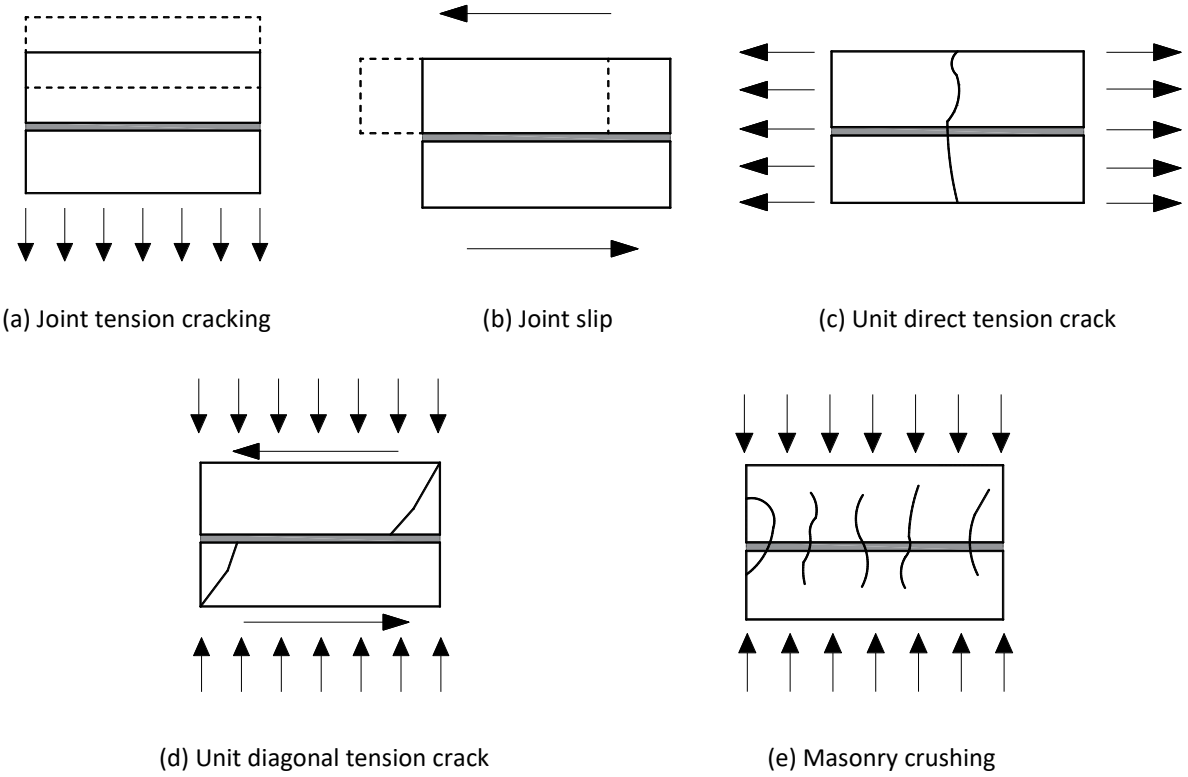

(a) Joint tension cracking (b) Joint slip (c) Unit direct tension crack

(d) Unit diagonal tension crack (e) Masonry crushing

Figure 2.2 Failure mechanisms of masonry [Adapted from (Lourenco, 1996)]

2.3.3 Simplified micro-models for masonry structures

The simplified micro-model method uses continuum elements for the masonry units, but both mortar joints and interfaces are modelled as whole discontinuous elements. This model type of modelling approach can be subclassified into three main methods; the Discontinuous Finite Element Method, the Discrete Element Method (DEM) and the Limit Analysis Method. The discrete element method then divides down into the Distinct Element Method, Discontinuous Deformation Analysis (DDA), the Particle Flow Method (PFM) and the Discrete-Finite Element Method. A review of these models is presented below.

2.3.3.1 Continuum finite element models

Due to the demand for developing suitable models to describe the true behaviour of old masonry buildings with piers and buttresses, masonry can modelled as a homogeneous continuum (Oliveira,

2003). As all the elements belong to a continuum, the meshing of the model tends to take a long time, and this approach is only suitable for the analysis of partial or detailed models. Some examples of analyses using this method can be found in (Mola and Vitaliani, 1995). The process of mesh generation occupies the majority of the analysis time because of the need for a large number of element meshes. The combination of computational time limits and the need for experimental data to validate models, means that these models are generally restricted to simplified non-linear models. This means that difference between linear and simple non-linear analysis is always significant and often a non-linear analysis can effectively be regarded as a linear analysis. However, continuum finite element models are feasible for some regular historical masonry structures although the range of their application is limited.

2.3.3.2 Discontinuum finite element model

The discontinuum finite element model takes the mortar joints as discontinuities where failure by cracking, slipping or crushing can take place. Interface elements are applied to represent the discontinuities, and the vector of stress and displacement along the interface can be defined by a constitutive model (Oliveira, 2003). Therefore, it is necessary to set up a proper model to simulate all the possible failure mechanisms and capture the real behaviour of the masonry. Based on (Lourenco, 1996), a composite interface model was proposed for masonry, including the tension model, a Coulomb friction model, and a compressive capacity model. All the models included different failure criteria consisting of a tension cut-off criterion, a Coulomb friction criterion and a compressive failure criterion, and then a composite yield criterion was introduced. This model had shown good agreement between the analysed load-displacement curves and experimental data, so it appeared that the model could represent the real behaviour of mortar. However, a situation might occur where the compression model was not spherical and therefore some parameters in the model need to be adjusted to take into account the effect of softening. In another study by (Lourenço et al., 1998) a model of a shear wall with an opening was validated by some experimental data and the results were discussed.

Similarly, according to (Lotfi and Shing, 1994), a model was suggested that considered the softening rule and non-associated flow Rule. Lotfi and Shing (1991) proposed a smeared-crack model for masonry shear walls. Using their model, reinforced masonry shear walls were tested and it was shown that the smeared-crack model could reflect the response of the shear wall accurately except for the brittle shear behaviour which was dominated by diagonal cracking. Based on (Sutcliffe et al., 2001), a

lower bound limit approach for unreinforced masonry walls was developed but use of this method needs to satisfy two assumptions. One was that the materials had to show good plastic capacity and the associated flow rule had to be obeyed without considering strain hardening or softening. The other was that the deformations of the body were able to remain unchanged under the collapse load. It is worth noting that Sutcliffe et al. (2001) used linear 3-noded triangular elements to model the field rather than the spherical cap model used by (Lourenco, 1996) when introducing the yield surface. Gambarotta and Lagomarsino (1997) proposed a damage model for mortar joints which considered the effects of the mortar damage and debonding of the mortar-brick interface, so the failure of opening and sliding could occur. This composite finite-element model has been applied to model experimental tests of masonry shear walls under static loads and cyclic forces and describes the failures in compression, tensile and shear. However, this method is too time-consuming to be applied to full-scale masonry walls and the model ignores some inelastic mechanisms with limits the flexible of the continuum model. Chaimoon and Attard (2007) suggested a model for unreinforced masonry walls with 2D brick units and mortar joints, where the mortar-brick interface was regarded as a zero thickness interface. Meanwhile, a similar failure surface was used by (Sutcliffe et al., 2001) who suggested the Mohr–Coulomb failure surface with a tension cut-off and a linear compression cap. But there are several differences between (Chaimoon and Attard, 2007) and (Sutcliffe et al., 2001) which meant that the linear compressive cap models used had different slope angles. Shieh-Beygi and Pietruszczak (2008) adopted a mesoscale method for masonry shear walls with a constitutive model that could implement pre and post-localisation behaviour, and this method has been verified against three different experimental tests. Based on (Avossa and Malangone, 2015), a new modified concrete model was used, and this paper compares three different models i.e. a Drucker–Prager model, a Concrete model and a CoDIC model (Concrete-Drucker–Prager-Ideal Spherical Compressive Cap). It was observed that the CoDIC model was able to represent the masonry behaviour more accurately, especially for the evaluation of 3D building performance. Akhaveissy and Desai (2011) describe a model which is called the DSC/HISS-CT model and this model relies on the Disturbed State Concept (DSC). The plasticity principle of a hierarchical single yield surface (HISS) model with the associated flow was used to model behaviour in compression and tension. This model had different yield surfaces applied in compression and tension to predict microcracking as well as the hardening and softening of the masonry and does not need as much calculation time as the cap model. Pegon et al. (2001) developed a model where the interface elements are controlled by an elastic-plastic Coulomb friction model. This model was implemented in 2D and 3D numerical simulations. It was shown that the 2D model produced good agreement for deformation and damage pattern compared with real tests.

However, for the 3D model, there was the challenge that the meshing of the models was too time consuming for realistic application to parametric studies.

2.3.3.3 Discrete element model

The discrete element model is interesting because large displacements can be applied to the model and the failure mechanisms of the masonry are easily observed. This method was firstly introduced by (Cundall, 1971) who developed the formulation for this method dealing with discrete bodies that can have finite displacements and rotations with contacts between blocks being recognised automatically. Later the method was extended to lots of areas where there is a need to identify the contacts between blocks or particles and this method is therefore particularly suitable for masonry structures. (Ghaboussi and Barbosa, 1990) developed a study showing how connections between blocks such as soil or other materials could be modelled using the discrete element method. Alexandris et al. (2004) applied the discrete element method successfully to model historic masonry structures and analysed the collapse mechanisms of masonry buildings. Lemos (Lemos, 1995, Lemos, 1998), presented studies modelling masonry arches with the discrete element method. Due to the behaviour of contacts being governed by the properties of the masonry joints, this method can be readily be applied to model masonry structures. Dimitri et al. (2011) carried out a 2D numerical study on the dynamic behaviour of masonry columns and arches based on the discrete element method. An example comparing 3DEC analyses with experimental data for plain and reinforced masonry walls can be found in (Dihrou L et al., 2018) and a 3DEC model of a masonry wall was built by Liu Z and Crewe AJ (2018) to explore the opening effects of masonry walls.

- **Distinct element method**

The Distinct Element Method (DEM) is based on the discrete element model and is used in the UDEC (Universal Distinct Element Code) and 3DEC software and can be applied to the analysis of static or dynamic models of 2D and 3D structures (Itasca, 2012). In 3DEC, the representations of contacts and blocks are similar to standard DEM method, and the blocks can be described as rigid or as deformable. A rigid block does not change shape even under applied loading, while deformable blocks are subdivided into triangular elements, which are based on the FE method, and these allow calculation of deformation of the blocks. The main difference between DEM in 3DEC and a standard FE model is the fact that for DEM models in 3DEC only the blocks need to be meshed and the joints are generated

automatically as additional blocks are added, as compared to FE where all the contact elements need to be specifically defined. In 3DEC, the mortar joints are built as zero-thickness interfaces and are represented by point contacts rather joint elements, and these points can be used to identify the stresses and displacements across the joint. According to (Dialer, 2002, Schlegel and Rautenstrauch, 2004, Dumova-Jovanosla and Churilow, 2009, Sarhosis et al., 2014b, Sarhosis and Sheng, 2014, Sarhosis et al., 2015), masonry walls can be modelled with DEM using UDEC or 3DEC. (Mohebkhah et al., 2008) developed a DEM model to evaluate the in-plane behaviour of masonry infilled walls. Haider (1995) , Lemos (Lemos, 1998, Lemos, 2004, Lemos, 2007, Lemos, 2001) and Sarhosis et al. (2014a) studied masonry arches with DEM method and described the theory of modelling masonry structures with 3DEC. In 2011 de Felice (2011) studied the out-of-plane behaviour of masonry walls based on the wall section morphology and proposed methods to determine the failure acceleration under a quasi-static loading case. Çaktı et al. (2016) developed an experiment for a scaled masonry structure and compared the dynamic response with 3DEC model.

Similarly, Lemos and Costa (2017) simulated a simplified shaking table test of masonry stone structures and compared the results with experimental data. This paper demonstrated that the DEM could reproduce the significant features of the shaking table tests. Low-bond strength masonry walls modelled using 3DEC to simulate the in-plane behaviour are described in (Sarhosis and Sheng, 2014), (Sarhosis et al., 2014a) and (Giamundo et al., 2014). These papers introduced specific methods of modelling masonry in 3DEC and compared the load-displacement curves of for different models. Bui et al. (2017) developed a 3D DEM numerical model to study the in-plane and out-of-plane behaviour of dry-joint masonry wall constructions. In this article simulated collapse patterns were compared with experimental data and obtained similar failure mechanisms were seen for the models and the actual masonry walls. Bui et al. (2019) identified both in-plane and out-of-plane behaviour of masonry panel using 3DEC and calibrated the results compared with experimental data. A DEM model was developed by (Tavafi et al., 2019) to identify the dynamic analysis for the Cube of Zoroaster Tower. Liu and Crewe (2020) identified the opening effects on URM walls subjected to in-plane loading. All the research present numerical analysis of URM structures considering the DEM model and the results show good agreement with experimental tests and can predict accurately the structural behaviour of masonry structures, which verify the reliability of the numerical model.

- **Discontinuous deformation analysis**

Discontinuous deformation analysis (DDA) is another method based on DEM, firstly developed by (Goodman, 1988) to solve the issues of stress-displacement problems in a jointed rock mass system.

Subsequently, this method was used to model masonry arches by (Bićanić et al., 2003). Compared to DEM, DDA considers the blocks to be deformable while the stress and strain should be distributed. Contacts are regarded as rigid, and interpenetration of blocks is forbidden, which is different from the discrete element method where the contact is soft and some overlap of blocks is permitted. However this method does not model shear displacements if blocks only slide. The algorithm solution of DDA is also based on the global stiffness matrix which is different to UDEC (which is based on an explicit algorithm), and this solution reaches the equilibrium by reducing the potential energy of the blocky rock mass system. A comparison of the DEM and DDA methods is described in detail by (Bobet et al., 2009) and (Milani, 2016).

- **Particle Flow and Discrete-finite element model**

A particle flow model (PFM) is another discrete element method that simulates the response of a system composed of arbitrarily shaped particles (Milani, 2016). This method had been applied in the simulation of old masonry arch bridges by (Tóth et al., 2009) and (Thavalingam et al., 2001). The particle flow code (PFC) is used in the software developed by Itasca Ltd can model problems in 2D as disks or in 3D using spherical shaped particles. An advantage of PFM is that it is computationally efficient due to the contact detection mainly depending on the calculation of the distance between the particle centres. However, this method is time consuming if the size of structure is large. In this method, the masonry blocks are generally regarded as larger particles and the mortar joints are taken as smaller particles. The interface elements can be represented by applying various bond strengths.

Discrete-finite element models can be considered as the combination of both DE and FE methods. The aim of this method is to increase the efficiency of calculation. The blocks in this method are regarded as FE models, meshed by triangular elements during the analysis. Similar to the FE method, plastic material properties need to be determined for the masonry blocks and mortar joints. Based on (Munjiza et al., 1995), a method was developed to simulate fracturing issues using a fracture mechanism criteria. Later (Mamaghani et al., 1999) considered an FE assumption for blocks and described the non-linear behaviour through iterations performed at every load increment and assembling the global stiffness matrix. Thus, this method can identify the stability analysis for different masonry structures. (Owen et al., 1998), applied a discrete-finite element model to estimate the load-bearing capacity of a masonry arch bridge. Masonry blocks were taken as deformable discrete elements, and the mortar joints were represented by the spherical discrete elements. The load-displacement curve for the structure was presented and compared with experimental data.

2.3.3.4 Limit analysis model

The limit analysis model for masonry structures can be described as rigid blocks connected by joints considering static or dynamic equilibrium. Based on (Orduña and Lourenço, 2003), there are two underlying assumptions, firstly that ultimate load occurs at a small overall displacement and secondly that the masonry has zero tensile strength; but only in dry jointed masonry would this actually occur. Garrity et al. (2010) developed several experiments to verify the method. Roca et al. (2010) considered some of the issues related to the above assumptions, especially when dealing with crushing behaviour that may not play an essential role under general situations, but can when there is significant vertical loading or the structural elements are shallow. Baggio and Trovalusci (1998) suggested that limit analysis using a 2D and 3D discrete system including rules for non-associative flow was successful in providing an effective way to estimate the ultimate load-carrying capacity and failure mechanisms for the masonry structures with dry joints and frictional interfaces. Gilbert et al. (2006) proposed a new limit analysis method for rigid block systems based on non-associative frictional interfaces. The behaviour of contacts is controlled by a Mohr-Coulomb failure surface at each contact interface. This proposed method can estimate the load-bearing capacity for a wide range of problems and is especially suitable to solve large problems which are normally prohibitively computationally expensive. (Gilbert, 2007), concluded that limit analysis provides a robust and straightforward way to evaluate the progress of collapse for masonry arch bridges and also increases the efficiency of computation.

2.3.4 Macro-model for the masonry structure

In macro-modelling of masonry, mortar joints are smeared out in the continuum, as stated by (Akhaveissy and Desai, 2011). Most of the material parameter need to be obtained via experimental tests of the masonry. Lourenco (1996) referred to two macro-modelling approaches, one using the single yield criterion to reflect the material behaviour, and the other using an extension of conventional formulations for isotropic quasi-brittle materials to describe the orthotropic characteristics. In (Lourenço et al., 1998), the yield surface of the continuum model was proposed using two different criteria, a Rankine-Type Criterion and a Hill-Type Criterion and then 12 walls were tested to compare the experiments results with the plastic model. Brasile et al. (2010) suggested a coarse-scale model for the in-plane analysis of masonry. Based on four assumptions, this approach reflected the global response of structures. However, it is essential to note that the use of a non-associated flow rule tended to ignore the effects of the unrealistic response of the associated plastic

modelling. Dhanasekar and Haider (2008) applied the Hill-type yield surface containing four parameters to model the biaxial compression and tension behaviours of URM (unreinforced masonry) walls and wide-spaced reinforced masonry (WSRM). Additionally, this paper proposed a damaged concrete plasticity model for grouted cores as well as an ABQUS rebar option for reinforcement. Based on (Belmouden and Lestuzzi, 2009), a novel equivalent plane-frame model with openings was proposed to analyse the pushover behaviour for unreinforced masonry walls and reinforced concrete buildings. The model uses a method that separates the walls with opening into piers and spandrels to formulate the phenomenon of inelastic flexural and shear deformation. Thus, the model can present any shape of failure criteria and shows good agreement with experimental data.

2.3.5 Determination of numerical model in the thesis

Based on all the modelling methods mentioned above, a comparison between finite element models and discrete element models are presented in Table 2.2.

Table 2.2 Comparison of micro-modelling methods between finite element models and discrete element models

	Advantages	**Disadvantages**
Finite-element models	➢ Produce a good prediction of masonry building response; ➢ Suitable for small deformations of masonry	➢ Time-consuming when running analysis of large structures; ➢ Difficult to mesh blocks and joints for 3D problem or create blocks with the complex arrangements; ➢ Once large displacement occurred, it is hard to auto-meshing, updating the information of the new contacts; ➢ When masonry unit overlap occurs, there is no warning; ➢ Pre-defined crack patterns are needed.

Discrete-element models	➢ Large displacements and rotations are allowed; ➢ Able to mesh the blocks and joints independently, without need to match nodal points; ➢ The algorithm is similar for both static and dynamic problems; ➢ Able to describe the post-peak behaviour; ➢ Overlap of blocks is limited and dilation effects are considered.	➢ The code is complicated and needs to be adjusted to analyse different problems; ➢ The stress distribution in the individual masonry units is not completely accuracy; ➢ Still time-consuming when dealing with large buildings.

Based on the comparison of both advantages and disadvantages for FE and DEM models, the main difference is that for FE model, it can describe the structural response of masonry structures accurately but is time-consuming when considering large structures, and it is also difficult to capture the movement of blocks if large displacement occurred. However, the thesis needs to observe the response when large displacements of structures occur and even the collapse behaviour. DEM can allow large displacements and rotations and evaluate post-peak behaviour for both static and dynamic problems, which satisfy the requirements of the research.

Therefore, DEM is considered more suitable for targeting the opening issues as it can represent the crucial large deformation dynamic behaviour of masonry structures when considering different opening cases and observe easily the crack propagation and progress of failure include collapse. The thesis prefers to DEM model to represent the masonry structures.

2.4 Seismic performance of unreinforced masonry structures

Typical URM structures include load-bearing walls arranged in orthogonal planes and rigid or flexible floors (Magenes and Calvi, 1997). Damage to URM buildings can be composed of connection failures, in-plane failures, out-of-plane failures of walls, diaphragm related failures and combined in-plane and

out-of-plane failures (Moon, 2003, Bruneau, 1994b, Tomazevic, 1999). The different failure modes in URM structures are further complicated due to effects such as boundary conditions, aspect ratios of walls, pre-compressive stress, variation in material properties etc. The following sections describe the specific failures in detail.

2.4.1 In-plane behaviour of unreinforced masonry walls

In-plane walls are critical to the stability of URM structures, and they provide stability and strength to prevent the collapse of buildings. The in-plane capacity of masonry walls is highly related to the strength of masonry and mortar (Wijanto, 2007) and a review of the failure modes, failure criteria and analytical application is presented below.

2.4.1.1 Failure modes of in-plane unreinforced masonry walls

(Abrams and Shah, 1992) carried out experimental tests of three unreinforced masonry walls subjected to vertical compressive stress and lateral deflections. For flexural failure, when the first crack occurred, the vertical compressive stress shifted towards the wall toe to form a lever arm, which could generate overturning moments. For shear failure, when stair-stepped diagonal tension cracks propagated, vertical stress could support frictional force to resist lateral loads. Unreinforced masonry walls are ductile elements capable of dissipating energy through hysteresis and it is reasonable that all unreinforced masonry elements should contribute to lateral strength of a structural system. Usually, these in-plane walls are divided into small piers and spandrels by window openings and door openings. These smaller structural components separated by openings form the resistance system against gravity and lateral loads. Typically, in-plane failures usually appear in one of these elements (Moon, 2003) and the final collapse of URM buildings in the past research is mostly driven by pier failure (Calvi et al., 1996). According to (Yi, 2004, ATC, 2000), the failure of masonry walls under in-plane loading comes from shear failure along the mortar joints, compressive failure at the toe of the wall and flexural failure, which can be summarised as diagonal tension cracking, bed-joint sliding and rocking failure (simplified into three behaviours in Figure 2.3).

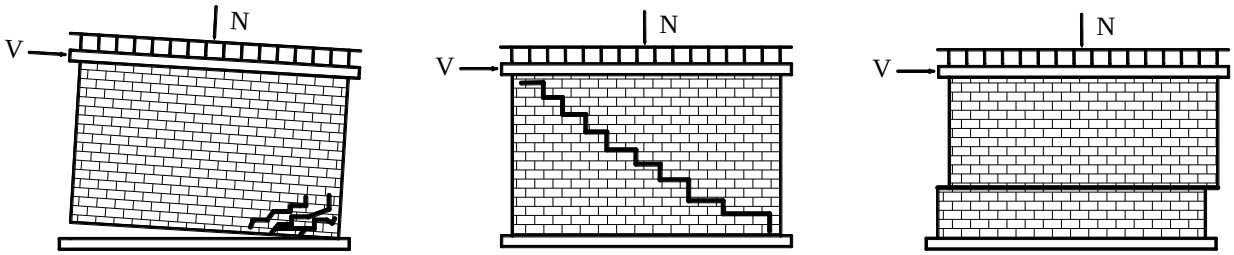

(a) Rock failure (b) Diagonal cracking (c) Bed-joint sliding

Figure 2.3 Failure patterns of masonry walls

Rocking failure and crushing failure can also be regarded as a flexural failure. As a large flexural moment occurs, and wide flexural cracks are propagated at the top or bottom of the pier, a rigid body rotation of pier is developed at the corner. As the toe of a pier now carries a high concentrated compressive stress, compressive failure is often generated around the toe area. Typically toe crushing is observed after rocking deformation.

Diagonal cracking is identified as a shear failure when the value of the maximum principal tensile stress based on vertical and horizontal loads is higher than the tension strength of the masonry. Then diagonal tension cracks occur and propagate in stair-stepped shapes along the mortar joints or sometimes go directly through the bricks. Diagonal cracking is not an good failure mode because it leads to a lower ductility for masonry walls and the strength of the masonry structures decreases with diagonal shear cracking.

Bed-joint sliding is dependent on the normal stress or friction coefficient between bricks. When the shear force in masonry walls has a higher value than the bed joint shear strength, which could be caused by low normal stress or low frictional resistance, the walls will sliding along the bed joints.

Considering the deformations of masonry walls, rocking failure and sliding failure lead to large displacements. The diagonal cracks along the bed and head joints allow large displacements as the bricks slide across each other, which cause energy dissipation. However, the diagonal cracks directly through units belong to a brittle failure mode because the bricks reduce in strength dramatically as cracks propagate between them, and this will lead to unstable walls. Toe crushing failure is also a brittle failure as the bricks can fail rapidly under high local loading.

2.4.1.2 Failure criteria for strength for in-plane URM walls

Failure criteria for strength are essential to predict the in-plane response of unreinforced masonry buildings accurately. Many researchers and codes have proposed relevant formulations to present different failure criteria for strength under in-plane behaviour (Andreaus, 1996). Based on a Mohr-Coulomb frictional law which considering the dependence of shear strength combined with normal stress, the failure modes such as mortar joints slipping, splitting and slipping of bed joints can be expressed accurately. Using the Saint-Venant criterion, other failure modes can be represented such as the splitting of bricks, and the splitting and slipping of mortar joints. When considering middle plane spalling, the Navier criterion could be used. All these criteria have been applied in 2D finite element models to analyse the in-plane behaviour of URM walls. Here are some specific failure criterions from taken from the literature and from design codes.

- **Magenes and Calvi, 1997**

(Magenes and Calvi, 1997) presented the issues of evaluation of strength, deformability and energy dissipation capacity of URM walls. In this paper, the role of the shear ratio in shear failure mechanisms is mentioned, and the relevant shear strength equation was proposed. The maximum horizontal shear resisted by a rocking pier can be expressed by Equation 2-1 as below:

$$V_r = \frac{D^2 t}{\alpha_v} \frac{p}{2} \left(1 - \frac{p}{\kappa f_u}\right) \quad 2\text{-}1$$

Where D is the pier length, t is the pier thickness, p is he mean vertical stress on the pier due to the axial load, f_u is the compressive strength of masonry, κ is a coefficient which takes into account the vertical stress distribution at the compressed toe, α_v is the shear ratio, which is related to the effective height of the pier H_0. $\alpha_v = H_0/D$.

For predicting shear strength concerning diagonal cracking, two methods were proposed. One was based on the assumption that diagonal shear failure occurs when the principal stress was located at the centre, taken as a reference tensile strength of masonry. The relevant shear strength was given by Equation 2-2 as below:

$$V_d = \frac{f_{tu} D t}{b} \sqrt{1 + \frac{p}{f_{tu}}} \quad 2\text{-}2$$

Where f_{tu} is the conventional tensile strength of masonry to be depended on shear tests of specific wall specimens, b is the pier aspect ratio.

Another approach was a Mohr-Coulomb equation based on mortar failure. The criterion was expressed by Equation 2-3 as below:

$$\tau_u = c + \mu\sigma_{\mathrm{v}} \qquad 2\text{-}3$$

In which τ_u is ultimate shear strength, c is cohesion coefficient, μ is the friction, σ_{v} is the vertical compressive stress.

For the sliding failure of the pier under seismic load, the horizontal joint could be formulated using Equation 2-4 as follows:

$$V_s = \mu P \qquad 2\text{-}4$$

In which μ referres to the sliding coefficient of friction of masonry joint without considering cohesion, as the joint had generated cracks in tension due to flexure already.

Notably, a proposed simplified formulation of shear strength could be expressed by Equation 2-5, Equation 2-6 and Equation 2-7:

$$V_d = Dt\tau_u \quad \text{with } \tau_u = \min(\tau_{cs}; \tau_{ws}) \qquad 2\text{-}5$$

$$\tau_{cs} = \frac{1.5c+\mu p}{1+3c\alpha_v/p} \quad \text{relevant to the cracked section} \qquad 2\text{-}6$$

$$\tau_{cs} = \frac{c+\mu p}{1+\alpha_v} \quad \text{relevant to the whole section} \qquad 2\text{-}7$$

- **Calderini et al., 2009**

Similarly, for identifying the in-plane load-bearing capacity of masonry piers, (Calderini et al., 2009) summarised most widespread strength criteria to reflect the in-plan failure modes (crushing, rocking, bed joints sliding and diagonal cracking) and discussed the conditions for proper use of the equations. Here are specific equations for considering different failure mechanism of masonry piers. For flexural failure, the maximum normal stress σ_c can be expressed by Equation 2-8 as below:

$$\sigma_c = \frac{\bar{\sigma}_y}{k_{2r}(1-2\kappa k_{1r})} \leq f_m \qquad 2\text{-}8$$

Where k_{1r} is a coefficient taking into account the slenderness and the boundary conditions of the pier; k_{2r} is a coefficient, which takes into account the assumed normal stress distribution at the compressed toe; κ is the ratio between the horizontal force and vertical force applied; $\bar{\sigma}_y$ is the mean

vertical stress acting on the section (*D* and *T* are the pier width and thickness); f_m is the compressive strength of the masonry.

For shear failure, a Mohr-Coulomb failure criterion was applied and the equations can be followed by Equation 2-9 as below:

$$\sigma_c = k_{1d}\bar{\tau} \leq k_{1s}\tilde{c} + \tilde{\mu}\bar{\sigma}_y \quad 2\text{-}9$$

Where $\tilde{c}$ and $\tilde{\mu}$ are cohesion and friction of masonry; k_{1d} refers to the slenderness of the pier *H*/*D*; k_{1s} is a coefficient that takes into account the actual compressed part of the reference section under the situation of ratios between uncracked and total height.

- **Chinese standards of low-rise unreinforced masonry buildings**

According to the (JGJ161-2008, 2008), the shear strength of masonry wall is expressed by Equation 2-10 as below:

$$V_b \leq \mu r_{bE}\xi_n f_{v,m}A \quad 2\text{-}10$$

In which, μ is the adjustment coefficient of seismic capacity. When there are no confined columns and ring beams, μ is 0.75; when there are confined columns, and ring beams but the structural measures are not good, μ is 0.85. V_b refers to the standard value of masonry wall shear strength under primary seismic intensity. r_{bE} is the adjustment coefficient of ultimate seismic bearing capacity, for the bearing walls, it is 0.95; for non-bearing walls, it is 0.85. $f_{v,m}$ refers to the mean of shear resistant for masonry without seismic design. A is the cross-sectional area of shear walls. ξ_n is the impact factor of normal stress for the masonry shear strength. Based on (GB50011, 2010), this can be calculated using Equation 2-11 as below:

$$\xi_n = \frac{1}{1.2}\sqrt{1 + 0.45\sigma_0/f_v} \quad 2\text{-}11$$

Where σ_0 is the average stress of masonry corresponding to the representative value of gravity load and f_v is the design value of hearing resistant for masonry structures.

Another shear strength dependent on diagonal cracking of masonry wall based on (GB50011, 2010) is expressed by Equation 2-12 and Equation 2-13 as below:

$$\mathrm{V} \leq f_{vE}A/\gamma_{RE} \quad 2\text{-}12$$

$$f_{vE} = \xi_n f_v \quad 2\text{-}13$$

Where σ_0 is the average stress of masonry corresponding to the representative value of gravity load and f_v is the design value of hearing resistant for masonry structures.

This indicates that the shear value from the seismic design code is more favourable than the regulations of rural housing, so the shear strength from the regulations should be used when considering the seismic performance of buildings.

For flexural strength of unreinforced walls, the formulation is given by Equation 2-14 as follows:

$$\mathrm{M} \leq f_{tm} W \tag{2-14}$$

Where

M is the moment design value; f_{tm} is the design value of bending tensile strength; W is the section modulus.

- **Eurocode 6**

According to part 1-1of (EN1996-1-1, 2005), the capacity of URM subjected to shear loading is given by Equation 2-15:

$$V_{Rd} = f_{vd} \cdot t \cdot l_c \tag{2-15}$$

In which f_{vd} is the design value of the shear strength of masonry, based on the average of the vertical stress over the compressed part of the wall that is providing the shear resistance, t is the thickness of the wall resisting the shear, l_c is the length of the compressed part of the wall, ignoring any part of the wall that is in tension.

There is also a simplified method to analyse shear strength according to part 3 of (EN1996-3, 2006) expressed by Equation 2-16 as below:

$$V_{Rd} = c_v \cdot \left[\frac{l}{2} - e_{Ed}\right] \cdot t \cdot f_{vdo} + 0.4 \cdot \frac{N_{Ed}}{\gamma_M} \leq 3\left[\frac{l}{2} - e_{Ed}\right] \cdot t \cdot f_{vdu} \tag{2-16}$$

In which

$e_{Ed} = \frac{M_{Ed}}{N_{Ed}}$; $c_v = 3$ filled head joints; $c_v = 1{,}5$ unfilled head joints; e_{Ed} : Eccentricity of load; t: the thickness of the wall; $f_{vdo} = f_{vko}/\gamma_M$; N_{Ed} : Vertical load; l: length of the wall; f_{vdu} : Ultimate shear strength

For flexural strength of masonry wall, the formulation is expressed by Equation 2-17:

$$M_{Ed} \leq f_{xd} Z \quad \text{2-17}$$

Where

M_{Ed} is the design value of the moment applied to the masonry wall; f_{xd} is the design flexural strength appropriate to the plane of bending; Z is the elastic section modulus of unit height or length of the wall.

- **FEMA (273, 274, 356)**

Based on (ATC, 1997a, ATC, 1997b, ATC, 2000), the expected lateral strengths of URM walls or pier components based on bed-joint sliding failure or rocking strength are given by Equation 2-18 and Equation 2-19:

$$Q_{CE} = V_{bjs} = \nu_{me} A_n \quad \text{2-18}$$

$$Q_{CE} = V_r = 0.9 \alpha P_{CE} \left(\frac{L}{h_{eff}}\right) \quad \text{2-19}$$

Where

A_n is the area of net mortared/grouted section; h_{eff} is the height of resultant of lateral force; L is the length of the wall or pier; P_{CE} is the expected vertical axial compressive force per load combination; ν_{me} is the expected bed-joint sliding shear strength; V_{bjs} is the lateral strength of wall or pier based on bed-joint shear strength; V_r is the lateral rocking strength of wall or pier component; α is factor equal to 0.5 for fixed-free cantilever wall, or equal 1.0 for the fixed-fixed pier.

The lower bound lateral strength of URM walls or piers controlled by diagonal tension stress or toe compressive stress is expressed as below.

If L/h_{eff} is larger than 0.67 and less than 1.00, then the Equation 2-20 and Equation 2-21 is as follows:

$$Q_{CL} = V_{dt} = f'_{dt} A_n \left(\frac{L}{h_{eff}}\right) \sqrt{1 + \frac{f_a}{f'_{dt}}} \quad \text{2-20}$$

$$Q_{CL} = V_{tc} = \alpha P_{CL} \left(\frac{L}{h_{eff}}\right) \sqrt{1 + \frac{f_a}{0.7 f'_m}} \quad \text{2-21}$$

Where

f_a is the upper bound of vertical axial compressive stress; f'_{dt} is the lower bound of masonry diagonal tension strength; f'_m is the lower bound of masonry compressive strength; P_{CL} is the lower bound of

vertical compressive force from load combination; V_{dt} is the lateral strength limited by diagonal tension stress; V_{tc} is the lateral strength limited by toe compressive stress.

2.4.1.3 Review of applications of unreinforced masonry structures under in-plane behaviour

There is lots of research identifying the in-plane behaviour of unreinforced masonry structures, and some analytical applications for the in-plane response of URM are presented. Bruneau (1994b) identified the seismic performance of unreinforced masonry buildings in North America and pointed out the limitation of current design codes and standards. Costley and Abrams (1996) indicated that flexural tension was the primary failure mode for all piers, which could lead to horizontal cracks located at the bases of the door and window piers. Besides, when flexural tension cracks occurred, the rocking failure would control the response of buildings. Due to rocking failure regarded as a stable and repeatable response, an expected aspect ratio of piers was suggested from 1:1 to 2:1. A similar conclusion was obtained by (Badoux et al., 2002). Lourenço et al. (2005b) tested the structural behaviour of dry joint masonry walls subjected to in-plane combined loading. The experimental results showed the stiffness of masonry walls increased dramatically when a vertical load was applied. Depending on a simple ultimate mechanism, a simplified analysis method was also identified and compared well with the experimental results. Yi et al. (2006) developed three nonlinear methods consist of rigid body analysis, three-dimensional nonlinear FE analysis and two-dimensional nonlinear pushover analysis to simulate the response of a full-scale, two-storey URM structure. Through comparison with experimental results, all the methods could predict the nonlinear in-plane behaviour, and a 2D nonlinear pushover analysis was identified as a better way to analyse the in-plane behaviour efficiently and accurately. Garbin (2010) carried out experimental research targeting the in-plane cyclic response of three types of load-bearing masonry walls using uniaxial, diagonal compression and cyclic shear-compression tests. Finite-element models were applied, and two simplified criteria were used for calibration. According to the results, the isotropic micromodel, in particular, can describe shear-compression tests accurately and the implemented model can be applied by other types of units. It was found that the ultimate horizontal load and drift decreased with unit strength, and the displacement capacity of thin-layer masonry was lower than other types of masonry.

Ingham et al. (2011) developed an experimental test of unreinforced masonry walls to indicate that current NZSEE guidelines for seismic assessment of URM walls did not consider the effects of a spandrel when calculating the lateral strength of a perforated wall. The spandrel was usually regarded as infinite stiffness and strength. However, the strength of the failure mode of spandrel affected the

effective height of the pier aspect ratio, which is vital to in-plane strength and capacity. Caliò et al. (2012) introduced a new discrete-element model to represent the in-plane behaviour of unreinforced masonry buildings. The analysis method in this paper simulated the typical in-plane nonlinear behaviour of URM walls using an equivalent discrete element under seismic loading. The masonry units were meshed by macro-element discretisation with 48 quadrilaterals and 192 degrees of freedoms, the interface of joint was described as different springs to represent three in-plane failure modes. Through calibration with previous experimental and theoretical results, this approach was reliable and was suggested as a useful tool to evaluate the seismic performance of unreinforced masonry structures.

Similarly, Ghiassi et al. (2012a) proposed a macro-model (called a contact density model) to describe the nonlinear static analysis of unreinforced masonry walls. The model could predict all masonry in-plane failure modes such as crushing toe, rocking, diagonal tension cracking and bed-joint sliding. The results also had a good agreement with experimental research and there was improved computational efficiency. Penna et al. (2014) developed a microelement model for representing the cyclic in-plane behaviour of masonry walls. The two-node microelement allowed simulation of the main features of the lateral response of masonry piers, which were bending-rocking behaviour and shear failure, and the element could be applied for meshing equivalent frames representative of global masonry walls. Parisi et al. (2014) focused on the in-plane behaviour of spandrels and carried out lots of tests. Two full-scale lateral loading tests on masonry walls with different spandrel types were completed and the results were compared with a previous specimen. For considering the energy dissipation capacity of walls with openings and rocking piers, this paper recommended a damping ratio with 2% with respect to masonry arch and 4% with wooden lintel, respectively.

2.4.2 Out-of-plane behaviour of unreinforced masonry walls

Out-of-plane collapse usually occurs at relatively low excitation levels and regularly appears without warning, which is dangerous to life and property. Based on a few studies looking at post-earthquake assessment, the out-of-plane collapse of masonry walls has been taken as one of the predominant failure modes in URM buildings (Bruneau, 1994a, Bruneau, 1994b, Doherty, 2000, Yi, 2004, Griffith et al., 2007). Compared with in-plane behaviour, out-of-plane action cannot be regarded as a component of the seismic load path, the capacity of walls to remain stable and avoid out-of-plane collapse is the focus of current research. Local failures or failure of part of the loadbearing wall system can lead to failure or collapse of the complete structures. If the boundary conditions mean the wall spans between

floor levels or between orthogonal URM walls, the wall can be assumed to act as a one-way slab when subjected to out-of-plane loading. In the other case that the wall spans between floor levels and also between orthogonal URM walls, the wall can be assumed to act as a two-way slab.

2.4.2.1 Out-of-plane Failure for unreinforced masonry walls

When subjected to an earthquake, vibration is transferred to the out-of-plane URM by the in-plane walls and roof or floor diaphragms and via the inertial mass on the wall itself (Yi, 2004). The seismic vibration and associated bending deformation can cause cracking and even collapse of URM walls. After cracking, each part of the wall will act as a small rigid body in rocking and sufficient vertical loading is vital to support stability and stop overturning of individual bodies. Also, if the connection between the out-of-plane walls and the floor diaphragms or in-plane walls is not strong, the walls can become unstable leading to collapse. According to (Wijanto, 2007), the out-of-plane capacities of a URM wall is strongly related to the wall aspect ratio, the thickness of the wall, the boundary conditions, the types of diaphragm, and the material properties of the masonry. FEMA-273 and FEMA-274 (ATC, 1997a, ATC, 1997b) state that the stiffness of out-of-plane URM walls should be neglected in analytical models of the global structural system if in-plane walls exist and the stability of out-of-plane URM walls was highly related to the effective height to thickness ratio.

Vaculik (2012) introduced different failure mechanism of URM walls under out-of-plane behaviour depending on various boundary conditions. For one-way spanning walls, the boundary conditions are either one-side supported or two-side supported. For two-way spanning walls, two-side supported, three-side supported and four-side supported are possible. Sketches of these options are shown in Figure 2.4.

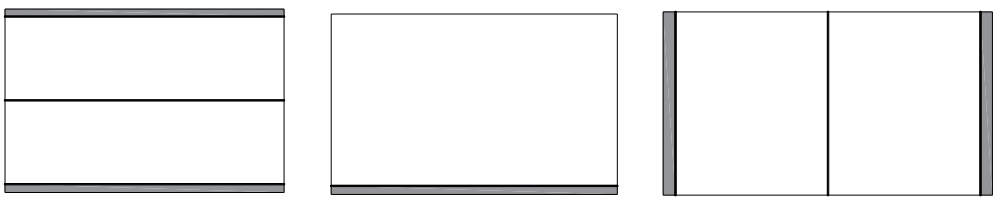

(a) Vertically spanning one-way wall 1; (b) Vertically spanning one-way wall 2; (c) Horizontal spanning one-way wall

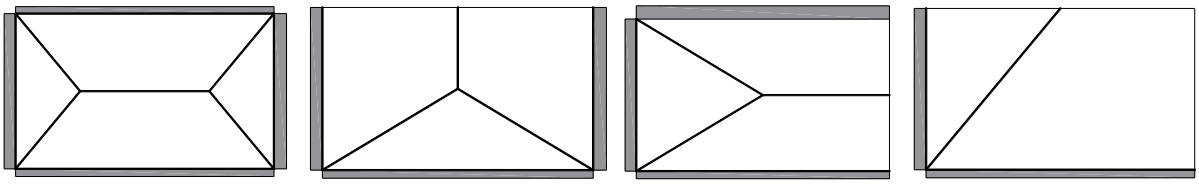

(d) O shaped spanning two-way wall; (e) U shaped spanning two-way wall; (f) C shaped spanning two-way wall; (g) L shaped spanning two-way wall

Figure 2.4 Different failure mechanisms of one-way and two-way spanning walls [Adapted from (Vaculik, 2012)]

For a vertical spanning a one-way wall, (Doherty, 2000, Doherty et al., 2002) proposed rigid body idealisation and a trilinear model for vertically one-way spanning walls. The detailed information for these models can be seen in Figure 2.5.

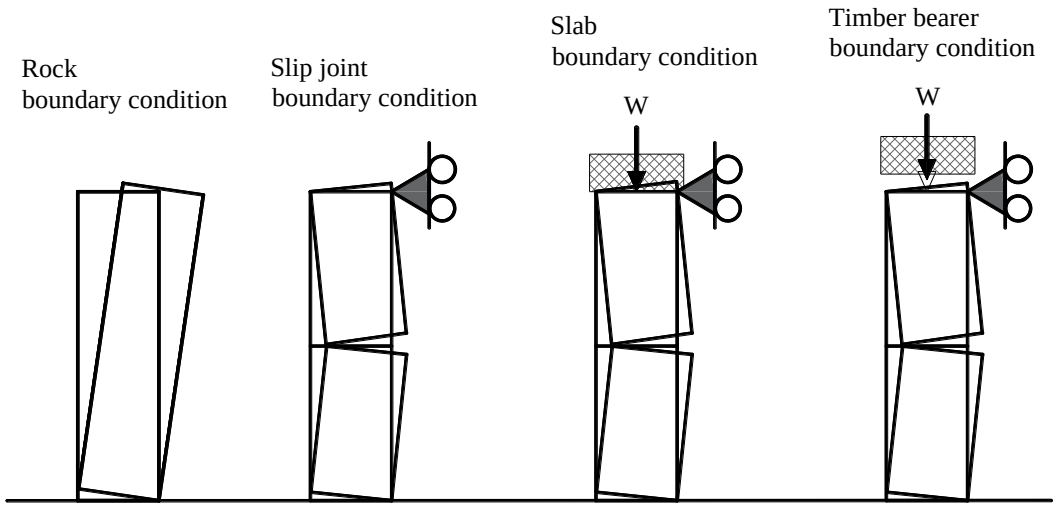

(a) Parapet wall; (b) Simply-supported non-loadbearing wall; (c) Simply-supported loadbearing wall with rigid diaphragms; (d) Simply-supported loadbearing wall with flexible diaphragms

Figure 2.5 Support configurations for vertical one-way spinning unreinforced masonry wall [Adapted from (Doherty et al., 2002)]

Doherty (2000) proposed a quasi-static linear elastic design methodology from Australia (AS3700-1998) for vertical one-way bending URM walls (described in Figure 2.6). The moment is expressed by Equation 2-22, Equation 2-23 and Equation 2-24 below:

$$M_e = \frac{t^2 l}{6}\left[\frac{O+\frac{W}{2}}{tl} + f_t'\right] \qquad 2\text{-}22$$

The predicted inertia distributed load leading to cracking is given by

$$w = \frac{8}{h^2}\left[\frac{t^2}{6}\left(\frac{P+\frac{W}{2}}{t} + f_t'\right)\right] \quad 2\text{-}23$$

The predicted cracking acceleration is shown as

$$a = \left[\frac{4t}{3\gamma g h^2}\left(\frac{O+\frac{W}{2}}{t} + f_t'\right)\right] \quad 2\text{-}24$$

Where W is the self-weight of the URM wall; w is the earthquake inertia load; γ is the specific weight of the URM wall; f_t' is the flexural tensile strength; O is the superimposed load (take concrete slab for instance). However, this method was limited to un-cracked walls and the elastic stress-strain assumption is not suitable for a post-cracked situation.

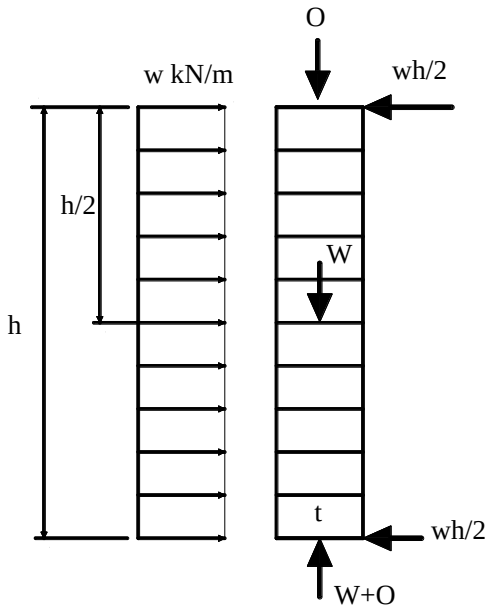

Figure 2.6 Quasi-Static Linear Elastic Design Methodology [Adapted from (Doherty, 2000)]

For a nonlinear analysis procedure, taking the object as rocking at Mid-height for instance, the moment equilibrium about the base corner can be expressed by (Griffith et al., 2003) Equation 2-25 and is shown in Figure 2.7:

$$R_t \cdot h + \frac{W}{2} \cdot \left(\frac{t}{2} - \frac{\Delta}{2}\right) \cdot 2 + M \cdot \frac{a_m}{2} \cdot \frac{h}{2} - M \cdot a_g \cdot \frac{h}{2} = 0 \quad 2\text{-}25$$

Where t is the wall thickness; h is the wall height between supports; M and W are the total mass and total weight of the wall, respectively; a_g is the ground acceleration; a_m and Δ are the acceleration and the displacement of the wall at mid-height.

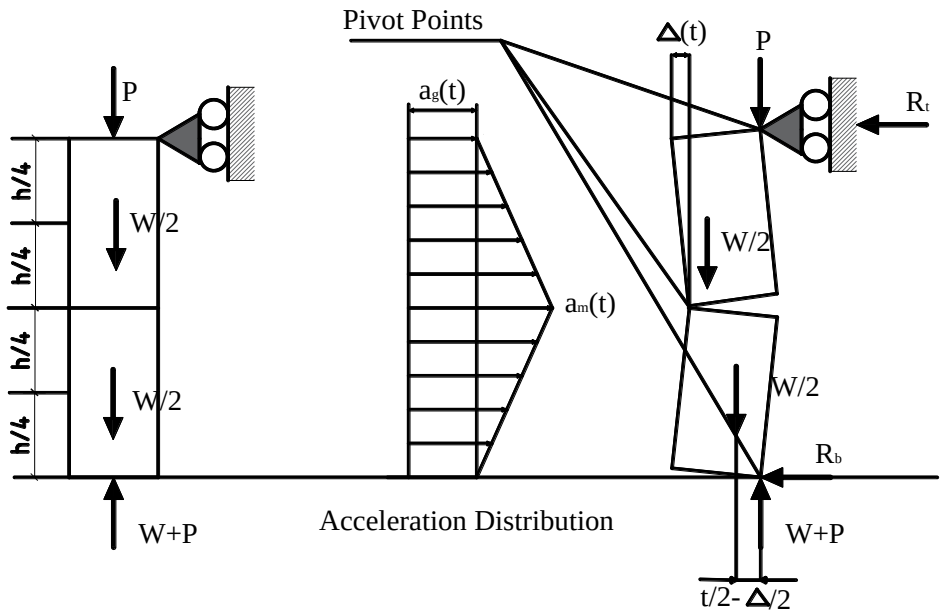

Figure 2.7 Rigid body idealisation of the cracked URM wall at rocking at Mid-height [Adapted from (Griffith et al., 2003)]

For the moment equilibrium of the upper half of the wall about the contact point at mid-height, the Equation 2-26 is given by

$$R_t \cdot \frac{h}{2} + \frac{W}{2} \cdot \frac{a_m}{2} \cdot \frac{h}{6} - \frac{M}{2} \cdot a_g \cdot \frac{h}{4} - \frac{W}{2} \cdot \left(\frac{t-\Delta}{2}\right) - P \cdot (t - \Delta) = 0 \qquad 2\text{-}26$$

Willis (2004) described the failure mechanism of diagonal bending including the flexural tensile strength of perpend joints, the torsional capacity of the bed joints, the torsional capacity of the perpend joints and the flexural tensile strength of the bed joints (shown as 1,2,3,4 in Figure 2.8).

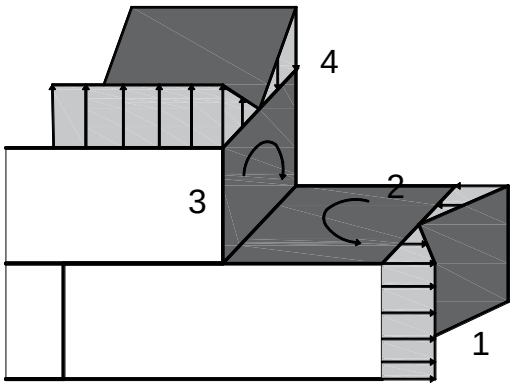

Figure 2.8 Failure mechanism of diagonal bending [Adapted from (Willis, 2004)]

Thus, the moment depended by each perpend joint, M_p , is expressed by Equation 2-27:

$$M_p = (f_{mt} - v_m[\sigma_V + f_{sw}]) \frac{(h_u + t_m)t^2}{6} \quad 2\text{-}27$$

The torque developed by bed joint, T_b is given by Equation 2-28:

$$T_b = \tau_b k_b 0.5(l_u + t_m)t^2 \quad 2\text{-}28$$

The torque developed by perpend joint, T_p, is determined by Equation 2-29:

$$T_p = \tau_p k_p t(h_u + t_m)^2 \quad 2\text{-}29$$

The moment, M_b, developed by bed joint is shown as Equation 2-30:

$$M_b = (f_{mt} + \sigma_V + f_{sw}) \frac{0.5(l_u + t_m)t^2}{6} \quad 2\text{-}30$$

Where f_{mt} is the flexural tensile strength of masonry perpendicular to bed joints, f_{sw} is the compressive due to self-weight, v_m is the Poisson´s ratio of mortar, σ_V is compressive stress, h_u is the height of the brick unit, t_m is the thickness of mortar joint, t is the thickness of the brick unit, l_u is the length of the brick unit, τ_b is the ultimate shear stress of bed joint, τ_p is the shear stress of perpend joint, k_b is the numerical factor used to calculate τ_b, k_p is the numerical factor used to calculate τ_p.

Based on (EN1996-1-1, 2005) 5.5.5, when the wall is supported along 3 or 4 edges, the calculation of the applied moment, M_{Edi}, may be taken as:

When the plane of failure is parallel to bed joints, in the f_{xk1} direction, the Equation 2-31 is as follows:

$$M_{Ed1} = \alpha_1 W_{Ed} l^2 \quad \text{per unit length of the wall} \quad 2\text{-}31$$

When the plane of failure is perpendicular to the bed joints, in the f_{xk2} direction, the Equation 2-32 is as follows:

$$M_{Ed2} = \alpha_2 W_{Ed} l^2 \quad \text{per unit height of the wall} \quad 2\text{-}32$$

Where

$\alpha_1 \alpha_2$ are the bending moment coefficient taking account of the degree of fixity at the edges of the walls, the height to length ratios of the walls; they can be obtained from a suitable theory;

l is the length of the wall;

W_{Ed} is the design lateral load per unit area.

Note: values of the bending coefficient α_1 and α_2 may be obtained form Annex E for single leaf walls with thickness less than or equal to 250mm, where $\alpha_1 = \mu\alpha_2$

μ is the orthogonal ratio of the design flexural strengths of the masonry.

FEMA-274 (ATC, 1997a) proposed the out-of-plane strength of URM walls consist of a lower limit and upper limit. For lower limit, no axial load, no edge confinement, no continuity with the adjacent wall and low tensile strength are considered. In that situation, the out-of-plane strength and stiffness should be neglected. For the upper limit, the tensile strength is ignored and the uniform transverse load equations q_{cr} are given by Equation 2-33:

$$q_{cr} = \frac{2Pt}{h^2} \quad 2\text{-}33$$

Where P is the vertical compressive load, and h and t are the height and thickness of walls. When considering arching action, the wall can sustain transverse loads with a reasonable upper bound expressed by Equation 2-34:

$$q_{cr} = \frac{6Pt}{h^2} \quad 2\text{-}34$$

Considering the maximum load level, the wall stiffness is ignored, and the structural integrity of the walls is directly related to dynamic stability.

Willis (2004) identified the failure mechanisms of horizontal one-way bending walls and diagonal bending walls, certain non-linear failure modes were proposed and compared with experimental data and with the Australia code. Vaculik (2012) carried out cyclic testing and shaking table testing specifically for two-way bending walls, then load-displacement modelling was developed and compared with experimental results.

2.4.2.2 Review of applications for unreinforced masonry walls under out-of-plane behaviour

Casolo (Casolo, 1999, Casolo, 2000) developed a rigid element model to identify the dynamic response and damage of masonry walls under out-of-plane loading. This model successfully described the failure modes and produced an accurate prediction of the general wall behaviour. This model was considered suitable for studying the seismic vulnerability of large scale of masonry buildings. (Doherty et al., 2002) and (Doherty, 2000) developed a trilinear model to predict the seismic performance of URM structures subjected to out-of-plane behaviour. (Lam et al., 2003) proposed a single-degree-of-freedom macro model to evaluate the out-of-plane response of URM walls under vertical one-way

bending conditions. A time-history analysis procedure was applied, and the results from the experiments and the analytical model were compared. The outcomes indicated that displacement was a better indicator of performance than acceleration and the response displacement derived from the dynamic analysis were consistent with the expected linear system. (Willis, 2004) focused on the study of URM walls under out-of-plane behaviour with three different bending conditions including one-way vertical bending, one-way horizontal bending and diagonal bending. Analytical models were developed to use basic non-linear stress-strain rules and improvements to design methods were proposed. Based on the results, the critical factors for the out-of-plane wall capacity were the material properties, specimen geometry, failure patterns and support conditions. Casapulla et al. (2014) applied two numerical models including macro and micro-block models to estimate out-of-plane performance for URM walls. A rigid-perfectly plastic model with dry contact interfaces controlled by Coulomb failure criterion was considered. A good agreement was achieved by comparing experimental results with numerical and analytical models.

(Griffith et al., 2007) and (Griffith, 2007) conducted a cyclic test for eight full-scale URM walls using an airbag system. Combined supports for vertical and horizontal edges were used and the boundary condition was determined to be two-way bending. The experimental results showed a good post-peak strength and displacement capacity. Derakhshan and Ingham (2008) implemented out-of-plane testing for URM walls with one-way bending. A tri-linear model was applied to validate the experimental results, which illustrated that different levels of overburden could change the response of the wall. Dazio (2008) implemented a shaking table test to identify the out-of-plane response of typical URM walls in Switzerland with different boundary conditions. The slenderness ratios, axial load ratio and restraints of walls were all considered. This paper showed that simple boundary conditions] are not always the most critical condition, but that more restrained boundary conditions can introduce an eccentric axial force to the wall that can cause failure of the wall at considerably smaller shaking levels. This means a simply supported wall can not always be taken as a worst-case situation. Shi et al. (2008) reported pseudo-static tests of URM walls under out-of-plane loading. For the experimental results, the corner connection was regarded as the most important factor for the out-of-plane response. Costa (Costa et al., 2012, Costa et al., 2013) discussed an experimental investigation of stone masonry structures subjected to out-of-plane loading and some simple theoretical models were calibrated to predict the ultimate strength of specimens. Vaculik (2012) developed a displacement-based seismic design method for URM walls subjected to two-way bending. Using this approach, a prediction of ultimate strength considering tensile strength and the strength for post-cracking behaviour could be achieved. Quasi-static cyclic and shaking table tests were carried out and

compared with the analytical results. Tis research did not consider the interaction of both in-plane and out-of-plane performance or the effects of floor/roof diaphragms.

Ferreira et al. (2015) presented the current issues for out-of-plane performance for URM structures. Different analytical methods were introduced including force and displacement-based approaches and useful numerical tools. In general, force-based methods were suitable to identify minimum acceleration capacities while displacement-based methods were more suitable for post-cracking modelling. Doherty et al. (2002) studied the displacement-based (DB) seismic analysis for URM walls subjected to out-of-plane loading. Through the comparison between quasi-static procedures and time-history analysis, the DB procedure was shown to give a better prediction than a force-based approach. A similar simplify procedure was developed by (Griffith et al., 2003). Derakhshan (2011) identified the rocking response of URM walls subjected to out-of-plane behaviour. The one-way bending response was determined and the force-displacement response was evaluated. The based on the results, a simple seismic assessment method was proposed based on (NZSEE, 2006). Similarly, Shawa et al. (2012) applied two methods; a discrete element model and a SDOF analytical model to evaluate the seismic behaviour of rocking masonry walls. Both models successfully simulated the experimental response, and the results were compared with the Italian seismic code.

2.4.3 Connection failure and diaphragm related failure of unreinforced masonry walls

Connection failure in URM masonry structures is common due to faulty connections between members in buildings. One type of failure is a poor anchorage between the diaphragm and the out-of-plane walls, which reduces the strength of the walls significantly often leading to walls that act as unstable cantilevers, which collapse during earthquakes. (Moon, 2003, Bruneau, 1994b). Another type of failure is low capacity shear connections between the in-plane walls and the diaphragms. This outcome will lead to severe damage at the corners between in-plane and out-of-plane walls, and can even lead to the total collapse of the out-of-plane walls.

Diaphragm related failures appear occasionally during seismic excitation. Membrane action in the URM structure can be created by structures such as deep beams, which can lead to corner damage in the URM wall under lateral force. However, for a flexible diaphragm, which results in the out-of-plane wall supports behaving as a spring, this can lead to out-of-plane failure due to the poor connections with the masonry walls (Yi, 2004). Simsir et al. (2004) also showed that flexible floor and roof

diaphragms dramatically increased the out-of-plane displacement response and acceleration response of the in-plane walls.

2.5 Seismic analysis procedures of unreinforced masonry structures

Based on (EN1998-1, 2004), there are several possible analytical approaches targeting the seismic performance of URM structures, including linear methods and non-linear methods. For linear methods, lateral force analysis and modal response spectrum analysis are possible and for non-linear methods, static (pushover) analysis and time-history analysis are possible. The linear analytical procedure is simplified so results can be calculated quickly, but this method cannot capture any plastic behaviour, so it does not really describe the global seismic capacity of URM structures. Non-linear methods expand the models into a post-elastic range, and a force-displacement relationship can be obtained. To present the seismic analysis methods in detail, the lateral shear force method, pushover procedure and dynamic analysis methods are introduced below.

2.5.1 Seismic force based on current codes or standards

This type of method is suitable for URM buildings which are not affected by modes of vibration higher than the fundamental mode in principle direction (EN1998-1, 2004). Before identifying the seismic performance of structures, there are two safety indicators that need to be checked; the ultimate limit states (strength verification) and damage control (deformation demands). Ultimate limit states relate to failures that might endanger the safety of people. Damage limit states identify when some structural requirements are no longer met (EN1998-1, 2004). Generally, when checking the ultimate limit states of masonry structures, the seismic force is calculated based on the elastic acceleration response spectrum, and the shear resistance is obtained according to the failure mechanism and material properties. For evaluating seismic performance of URM buildings, the lateral force methods from Chinese code, Eurocode and EERI are discussed and a comparison is also presented later.

2.5.1.1 Chinese earthquake resistance code

According to (GB50011, 2010), to analyse the seismic performance of structures, a simple earthquake resistant design method called equivalent base shear method is proposed. As the weight and stiffness

of masonry structures along the height are relevant distributed uniformly and the deformation of the structures is based on shear deformation, this method can be applied to calculate the seismic bearing capacity.

- **The calculation of horizontal earthquake force**

Based on (GB50011, 2010), the relationships between the seismic intensity and design basic acceleration of ground motion are shown in Table 2.3 below.

Table 2.3 The relationship between the seismic intensity and design basic acceleration of ground motion

Seismic intensity	6	7	8	9
Design basic acceleration of ground motion	0.05g	0.10 (0.15) g	0.20 (0.30) g	0.40 g

When calculating the horizontal earthquake force, the horizontal seismic effect coefficient α is needed and when the damping ratio is equal to 0.05, it is defined by Equation 2-35 as follows:

$0 \leq \mathrm{T} \leq 0.1$: $\alpha = 10 \cdot (\eta_2 - 0.45) \cdot \alpha_{max} \cdot T + 0.45 \cdot \alpha_{max}$

$0.1 \leq \mathrm{T} \leq T_g$: $\alpha = \eta_2 \cdot \alpha_{max}$

$T_g \leq \mathrm{T} \leq 5T_g$: $\alpha = (\frac{T_g}{T})^{\gamma} \eta_2 \alpha_{max}$

$5T_g \leq \mathrm{T}$: $\alpha = [\eta_2 0.2^{\gamma} - \eta_1(\mathrm{T} - 5T_g)]\alpha_{max}$ 2-35

In which T is the vibration period; η_2 is the adjustment factor of damping, $\eta_2 = 1 + \frac{0.05-\xi}{0.06+1.7\xi}$, $\eta_2 = 1$ for 5% viscous damping; T_g is characteristic period; γ is the reduction factor, $\gamma = 0.9 + \frac{0.05-\xi}{0.5+5\xi}$, $\gamma = 0.9$ for 5% viscous damping; η_1 refers to decline slope adjustment factor, $\eta_1 = 0.02 + \frac{0.05-\xi}{8}$, $\eta_1 = 0.02$ for 5% viscous damping; α_{max} is the maximum horizontal earthquake response factor; T_g is the characteristic period; T is the vibration period

The α_{max} and T_g can be determined in Table 2.4 and Table 2.5.

Table 2.4 The maximum value of horizontal earthquake effect coefficient α_{max}

Seismic intensity	6	7	8	9
Frequent seismic	0.04	0.08 (0.12)	0.16 (0.24)	0.32
Fortification seismic	0.12	0.23(0.36)	0.45(0.68)	0.90
Rare seismic	0.28	0.50 (0.72)	0.90 (1.20)	1.40

Table 2.5 Characteristic period T_g

Design seismic group	Ground-type			
	I	II	III	IV
One	0.25	0.35	0.45	0.65
Two	0.30	0.40	0.55	0.75
Three	0.35	0.45	0.65	0.90

(GB50011, 2010) proposes a standard method for calculating seismic action, the maximum seismic action for the single degree of freedom system is expressed by Equation 2-36 as follows:

$$F_{Ek} = G\alpha \quad \text{2-36}$$

Where the F_{Ek} is the seismic action force; G is the representative value of gravity load; α refers to horizontal seismic effect factor.

Therefore, the base shear force can be obtained based on the equivalent base shear method for masonry structures, which is proposed in (JGJ161-2008, 2008) using Equation 2-37 as follows:

$$F_{Ekb} = \alpha_{max\,b} G_{eq} \quad \text{2-37}$$

In which F_{Ekb} refers to the standard value of horizontal structural earthquake force, α_{maxb} refers to the maximum value of the horizontal earthquake influence coefficient, G_{eq} refers to the equivalent gravity load of the structure. For the one-storey buildings, the value should be the value of the gravity load, and for the two-storey structures, the value should be 95% of the representative value of gravity load.

The Equation 2-38, 2-39 and 2-40 of The Characteristic Value of Horizontal Earthquake force are as follows:

For the single-storey housing: $$F_{11} = F_{EX} \quad (2\text{-}38)$$

For the two-storey housing: $$F_{21} = \frac{G_1 H_1}{G_1 H_1 + G_2 H_2} F_{EX} \quad (2\text{-}39)$$

$$F_{22} = \frac{G_2 H_2}{G_1 H_1 + G_2 H_2} F_{EX} \quad (2\text{-}40)$$

Where the F_{11} refers to the Characteristic Value of Horizontal Earthquake force (kN), F_{21} refers to the Characteristic Value of Horizontal Earthquake force of Particle 1 for the two stories housing (kN), F_{22} refers to the Characteristic Value of Horizontal Earthquake force of Particle 2 (kN). G_1 and G_2 refer to the representative value of gravity load of Particle 1 and Particle 2 (kN), and the value should take the sum of Characteristic Value of self-weight, 50% of the floor live load and 50% of the roof snow load. H_1 and H_2 refer to the height of Particle 1 and Particle 2. This information is shown in Figure 2.9.

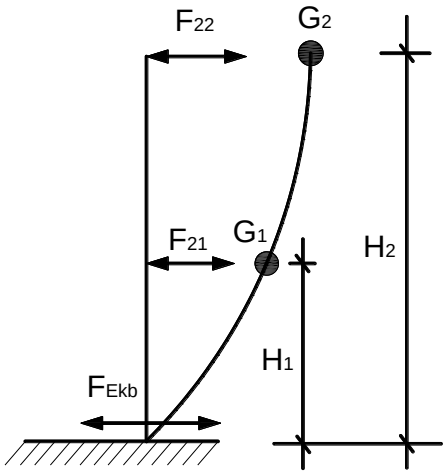

Figure 2.9 Simple calculation sketch of horizontal earthquake force

It can be seen in Equation 2-37 that the seismic action is only taken as the maximum value of the horizontal earthquake influence coefficient, which means you only need to consider the maximum seismic activity. To simplify calculation, masonry structures can directly Equation 2-37 to obtain the seismic design force.

2.5.1.2 Eurocode 8

- **The calculation of base shear force**

Based on (EN1998-1, 2004), for the horizontal components of the design acceleration spectrum, $S_d(T)$, are defined by the following expressions Equation 2-41:

$0 \leq \mathrm{T} \leq T_B$: $S_d(T) = a_g \cdot S \cdot [\frac{2}{3} + \frac{T}{T_B} \cdot (\frac{2{,}5}{q} - \frac{2}{3})]$

$T_B \leq \mathrm{T} \leq T_c$: $S_d(T) = a_g \cdot S \cdot \frac{2{,}5}{q}$

$T_c \leq \mathrm{T} \leq T_D$: $S_d(T) \begin{cases} = a_g \cdot S \cdot \frac{2{,}5}{q} \cdot [\frac{T_c}{T}] \\ \geq \beta \cdot a_g \end{cases}$

$T_D \leq \mathrm{T}$: $S_d(T) \begin{cases} = a_g \cdot S \cdot \frac{2{,}5}{q} \cdot [\frac{T_c T_D}{T^2}] \\ \geq \beta \cdot a_g \end{cases}$ 2-41

Where

a_g is the design ground acceleration on type A ground;

T is the vibration period of a linear single-degree-of-freedom system;

T_B is the lower limit of the period of the constant spectral acceleration branch;

T_C is the upper limit of the period of the constant spectral acceleration branch;

T_D is the value defining the beginning of the constant displacement response range of the spectrum;

S is the soil factor;

$S_d(T)$ is the design spectrum;

q is the behaviour factor;

β is the lower bound factor for the horizontal design spectrum. The recommended value for β is 0,2

The seismic base shear force F_b, for each horizontal direction in which the building is analysed, shall be determined using the following expression Equation 2-42 and Equation 2-43:

$F_b = S_d(T_1) \cdot m \cdot \lambda$ 2-42

$$T_1 = C_t \cdot H^{3/4} \quad \text{2-43}$$

Where

$S_d(T_1)$ is the ordinate of the design spectrum at the period T_1;

T_1 is the fundamental period of vibration of the building for lateral motion in the direction considered;

m is the total mass of the building, above the foundation or the top of a rigid basement;

λ is the correction factor, the value of which is equal to $\lambda = 0{,}85$ if $T_1 \leq 2T_C$ and the building has more than two stories or $\lambda = 1$ otherwise.

C_t is 0,085 for moment resistant space steel frames, 0,075 for moment resistant space concrete frames and eccentrically braced steel frames and 0,050 for all other structures;

H is the height of the building, in m, from the foundation or the top of a rigid basement.

- **Distribution of the horizontal seismic forces**

The fundamental mode shapes in the horizontal directions can be approximately obtained by assuming horizontal displacements increase linearly up the height of the masonry building. Therefore, the horizontal forces F_i can be expressed using Equation 2-44 below:

$$F_i = F_b \cdot \frac{z_i \cdot m_i}{\sum z_j \cdot m_j} \quad \text{2-44}$$

Where

F_i is the horizontal force acting on storey i;

F_b is the seismic base shear following Equation 2-8;

z_i, z_j are the heights of masses m_i, m_j above the level of application of seismic action;

m_i, m_j are the storey masses

It should be noted that, when considering this method, the floors are assumed rigid in their plane.

- **Torsional effects**

If the lateral stiffness and mass are symmetrically distributed in plan but accidental eccentricity occurs, the horizontal force must consider torsional effects and be multiplied by a factor δ given by Equation 2-45.

$$\delta = 1 + 0.6 \cdot \frac{x}{L_e} \quad \text{2-45}$$

where

x is the distance of element under consideration from the centre of mass of the building in plan, measured perpendicularly to the direction of the seismic action;

L_e is the distance between the two outermost lateral load resisting elements, measured perpendicularly to the direction of the seismic action.

2.5.1.3 EERI method

- **The calculation of base shear force**

In (Network, 2011) a simplified method using calculations of wall density was proposed to analyse the seismic behaviour of buildings. The assumptions are that the storey shear strength is the sum of the shear capacities of all walls in the direction under consideration. Floor-roof systems act as rigid diaphragms. Wall stiffness is mainly governed by shear deformations, and all confined masonry walls can reach their shear strength before the failure of any storey in the building takes place.

It is assumed that the building will remain safe when exposed to the design earthquake under consideration, provided that the shear strength of each storey ($F_R V_R$) exceeds the factored seismic shear force ($F_C V_u$) according to the following criterion Equation 2-46:

$$F_R V_R \geq F_C V_u \quad \text{2-46}$$

In which V_R is the seismic shear strength for each storey; V_u refers to the seismic force; F_R is 0.7 strength reduction factor; F_C refers to 1.1 load factor. This check needs to be performed for each orthogonal direction of the building plan.

Seismic force (V_u), also known as the seismic base shear force, depends on the building properties and site conditions. It can be computed by multiplying the total building weight (W_T) by the corresponding seismic coefficient (c) as described by Equation 2-47:

$$V_U = cW_T \quad \text{2-47}$$

Building weight (W_T) should be calculated using Equation 2-48:

$$W_T = A_p nw \quad \text{2-48}$$

Where A_p is area of floor plan for one storey; w refers to the weight for unit area of floor-roof system, which includes the wall self-weight; typical values range from 6 kPa (600 kg/m2) to 8 kPa (800 kg/m2) for light and heavy floor or roof system respectively; n is the numbers of stories.

The seismic coefficient, c, should be computed from the following Equation 2-49:

$$c = (IK_T S/R)a_o \quad \text{2-49}$$

In which a_o is the peak ground acceleration (PGA) specified by the local code or based on the seismic hazard map; K_T refers to the dynamic amplification factor which transforms a_o into the spectral acceleration for a system with 5% modal damping. K_T depends on the fundamental period of the building. The buildings under consideration are characterized by low primary periods in the range from 0.1 to 0.4 s. Most seismic codes prescribe a constant spectral acceleration for low-period structures, thus a constant value of 2.5 can be conservatively assigned to K_T (this corresponds to a spectral acceleration of 2.5 a_o); I is the building important factor, 1.0 for normal-importance buildings (housing – residential buildings), 1.3 for high-importance buildings, including schools and places of assembly that could be used as refuge in the event of an earthquake and 1.5 for post-disaster facilities (hospitals, emergency control centres, etc.); S is soil amplification factor, which depends on the building site location, 1.0 for rock or firm soil conditions, 1.2 for compact granular soil conditions and 1.4 for soft clay conditions; R is a response reduction factor that takes into account ductility and overstrength, 3 for hollow masonry units and 4 for solid masonry units.

- **Distribution of the horizontal seismic forces (wall density index method)**

For the first storey, the average compressive stress σ can be obtained as the ratio of the total building weight, W_T, and the sum of the cross-sectional areas of all walls at the first storey level in both directions, $\sum A_W$, the Equation 2-50 is below:

$$\sigma = \frac{W_T}{\sum A_w} = \frac{nwA_p}{\sum A_w} = \frac{nw}{\sum A_w/A_p} = \frac{nw}{\sum d} \quad \text{2-50}$$

In which W_T is substituted from Equation 2-3, and $\sum d$ is the sum of wall densities in both orthogonal directions of the building plan, that is, longitudinal (x) and transverse (y), the Equation 2-51 is as follows:

$$\sum d = d_x + d_y \quad 2\text{-}51$$

The calculation of wall density index is an iterative process because the d value is required to find the σ value, and subsequently, the masonry shear strength (v) value. Moreover, the number of walls and the corresponding d value influence the floor weight w.

According to the equations presented earlier in this section, the ratio of the shear strength at the storey level (V_R) and the seismic force (V_u) is given by Equation 2-52:

$$\frac{V_R}{V_u} = \frac{v\,A_w}{c\,n\,w\,A_p} = \frac{v}{c\,n\,w}d \quad 2\text{-}52$$

In which the wall density index (d) is a ratio of the total wall area (A_w) in one orthogonal direction and the building plan area (A_p) as in Equation 2-53 below:

$$d = A_w/A_p \quad 2\text{-}53$$

Based on the fundamental design requirement stated at the beginning of Equation 2-12, Equation 2-54 is follows:

$$\frac{V_R}{V_U} \geq F_s \quad 2\text{-}54$$

Then Equation 2-55 is below:

$$\frac{v}{c\,n\,w}d \geq F_s \quad 2\text{-}55$$

Based on the Simplified Method, the building can be considered to be safe for the specified seismic loads provided that the wall density index, d, is greater than or equal to the following value, given in Equation 2-56 below:

$$d \geq \frac{F_s\,c\,w\,n}{v} \quad 2\text{-}56$$

2.5.2 Nonlinear static procedure (push-over analysis)

Nonlinear static analysis (pushover analysis) is a necessary procedure for evaluating the seismic performance of buildings. Based on (ATC, 2000, ATC, 2005, EN1998-1, 2004), there are usually four

analysis methods for seismic assessment, a Linear Static Procedure (LSP), a Linear Dynamic Procedure (LDP), a Nonlinear Static Procedure (NSP) and a Nonlinear Dynamic Procedure (NDP). Pushover analysis is a nonlinear static analysis that assumes that only first few modes of vibration control the seismic response, which means that dynamic problems can be transformed in equivalent static problems. Non-linear static procedures (NSP) have been verified as a useful tool to predict the seismic performance of structures under different earthquake inputs. According to (Parisi, 2010), the main advantages of this method are, the inclusion of the selection and scaling of seismic input, the definition of evolutionary hysteretic models and the interpretation of analysis results. The seismic performance assessment method requires the evaluation of capacity and demand.

2.5.2.1 Generally remarks

The procedure for a pushover analysis generally includes applying a pattern (adaptive or not) of monotonically-increasing lateral loads (force or displacement) while subjected to gravity loads and then evaluating the seismic performance by pushing the structure to failure. The structural analysis stops in one of following three cases: a pre-defined limit state is reached, global collapse occurs or there is a loss of numerical stability. A pushover curve is then proposed to reflect the structural response. The horizontal displacement of monitor points (generally assumed as the centre of mass at the roof level) can be taken as the x-coordinate and the base shear of structure regarded as Y-coordinate of pushover curve. Using an equivalent single degree of freedom system (ESDOF), buildings with multiple degrees of freedom (MDOF) can be modelled by analysing the relationship between base shear and top displacement, which is called capacity curve (as described in Figure 2.10). It can be seen from the pushover curve that some information on the nonlinear behaviour of structure, once it exceeds its elastic limits, is revealed.

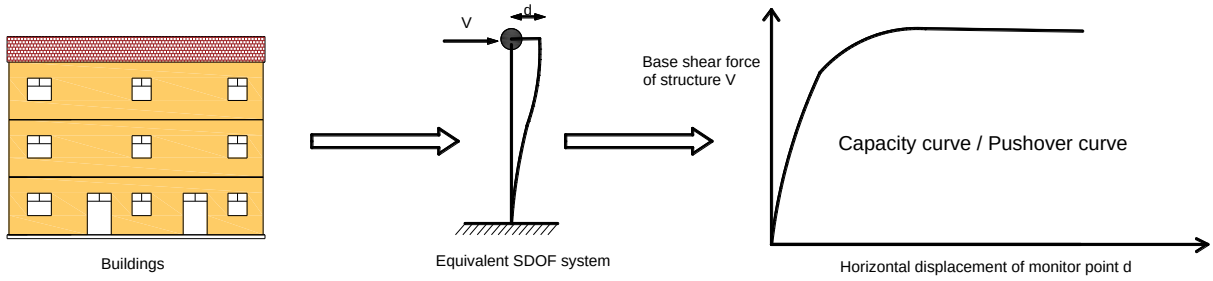

Figure 2.10 Non-linear static (pushover) procedure

A number of different loading patterns can be applied to the structure. According to (Themelis, 2008), seven load patterns were introduced, and the most common types for static pushover analysis are the

mode shape distribution, the inverted triangular distribution and the uniform load distribution. The modal force pattern can capture the elastic response of structure while the uniform force pattern can capture the inelastic response after significant damage. The uniform pattern has been verified as giving better seismic performance compared to both modal and inverse triangular patterns, leading to a higher overturning moment (Mwafy and Elnashai, 2001). In addition to load-based procedures, displacement-based procedures can also be applied where the pushover analysis is based on the application of lateral displacements, rather than forces, especially for plastic structural systems.

Control strategies are then either load control and displacement control. For load control, a monotonically increasing load factor is applied, and a corresponding displacement vector is monitored. This strategy allows prediction of the peak base shear force but is not suitable for evaluating the behaviour after failure. When trying to identify the post-failure action, displacement control is more useful. The main procedure involves defining a target displacement at a control point, calculating relevant base shear force and monitoring the displacement of the control point. A displacement control strategy allows identification of the structural response after massive damage and it is easy to find a peak value of base shear. Load control is widely utilised when considering the out-of-plane behaviour of masonry walls while displacement control has been applied to the in-plane behaviour of masonry structures.

In addition to the basic load patterns and control strategies, some of the different pushover analysis methods are also introduced below. There are three main methods; Static Pushover Analysis Methods, Adaptive Pushover Analysis Methods and Energy-Based Pushover Analysis Methods. For static pushover analysis methods, several options are discussed by (Themelis, 2008) which include the Capacity Spectrum Method (CSM), the Improved Capacity Spectrum Method (ICSM), the N2 method, the Displacement Coefficient Method (DCM) and the Modal Pushover Analysis (MPA). The Capacity Spectrum Method was widely used in (ATC, 1996) and has been applied in many different analysis packages. This method idealises the capacity curve as bilinear curve and transfers the capacity curve to the spectrum curve to achieve the performance point through applying the design spectrum curve into the capacity curve. Additionally, once the performance point has been determined, it can be replaced by a target displacement to evaluate the seismic performance like plastic hinge distribution, total lateral displacement and storey drift ratio. However, if there is a difference between demand spectra and the capacity spectra, it is seen that the structure has a low seismic capacity and needs to be redesigned. The details of the Capacity Spectrum Method can be seen in Figure 2.11.

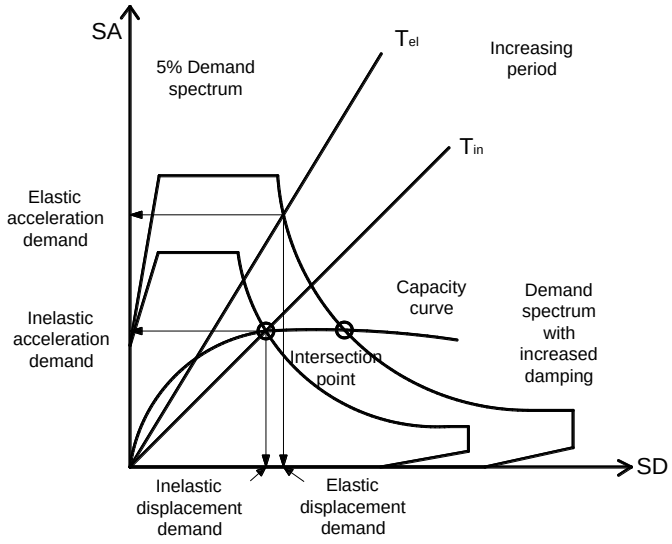

Figure 2.11 Illustration of Capacity spectrum method (Adapted from (Mwafy, 2001))

Other methods of static pushover analysis are also worth mentioning. The Improved Capacity Spectrum Method is based on the Capacity Spectrum Method, replacing the elastic design spectrum with constant-ductility inelastic design spectra which were introduced by (Chopra and Goel, 2000). The N2 method is a choice for CSM, and this method regards the demand spectra as the evaluation standard of the target displacement. A difference between the Displacement Coefficient Method (DCM) and the above methods is that the capacity curve does not need to be converted to a capacity spectrum, and the target displacement can be calculated by relative equations. Compared with the Static Pushover Analysis Methods, the Adaptive Pushover Analysis mainly considers the accuracy of every force vector increment and makes sure the strength or stiffness is actually changing. This method was introduced primarily by (Gupta and Kunnath, 2000). The Base-Energy Pushover Analysis developed by (Albanesi et al., 2002) presents satisfactory results for both forces. The outcomes of both dynamic and quasi-static adaptive analyses are consistent . Based on the results, the proposed energy based push over analysis is a simple and accurate tool to identify seismic behaviour of multi-storey structures with a given seismic input.

2.5.2.2 Application of pushover procedures for masonry buildings

Many researchers have applied pushover procedures for unreinforced masonry buildings (Galasco et al., 2004, Augenti and Parisi, 2009). Magenes (2000) introduced a method for seismic assessment

procedures based on pushover analyses. This method depends on an equivalent frame idealisation of the structure to apply a simplified constitutive law. However, this paper showed that a satisfactory model for monotonic analysis is not sufficient for predicting the seismic response of structures. Unreinforced masonry structures being sensitive to the duration, frequency and energy content of the earthquake input. Tomaževič et al. (2004) discussed the ranges of values of structural behaviour factor q, proposed in EC8 for different masonry construction systems. It was shown that the values of behaviour factor q cannot be assessed only depending on ductility tests of masonry walls. Penelis (2006) focused on a new method for calculating the moment-rotation curves of URM based on a solution for flexure using a parabolic compression stress block assumption and a Mohr-Coulomb failure criterion for shear strength. This method was applied as a useful design and assessment tool to specific URM buildings, and it allowed the prediction of the failure mechanism by identifying the development of plastic hinges at different location of the buildings. Galasco et al. (2006) introduced a new displacement-based adaptive pushover procedure for both masonry walls and buildings. This method has been identified as a useful tool for in-plane behaviour of masonry walls but some corrections were still needed when considering 3D issues. Augenti and Parisi (2009) showed that the current non-linear static procedures were the only practical alternative to traditional methods of linear seismic analysis due to the complexity of non-linear time-history analysis. They presented a new approach based on a displacement-based NSP to predict the seismic response of masonry buildings as well as considering torsional effects. Akhaveissy et al. (2013) introduced a 2D model based on a so-called disturbed state concept (DSC) with modified hierarchical single yield surface (HISS) plasticity. Three large scale masonry walls were tested under pushover analysis, and pushover curves were obtained for comparison with the actual test results. The results showed good agreement with equivalent frame models and involved relatively small computational times especially compared to full smeared 3D models.

In summary, pushover procedures have been widely applied to the analysis of masonry buildings. Many studies have compared different models of masonry structures and validated them against pushover analysis. Therefore, pushover analysis procedures can been taken as one of the most useful tools for identifying the seismic behaviour of masonry structures and this thesis evaluates the seismic performance of masonry structures using this method.

2.5.3 Nonlinear time-history procedure of unreinforced masonry structures

Time-history analysis procedures are dynamic analyses which identifies the structural response through the direct integration of the equations of motion or spectral analysis (Parisi, 2010). The equation of motions can be interpreted in the time domain and applied to any structural type, while spectral analysis considers the frequency domain and is only suitable for a linear system. The fundamental equation for any dynamic analysis is shown in Equation 2-57:

$$M\ddot{x}(t) + C\dot{x}(t) + Kx(t) = F(t) \qquad 2\text{-}57$$

Where

t is the time variable; M is the mass matrix; C is the damping matrix; $\ddot{x}$ is the relative acceleration vector, $\dot{x}$ is the velocity vector, and x is the displacement vector; F is the load factor.

For the dynamic analysis of unreinforced masonry structures, many researchers have focused on the out-of-plane failure of URM walls under seismic excitation by comparing shaking table tests and the related numerical models (Doherty, 2000, Griffith et al., 2003, Lam et al., 2003, Simsir et al., 2004, Dazio, 2008, Hamed, 2008, Vaculik, 2012, Russo, 2013, Costa et al., 2013). Zhuge et al. (1998) investigated the in-plane behaviour of an unreinforced masonry under dynamic loads. A failure envelope had been proposed to predict failure modes including both sliding and cracking and a simplified secant-type unloading curve was developed. (Doherty, 2000) and (Doherty et al., 2002) proposed a simplified procedure based on a linearised displacement-based (DB) method to identify the seismic performance of URM structures. A trilinear relationship was applied to describe the real nonlinear force-displacement relationship for URM walls, and the results were compared with the quasi-static analysis and the time-history outcomes. This procedure was proved to be a better method for evaluating seismic capacity for the design or assessment of existing URM structures but some refinements were still needed. Bothara et al. (2010) describe experimental tests used to identify the seismic performance of two-storey URM buildings. The structures experienced different levels of damage depending on the seismic loading, ranging from rocking piers and partial out-of-plane failure of walls. A numerical model was built to compare with the experimental results, and a seismic fragility curves for URM buildings were proposed. Lourenco et al. (2011) reviewed the seismic analysis of masonry structures without box behaviour. Various analysis methods were discussed and in particular a pushover analysis and a nonlinear dynamic analysis were compared. The box behaviour, in this research, referred to stiff floors that can provide diaphragm behaviour for the whole building, but it should be noted that, in general, historic masonry structures do not show this behaviour.

Overall, due to the complex nature of dynamic analysis for unreinforced masonry structures and time-consuming process of creating accurate models, insufficient research about this area is available. In

addition, few papers consider the global behaviour of real URM buildings under seismic excitation and more study is needed in this area.

2.6 Seismic assessment procedures for unreinforced masonry structures

Seismic assessment procedures of unreinforced masonry buildings are essential to identify the seismic performance of URM structures before an earthquake occurs and are helpful for the development of proper retrofitting methods that can reduce damage. There many traditional assessment procedures around the world, like FEMA 306 (ATC, 1999), (NZSEE, 2006) and (ASCE, 2007). In addition, some researchers have developed analysis methods or analytical models to identify the seismic performance of URM walls and compare the results with tests (Bruneau, 1994a, Bruneau, 1994b, Magenes, 2000, D'ayala and Speranza, 2002, Restrepo-Velez and Magenes, 2004, Wijanto, 2007, Derakhshan, 2011). Most assessment methods for structures usually assess a structure's conformance to a design code but there are many older or self-built structures which do not satisfy the current codes, and these buildings are more likely to suffer severe damage in a seismic event.

According to (Jain et al., 2010), most seismic assessment methods focus on three different levels of performance, level one is rapid visual screening, level two is a preliminary assessment and level three is detailed evaluation. Of the three methods, rapid visual screening (RVS) is a simple and quick procedure to evaluate buildings and may only require 15-30 minutes to walk down surveys. There is no need to calculate the specific seismic response data and a rapid visual screening method can be used when the number of buildings to be assessed is large. (FEMA-154, 1988) first published the RVS method, which was then revised in 2002 as (FEMA-154, 2002). The current edition is the third edition which came out in 2015 as (FEMA-154, 2015). The FEMA P-154 report is a comprehensive score evaluation system based on different parameters such as seismic ground motion parameter zonation, structural type, stories of housing, plan and vertical irregularities, soil type etc.. It mainly considers the lateral force-resisting system of the building and a finally a score is assigned that describes the vulnerability of the building. Other countries which have done some research combined with FEMA methods. Sinha and Goyal (2004) applied the FEMA-154 method in India as a general evaluation method and produced a series of comprehensive assessment forms. Jain et al. (2010) proposed a rapid visual screening procedure based on limited data from damages in one Indian city, particularly looking at RC buildings. Sucuoğlu et al. (2007) combined a screening procedure theory with 454 damaged buildings surveyed after the 1999 Düzce earthquake in Turkey, and then suggested a risk assessment for three- to six-storey substandard concrete structures through a side-walk survey. Achs and Adam

(2012) adopted a rapid visual screening (RVS) method to appraise historic brick-masonry buildings located in Vienna city in Austria.

China has not done much development of RVS methods, and according to the current seismic assessment guidelines of China (GB50023, 2009), the evaluation method contains only two levels. Level One focuses on the assessment of macro-control and structural measures, Level Two concentrates on anti-seismic checking and needs to be calculated. However, compared with FEMA-154, Level One is the only necessary requirement for buildings with 30-year seismic design life. For buildings with a 40-year or more seismic design life, Level Two is necessary. Also, there are no clear quantitative criteria for Level One so it cannot really be called a true RVS method, nor is it a rapid evaluation method. Additionally, the current seismic assessment guidelines are hard to apply widely in rural areas because there are no simple and clear criteria to identify the seismic capacity of structures and lots of calculations are still needed. Thus, it is necessary and important to develop a seismic assessment method that combines RVS and is appropriate for assessing rural housing in China.

Overall, by analysing the damage statics for typical Chinese buildings (masonry structures and RC structures), it can be seen that both types of structure have suffered significant damage in earthquakes and the reasons of failure are clear. It also needs to be noted that masonry infill walls in RC buildings and masonry walls in masonry buildings have a significant influence on the seismic performance of both types of buildings and combined with the current seismic assessment methods, a clear index factor reflecting the seismic capacity of masonry walls should be developed. Thus, a quick and straightforward seismic evaluation guideline should be proposed, especially for URM structures, using the concept of a rapid visual screen to calculate the capacities of existing URM structures with openings

2.7 Summary

This chapter presents the literature review for the whole thesis, including opening effects of URM structures, modelling methods for masonry structures, seismic analysis procedures, seismic performance and seismic assessment methods for unreinforced masonry structures. This chapter summarises the state-of-art in modelling methods for URM structures and compares the advantages and disadvantages of the different methods. This work strongly suggests that the discrete element method a good way to model URM walls and that opening effects under in-plane and out-of-plane loading should be studied. Concerning the seismic analysis and performance of URM structures, the

linear method is considered for calculating the ultimate strength of the walls but it does not deal with complex nonlinear issues, which means that analysis using pushover and time-history procedures will be important. In-plane and out-of-plane behaviour of URM walls are the essential seismic characteristics that need to be identified and relevant failure modes and research progress are presented. It is noted that there is little previous research or mention in current codes of the effects of opening on URM structures. The relationships between opening factors and seismic capacity are therefore worth developing. Seismic assessment procedures have been developed by lots of researcher and are embedded in some codes. However, a simple rapid method is still missing, especially for URM housing stock in rural areas in developing countries. In summary, the content of this chapter offers theoretical support for the analysis of URM walls in the following chapters.

Chapter 3 METHODOLOGY OF UNREINFORCED MASONRY MODELLING IN 3DEC

3.1 Introduction

3DEC is software based on the UDEC code (Universal Distinct Element Code) that has been applied in many different analysis areas. Unlike Finite Element methods, DEM in 3DEC allows significant displacements to develop between the blocks, and new contacts are automatically recognized as part of the analysis. This analysis method can capture the appearance of cracks, crack propagation and the failure patterns of the masonry walls. However, this numerical software is still a relatively new analytical tool and more detailed information and validation are necessary to show that this analysis method is valid for modelling masonry structures. Therefore, this chapter outlines the basic methodology for this analysis method including fundamental assumptions, the solution algorithm, the building of models, failure criterion, static analysis procedures and dynamic procedures. Finally, a sensitive study of 3DEC and calibration against experimental data are considered to verify the reliability of this method and support the analytical processes in the following chapters.

3.2 Fundamental assumptions in 3DEC

3.2.1 Block assumptions in 3DEC

The representation of blocks in 3DEC assumes that the blocks are rigid bodies that only interact at their boundaries. In 3DEC, blocks are characterized as polygons which need to be convex. For non-convex blocks, convex sub-blocks are formed and 'glued' together so they move together without relative displacement. However, non-convex blocks in masonry applications are generally of limited interest. Larger blocks can also be split by a series of cuts, with each cutting plane splitting the whole block in two. This joining method still allows composite blocks to behave as a single block. As an alternative to rigid blocks, 3DEC can create deformable block models where the bocks are meshed and this is useful when considering blocks made from weaker materials where stress concentration is important. In this case the model converts every block into a mesh like an FE model, and can be taken as a simplified micro-model with zero thickness joint elements. For deformable blocks, the Mohr-Coulomb elastoplastic model is widely used to reflect the tensile and shear failure in the block material. If there are not too many blocks then, when choosing deformable blocks in 3DEC the run time is similar to that for rigid blocks with a static analysis due to the efficiency of the code. However, for a dynamic analysis, rigid blocks are more often used (rather than deformable blocks) because they need significantly less analysis time.

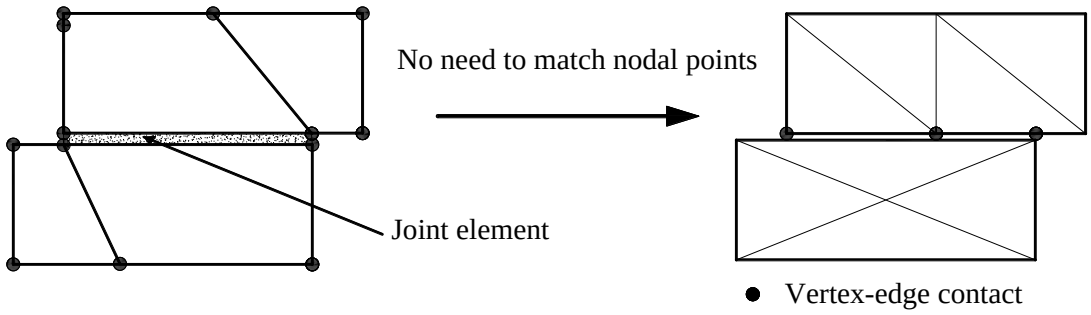

(a) Representation of contact by joint element (b) Representation of contact by point (vertex-edge)

Figure 3.1 Representation of contact between blocks [Adapted From (Lemos, 2007)]

3.2.2 Contact assumptions in 3DEC

The contact assumption is a distinctive feature in DE codes and reflects the relationships between the model components. According to (Lemos, 2007), a point contact assumption is applied in UDEC and 3DEC, which means that the internal forces between two blocks are obtained and used at a set of discrete points. These forces are a function of relative displacement between the two blocks at that point. Every contact point is assigned an area, and the total contact surface can be obtained by adding up these point areas. Thus, the joint force or stress can be identified at a point contact, and then a joint model can be applied. The advantage of this contact assumption is that it can handle arbitrary types of interactions and is very convenient for dealing with large displacement problems where the contact types change and point locations are updated as the blocks move, the new contacts are automatically detected. In 3DEC, the contact area is defined using the concept of a common-plane. Two types of point contacts including vertex-to-face and edge-to-edge are possible. The total contact area can be presented by the sum of the areas of point contacts.

Furthermore, 3DEC contacts also are divided into hard contacts or deformable contacts. The hard contact assumption is mainly useful for rigid blocks analysis and no overlaps can be tolerated. For the deformable contact type, 3DEC considers both normal and shear contact stiffnesses where the contact forces are defined by the overlap between blocks. What is key, in the case of mortared joints, is that the normal stiffness can be reflected by the mortar properties. For shear behaviour, the joints can be modelled using Coulomb friction. For a quasi-static analysis, the shear force can be obtained by the shear stiffness when arriving at the maximum friction. Thus, the normal contact force and shear force can be calculated by the normal and shear stiffness, the relative contact displacements and the contact area. In some cases, finite tensile and shear-bond strength are used to reproduce the correct fracture energy under post-peaking softening and prevent the numerical perturbation caused by sudden bond failure. Coulomb friction models are used widely for dry masonry joints and a full Mohr-Coulomb model including tensile and shear strength is applied in masonry joints.

3.3 Solution algorithm in 3DEC

A time-stepping explicit algorithm is used in 3DEC to solve the equations of motion of the block system. Compared with the stiffness matrix approach in finite element codes, an explicit algorithm is capable of handling a system of blocks undergoing a collapse mechanism containing large displacements and

can cope with the challenges of unconnected blocks or rapidly changing contact conditions. Although the solution method is a real dynamic technique, it can also be used for static or quasi-static problems. For static problems, the same time-stepping algorithms are applied until static equilibrium is achieved (Lemos, 2007). Damping is also applied in static analyses as it increases the convergence of equilibrium or leads to a steady failure pattern.

In static solutions, inertial masses (but not weights) can also be scaled to speed the convergence. For dynamic problems, the block masses and damping are applied (normally Rayleigh damping is used) and stiffness-proportional components are added to the boundaries. In case of deformable blocks, the nodal mass is used instead of the block mass, but the solution algorithm is very similar and the only extra things that need to be considered are the extranodal forces induced by element stress. The disadvantage of the explicit algorithm is that small-time steps are required to make the results stable. The solver in 3DEC calculates the time step based on a function of masses and stiffness. However, the time step will be reduced dramatically if stiff materials or joints are used or if the variation in size of elements in the model is large. Therefore, it is helpful to optimise the analysis time by trying different values of block Young´s modulus, joint stiffness and zone sizes. Because DE model solution methods are time-consuming it is vital to increase the efficiency of analysis and this is best done by optimising the time step for a particular analysis.

Based on (Cundall, 1987), a solution scheme based on the equations of motion is to be better-suited to indicate potential failure modes of discontinuum systems than schemes which disregard velocities and inertial forces (e.g., successive over-relaxation). At each timestep, the laws of movement and the constitutive equations are applied. For both rigid and deformable blocks, sub-contact force-displacement relations are prescribed. The integration of the law of action provides the new block positions, and therefore the contact displacement increments (or velocities). The sub-contact force-displacement law is then used to obtain the new sub-contact forces, which are to be applied to the blocks in the next timestep. The mechanical calculation cycle can be shown in Figure 3.2. When the block motion update, the relative contact velocities are automatically generated and the sub-contact force is updated, so the block centroid forces are calculated.

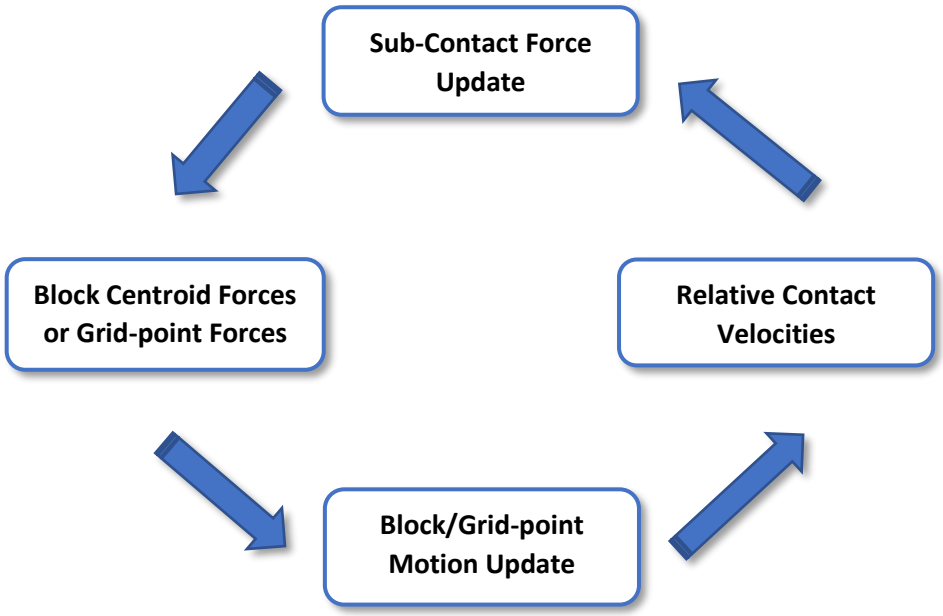

Figure 3.2 Schematic diagram of mechanical calculation cycle in 3DEC [Adapted from (Itasca, 2012)]

3.4 Application issues for masonry structures in 3DEC

3.4.2 Generation of blocks

In 3DEC, blocks can be defined as convex polyhedra. Simple shapes can be created with “poly brick” or “poly prism” commands, and shapes with arbitrary convex polygonal faces can be defined by the “poly face” commands. Additionally, Fish (a programming language within 3DEC) functions can be applied to build the specific block shapes, or block geometry can be created with CAD software and then input, via a text data file, into 3DEC code using the relevant format. Furthermore, non-convex blocks can be built using commands to join convex blocks. For rigid blocks, this method is used for a single composite rigid body, while the contacts with adjacent blocks are detected and applied, following the logic of common plane. For deformable blocks, a joining command can create a rigid connection between the coincident grid-points of sub-contacts to make the sub-blocks move together.

3.4.3 Models of blocks

The possible constitutive models for the blocks include four basic models: null model, elastic - isotropic model, elastic-anisotropic model and Mohr-Coulomb plasticity model (Itasca, 2012). The null model just means that the material of the block built with this model is removed or excavated, and the stress of the model is set to zero. The elastic-isotropic model is the simplest model that reflects material behaviour. This model mainly contains the isotropic and continuous materials representing by linear stress-strain behaviour without hysteresis on unloading and the linear response follows Hooke's law. The input material parameters for elastic models are density, Poisson ration, elastic modulus (E) or bulk modulus (K) and shear modulus (G).

The elastic-anisotropic model is usually used to reflect materials with a sharp difference in elastic properties in different directions. This model is available as an anisotropic model, orthotropic model or transversely isotropic model. The last model is the Mohr-Coulomb model. This model is particularly suitable for plastic problems comprising soil and rock mechanisms. The failure criterion of this model is based on the Mohr-Coulomb tension cut off (Lourenco, 1996) and the shear failure follows the non-associated flow rule (Lotfi and Shing, 1994). The failure criterion, based on tension cut off, is shown in Equation 3-1, concerning the three principal stresses:

$$\sigma_1 \leq \sigma_2 \leq \sigma_3 \tag{3-1}$$

The criterion can be reflected in the plane (σ_1, σ_3) and it is shown in Figure 3.3. The failure envelope $f(\sigma_1, \sigma_3) = 0$ is determined from A to B according to the Mohr-Coulomb failure rules $f^s = 0$ with Equation 3-2:

$$f_s = \sigma_1 - \sigma_3 N_\emptyset + 2c\sqrt{N_\emptyset} \tag{3-2}$$

And from B to C the failure can be illustrated by the form $f^t = 0$ with Equation 3-3:

$$f_t = \sigma_3 - \sigma_t \tag{3-3}$$

In which Ø is the friction angle, c is the cohesion, σ^t is the tensile strength, and $N_\emptyset$ is defined in Equation 3-4 as follows:

$$N_\emptyset = \frac{1+\sin(\emptyset)}{1-\sin(\emptyset)} \tag{3-4}$$

The maximum value of tensile strength can be given by Equation 3-5:

$$\sigma_{max}^{t} = \frac{c}{\tan \emptyset} \quad 3\text{-}5$$

The shear plastic flow based on the non-associated law is defined by Equation 3-6:

$$g_s = \sigma_1 - \sigma_3 N_\omega \quad 3\text{-}6$$

In which ω is the dilation angle, and N_ω is defined in Equation 3-7 below:

$$N_\omega = \frac{1+\sin(\omega)}{1-\sin(\omega)} \quad 3\text{-}7$$

When shear failure occurs, the stress can be limited by the function g^s on the curve $f^s = 0$ and if tensile failure takes places, the stress follows the curve $f^t = 0$.

Notably, all the Mohr-Coulomb models are applied using a tension cut-off criterion, but the tensile failure may differ, and it can be determined by the plastic flow in the specific derived model. Furthermore, there are several other plastic models available such as a Drucker-Prager model, a strain-hardening/softening model, a bilinear strain-hardening/softening ubiquitous-joint model etc. In addition, custom self-built models can be defined using a Fish function (the basic programming language within 3DEC). Whichever types of model are used they must follow the rule that only one type of model can be used within the zones in any block; two or more models cannot be assigned to a single block.

3.4.4 Models of joints

In 3DEC, the joints between the blocks are presented by a zero-thickness interface between the adjacent blocks, as mentioned in Chapter 2. Along with the interfaces, contacts are defined by checking all potential contact points. These contact points are defined at the edges or corners of the blocks and they are connected by two assumed springs such that they can transfer normal and shear forces between the blocks, as illustrated in Figure 3.3.

For the joint, there are two typical models: a continuously yielding joint model and a Coulomb-slip joint model. The continually yielding joint model is regarded as an intrinsic mechanism for analysing some nonlinear behaviours like joint shearing damage, normal stiffness dependence on stress etc., and the main characteristics are defined below:

1. The shear-displacement curve reflects the target shear strength for the joint, for example, the instantaneous gradient of the curve is determined by the difference between the strength and stress.
2. The demand shear strength decreases continuously when the plastic displacement is reached.
3. The dilation angle is used to distinguish the apparent friction angle (depended on the current shear stress and normal stress) and residual friction angle.

Thus, the model can be evaluated for peak or residual behaviour and hysteresis behaviour can be applied for unloading and reloading cycles at all strain levels.

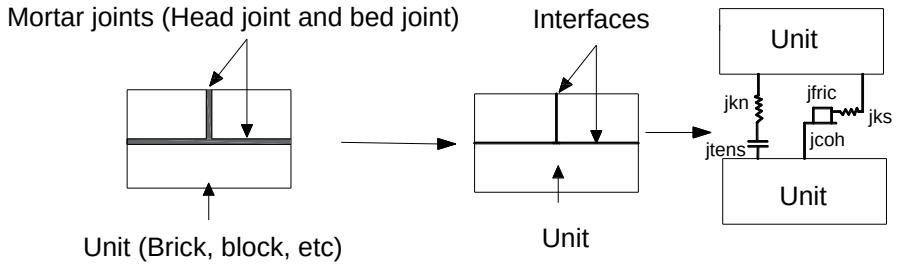

Figure 3.3 Interface model [Adapted from (Çaktı et al., 2016)]

Another joint model, called Coulomb-slip joint model, is the basic constitutive model applied in 3DEC. Both sub-contacts between the rigid block and deformable block follow the Coulomb friction rules, and shear failure, tensile failure and joint dilation are all considered. In the elastic range, the behaviour can be defined by the joint stiffness and shear stiffness, K_n and K_s and the Equation 3-8 and Equation 3-9 describes these relationships (take compressive force as positive):

$$\Delta F^n = -K_n \Delta U^n A_c \quad 3\text{-}8$$

$$\Delta F_i^s = -K_s \, \Delta U_i^s \, A_c \quad 3\text{-}9$$

Where ΔF^n is the normal force vector increment, ΔU^n is the normal displacement vector increment, ΔF_i^s is the shear force vector increment, and ΔU_i^s is the shear displacement vector increment, A_c is the area of the sub-contact.

For an intact joint (without previous slip or separation), the normal tensile force is given by Equation 3-10:

$$T_{max} = -T \, A_c \quad 3\text{-}10$$

Where T is the joint tensile strength.

The maximum shear force can be calculated using Equation 3-11:

$$F_{max}^{s} = c\,A_c + F^n \tan\emptyset \qquad 3\text{-}11$$

In which c is the interface cohesion (stress) and ∅ is friction angle. Once the onset of failure is identified at the sub-contact, in either tension or shear, the tensile strength and cohesion are taken as zero, giving Equation 3-12 and Equation 3-13 as follows:

$$T_{max} = 0 \qquad 3\text{-}12$$

$$F_{max}^{s} = F^n \cdot \tan\emptyset \qquad 3\text{-}13$$

Also, dilation will occur after joint slipping and this is calculated using Equation 3-14:

$$\Delta U^n(dil) = \Delta U^s \tan\psi \qquad 3\text{-}14$$

Where ψ is the dilation angle, ΔU^s is the shear increment magnitude.

Then the normal force needs to be corrected as in Equation 3-15:

$$F^n = F^n + K_n\,A_c\;\Delta U^s \tan\psi \qquad 3\text{-}15$$

It can be seen from the equations that the dilation controls the direction of shearing. If the shear displacement increment is in the same direction of global shear displacement, the dilation will increase; alternatively it will decrease if the directions are opposing.

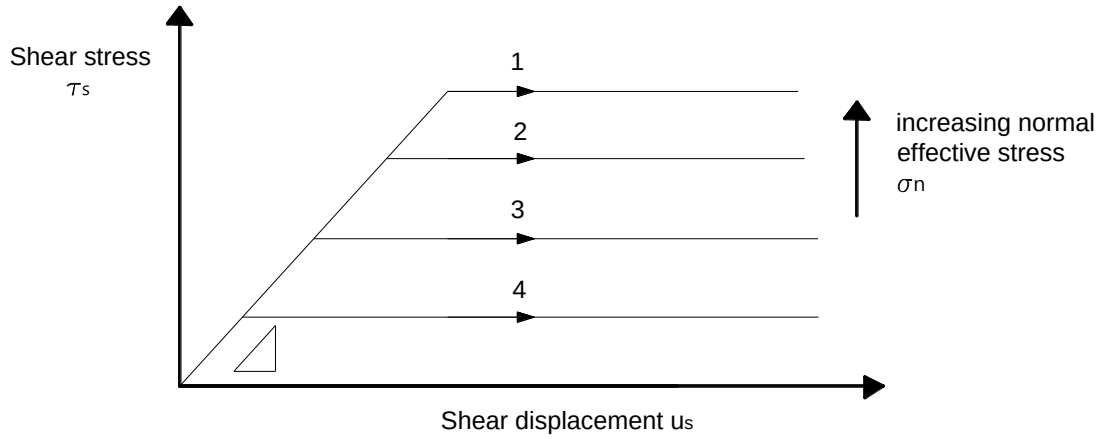

Figure 3.4 Mohr-Coulomb slip model in 3DEC [Adapted from (Itasca, 2012)]

3.4.5 Rigid and deformable blocks

For rigid blocks, the deformation of models is dependent on the joints between the blocks. The contact normal and shear stiffnesses impact the deformability during the elastic range. However, the use of rigid blocks does not allow modelling of local brick crushing or failure, because masonry walls usually fail along the joints depending on (Bruneau, 1994b, Lourenco, 1996, Çaktı et al., 2016) rather than through the blocks, this modelling approach remains valid for global modelling of walls, at least up to the point where significant cracking has concentrated local stresses to the point that bricks would start to experience local failure. For deformable blocks more information is needed to define the joints and unit materials must also be characterized. The internal mesh in deformable blocks is created automatically when the average element size is given. If a detailed stress analysis of the block is not needed, then a coarse mesh may be suitable. For static analysis, the solution of a coarse mesh deformable block model is similar to a rigid block model, and thus deformable blocks with coarse meshes can be used for most problems, especially for more straightforward assignment of joint properties.

However, the use of rigid blocks is crucial in dynamic analysis. In static analysis, the use of mass scaling techniques makes deformable blocks relatively quick to analyse but for a dynamic analysis the blocks need to have their true masses and the small elements in the mesh lead to minimal time steps to keep the stability of explicit algorithm, which leads to substantial computational time. Therefore, rigid block models are more suitable for dynamic analysis, unless the structure being modelled precludes their use.

3.4.6 Determination of failure load for quasi-static problems

For pushover analyses of multi-storey buildings, as described by (EN1998-1, 2004), a non-linear static analysis is carried out under conditions of constant gravity load and monotonically increasing horizontal loads, with the lateral loads being applied at the location of the masses in the building, typically each floor level. For low-rise masonry buildings, in which structural wall behaviour is dominated by shear, Eurocode 8 (EN1998-1, 2004) additionally states that each storey may be analysed independently. Therefore, in the thesis single storey masonry walls are analysed and two different loading methods have been used to simulate in-plane seismic loading on the walls.

In the first case a load-based analysis is performed by applying a gradually increasing horizontal acceleration is applied to the whole URM wall to create the pushover analysis, where every brick

experiences a force proportional to its mass. Initially the vertical gravity load is applied, then a uniform horizontal acceleration is applied to the masonry wall, in increments, until failure takes place. To determine the failure load, the horizontal displacements need to be monitored carefully at each load step. Under this type of load-based analysis, once failure takes place, the horizontal displacements increase dramatically. Therefore, the displacement at each load step is monitored and the ultimate capacity of the wall is based on the flattening of the acceleration/displacement curve. This type of load-based pushover analysis procedure is simple and fast; however, the displacements and failure patterns cannot be found after the maximum load is reached. Therefore, a displacement-based pushover analysis method was also implemented, which allowed tracking of any post-peak softening but required more computation as the displacement needed to be applied at a low velocity to allow a smooth response to be simulated.

In 3DEC, the displacement-based pushover analysis was achieved by applying constant velocity to a loading block at the top of the wall after the vertical gravity load had been applied to the wall. It was important, for the displacement-based analysis procedure, to validate whether the deformation and failure process was smooth or whether any artificial vibration motion occurred, and if so, the loading velocity was reduced so that the loading was effectively quasi-static. In order to obtain the collapse load, the reaction forces being applied at the prescribed velocity boundaries were calculated at every time step (Sarhosis et al., 2014a). While this type of displacement-based analysis allowed tracking of any post-peak softening and captured the failure patterns in the masonry, the loading pattern is less representative of the forces on a URM wall under seismic loading, as the loading is only applied at a single point at the top of the wall. However, if significant loading on the URM wall is coming from a supported floor or roof, then it is more reasonable to ignore the forces generated by the mass of the URM wall itself. This type of displacement-based loading regime is also commonly used in experimental test programmes.

Because both the load-based and the displacement-based analysis procedures offer different advantages both methods have been used in this research to create pushover curves for URM walls with openings and the results have been compared. It is particularly relevant to compare results from a displacement-based single point loading regime, which is widely used in experiments, with a load-based distributed loading procedure which is more representative of actual loading in a seismic event, to identify any differences in in-plane capacities and in failure patterns.

3.4.7 Dynamic analysis and Rayleigh Damping

Based on (Itasca, 2012), the dynamic input in 3DEC can be applied in one of two ways: (a) as a prescribed velocity history; or (b) as a stress history. Option (a) enforces an exact given velocity history. If an acceleration history is available, it must first be integrated numerically to produce a velocity history for 3DEC. The disadvantage of the option (a) is that this boundary will not be an absorbing (or non-reflecting) boundary (i.e., it will reflect back into the model any outgoing stress waves). To avoid this, option(b) can be used: the velocity record is transformed into a stress record and applied to a non-reflecting (viscous) boundary.

For damping, 3DEC uses a dynamic algorithm for problem-solving. Natural dynamic systems contain some degree of damping of the vibrational energy within the system; otherwise, the system would oscillate when subjected to driving forces. Damping is due, in part, to energy loss as a result of slippage along with contacts of blocks within the system, internal friction loss in the intact material, and any resistance caused by air or fluids surrounding the structure. 3DEC is used to solve two general classes of mechanical problems: quasi-static and dynamic. Damping is used in the solution of both classes of questions, but quasi-static problems require more damping. Two types of damping (mass-proportional and stiffness-proportional) are available in 3DEC. Mass-proportional damping applies a force which is proportional to absolute velocity and mass, but in the direction opposite to the velocity. Stiffness proportional damping applies a force, which is equivalent to the incremental stiffness matrix multiplied by relative velocities or strain rates, to contacts or stresses in zones. In 3DEC, either form of damping may be used separately or in combination. The use of both types of damping in combination is termed Rayleigh damping. For dynamic analyses, either mass-proportional or stiffness-proportional or both (i.e., Rayleigh), types of damping may be used.

In performing dynamic analysis with any code, it is usually necessary to account for energy losses in the physical system (e.g., heat, hysteresis) which are not accounted for in the numerical algorithm. In general, damping is used for highly elastic systems, and more damping is used for geomechanical materials, especially soils. In the continuum analysis of structures, proportional Rayleigh damping is typically used to damp the natural oscillation modes of the system. In the dynamic finite-element analysis, a damping matrix, C, is formed with components proportional to the mass (M) and stiffness (K) matrices, as shown in Equation 3-16:

$$\mathrm{C} = \alpha\,\mathrm{M} + \beta\,\mathrm{K} \qquad 3\text{-}16$$

Where α is the mass-proportional damping constant; and β is the stiffness-proportional damping constant.

3.4.8 Mechanical damping and mass (density) scaling

In 3DEC a static analysis uses a dynamic solver (Itasca, 2012) and mechanical damping is used to help improve the stability of the 'static' solver. For static problems, the approach used is similar to that used in dynamic relaxation solvers and the procedure applies a damping force proportional to the velocity of the blocks (velocity-proportional damping). There are two forms of velocity-proportional damping including in 3DEC, namely adaptive global damping and local damping. The global damping approach adjusts the damping constant automatically and applies viscous damping forces to the blocks. The local damping approach applies a damping load to each block node proportional to the magnitude of the unbalanced force on the block. Both damping approaches converge to the same solution, but the local damping approach is preferable when solving problems where there is the possibility of sudden load changes or failure within the model.

Mass scaling is a way of speeding up the convergence of static problems containing very non-uniform block sizes and increases the efficiency of calculation. It is mainly useful when the model is non-uniform and is typically applied to the quasi-static problem. In 3DEC, mass scaling is activated if either local damping or global damping is being used.

3.5 Sensitivity study of a 3DEC masonry model for a quasi-static analysis

As mentioned in section 3.4.6, for static problems, the analysis of masonry walls can be done using a load-based analysis procedure or a displacement-based procedure. While the two methods use different applied loads and monitor different data, there are many similar features in the analyses such as the types of blocks and model scaling however, there are still many possible analysis parameters (such as load or displacement increments) that can be applied. Therefore, to check the sensitivity of the analyses to these parameters and analyse which parameter is stable and consistent while which parameter is sensitive and needs to be careful in the future analyisis, a number of sensitivity analyses were done.

3.5.1 Numerical model in 3DEC

To study the sensitivity of a 3DEC masonry model to various analysis parameters a relatively simple numerical model in 3DEC was built. The length × height × thickness of masonry wall was taken as 3.2m × 1.56m × 0.24m. The top of the wall capped by a concrete beam and the bottom was fixed. Detailed information can be seen in Figure 3.5. The material properties of units and joints are described in Table 3.1 and Table 3.2.

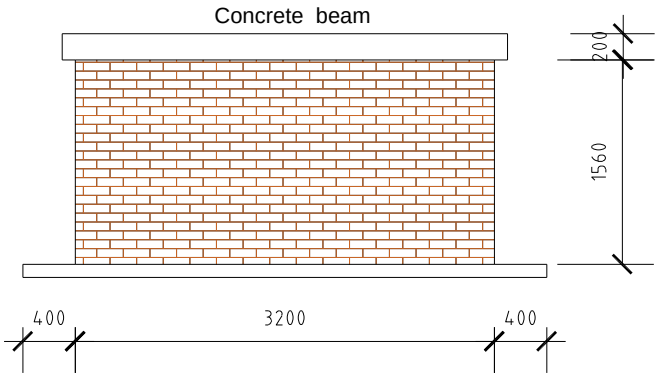

(a) Schematic diagram of numerical model

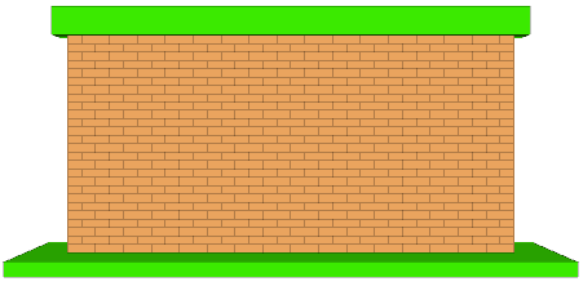

(b) Numerical model in 3DEC

Figure 3.5 Geometry information of numerical model in 3DEC

Table 3.1 Properties of masonry blocks

Density [kg/m^3]	Young modulus [GPa]	Poisson's ratio [-]
1890	5.17	0.15

Table 3.2 Properties of joints

Joint normal stiffness [MPa/m]	Joint shear stiffness [MPa/m]	Joint friction angle [Degrees]	Joint tensile strength [MPa]	Joint cohesion [MPa]
17400	8680	35	0.2	0.1

Using the data above, the in-plane capacities of the URM wall were identified using both load-based and displacement-based pushover procedures looking at the sensitivity of the analyses to different analysis parameters.

3.5.2 Horizontal acceleration increments

Horizontal acceleration increments could affect the accuracy of analyses because the analysis will stop as soon as a loading is applied that results in collapse. For example, if the loading increment is large then the applied load that leads to the collapse of the wall might be significantly higher than the minimum load needed to cause collapse. For this reason, it was necessary to investigate the impact of acceleration increments to find the optimum increment to accurately capture the collapse load without requiring an excessing number of increments (and computing time). For the in-plane masonry wall above, acceleration increment values of 0.01 m/s², 0.03 m/s², 0.06 m/s², 0.09 m/s², 0.15 m/s², 0.3 m/s², 0.6 m/s² and 1.3 m/s² were chosen as possible horizontal acceleration increments. The model built was as described in section 3.5.1. Acceleration-displacement curves for the in-plane wall behaviour were obtained and are shown below (Figure 3.6).

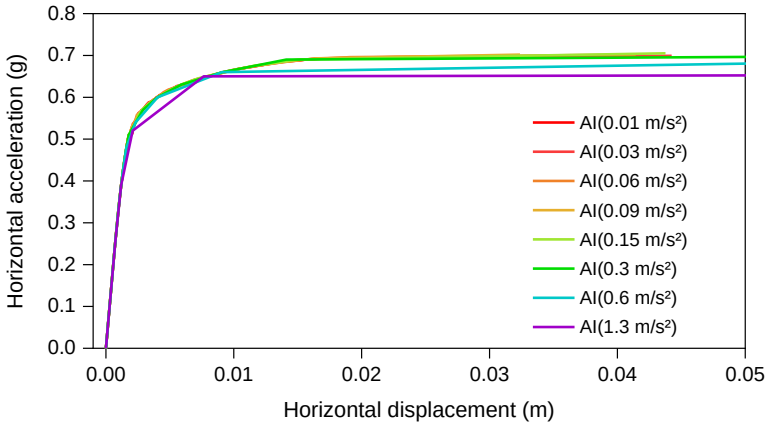

Figure 3.6 Pushover curves for different acceleration increments (0.01m/s²-1.3m/s²)

It can be clearly seen that acceleration increments have a significant effect on the pushover curves when the acceleration increments (AI) exceed 0.3m/s². During the range of AI from 0.01m/s² to 0.15m/s², the pushover curves follow very similar patterns due to the small values of AI applied. However, if the increments surpass 0.3m/s², the pushover curves miss the failure point, which makes the maximum accelerations hard to identify. In addition, the failure mechanisms also changed when a high value of acceleration increment was applied. A distinct difference in failure mechanisms can be seen in Figure 3.7, where top beam slides quickly when a much high instantaneous acceleration is applied. Thus, when running an analysis in 3DEC, the acceleration increment can affect the results of analysis and a suitable acceleration increment needs to be limited.

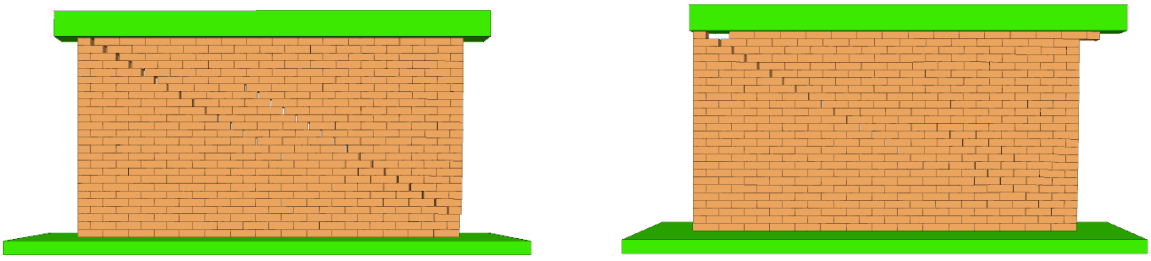

(a) Failure pattern with AI (0.01)

(b) Failure pattern with AI (0.5)

Figure 3.7 Failure pattern with different acceleration increments

3.5.3 Solution cycles

The limit placed on the number of solution cycles is a key part of analyses in 3DEC because sufficient cycles need to be applied to make sure the structures has reached equilibration and the results are stable. If insufficient cycles are applied, the models may not reach equilibrium at each load increment leading to an overestimation of the wall's capacity. To identify the influence of the number of solution cycles (SC), a range of a number of solution cycles were tested with (SC) ranging from 1000, 2000, 5000, 10000, 20000, 50000, 100000 to 200000. The horizontal acceleration-displacement plots from these analyses are given in Figure 3.8.

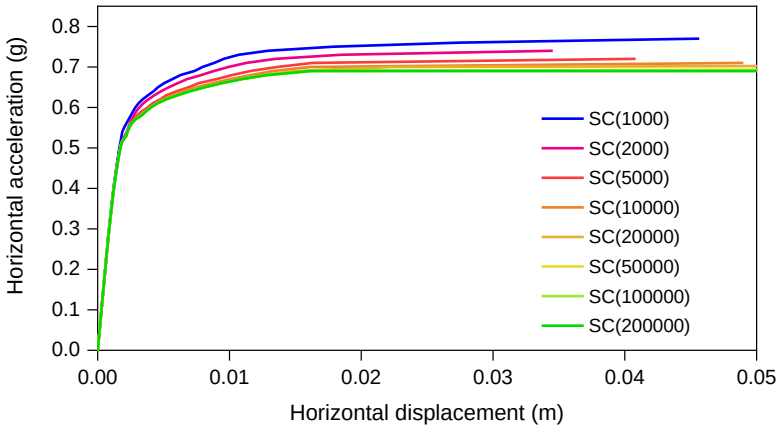

Figure 3.8 Pushover curves for different solution cycles (1000-200000)

This figure shows that different numbers of solution cycles have an impact on the maximum horizontal accelerations of masonry walls recorded. When the number of solution cycles is less than 10000, the maximum horizontal accelerations show some differences, but when the number of solution cycles is greater than 20000, the maximum accelerations recorded are very similar. It is notable that the number of solution cycles does not dramatically affect the curves in the elastic range because the solver rapidly converges to a stable solution. However, when in the plastic phase, it is important to allow enough solution cycles for the solver to stabilise and hence determine the ultimate strength of the walls. Although running too many cycles is very time-consuming, an appropriate minimum number of solution cycles must be allowed to maintain the accuracy and efficiency of the analysis in 3DEC. It should be noted that the failure mechanisms did not change for the different numbers of solution cycles because no internal forces had changed. From this study, for a standard analysis of a masonry wall, the number of solution cycles should not be less than 20000. However, higher solution cycles may be needed when considering specific issues.

3.5.4 Deformable blocks and rigid blocks

In 3DEC, the blocks can be assumed to be deformable or rigid, and the differences in results for these two options was also considered. A rigid block is assumed to allow no deformation and the only relevant parameter for the block is its density. This type of assumption is suitable for low bond strength masonry structures because the failure typically occurs along the joints and the crushing of blocks can be ignored as mentioned in 3.4.5. For deformable blocks, many different failure criteria can be applied, and the material properties will vary depending on the type of material model being employed within the blocks.

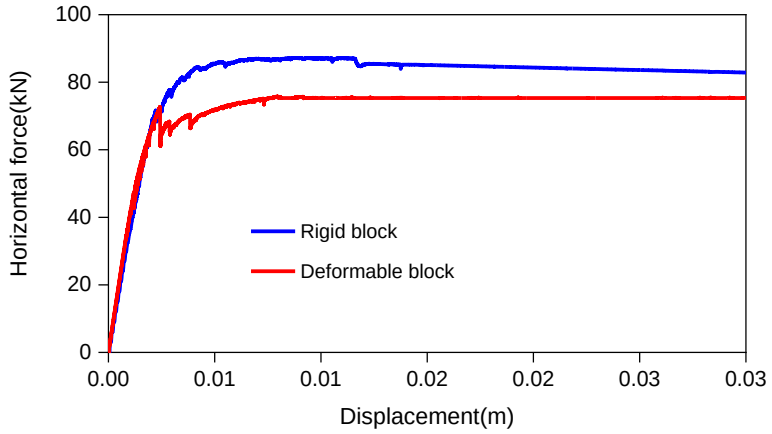

Figure 3.9 Pushover curves for different block assumption

The horizontal force-displacement curves for the two types of blocks can be seen in Figure 3.9. The peak value of horizontal force, based on the rigid block model, is a bit larger than for the deformable blocks. This can be explained by noting that rigid blocks allow no overlap between units. When the joints fail and begin to slip, it is possible for the blocks to form local arching patterns, which could increase the peak value of force to a certain extent. It also can be seen that the curve for the deformable block assumption is not as smooth as that for the rigid block assumption. This lack of smoothness is mainly a result of the deformable blocks needing more calculation time because of the number of elements into which each block was divided. The comparison between rigid and deformable blocks in 3DEC analysis was also identified by (Galvez et al., 2018) and the results are similar. Another challenge when choosing deformable blocks is that the outcome of analysis will change a little between repeated calculations. The main reason for this is that deformable blocks in 3DEC are meshed automatically and randomly. When the simulation starts, a slight variation in the meshing zones can occur, and the results will therefore differ slightly. However, the rigid blocks do

not have this problem as no meshing takes place. Therefore, to improve the efficiency of analysis, rigid block or coarse-mesh deformable blocks assumption should be concerned preferentially and determined based on the specific demand.

3.5.5 Model size scaling effects

Model size scaling issue is typically considered when reducing the size of test specimens to satisfy the requirements of an experiment, and consistency of outcomes for both real structures and scaled structures is important to check. It is helpful to investigate the difference in behaviour between the real models and scaled models through numerical simulation in 3DEC. Five different scaled walls, built with an identical pattern and number of bricks (but with bricks scaled to different lengths) were created i.e. wall sizes of 6m × 3.12m, 4.5m × 2.34m, 3m × 1.56m, 2m × 1.17m and 1.5m × 0.78m. Of these, model 3 having a size of 3m × 1.56m is the actual model. The resulting pushover curves can be seen in Figure 3.10.

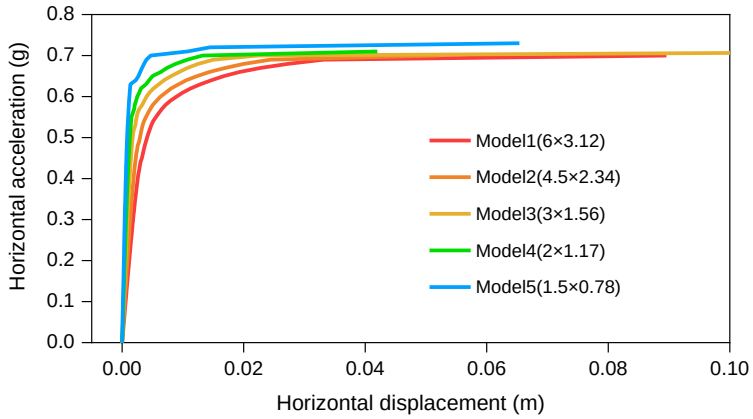

Figure 3.10 Pushover curves for different size models (Model 1-Model 5)

It can be seen in Figure 3.11 that very different outcomes have been obtained for the different sizes of models. As the size of the model increases, the maximum horizontal acceleration and the slope of pushover curves rise as well. This means that the sizes of numerical models may affect the in-plane behaviour of masonry walls. However, when the dimensions of numerical models change, some material properties of models such as normal stiffness and shear stiffness of joints should also vary, which could affect the outcomes of the analysis. According to (Sarhosis and Sheng, 2014) and (Lourenco, 1996), the normal and shear stiffness of mortar joint can be estimated using Equation 3-17, Equation 3-18 and Equation 3-19 as below:

$$JK_n = \frac{E_b E_m}{h_m(E_b - E_m)} \quad 3\text{-}17$$

$$JK_s = \frac{G_b G_m}{h_m(G_b - G_m)} \quad 3\text{-}18$$

$$G = \frac{E}{2(1+v)} \quad 3\text{-}19$$

Where E_b and E_m are Young's moduli of block and mortar, G_b and G_m are the shear moduli of block and mortar, respectively, h_m is the actual thickness of the mortar joint. Equation 3-17 and 3-18 show that normal stiffness and shear stiffness of a joint is related to the thickness of joint, so once the size of a models changes, the normal stiffness and shear stiffness of joints should be modified to fit the actual models. To solve this problem, an adjustment for the stiffness of joints was implemented depending on the thickness of the joints and the resulting pushover curves obtained are shown in Figure 3.11.

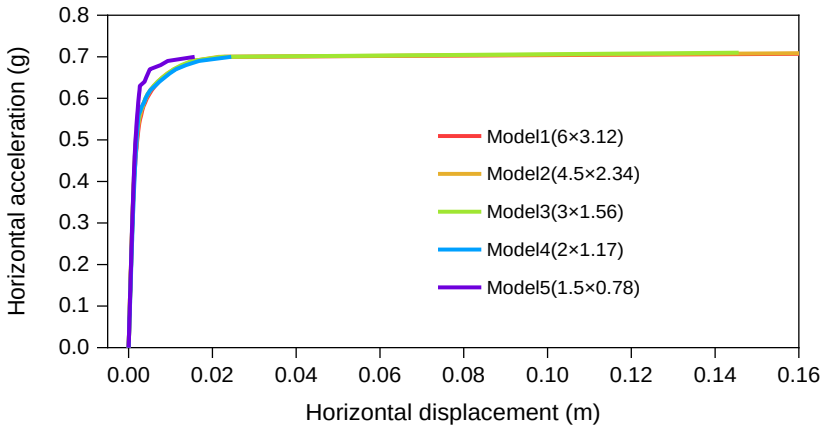

Figure 3.11 Pushover curves for different size models with adjustment of joint stiffness (Model 1-Model 5)

This figure shows that the pushover curves for different sizes of models will follow a similar trend only when the stiffness of mortar joints is changed to compensate for the scaling effects. This means that when considering model scaling issues for in-plane behaviour, the numerical models in 3DEC should use the correct joint stiffness if the model size is changed.

3.5.6 Input velocity values

The value of any input velocities is important in 3DEC because some aspects of static analyses and several aspects of dynamic analyses are related to the velocity inputs. For displacement-based pushover tests, the velocities are applied to an input block with quite low values to keep the structure

stable. The impact of different velocity input values is, therefore, important to evaluate. The model tested was as shown in section 3.5.1 and was built with the same material properties. The load-displacement curves resulting from the application of different loading velocities can be seen in Figure 3.12, and it is clear that different velocity values affect the ultimate in-plane capacity of the masonry walls to a certain extent. For the lower velocities (from 0.003m/s to 0.03 m/s) the ultimate load remains constant. When the velocities are above 0.03 m/s, the ultimate loads are similar but the initial stiffnesses are different.

Overall then velocity does not affect the ultimate load of URM walls significantly, but when the velocity is too high, the structure fails quicker resulting in a lower effective stiffness. Therefore, when considering input velocities for structures in 3DEC, a high velocity input should be avoided.

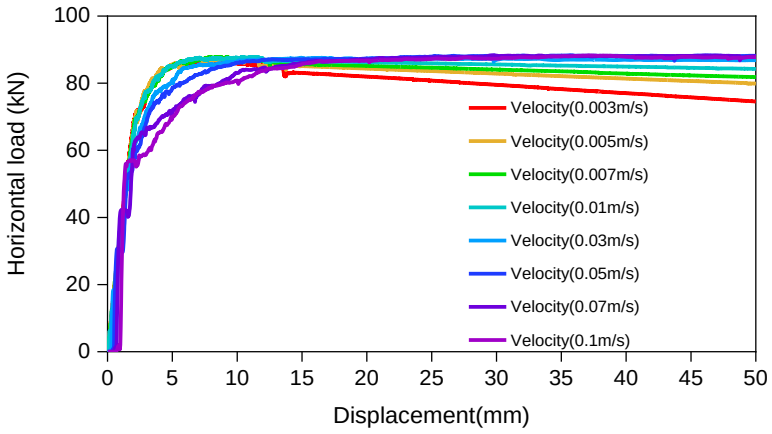

Figure 3.12 Load-displacement curves of different velocities (m/s)

In summary, a sensitive study is vital for any analysis study in 3DEC, as it supports the robustness and stability of analysis procedures being followed. For essentially the same type of analysis, a number of factors have been considered. Of all the factors considered for the model being considered this model was most sensitive to the applied velocity value but the choice of all the analysis parameters needs to be based on a detailed knowledge of the structure being analysed and the underlying analytical procedures.

3.6 Validation of numerical model in 3DEC

3.6.1 Validation of the numerical model under in-plane behaviour

To further check the validity of numerical models in 3DEC, a model of a simple dry-jointed masonry wall was built and was subjected to combined shear and vertical pre-compression loads for comparison with published experimental data by (Lourenço et al., 2005a). Models of four wall sections (wall I, wall II, wall III and wall IV) with different vertical loads applied (30kN, 100kN, 200kN and 250kN) were analysed to observe the different failure crack patterns and maximum horizontal loads. The size of all the masonry walls was 1000mm x 1000mm x 200mm (height x span x breadth) and the blocks were 100mm x 200mm x 200mm (height x span x breadth) in dimension. The density of blocks was 2200 kg/m^3, Young's modulus of blocks was 15500 N/mm^2 and the Poisson's ratio was 0.2. The joint properties were determined using equations from (Lourenço et al., 2005a) and (Bui et al., 2017) and took into account measurements of the variation of the stiffness of the walls with the applied vertical load. A comparison of crack patterns for the numerical and experimental tests is shown in Figure 3.13 and load-displacement plots are shown in Figure 3.14.

Table 3.3 The material properties for numerical models in 3DEC for validation [From (Bui et al., 2017)]

Wall	(MPa/m)	(MPa/m)	(MPa/m)	Friction angle
W I	556	5.87	2.45	32^o
W II	768	8.08	3.37	
W III	1057	11.40	4.73	
W IV	1202	13.00	5.43	

The failure modes and load-deflection curves can be seen in Figure 3.14 and Figure 3.15.

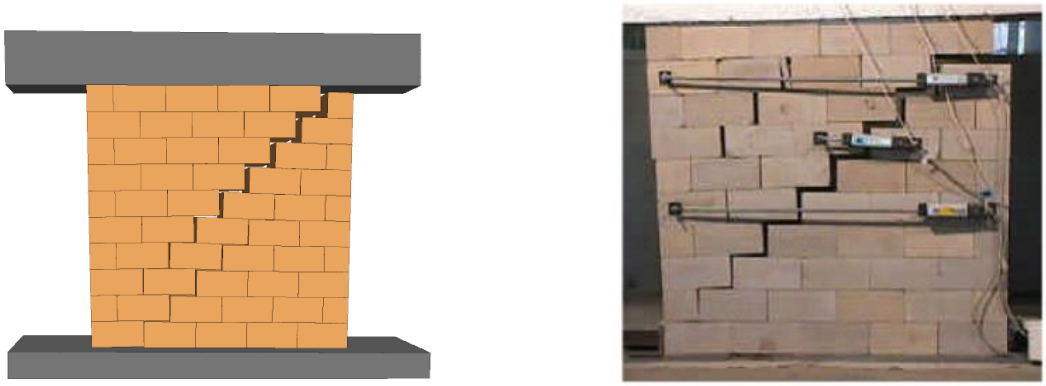

(a) Crack patterns for wall I - 30kN vert. load

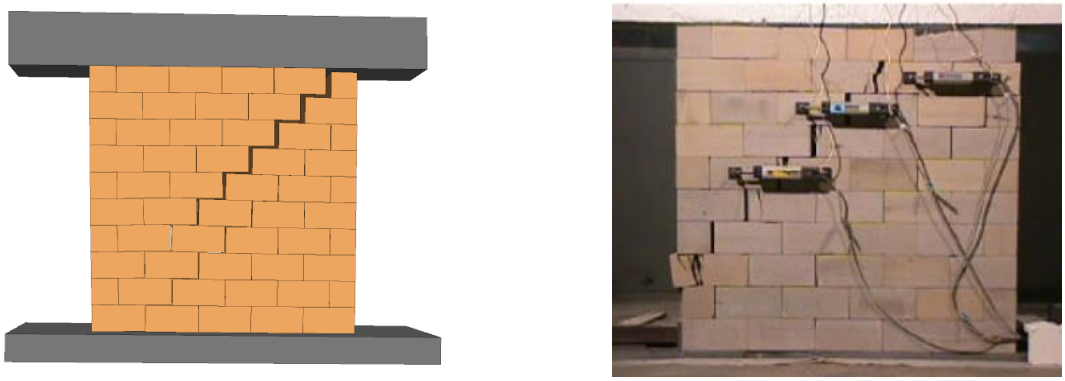

(b) Crack patterns for wall II - 100kN vert. load

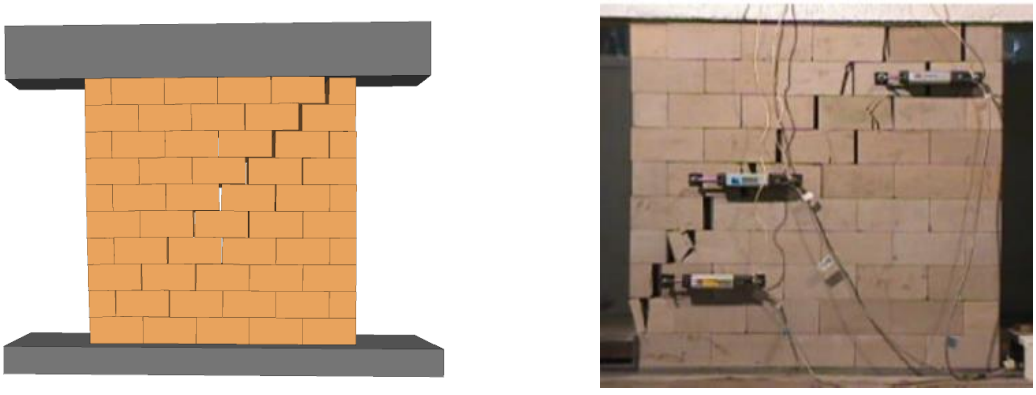

(c) Crack patterns for wall III - 200kN vert. load

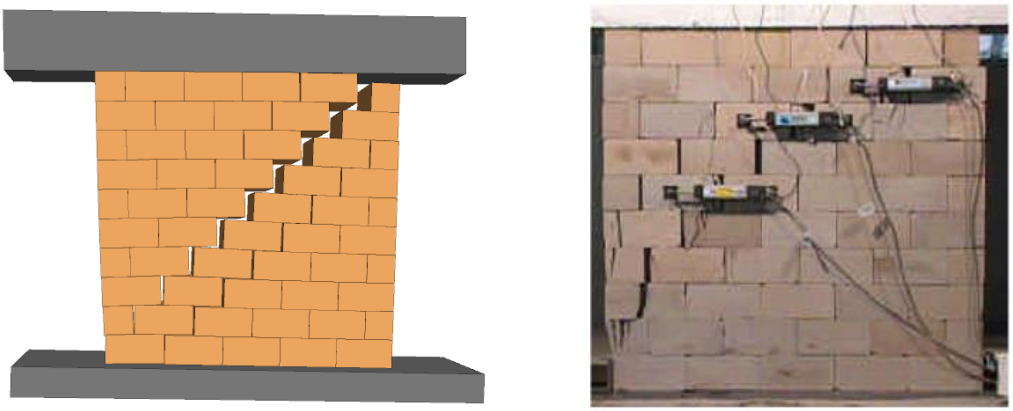

(d) Crack patterns for wall IV - 250kN vert. load

Figure 3.13 Crack pattern comparison: Numerical models and experiment data (With permission from ASCE)

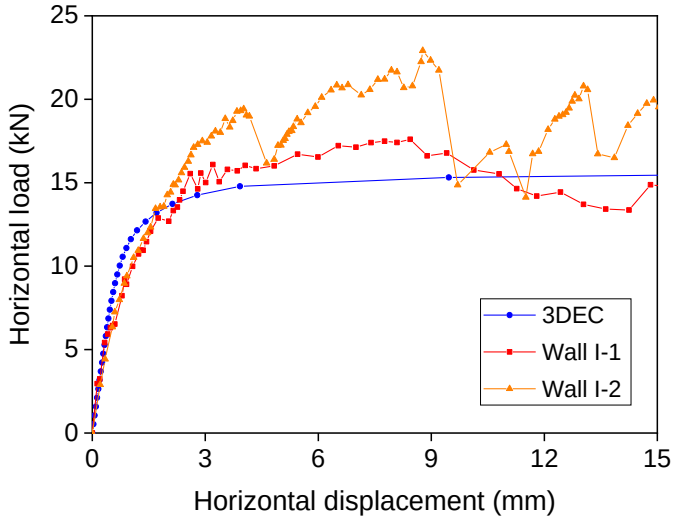

(a) Experiment and 3DEC model for wall I

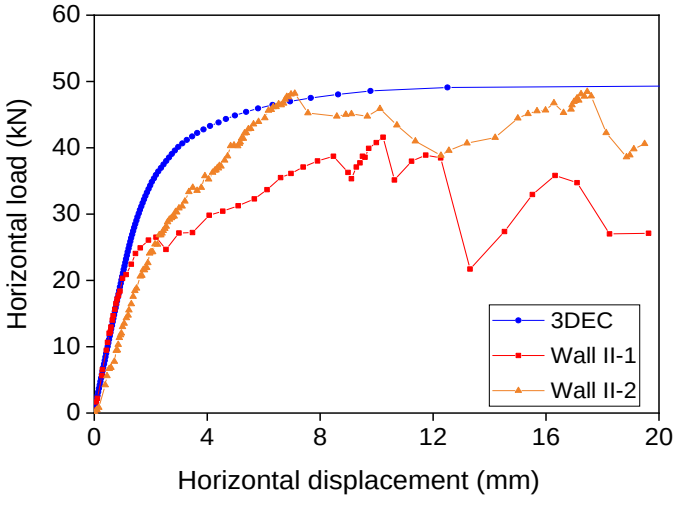

(b) Experiment and 3DEC model for wall II

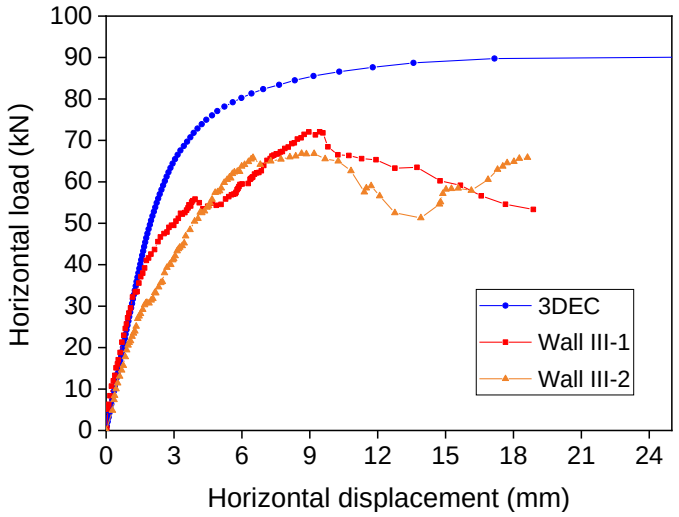

(c) Experiment and 3DEC model for wall III

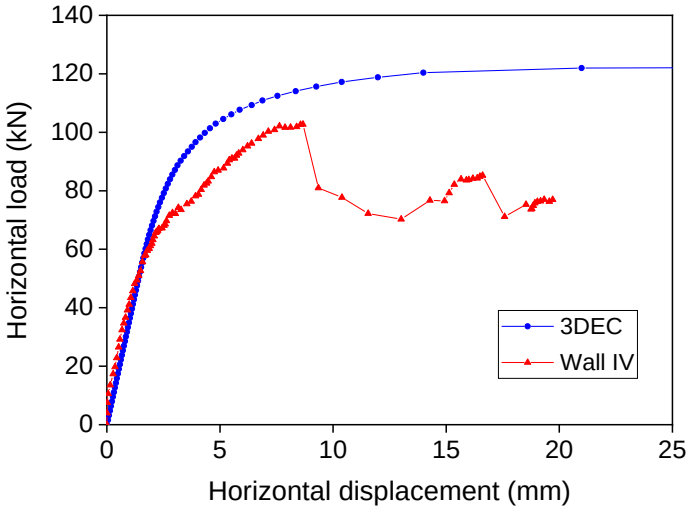

(d) Experiment and 3DEC model for wall IV

Figure 3.14 Load-deflection curve comparison: Experiment and numerical DE model

Comparing the crack patterns for the numerical and experimental data, it can be seen that the 3DEC numerical models show very similar failure crack patterns to the experiments (Bui et al., 2017). The main failure modes in the 3DEC models are the de-bonding of the top concrete beam and a diagonal crack, as happened in the experimental tests. For all the wall cases (I to IV) the mean (-6%, +28%, +37%, +32%) and RMS (14%, 31%, 40%, 42%) differences were calculated relative to the experimental data. For walls I to III the experimental data from the two tests were averaged before calculating the differences, and in all cases the statistics are calculated over the displacement range 0-15mm to allow

comparison between the walls. The 3DEC models generally overestimated the wall forces by ~30%. However, because of the rigid block assumption made in the analyses, the numerical model could not capture the crushing or cracking of the masonry blocks which was seen in some of the experiments. In particular, for the walls with higher vertical loading (Figure 3.14(c) and Figure 3.14(d)), where local block crushing and cracking occurred, the numerical model overestimates the load at the failure by up to 30%. This means that some caution is needed when using simplified models if there is a possibility of local block failure.

Overall, the two validation cases presented above show that 3DEC can successfully simulate the quasi-static response of masonry walls under in-plane loading and can reproduce the failure mechanism of these structures. Even though the properties of bricks were simplified for these comparisons, the results are comparable, showing that 3DEC is an appropriate tool for modelling URM under in-plane loading.

3.6.2 Validation of 3DEC model compared with experiments of masonry structures

To assess the reliability of 3DEC for in-plane static analysis of URM, data from an experimental test of a masonry wall (Augenti et al., 2010, Parisi, 2010) was compared with 3DEC analyses. The geometry of the masonry wall test is shown in Figure 3.15. Table 3.4(a) gives the mechanical properties of the masonry taken from the experimental data: tensile strength f_t; compressive strength f_c; Young´s modulus E; and shear modulus G. The mechanical parameters of the masonry were identified both parallel and orthogonal to the mortar bed joints to allow individual modelling of the spandrel and piers respectively. Based on the properties in Table 3.4(a), and the calculation methods of joint stiffness and strengths given in section 3.4, the properties of joints for the 3DEC model were calculated and are given in Table 3.4(b). The density of bricks was taken as 1600 kg/m³ and two 100kN vertical load blocks were applied at the top of the piers. To simulate this experiment in 3DEC, a constant velocity was applied to a loading block. The horizontal force in, and displacement of this block were recorded, and relevant masonry crack patterns and pushover curves were obtained.

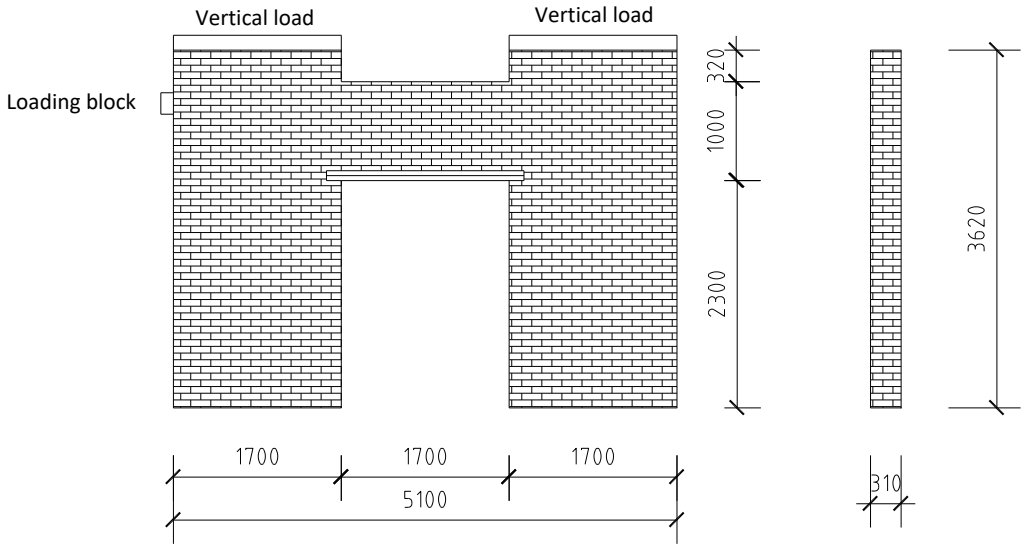

Figure 3.15. The geometry of experimental specimen (dimensions in mm) [Adapted from (Parisi, 2010)]

Table 3.4 (a) Mechanical properties of constituent materials

	f_t [MPa]	f_c [MPa]	E [GPa]	G [GPa]
Pozzolana-like mortar	1.43	2.50	1.52	0.66
Tuff masonry (compression parallel to bed joints)	-	3.85	2.07	0.86
Tuff masonry (compression orthogonal to bed joints)	-	3.96	2.22	0.92

Table 3.4 (b) Material properties used in 3DEC for modelling of the joints

	Joint normal stiffness [MPa/m]	Joint shear stiffness [MPa/m]	Joint friction angle [Degrees]	Joint tensile strength [MPa]	Joint cohesion [MPa]
Vertical joints	6680	2770	35	0.8	1.6
Horizontal joints	20200	8360	35	0.8	1.6

Figure 3.16 shows the failure patterns in the experimental specimen, including (a) a graphical interpretation and (b) a photo of the crack patterns in the masonry wall from (Parisi, 2010) and (Augenti et al., 2010).

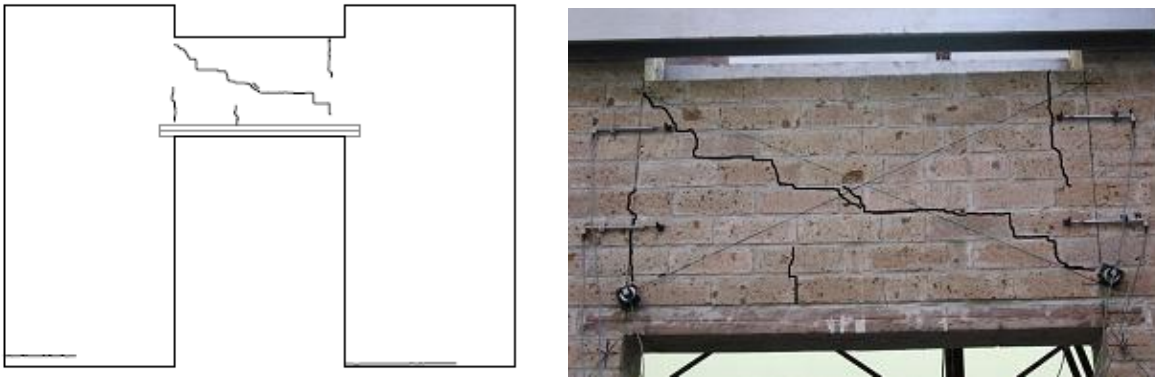

(a) Damage patterns for the masonry wall [From (Parisi, 2010)]; (b) Crack development in the masonry wall (From (Augenti et al., 2010))

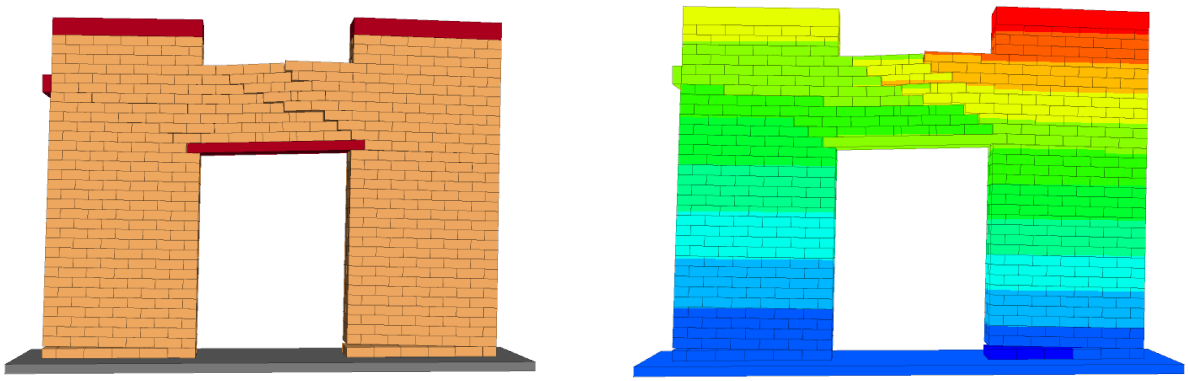

(c) Damage pattern for the masonry wall in 3DEC

Figure 3.16 Comparison of crack patterns for the experiment and the 3DEC model

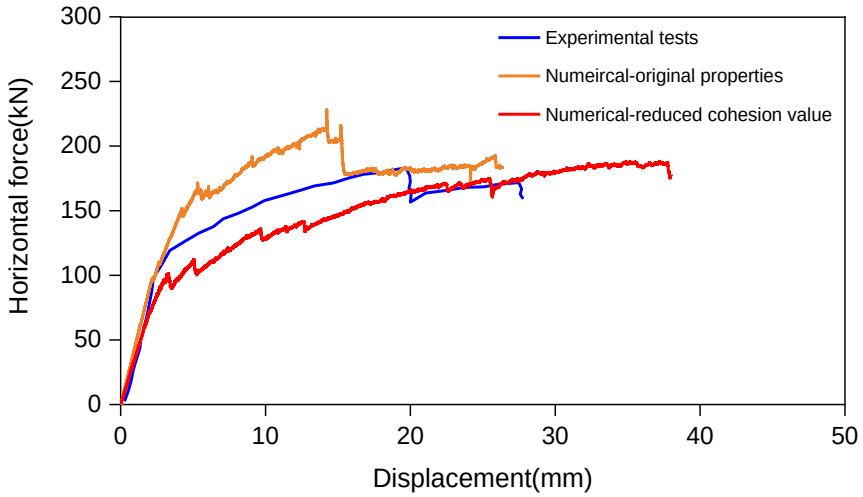

Figure 3.17 Comparison of pushover curves from 3DEC with experimental data

The 3DEC analysis produced very similar crack patterns to the experimental tests, with the numerical model (Figure 3.16(c)) displaying diagonal cracks in the middle part of the horizontal beam component and rocking failure at the bottom of the piers. The 3DEC and experimental pushover curves are also similar (Figure 3.17). While the experimental specimen displayed a lower maximum horizontal capacity compared to 3DEC when using the tensile and cohesion properties of the mortar given in the experimental data (Table 3.4(b)), it is worth noting that the model is sensitive to these properties and a 50% reduction (1.6 MPa to 0.8 MPa) in the cohesion value used for the joints resulted in a much closer match to the peak wall capacity. Results from the 3DEC model with the original properties had a mean difference of +16% (i.e. predicted higher forces) and an RMS difference of 23% compared to the experimental data, while the 3DEC model with modified cohesion values had a mean difference of -9% and an RMS difference of 17% compared to the experimental data (these statistics are calculated over the displacement range of the experimental data). Another reason for the differences in the curves is that the bricks in the 3DEC model were modelled as rigid blocks (ignoring the possibility of crushing or cracking of the masonry) with failure controlled only by the properties of joints. Thus the numerical model could be expected to be stronger than the experiment, where some local cracking of the masonry bricks was evident during the testing (Figure 3.16(b)). While it is possible to create a 3DEC model that incorporates elastic, elastic-plastic, or even cracking blocks, rather than rigid blocks, the simpler rigid block modelling approach remains valid at least until significant cracking has concentrated local stresses to the point that bricks would start to experience local failure. This

comparison shows that numerical modelling in 3DEC can simulate the quasi-static behaviour of URM walls and is appropriate for modelling pushover tests.

3.6.3 Validation of the numerical model for out-of-plane behaviour

To check the validity of 3DEC when analysing the out-of-plane behaviour of masonry walls, results from some 3DEC numerical models were validated against experimental data (Restrepo Vélez et al., 2014). A 1:5 scale dry stone masonry wall was built to investigate collapse mechanisms under out-of-plane loading and had a size of 280mm×800mm×400mm (height × length × width), and a masonry unit weight of 2680kg/m³. According to (Restrepo Vélez et al., 2014), initially, the experimental specimens were brought into equilibrium under their self-weights and then the structures were raised incrementally with tilting table up to the point where the collapse occurred. Forty-two tests were carried out, and two typical masonry walls were selected to compare some 3DEC models with the experimental data. Based on details from the experimental tests, the 3DEC numerical model produced are shown in Figure 3.18.

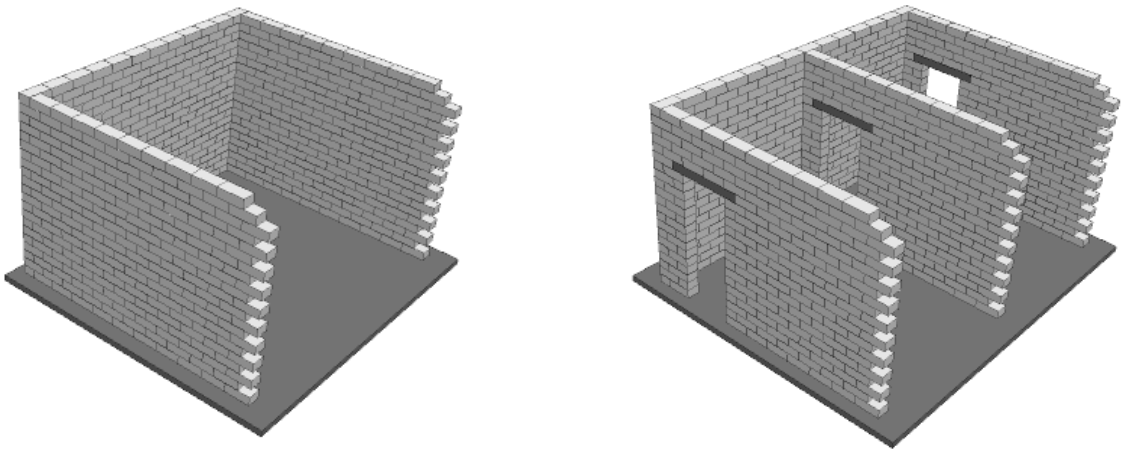

(a) Masonry wall I (b) Masonry wall II

Figure 3.18 The numerical model of masonry walls in 3DEC based on the geometry information from (Restrepo Vélez et al., 2014)

A comparison between the 3DEC models and the collapses seen in the experimental models can be seen in Figure 3.19. Fig 3.19(a) shows the onset of failure for Wall I and Fig 3.19(b) shows the post-

failure shape of Wall I. Fig 3.19(c) shows the onset of failure for Wall II and Fig 3.19(d) shows the post-failure shape of Wall II.

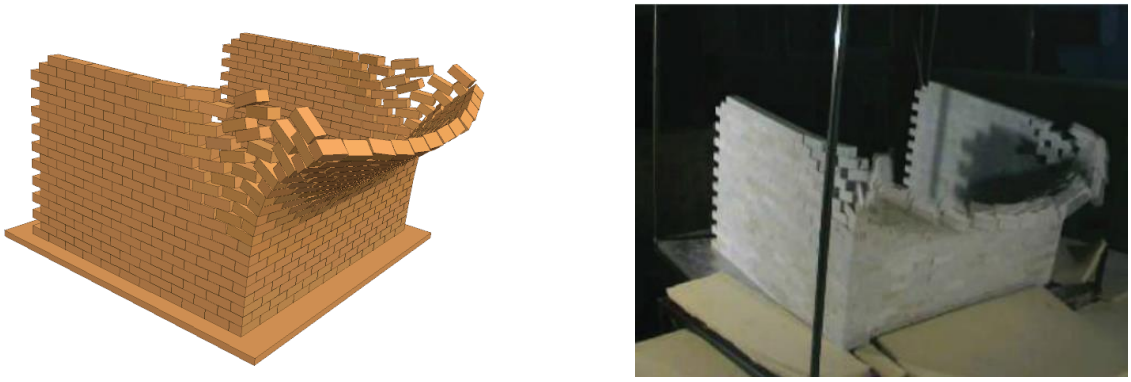

(a) The out-of-plane collapse mechanism A comparison: 3DEC analysis and experimental masonry wall I

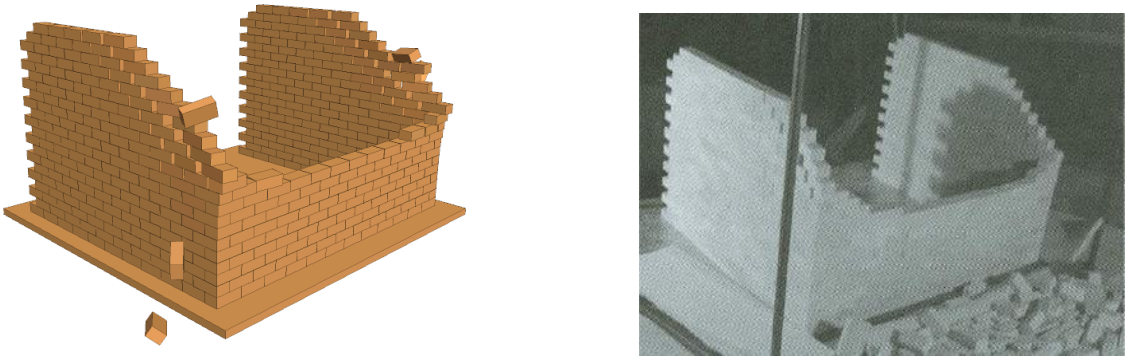

(b) The out-of-plane collapse mechanism B comparison: 3DEC analysis and experimental masonry wall I

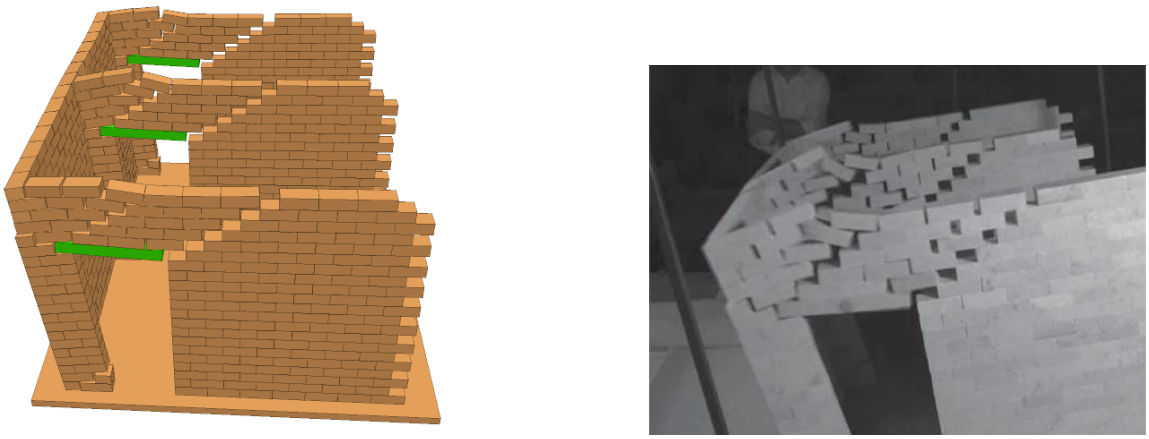

(c) The out-of-plane collapse mechanism C comparison: 3DEC analysis and experimental masonry wall II

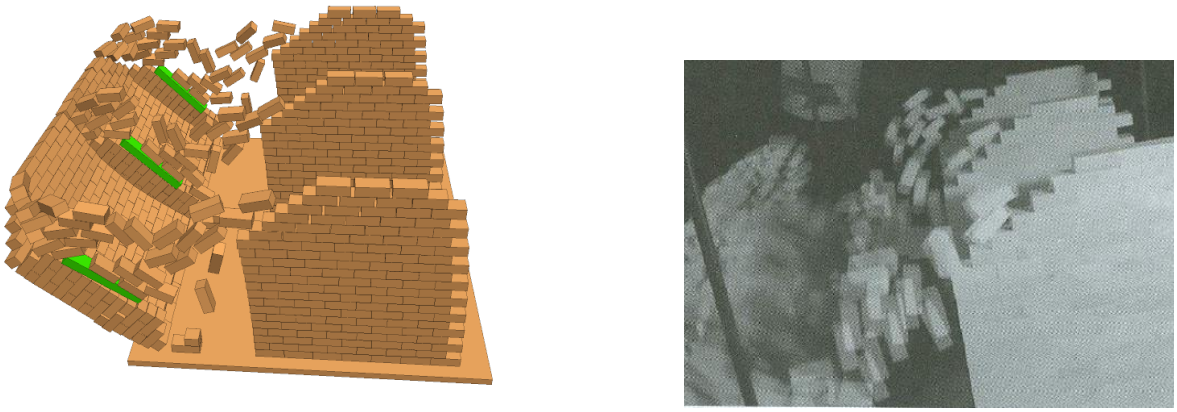

(d) The out-of-plane collapse mechanism D comparison: 3DEC analysis and experimental masonry wall II

Figure 3.19 Different collapse mechanisms comparison: Numerical models and experimental results from (Restrepo Vélez et al., 2014)

Looking at Figure 3.19, the collapse mechanisms for numerical models in 3DEC are very similar to those recorded in the experimental tests. The failure mechanisms that can be seen display two typical types of failure i.e. vertical cracks and diagonal cracks. The vertical cracks are generated because of the pure frictional resistance between the adjacent masonry blocks, and the shear cracks are derived from the shear stresses or the rotation due to the out-of-plane bending moments. Looking at the results above it is clear that numerical models in 3DEC can simulate the out-of-plane response of dry stone masonry wall accurately. Similar comparisons between 3DEC models and experimental tests have also been done by (Bui et al., 2017) and they present similar results, which means that using 3DEC analyses for the out-of-plane of masonry walls is valid.

3.6.4 Comparison with experiments of masonry walls under out-of-plane behaviour

Another comparison between a 3DEC numerical model and some experimental data for masonry walls under out-of-plane behaviour is presented below. According to (Griffith, 2007), the experimental specimen consisted of two long walls with and without vertical load (wall 1 and wall 2), the sizes of walls were 4000mm×2500mm and the properties of masonry blocks and joints are shown in Table 3.5. One wall had a 0.1MP vertical pre-compression and the other had no additional load applied. In both cases walls were supported at all four edges. The geometry of the walls is shown in Figure 3.20 below. In order to achieve the equivalent four-sided boundary conditions in the 3DEC model of the wall, the boundary blocks needed to have high joint stiffness to be effectively rigid while still allowing rotational

freedom to avoid arching issues. The reaction forces on the fixed blocks were recorded during the analysis and the wall displacement was monitored in line with (Griffith, 2007). In the experiment lateral loading was applied to the wall using airbag. The properties of blocks and joints are determined following (Gálvez et al., 2017) and are described in Table 3.5

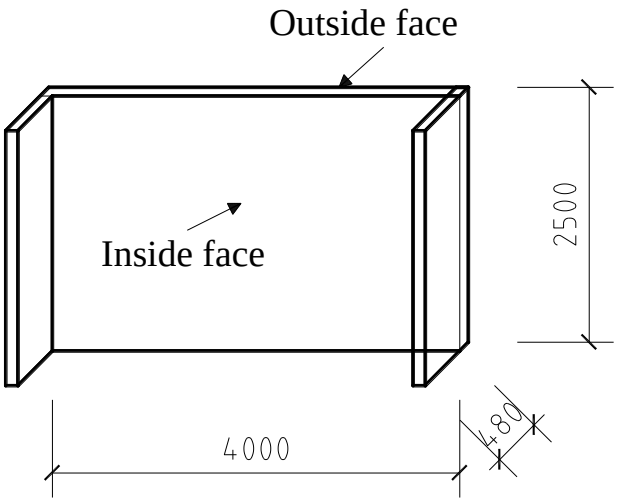

(a) geometry information from experiments (Adopted from (Griffith, 2007))

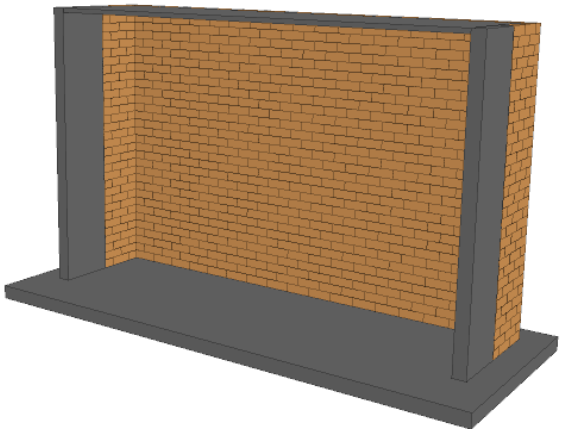

(b) numerical model in 3DEC

Figure 3.20 Geometry information for experiments and numerical model

Table 3.5 Properties of masonry blocks and joints [Adapted from (Gálvez et al., 2017)]

The density of blocks [kg/m³]			Joint normal stiffness [MPa/m]	Joint shear stiffness [MPa/m]	Joint friction angle [Degrees]	Joint tensile strength [MPa]	Joint cohesion [MPa]
1900	Wall 1	Horizontal joints	3600	2400	30	0.45	0.6
		Vertical joints	2000	1333	30	0.45	0.6
	Wall 2	Horizontal joints	3200	2130	30	0.35	0.5
		Vertical joints	1700	1130	30	0.35	0.5

The results are presented through cracks patterns, and peak applied pressure. Comparing the crack patterns of both numerical analysis and experimental tests (Griffith, 2007), it can be seen that the 3DEC model simulates similar crack patterns to the experiments. For the masonry wall with the vertical load, both the test specimen and the numerical model are almost the same, although for the masonry wall without the vertical load, there are a few differences between test specimen and the numerical model, with the 3DEC model showing more cracks and failure at the top part of the wall. In general, the 3DEC model simulates the crack patterns of the masonry walls under out-of-plane behaviour correctly.

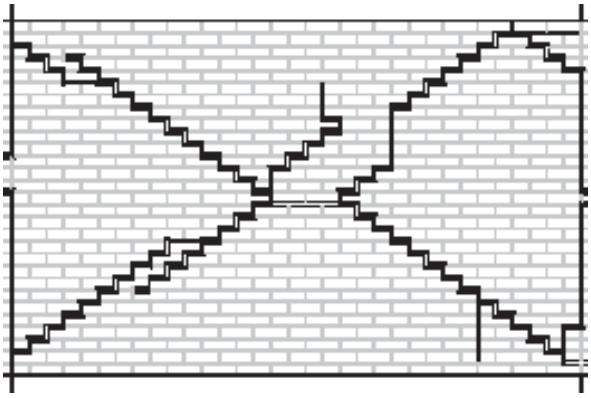

(a) Crack patterns of Wall 1 under experiment [Adapted from (Griffith et al., 2007)];

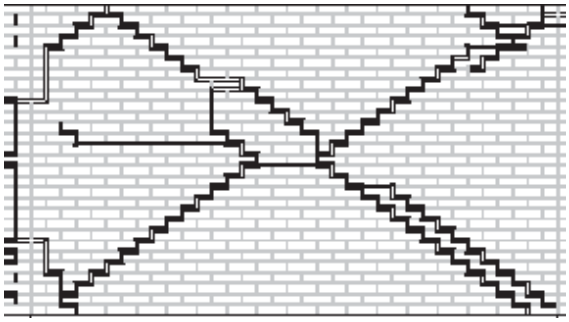

(b) Crack patterns of Wall 2 under experiment [Adapted from (Griffith et al., 2007)]

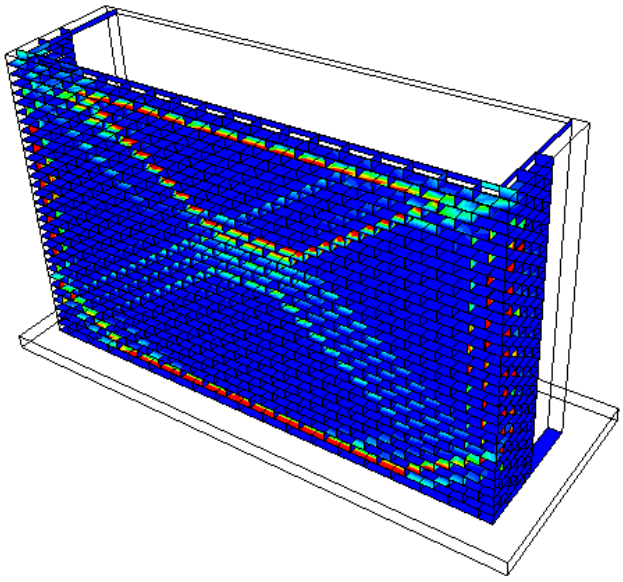

(c) Crack patterns of Wall 1 for numerical analysis

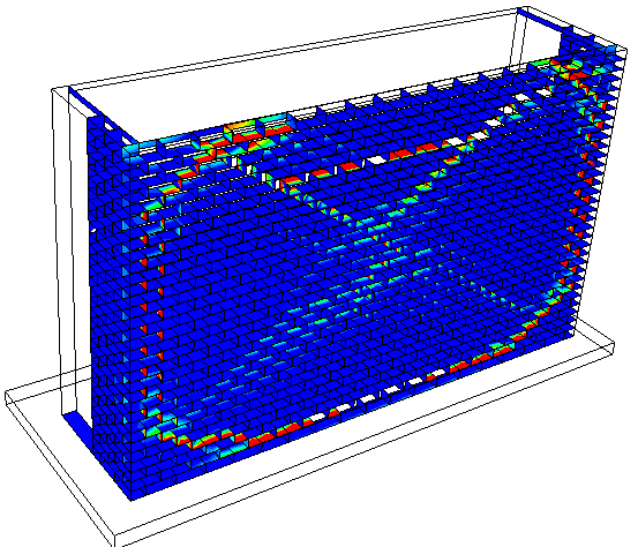

(d) Crack patterns of Wall 2 for numerical analysis

Figure 3.21 Crack patterns of masonry walls between numerical analysis and experiment

The pressure-displacement curves for the experimental results and the 3DEC numerical models are presented in Figure 3.22 and the peak applied pressures are shown in Table 3.6 below. It can be seen that the masonry walls with vertical pressure and without vertical pressure carry different peak applied pressures. The masonry walls with vertical pressure show a better out-of-plane performance than the walls without vertical pressure. Comparing the numerical model and experimental test for the masonry wall with a vertical pressure, the curves show a similar trend and the peak pressures are close. The results for the masonry walls without vertical pressure are also similar. Nevertheless there are still some differences between the numerical analyses and experiments, and in particular Figure 3.22(b) shows that the experiment and model have a rather different initial stiffness. When thinking about the difference in results it is worth noting that the properties of blocks and joints in the numerical model are different to those in the experimental tests because the blocks in the numerical model are considered to be rigid. However, while the 3DEC models could be created using the mode complex deformable blocks, the results using the simpler rigid block model are still acceptable.

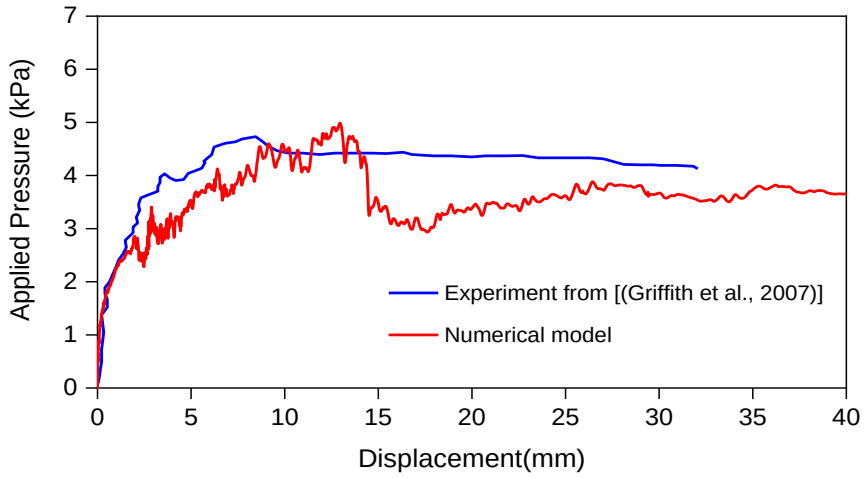

(a) Wall 1 with vertical pressure

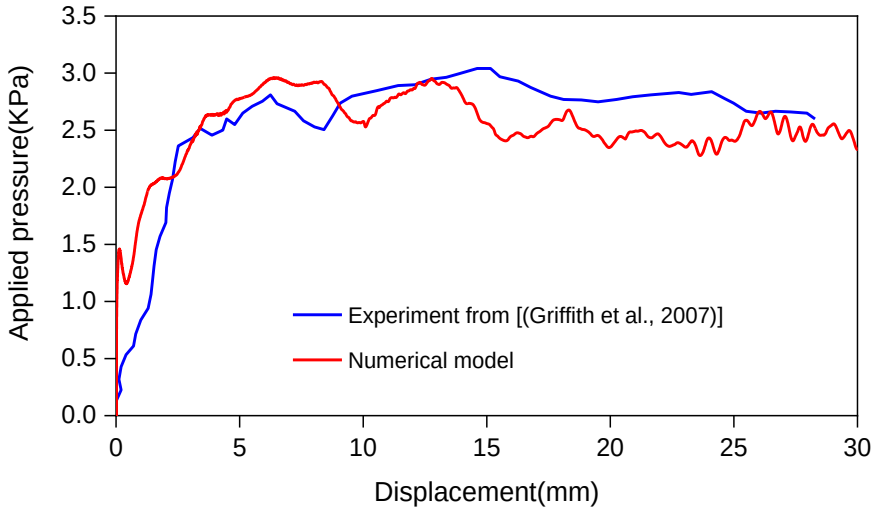

(b) Wall 2 without vertical pressure

Figure 3.22 Load-displacement curves of masonry walls between numerical analysis and experiment

Table 3.6 Results of experiment and numerical analysis for masonry wall

	Wall	Peak applied pressure (kPa)
Experiment (by (Griffith, 2007))	Wall 1 (with vertical load)	4.76
	Wall 2 (without vertical load)	3.0
Numerical analysis	Wall 1 (with vertical load)	5.0
	Wall 2 (without vertical load)	2.85

Numerical models in 3DEC can successfully simulate the out-of-plane behaviour of masonry walls. Because the 3DEC models assumed the bricks were rigid, the wall capacities would be expected to be higher than in the experiments where localised brick crushing was possible. For analysing failure modes and crack patterns, 3DEC also shows good agreement with experimental tests. The comparisons above show that DE models can successfully be used to model the in and out-of-plane behaviour of masonry walls.

Overall, based on the all the validation of numerical model in 3DEC, it can be verified that the software is able to simulate both in-plane and out-of-plane behaviour successfully. Even though there are still some differences for ultimate loads between numerical analysis and experimental test, this numerical model can still predict accurate failure pattern. What is notable, there is no calibration for dynamic analysis. The reason is illustrated that the thesis mainly focus on the static analysis and the dynamic analysis is applied by verifying the stability of static analysis. Besides, the dynamic issue is complicated and it is hard to make all the parameters similar to calibrate and also the dynamic analysis is time consuming. Therefore, the calibration for dynamic analysis in the thesis is ignored.

Even the DEM in 3DEC is ideal for analysis is the thesis, there are some limitations which need to be considered. For improving the efficiency of analysis, the block is regarded as rigid block and there is no deformation allowed. This assumption could lead to the structures stiffer and the ultimate load

higher than real response. Not all models are perfect but this model can also offer valuable information.

3.7 Summary

This chapter presents the methodology for 3DEC modelling, the issues relating to the application of 3DEC for masonry modelling, sensitive studies of 3DEC numerical analyses and has compared some numerical models with experimental data. It has been shown that numerical models in 3DEC can be used to analyse masonry structures successfully and accurately. For a nonlinear static analysis procedure, both a load-based analysis procedure and displacement-based analysis procedure are viable, but a number of analysis options relating to the numerical solver need to be considered carefully. For dynamic analysis, input data such as the applied velocity and damping are important and should be applied carefully. It should be noted that the application of appropriate levels of velocities is key to maintaining the accuracy of displacement-based static analyses. Some example comparisons between 3DEC results and experimental results have been presented and it has been shown that 3DEC is robust and can predict wall failure mechanisms and the wall strengths.

In summary, this chapter shows that modelling masonry in 3DEC is possible and can identify failure modes and capacities of masonry walls. In the next chapters, nonlinear and dynamic analyses will be applied in 3DEC to investigate the effects of openings in unreinforced masonry walls. In-plane, out-of-plane and time-history analyses are included.

Chapter 4 EFFECT OF OPENINGS ON IN-PLANE STRENGTH OF URM WALLS

4.1 Introduction

In general, the effect of openings on the in-plane unreinforced masonry walls is a reduction in the lateral stiffness and strength of the wall, as highlighted in section 2.6. Quite a lot of research has focussed on the effects of opening in URM infilled walls but little work has been done on the effects of openings in plain URM walls. In this chapter, a detailed analysis of the effects of openings, including opening sizes and opening positions, on the in-plane capacity of URM walls is discussed. The relationships between in-plane strength capacity and opening percentage or location are developed and the specific crack patterns of different opening cases are discussed. Two different pushover procedures are applied and the differences in the results are compared. Using comparisons with previous work, the numerical results are validated and the fundamental relationships between the in-plane capacity of URM walls size and location of openings are presented.

4.2 URM walls modelling in 3DEC

4.2.1 Geometry

When considering the modelling of a typical URM building, the individual masonry walls can be divided into two categories i) square walls and ii) rectangular walls, as illustrated in Figure 4.1(a) and 4.1(b) (Abrams and Shah, 1992, Ghiassi et al., 2012b). Geometric models both types of masonry walls, with typical dimensions, were built in 3DEC. To replicate the response of realistic URM walls, the models were built using a Flemish bond, the size of each masonry block was set as 0.06m x 0.24m x 0.12m (height x length x depth), and the dimensions of masonry walls were 3.9m x 0.24m x 3.6m (length x thickness x height). Below each masonry walls, a block was created to represent the ground, and an embedded concrete beam with a size of 4.38m x 0.5m x 0.24m (length x width x height) was located at the top of masonry wall where vertical loads would be applied. The detailed geometry of the models is shown in Figure 4.1 and Figure 4.2.

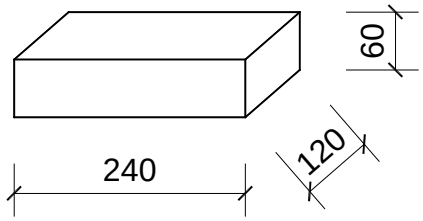

(a) The size of brick

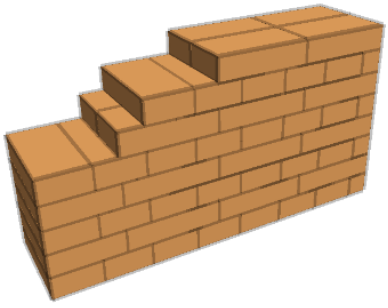

(b) Brick with a Flemish bond

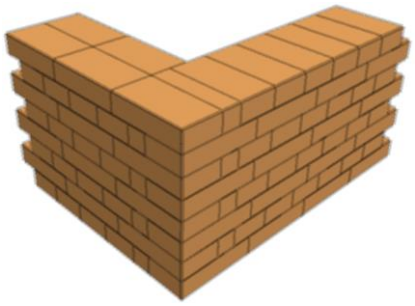

(c) The connection of corner for Flemish bond wall

Figure 4.1 Geometry and numerical models of bricks in 3DEC

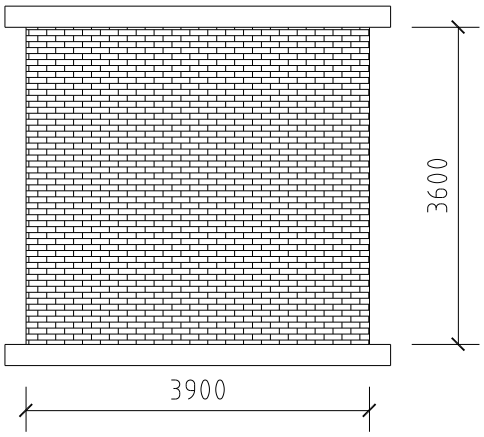

(d) Wall Section I in 3DEC

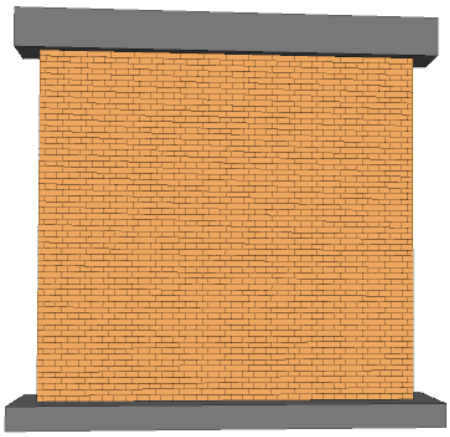

(e) Numerical model in 3DEC

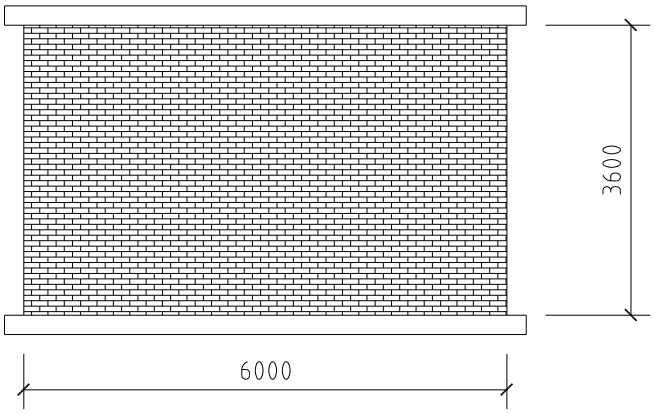

(f) Wall Section II in 3DEC

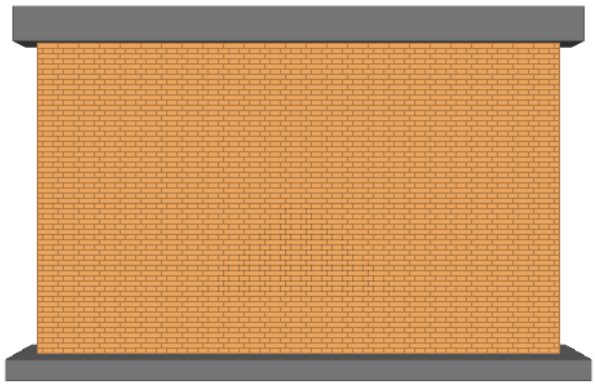

(g) Numerical model in 3DEC

Figure 4.2 Geometry and numerical models of different masonry walls in 3DEC

4.2.2 Material properties of blocks and joints

To simplify the analytical process, the bricks were modelled rigid blocks. For this type of rigid block model, the joint stiffness must represent the stiffness of both block and joint. If E and G are the Young's and shear moduli of the material, then joint stiffnesses can be calculated using Equations 4-1, 4-2 and 4-3 in Figure 4.3.

Horizontal joints $j_{kn} = E/h$ and $j_{ks} = G/h$ 4-1

Vertical joint1 $j_{kn} = E/d$ and $j_{ks} = G/d$ 4-2

Vertical joint2 $j_{kn} = E/l$ and $j_{ks} = G/l$ 4-3

Where h, d and l are the dimensions of the block plus the joint. It is worth noting that, because the blocks are not square, the joint properties are different between the horizontal joints and vertical joints, even though the mortar thicknesses are the same.

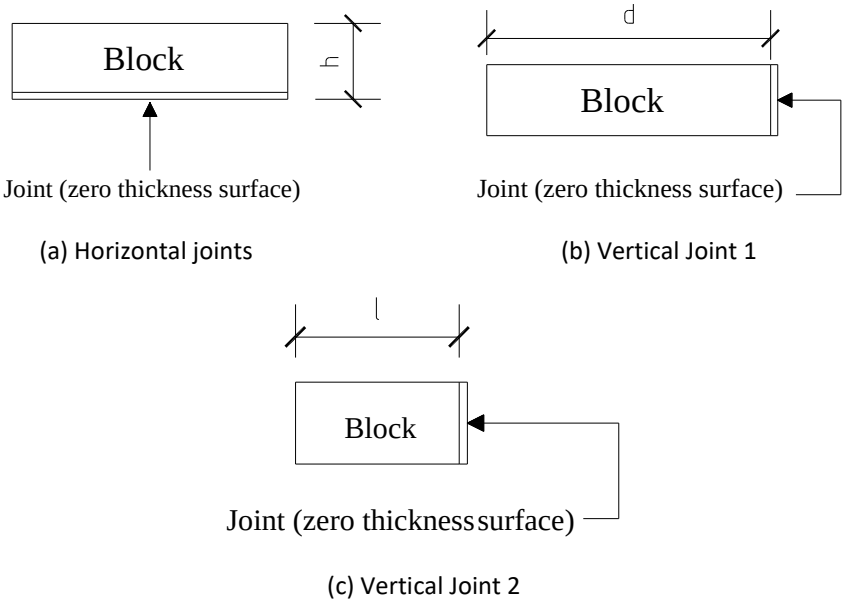

(a) Horizontal joints

(b) Vertical Joint 1

(c) Vertical Joint 2

Figure 4.3 Diagram showing calculation of joint stiffness

The cohesion properties of the joints in 3DEC are determined using Equation 3-11 where F^S_{max} and T_{max} are calculated from the compressive strength and tensile strength of bricks (based either on design code information or experimental results). The tensile strength of the joints was taken as half the cohesion force, based on (Lemos and Costa, 2017). For this work the compressive strength of bricks was taken as 1.83MPa, the average tensile strength of mortar as 0.13MPa and the shear strength of mortar as 0.11MPa. These values coming from the typical strengths are defined in the Chinese design code for masonry structures (GB50003-2011, 2012). The friction angle was assumed

to be 35 degrees, which is consistent with the values given in (Sarhosis and Sheng, 2014) for other 3DEC analyses. The final calculated properties used in the 3DEC model are given in Table 4.1.

Table 4.1 Properties of masonry blocks and joints

Density of blocks [kg/m³]		Joint normal stiffness [MP/m]	Joint shear stiffness [MPa/m]	Joint friction angle [Degrees]	Joint tensile strength [MPa]	Joint cohesion [MPa]
1800	Vertical joints 1	35600	14240	35	0.1	0.2
	Vertical joints 1	17800	7120	35	0.1	0.2
	Horizontal joints	71200	28480	35	0.1	0.2

4.3. Load-based and displacement-based analysis procedures in 3DEC

Pushover tests can be implemented in 3DEC using either a displacement-based analysis procedure or a load-based procedure. As discussed in chapter 3, a displacement-based loading procedure can be achieved by applying a constant loading velocity and the load-based analysis procedure can be achieved by applying a horizontal acceleration. For the load-based procedure, vertical load was applied first until arriving equilibrium, then a horizontal acceleration was applied in increments until the wall failed. For the displacement-based procedure, again the vertical load was applied first then, using a loading block attached to the concrete beam at the top of the wall, a constant velocity was applied until the wall collapsed. For both loading procedures the displacement of the top block (concrete beam) and the applied load/acceleration was recorded so the pushover curves could be determined, as shown in Figure 4.4. what is notable, the top blocks for both load patterns are not restrained for simulating the real response of masonry walls and thus the top blocks can move up and down.

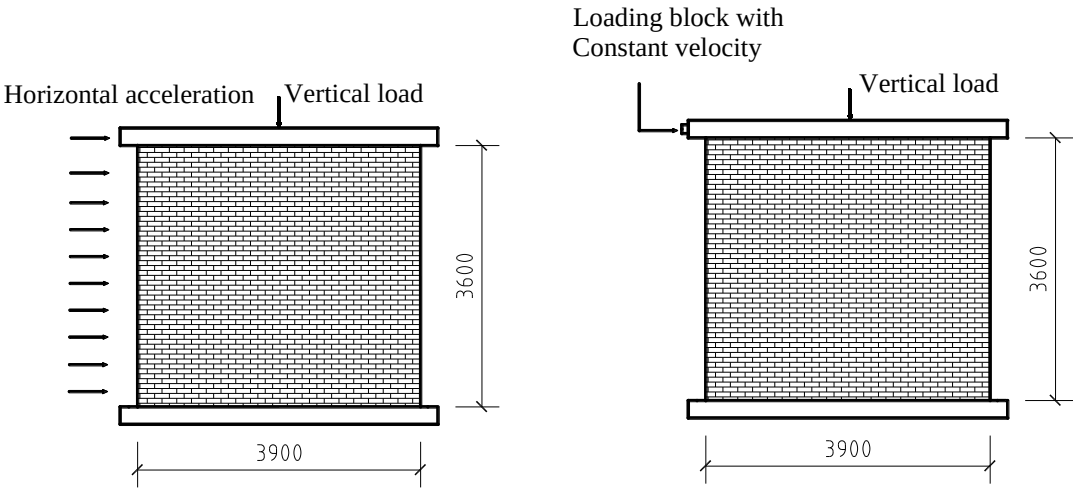

(a) Pushover load patterns under a load-based analysis procedure in 3DEC; (b) Pushover load patterns under a displacement-based analysis procedure in 3DEC

Figure 4.4 The pushover load patterns with different procedure and relationship from previous research

Taking a solid URM wall as an example case, the pushover curves for both procedures are shown in Figure 4.5(b). The results indicate that the maximum base shear force for a load-based analysis procedure is higher than for a displacement-based procedure. This is because for the load-based analysis procedure, the acceleration will generate vertical and horizontal forces in the top block and every other brick. The centroid of the global forces is therefore located between the top block and masonry bricks. However, for the displacement-based procedure, the forces are applied directly at the top block and the centroid of forces is located at the centre of the top block. In this case, the wall under the displacement-based analysis procedure will experience higher horizontal moments and a lower peak base shear force than the wall under the load-based procedure.

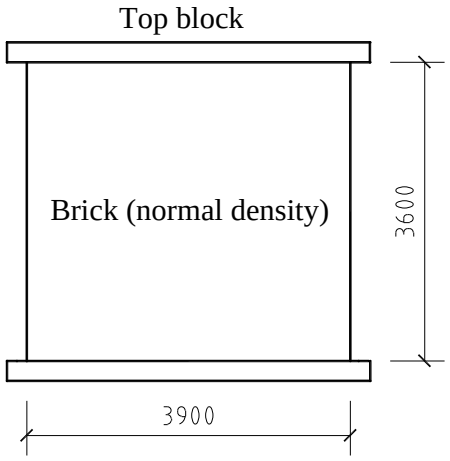

(a) The solid wall with normal density brick

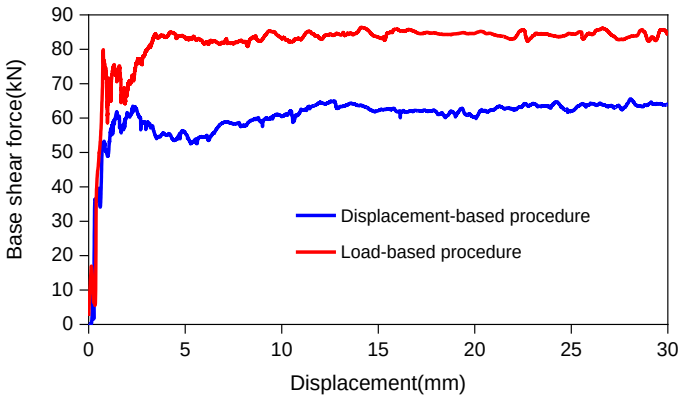

(b) Pushover curves of solid walls under both procedures

Figure 4.5 Results of solid walls with normal density brick

To check the validity of this explanation, a modified model was created to check whether it is possible to recreate similar responses under both loading procedures in 3DEC. For the modified wall under a load-based analysis procedure the bricks were assigned a very small density, i.e. effectively a zero density (because the density cannot be set as zero in 3DEC), and the top block had a normal density. When acceleration was applied, the horizontal forces were then only generated in the top block. The same model was used with a displacement-based analysis procedure again the bricks had a very low density to make sure horizontal forces were mainly determined by the top block. In this case both pushover results were expected to be similar and the results of these analyses are shown in Figure 4.6(b).

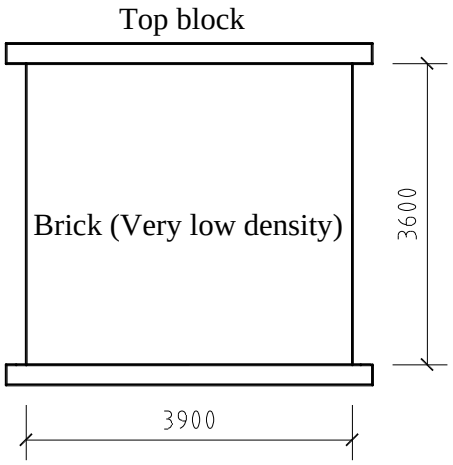

(a) The solid wall with very low density bricks

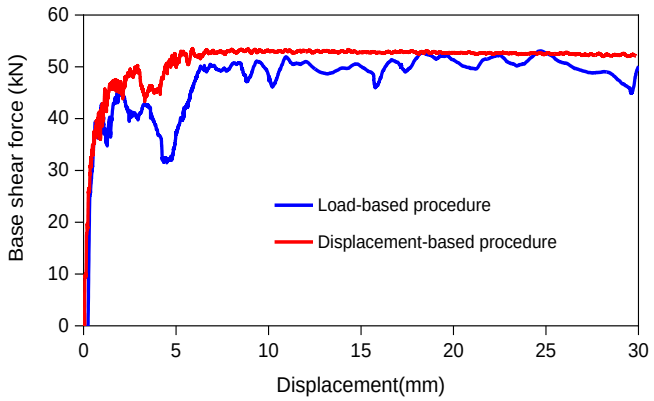

(b) Pushover curves of test models with very low density bricks under both procedures

Figure 4.6 Results of test models with very low density bricks

Looking at the results in Figure 4.6, both procedures now produce similar pushover curves and peak wall capacities, although there are still a few differences in the progression of failure because the density is almost taken as zero while for the load-based analysis procedure the acceleration is still applied to the bricks even the force is small, which may occur some local failure and reduce the base shear force resistance slightly. However, for real structures, the brick must have density, which means that the load-based analysis procedure gives a higher prediction of seismic capacity at collapse, but this does better reflect the loading that would be applied during a seismic event.

Nevertheless, the displacement-based approach is useful for investigating post-peak response and is more representative of most experimental tests. It is worth noting that there is also a significant difference in the computational cost of the two analysis methods. Using the solid wall as an example,

the load-based analysis procedure required ~202k analysis cycles while the displacement-based analysis procedure required ~523k analysis cycles to complete (just over twice as long). A larger number of cycles was necessary for the displacement-based approach as it was important to apply the loading slowly enough that the analysis replicated a pseudo-static loading condition. However, the analysis duration for the displacement-based approach only averaged 1 hour so both analysis procedures were viable. Therefore, in this research, both methods were used to determine the in-plane capacity of masonry walls with different opening percentages with the aim of identifying appropriate equations for capacity reduction as the opening size increases.

4.4. In-plane behaviour of masonry walls with different opening percentages

4.4.1 Cases studied for Opening percentage effects under in-plane behaviour

A total of five types of 3DEC model were built to identify the impact of opening percentage on URM walls. Based on (Voon and Ingham, 2008), which considered a range of openings in RC masonry infill walls, in this research, centralised square and rectangular window openings, single door openings, and combined door and window openings in URM walls with different aspect ratios have been all considered. These five different types of masonry wall are shown in Figure 4.7. For each basic wall type, the opening sizes were divided into eleven subcases, identified as OS1 to OS9 with opening percentages varying from about 2% to 64%, respectively. If the opening is too large such as the percentage is over 65%, the opening size is not realistic and the walls are almost similar to “frame” structures. To allow modelling of the walls using just full and ½ size bricks, the actual opening percentages in the five wall types vary slightly, but they have been kept as close as possible for each wall type. Detailed information about the sizes of openings can be seen in Figure 4.7 and Tables 4.2 and 4.3.

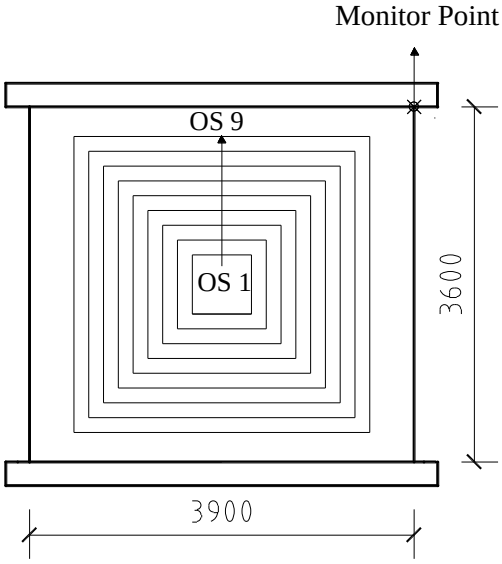

(a) Opening percentages situation I

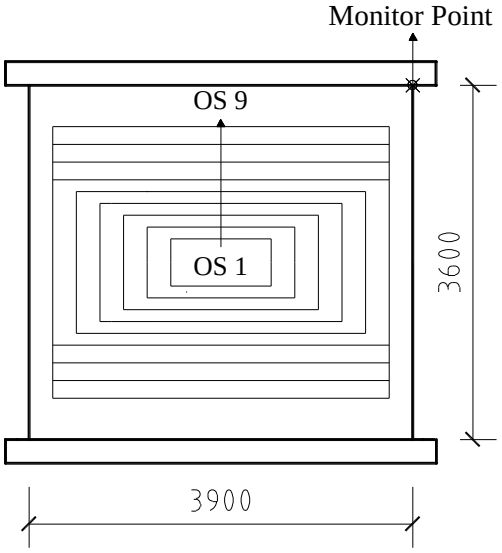

(b) Opening percentage situation II

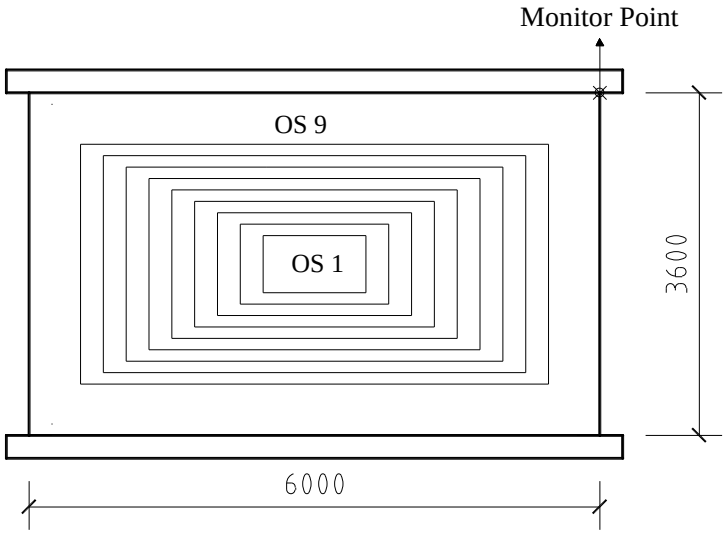

(c) Opening percentage situation III

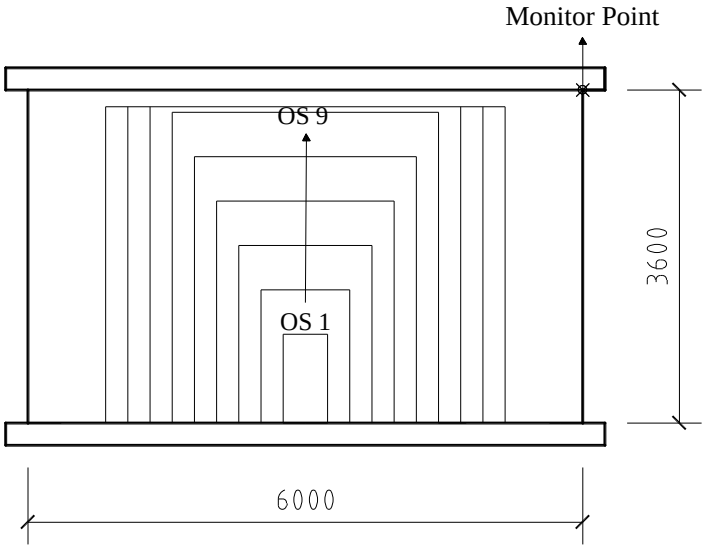

(d) Opening percentage situation IV

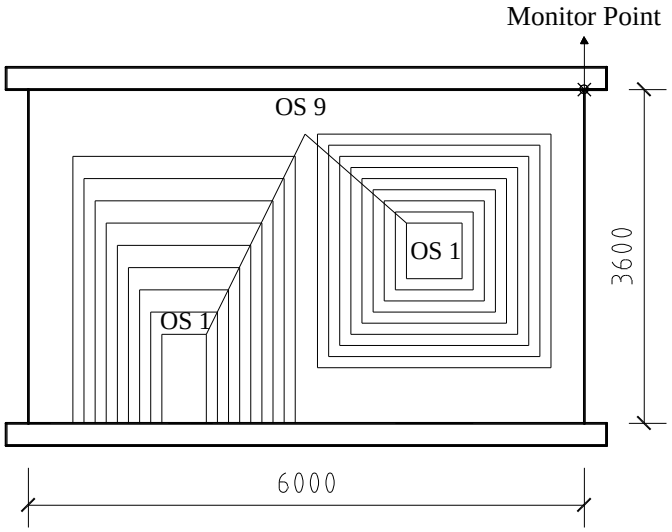

(e) Opening percentage situation V

Figure 4.7 Opening percentages in the five masonry wall types

Table 4.2 Opening percentage wall type I, Opening percentage wall type II and Opening percentage wall type III

Opening percentage wall type I			Opening percentage wall type II			Opening percentage wall type III		
Opening Case	Opening Size [mm]	Opening Percentage	Opening Case	Opening Size [mm]	Opening Percentage	Opening Case	Opening Size [mm]	Opening Percentage
OS1	600*600	3%	OS1	1020*480	3.5%	OS1	1080*600	3%
OS2	900*900	6%	OS2	1500*720	7.7%	OS2	1560*840	6%
OS3	1200*1200	10%	OS3	1980*960	13.5%	OS3	2040*1080	10.2%
OS4	1500*1500	16%	OS4	2460*1200	21%	OS4	2520*1320	15.4%
OS5	1800*1800	23%	OS5	2940*1440	30%	OS5	3000*1560	21.7%
OS6	2100*2100	31 %	OS6	3420*1680	41 %	OS6	3480*1800	29 %
OS7	2400*2400	41%	OS7	3420*2040	50%	OS7	3960*2040	37.4%

OS8	2700*2700	52%	OS8	3420*2400	58.5%	OS8	4440*2280	47%
OS9	3000*3000	64 %	OS9	3420*2580	63 %	OS9	4920*2520	57.4 %

Table 4.3 Opening percentage wall type IV and Opening percentage wall type V

Opening percentage wall type IV			Opening percentage wall type V		
Opening Case	Opening Size [mm]	Opening Percentage	Opening Case	Opening Size [mm]	Opening Percentage
OS1	480*960	2%	OS1	480*960 and 600*600	3.8%
OS2	960*1440	6.4%	OS2	720*1200 and 840*840	7.3%
OS3	1440*1920	12.8%	OS3	960*1440 and 1080*1080	11.8%
OS4	1920*2400	21.3%	OS4	1200*1680 and 1320*1320	17.4%
OS5	2400*2880	32%	OS5	1440*1920 and 1560*1560	24%
OS6	2880*3360	44.8 %	OS6	1680*2160 and 1800*1800	31.6 %
OS7	3360*3420	53.2%	OS7	1920*2400 and 2040*2040	40.6%
OS8	3840*3420	60.8%	OS8	2160*2640 and 2280*2280	50%
OS9	4320*3420	68.4 %	OS9	2400*2880 and 2520*2520	61.4 %

4.3.2 Pushover curves for load-based and displacement-based analysis procedures in 3DEC

To allow comparison between the results of the two loading procedures, for each procedure the pushover curves were created using the base shear forces calculated during the analyses. The pushover curves for masonry wall type I with different opening percentages, analysed using the two procedures, are given in Figure 4.8. For both methods the analytical parameters (damping and load/velocity increments) were chosen to optimize the numerical stability of the analyses while limiting analysis time. Generally, the results were insensitive even to significant changes in the analysis

parameters suggesting that a considerable proportion of the irregularity of the response in Figure 4.7 is coming from the development of sudden tensile failures between bricks as the analyses progress.

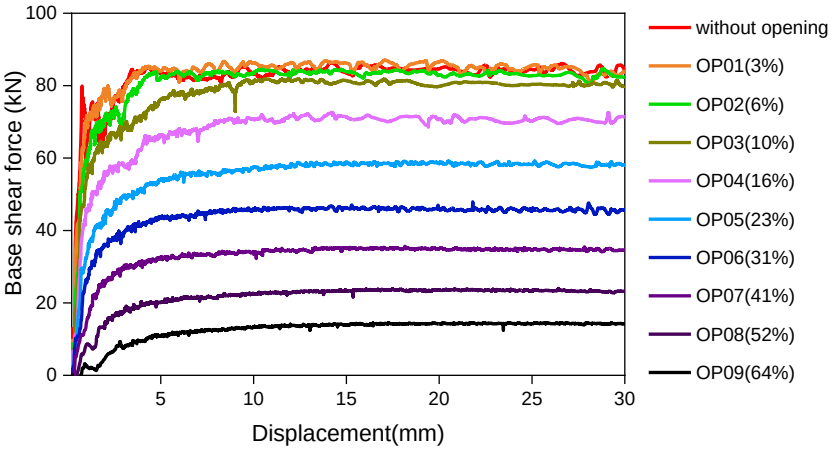

(a) The pushover curve for masonry walls under load-based analysis procedure

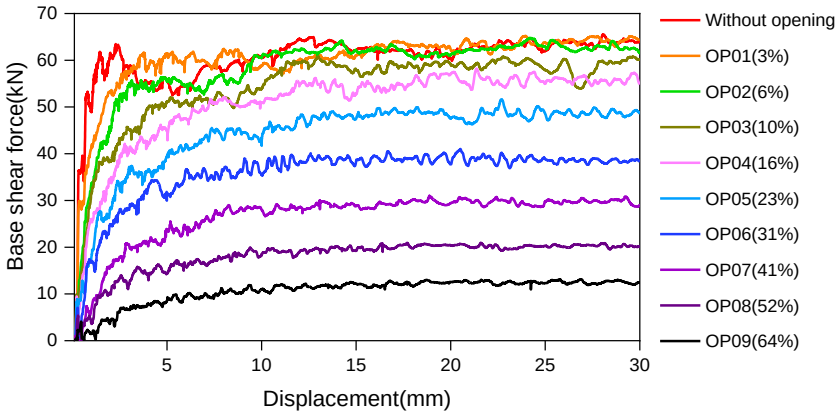

(b) The pushover curve for masonry walls under displacement-based analysis procedure

Figure 4.8 The pushover curves for masonry wall with the different opening percentage under different load patterns

The pushover curves created using a load-based analysis procedure show relatively smooth curves up to the point of maximum base shear force, at which point the displacement of the walls increases dramatically as the walls fail. For an opening percentage under ~10%, the base shear force of masonry wall is practically the same as for the solid wall. When the opening percentage is more than ~15% the wall capacity starts to drop significantly as the opening size increases. When the opening percentage is ~65% the wall only retains 15% of its solid capacity. For the displacement-based loading procedure, the pushover curves are quite similar, but the maximum values are lower. For an opening percentage over ~10% the decreasing wall capacity becomes obvious. When the opening percentage reaches ~40%

the wall in-plane capacity has reduced by ~40%. Once the opening percentage exceeds ~60%, the in-plane capacity has reduced to less 20% of the solid capacity.

The relationships between the opening size and the peak in-plane capacity for the two loading procedures are shown in Figure 4.9(a). Walls with openings less than 10% analysed using a load-based analysis procedure have a much higher capacity than those analysed using a displacement-based procedure, however as the opening percentage increases, the difference between the two methods reduces. When the opening size is greater than 40%, the capacity of the wall under both analysis methods is similar.

To allow further comparison between the results from the two loading procedures, for each procedure the pushover curves were normalised relative to the peak base shear force of the solid wall Figure 4.9(b). Both analysis methods result in very similar normalised curves for openings sizes up to 10% but the capacities from the load-based analysis procedure do drop below those from the displacement-based procedure once the opening is greater than 10%.

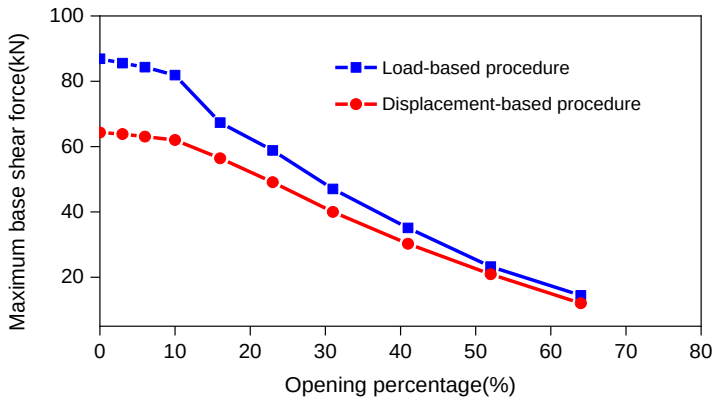

(a) Impact curves of opening percentage on maximum base shear force for the load and displacement-based procedures

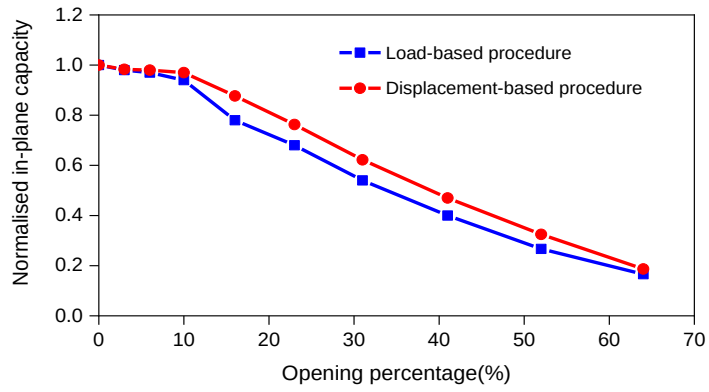

(b) Impact curves of opening percentage on normalised wall capacity for the load and displacement-based procedures

Figure 4.9 Comparison of the impact of opening percentage on wall capacity for the load and displacement-based analysis procedures.

To highlight the differences in the in-plane behaviour for the two analysis procedures, the crack patterns for four different opening percentages are shown in Table 4.4. The crack patterns for the walls produced by the two analysis procedures both show similar global failure mechanisms for the different opening percentages, however, some local differences can be observed. In particular, the masonry walls analysed using a load-based procedure generally display smaller distributed cracks compared to the walls analysed using a displacement-based procedure. The local differences in the failure patterns are a result of the different ways that the loading is applied to the walls. For the load-based analysis each brick is subjected to a force proportional to its mass, resulting in a very distributed loading applied the whole wall and more distributed cracking. However, for the displacement-based analysis procedure the loading is applied across the wall as a whole, resulting in fewer larger cracks.

Comparing the results in Figure 4.8 and Table 4.4, it is clear that there are some differences between the results from the two analysis methods and this is reflected in the different peak base shear forces calculated. However, both analytical procedures show a drop in the capacity as the opening size increases. In general, the displacement-based procedure gives a lower base shear force than the load-based procedure. However, when the opening percentage is over 40%, the base shear forces are similar.

Table 4.4. In-plane crack patterns for masonry walls with different opening percentages analysed using load-based and displacement-based procedures at 4% drift (0.15m)

	Load-based procedure	Displacement-based procedure
Masonry wall without opening	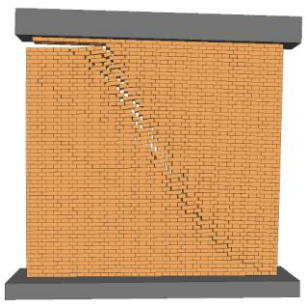	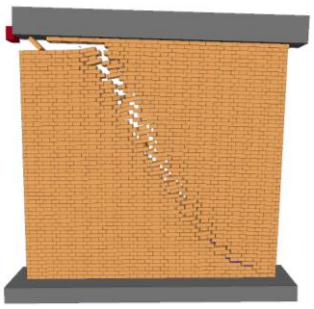

Masonry wall with OS 01 (3%)	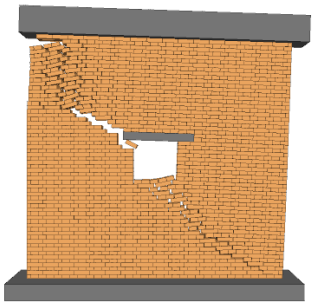	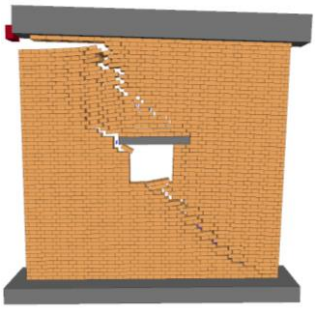
Masonry wall with OS 04 (16%)	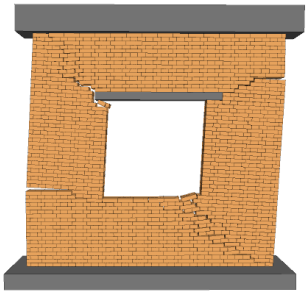	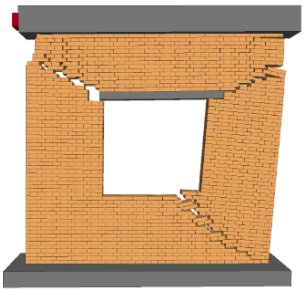
Masonry wall with OS 07 (41%)	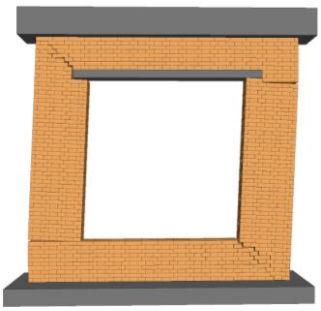	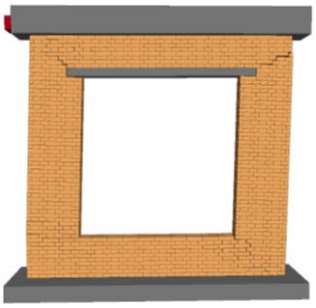

4.3.3 Comparison of the relationship between in-plane capacity and opening percentage from previous research and from the 3DEC numerical model

It is worth noting that in most experimental tests, a displacement-based procedure is used to load masonry walls, as it is much harder to conduct a test using a load-based analysis procedure (such tests requiring the use of a shaking table). Therefore, most experimental data comes from displacement-based pushover tests. In addition, because the previous research focusing on the effects of openings for URM cannot be found, it is unable to compare the results of opening effects with other studies. Therefore, to identify the opening effects through previous research, the data from pushover tests of RC infill walls are used. The comparison show that the relationship between in-plane capacity and opening percentage, from (Giannakas et al., 1987, Asteris, 2003), has been used to provide some comparison with the numerical results produced by 3DEC for URM walls. Curves showing the

relationship between stiffness reduction and opening percentage are shown in Figure 4.10. These curves show that the experimental performance of masonry walls in RC frames and equivalent displacement-based analytical solutions in 3DEC for URM walls are very similar, while the load-based analysis procedure in 3DEC predicts a higher in-plane performance for walls with the same opening percentage. For RC frame infill walls, when the percentage opening is higher than 50% the RC frame starts to carry all the load and there is no further degradation in wall stiffness while for the URM walls the stiffness continues to decrease. This load sharing mechanism between frame and masonry does not exist in URM walls. While the results from the load-based analyses of the URM walls do not match the displacement-based experimental data for RC infill walls, the load-based analysis results should not be dismissed because they reflect a loading pattern that is closer to that which would occur under seismic conditions. Therefore, both pushover procedures should be considered when designing or assessing URM.

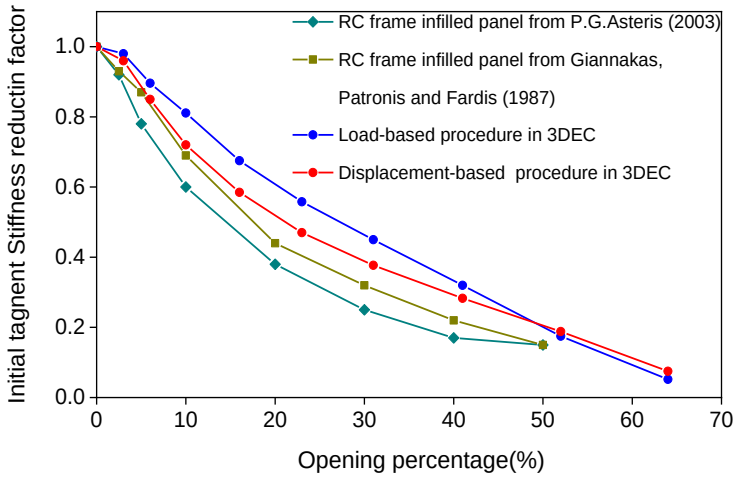

Figure 4.10 The comparison of relationship for opening percentage effects with different situations

Overall, the curves for URM produced by 3DEC show a similar trend to those given in previous papers. In addition, there are still some limitations in this comparison as the RC frame infilled walls eventually display different failure mechanisms because of load sharing between the RC frame and the masonry wall. However, the results still show some valuable information that for RC frame, once the opening size is over 50%, the frame would take the load completely and the stiffness reduction factor keep stable while for URM, as the opening size increase, the capacity would keep decreasing.

4.3.4 Effects of opening percentage considering different factors

As noted in section 4.4.1, five types of 3DEC model were built to identify the impact of opening percentage on a variety of URM walls; centralised square and rectangular window openings, single door openings, and combined door and window openings. Because a load-based analysis procedure gives a better representation of the inertial loading caused by earthquakes, pushover curves were only generated using the load-based analysis procedure and normalised curves showing the relationship between the maximum in-plane capacity and the opening percentage were calculated. In all cases the peak in-plane capacity of the walls reduces as the size of the opening increases, although the rate of the drop varies.

As shown in Figure 4.11(a), the capacity of the square and rectangular walls with central openings (cases I, II and III) follow a similar trend, with the in-plane capacity starting to drop significantly when the opening percentage exceeds ~10% until the opening percentage is ~65% at which point a residual wall capacity of ~10% is reached. For Case II (rectangular central opening in a square wall), the in-plane capacity is similar that to Case I (square opening in the square wall) when the opening percentage is below 10%, however above that percentage the wall capacity drops quickly until at a 40% opening percentage only a residual capacity of ~10% of the solid wall remains. However, for Case IV (door opening) the in-plane capacity remains higher than for the other cases for the same opening percentage, and it only drops to a 10% residual capacity when the opening percentage exceeds 80%. For Case V (door and window openings) the wall capacity reduces dramatically even with a relatively small opening percentage however once then the opening percentage is greater than 20%, the curve follows a similar trend to Case I and III.

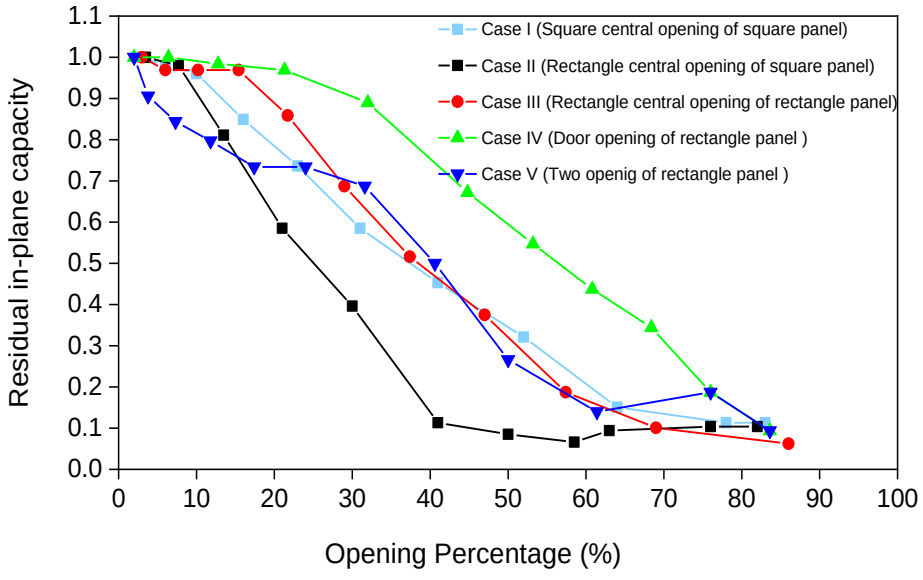

(a)

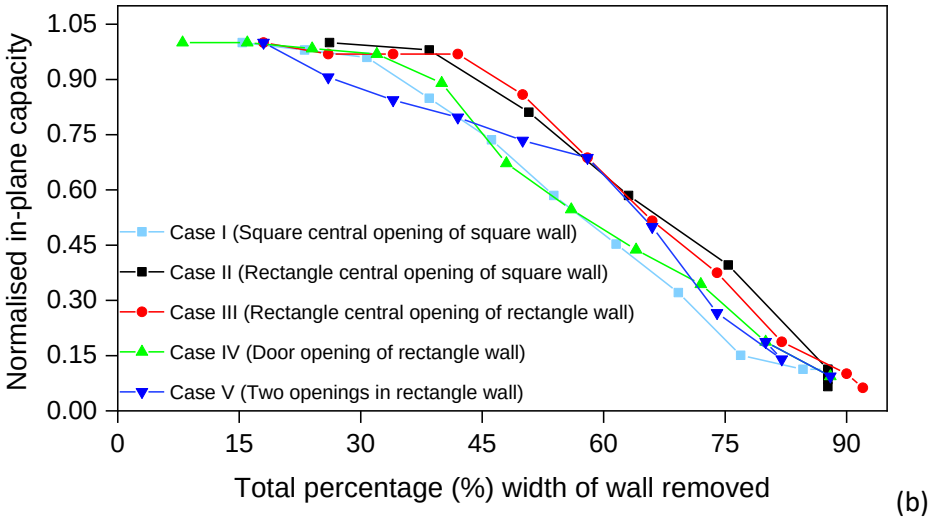

Figure 4.11 The relationships between residual in-plane capacity and (a) opening percentage (b) total percentage (%) width of wall removed for various opening cases

The differences in capacities for the cases shown in Figure 4.11(a) can be explained by looking at the failure patterns of masonry walls, shown in Table 4.5. Cases I and III display very similar failure mechanisms, the cracking starting on one diagonal and progressing to both diagonals as the opening percentage increases although the opening percentage at which the behaviour changes does vary between the two cases.

Case II displays a different behaviour compared to Cases I and III because the masonry piers on either side of the opening are proportionately thinner for the same opening percentage. This leads to quicker localised failure of the piers and a reduced capacity for any specific opening percentage.

For Case IV, the reverse is true as the piers around the door remain relatively wide while the spandrel becomes rapidly thinner as the percentage opening increases. In this case the masonry piers remain strong enough to resist the horizontal force and the wall performance is better than for the other cases. Therefore, as an alternative to considering the effect of the opening percentage on the wall capacity, Figure 4.11(b) shows the wall capacities compared to the total percentage width of wall removed by all the openings. This criterion reduces the differences in the curves for the more asymmetric opening cases i.e. the rectangular opening in a square wall and the two openings in one wall (Cases II and IV) but increases the variation for the more regular walls (Cases I and III).

In Case V, the location of the small window opening coincides with the crack location in the solid case inducing a localised failure at the window corner even though the opening percentage is small. The

wall behaviour becomes more similar to Case III as the opening percentage increases. This case shows the importance of the opening position, an aspect which is studied further in section 4.5.

Table 4.5 The in-plane crack patterns of opening percentage situation II of masonry walls at 0.15m top displacement

Masonry wall without opening	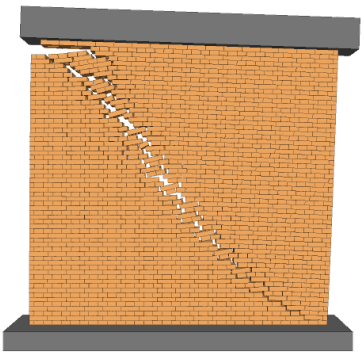	Masonry wall with OS 01 (3%)	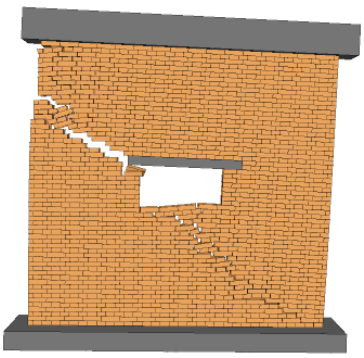
Masonry wall with OS 02 (8%)	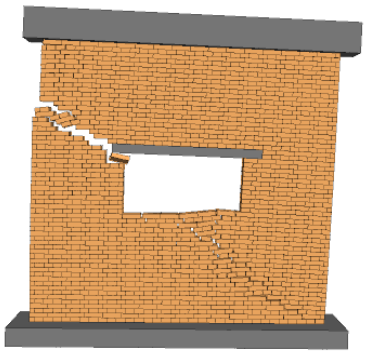	Masonry wall with OS 03 (13%)	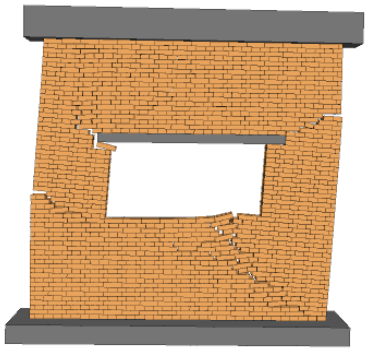
Masonry wall with OS 04 (21%)	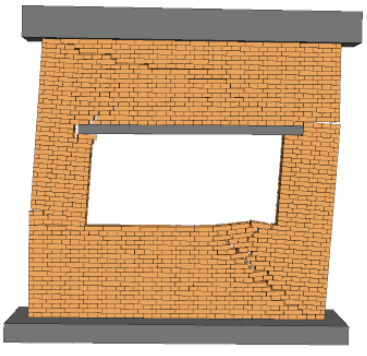	Masonry wall with OS 05 (30%)	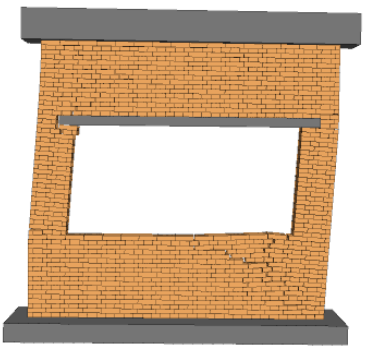

Masonry wall with OS 06 (41%)	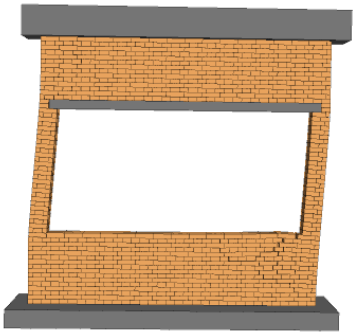	Masonry wall with OS 07 (50%)	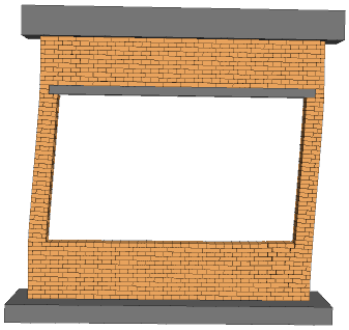

Table 4.6 The in-plane crack patterns of opening percentage situation III of masonry walls at 0.15m top displacement

Masonry wall without opening	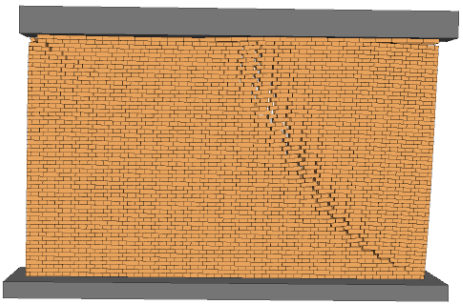	Masonry wall with OS 01 (3%)	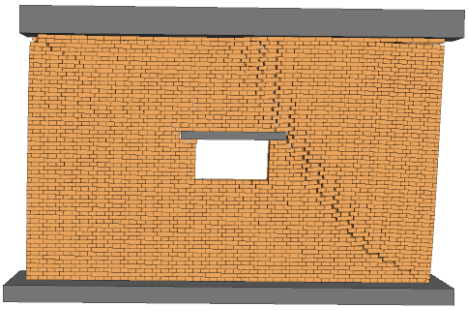
Masonry wall with OS 02 (6%)	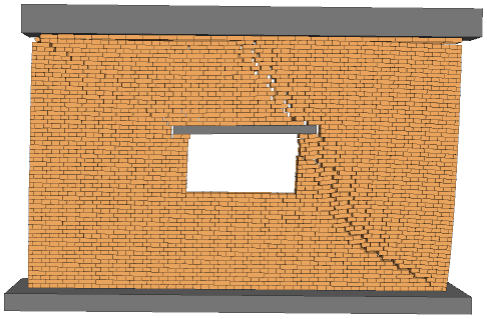	Masonry wall with OS 03 (10%)	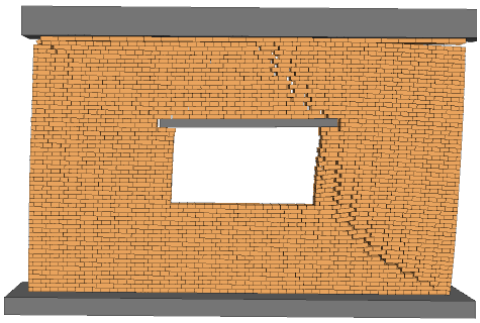

Masonry wall with OS 04 (15%)	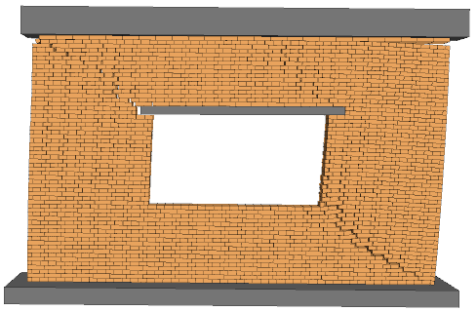	Masonry wall with OS 05 (22%)	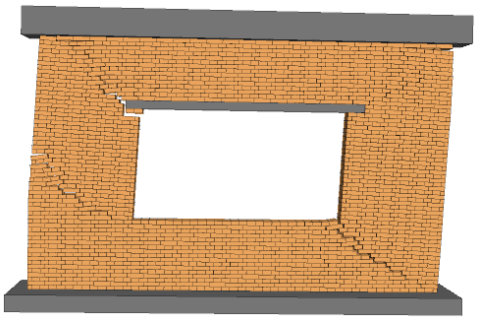
Masonry wall with OS 06 (29%)	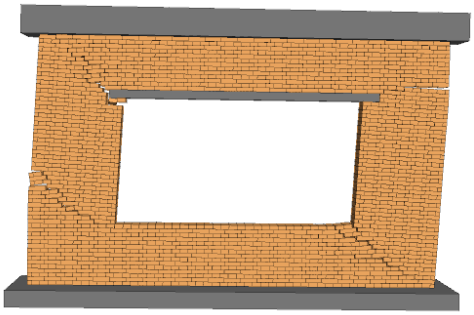	Masonry wall with OS 07 (37%)	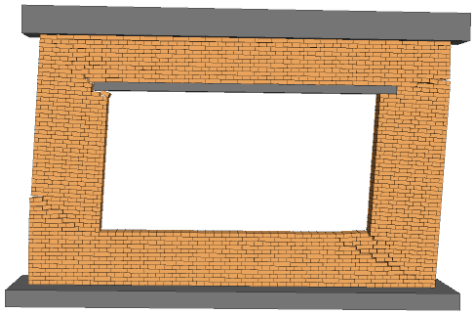

Table 4.7 The in-plane crack patterns of opening percentage situation IV of masonry walls at 0.15m top displacement

Masonry wall without opening	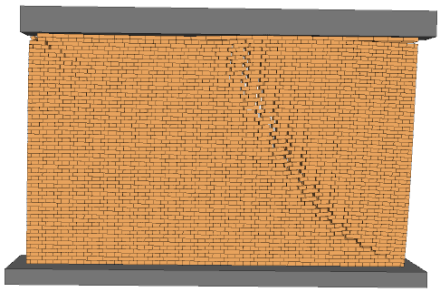	Masonry wall with OS 01 (2%)	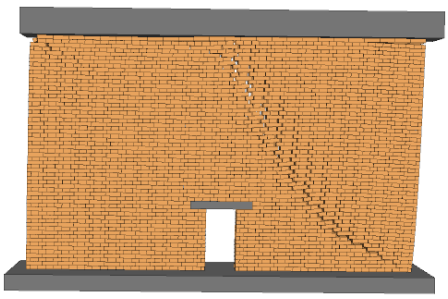
Masonry wall with OS 02 (6%)	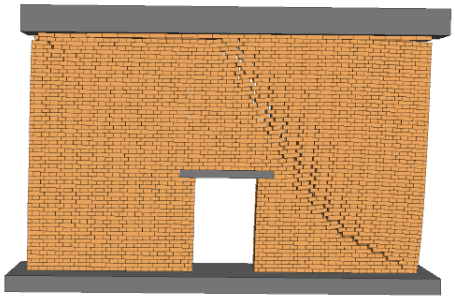	Masonry wall with OS 03 (13%)	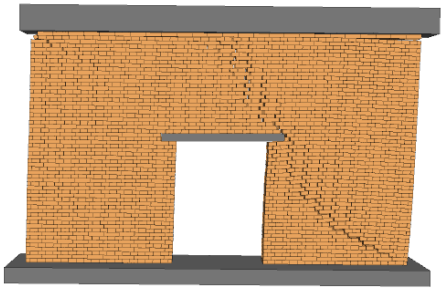

Masonry wall with OS 04 (21%)	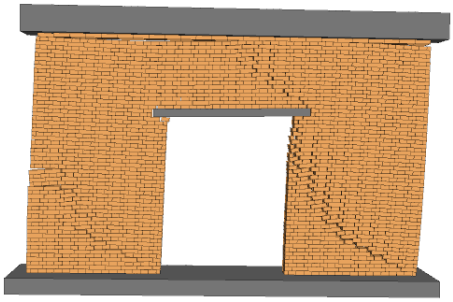	Masonry wall with OS 05 (32%)	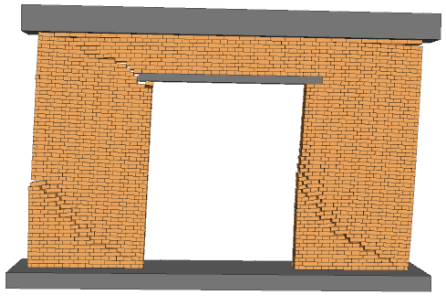
Masonry wall with 0S 06(45%)	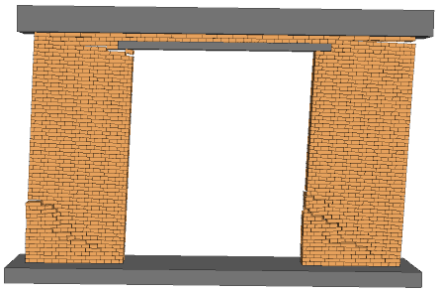	Masonry wall with OS 07 (53%)	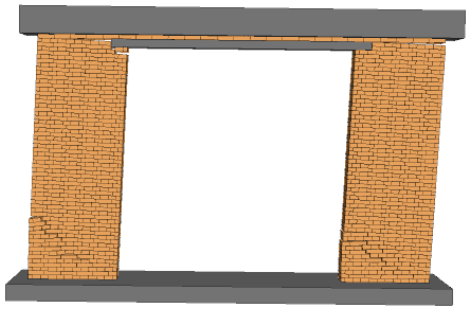

Table 4.8 The in-plane crack patterns of opening percentage situation V of masonry walls at 0.15m top displacement

Masonry wall without opening	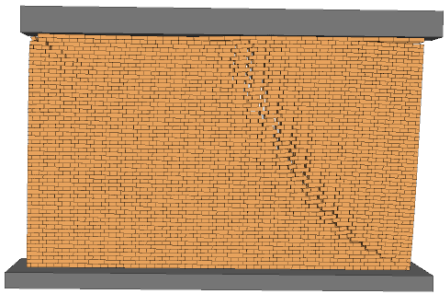	The masonry wall with OS 01 (4%)	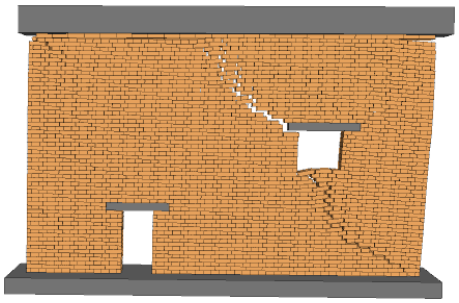
Masonry wall with OS 02 (7%)	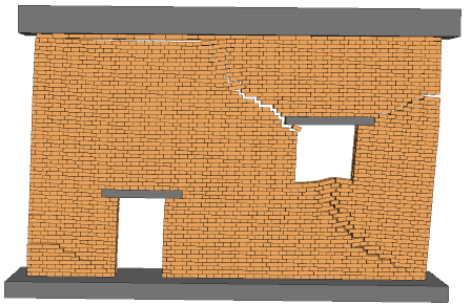	Masonry wall with OS 03 (12%)	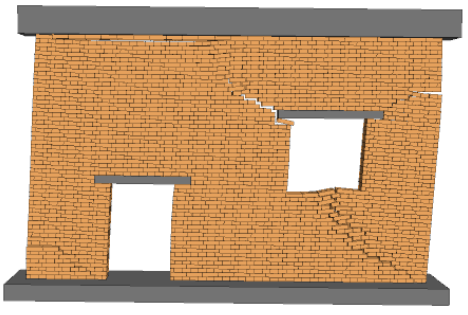

Masonry wall with OS 04 (17%)

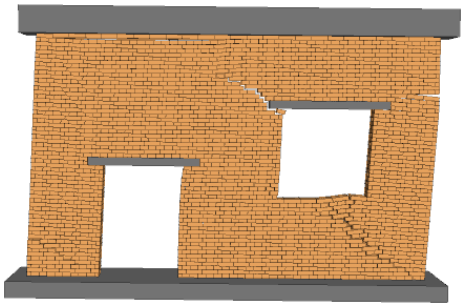

Masonry wall with OS 05 (24%)

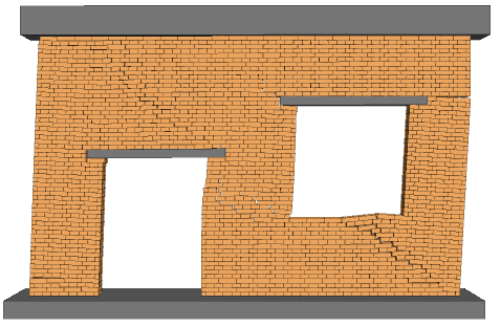

Masonry wall with OS 06 (32%)

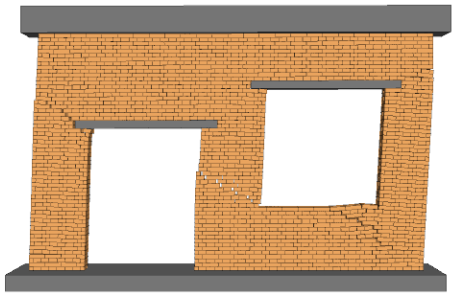

Masonry wall with OS 07 (41%)

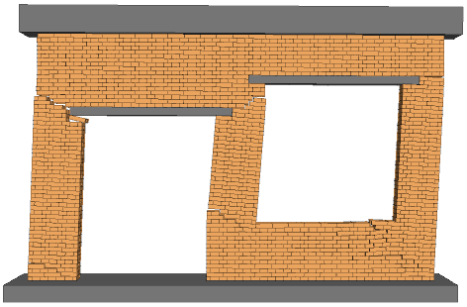

In summary, as the opening percentage increases the in-plane capacity reduces, often with changes to the failure mechanism. URM walls analysed using a force-based procedure show better capacity compared to walls analysed using a displacement-based procedure for the same opening percentage. For walls with the same opening percentage an adverse shape or location for the opening can result in significantly lower lateral strength and displacement capacity. Notably, the masonry walls with both door and window openings did not perform well even at small opening percentages which is of concern as this arrangement is common in real structures.

4.5. In-plane behaviour of masonry wall A with different opening positions

4.5.1 Cases considered for opening position effects under in-plane behaviour

As seen above, variation in the position of an opening in a URM wall can result in a change to the wall failure mechanism, creating more local failures and less wall integrity. To further evaluate the effect of opening position on the in-plane capacity of masonry walls, one model (Wall A) was built in 3DEC and many different opening positions were considered, see Figure 4.12. For Wall A, nine opening

positions (A1 to C3) were considered and analysed using both load-based and displacement-based pushover procedures.

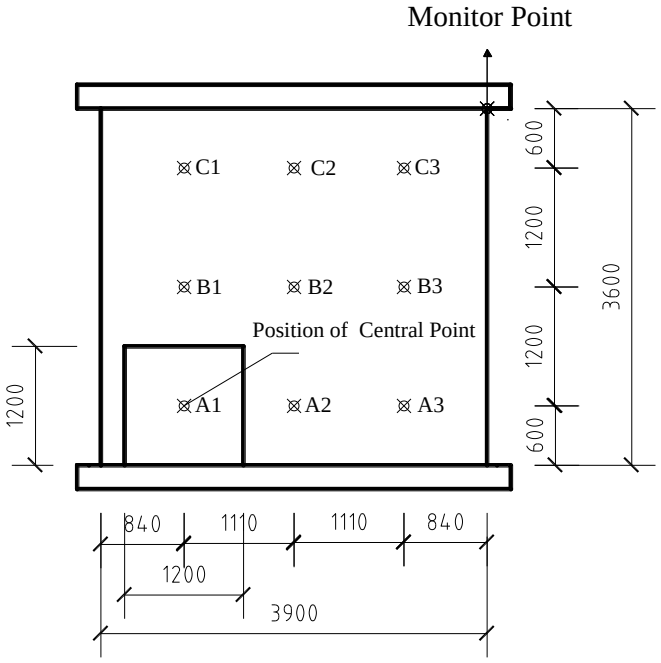

Figure 4.12 The geometry of numerical models in 3DEC with the different opening position for Case A

4.5.2 The in-plane capacity of masonry wall A with different opening positions under both loading patterns

To visualise the change in wall capacity for different opening positions using a load-based analysis procedure, contour plots of the wall capacity were created based on the centre point of the opening, see Figure 4.13. Similar plots using a displacement-based analysis procedure are shown in Figure 4.14.

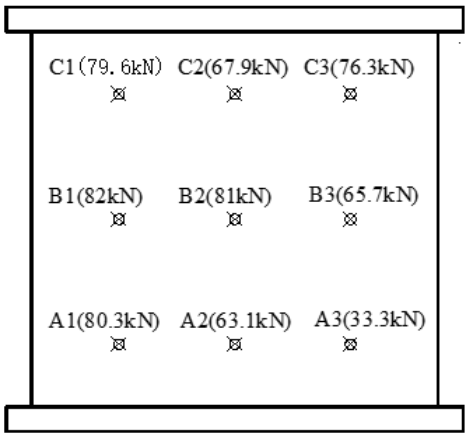

(a)

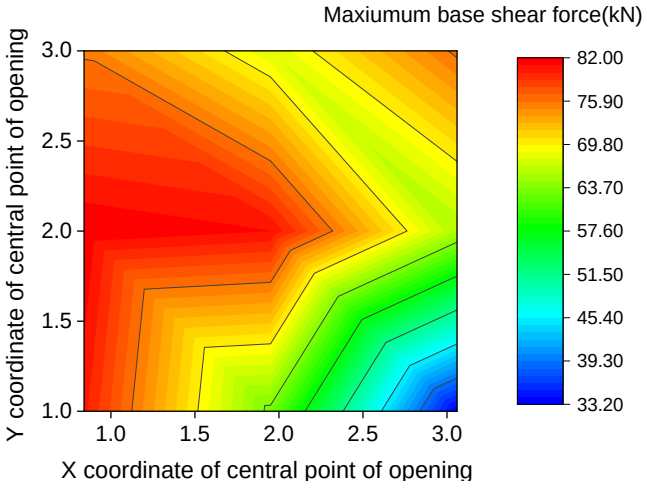

Figure 4.13 (a) Maximum base shear forces for the wall A for the 9 different opening positions, (b) Contour plot of maximum in-plane strength capacity of the wall for different opening positions; analysed using a load-based procedure

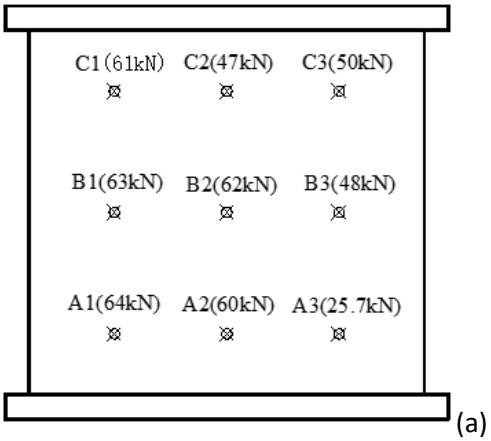

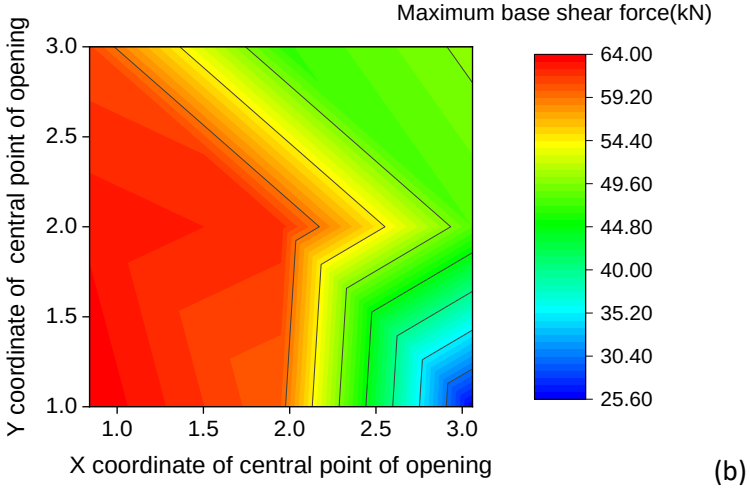

Figure 4.14 (a) Maximum base shear forces for the Wall A for the 9 different opening positions, (b) Contour plot of maximum in-plane strength capacity of the wall for different opening positions; analysed using a displacement-based procedure

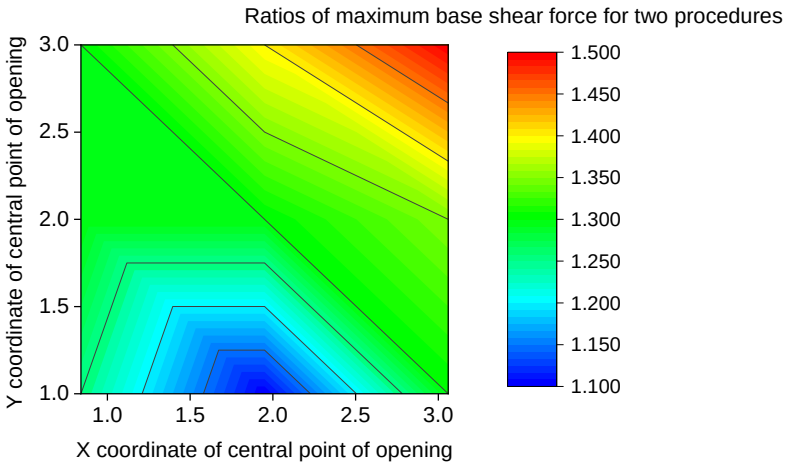

Figure 4.15 The comparison of maximum in-plane capacity for Wall A under the load-based analysis procedure and the displacement-based analysis procedure

Figure 4.13 shows that, for a load-based analysis, the in-plane capacity of the wall with an opening in the left or middle is higher than when the opening is in the right-hand side of the wall. The maximum capacity of the wall is lowest when the opening is located at the bottom right end of the diagonal compression strut. Figure 4.14 shows that the displacement-based analysis procedure results in similar distributions of in-plane capacity for the various opening positions although the wall capacities are lower for this analysis procedure.

In order to compare the differences in in-plane capacity for the two analysis approaches more easily, the ratios of the normalised in-plane capacity calculated using the load and the displacement-based methods are shown in Figure 4.15. This figure shows that the different analysis approaches generally produce similar distributions in both walls. The range of ratios varies from 1.1 to 1.5 but for most opening positions the difference in capacity from the two analysis methods is close 1.3. The only real differences are that for a displacement-based analysis an opening in the top right has a much worse impact on the wall capacity compared to a load-based analysis and while the reverse is true for an opening in the bottom middle of the wall. Overall, a central opening has the least impact on the wall performance, openings on the right side of the wall reduce the wall capacity, with openings in the bottom of the compression diagonal having a significant impact on the wall capacity.

4.5.3 Crack patterns for masonry walls with different opening positions

In Figure 4.14 the change of maximum in-plane capacity for Case A between the two loading patterns is displayed. It is noticeable that, when the opening occurs in a few particular locations, there is a distinct difference in the maximum in-plane capacity calculated for the load-based analysis procedure and the displacement-based analysis procedure. However, when the opening is in other locations there is very little difference between the results from the two analysis methods. The main differences are that for a displacement-based analysis an opening in the top right has a much worse impact on the wall capacity compared to a load-based analysis and while the reverse is true for an opening in the bottom middle of the wall. The difference between the capacities from the two procedures is then more than 50%. When the opening is located at the lower-left both analysis procedures give similar results. When the opening is located in other positions the difference in results ranges from 10% - 30%. It is clear that that the pushover procedure under different load patterns significantly affects the in-plane behaviour of walls with different opening positions and so the differences between the methods need to be explored further. To explore the reasons for the differences, the cracks patterns for different opening positions when the displacement of the top of the wall is 0.15m (4% drift) for both loading patterns are given in Table 4.9.

Table 4.9 In-plane crack patterns for Wall A with different opening locations when wall drift reaches 4% (0.15m)

	Load-based procedure	Displacement-based procedure
Opening position A1	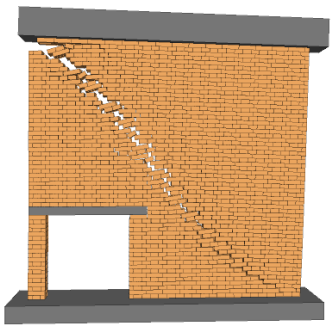	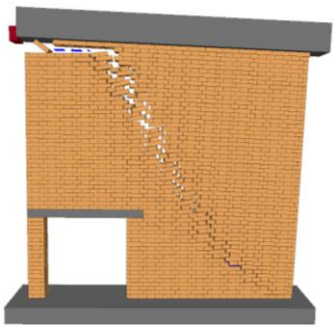
Opening position A2	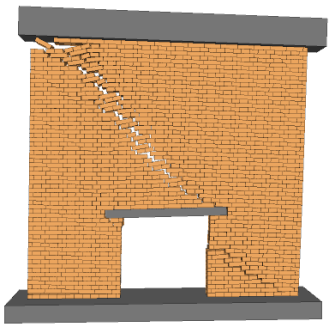	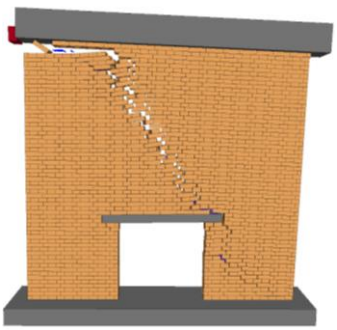

Opening position A3	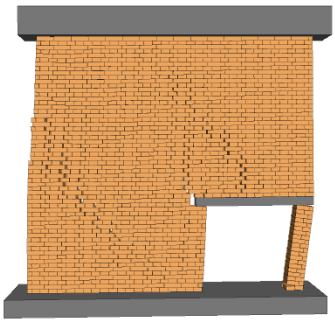	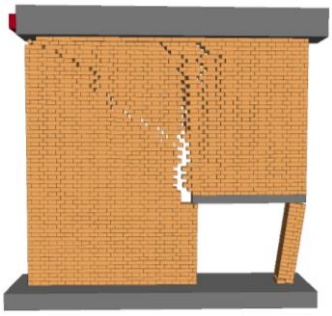
Opening position C1	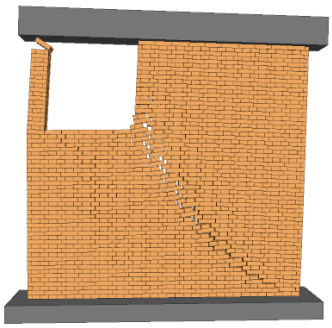	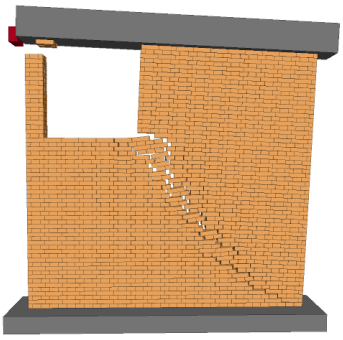
Opening position C2	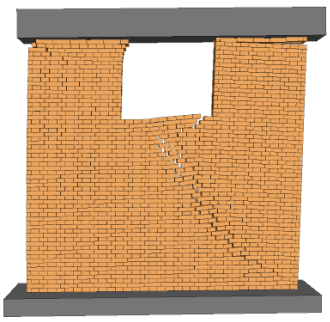	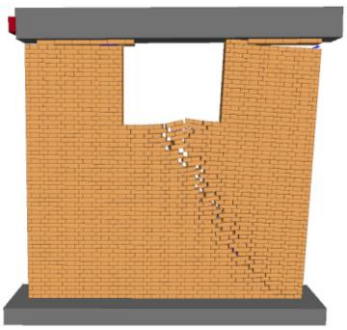
Opening position C3	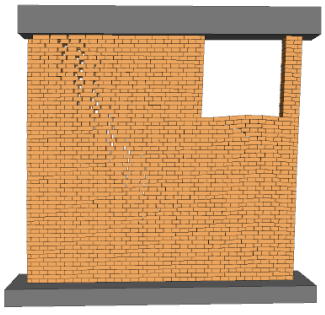	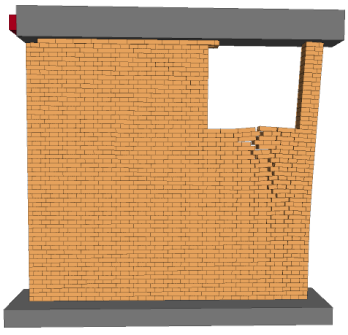

Opening position B2	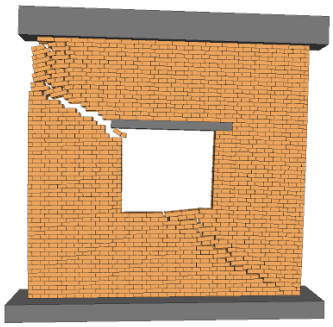	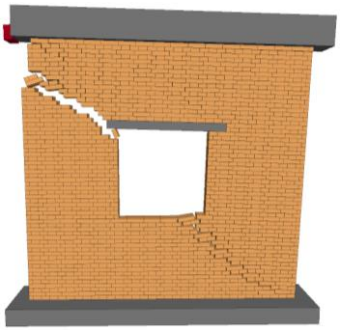

The variations in crack patterns shown in Table 4.9 help to explain the differences in the in-plane capacity calculated by the two methods and also show why locating the opening in the top left or bottom right of the wall has such a substantial effect on the wall capacity.

For opening position C3, where the difference in-plane capacity calculated by the two analysis methods is largest (see Figure 4.14), the crack patterns in the masonry wall are very different. Using a displacement-based analysis results in localised cracking below the opening whereas for the load-based analysis procedure the crack runs as one diagonal through the wall. For opening position A3, again there is an obvious difference in the behaviour of the walls, the masonry walls analysed using a load-based analysis procedure displaying more distributed cracking than the walls analysed using a displacement-based procedure. These results again highlight the importance of accounting for the way the loading is applied to the walls. For the load-based analysis where each brick is subjected to a force proportional to its mass, the distributed loading applied the whole wall results in more distributed cracking. However, for the displacement-based analysis method where the loading is applied across the wall as a whole this results in fewer larger localised cracks. These differences are emphasised when the opening is moved closer to the edges of the wall as any change to a local failure pattern leads to a significant change in wall capacity.

Overall, the in-plane capacity of masonry walls is sensitive to both location and size of opening under both load patterns, but in different ways. The masonry walls analysed using a displacement-based procedure were sensitive to local failures and generally showed a lower in-plane capacity compared to identical walls analysed using a load-based procedure. However, pushover tests using a load-based analysis procedure closer reflect the global behaviour of structures and are a better representation of seismic loading, so both load procedures can be helpful for identifying the capacity of URM walls with openings.

4.6. In-plane behaviour of masonry wall B with different opening positions

4.6.1 Cases considered for opening position effects under in-plane loading

As discussed in 4.5.1, to further evaluate the effect of opening position on the in-plane capacity of masonry walls, another model (Wall B) was built in 3DEC and many different opening positions were considered, see Figure 4.16. For Wall B, fifteen opening positions (A1 to C5) were considered and analysed using both load-based and displacement-based pushover procedures.

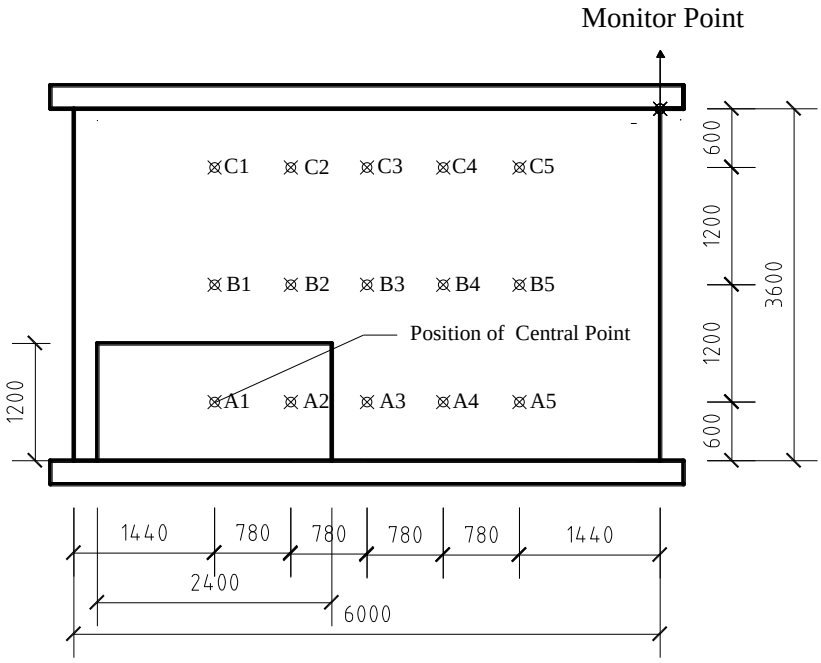

Figure 4.16 The geometry of numerical models for Wall B in 3DEC with different opening positions

4.6.2 The in-plane capacity of masonry wall B with different opening positions under both loading patterns

To visualise the change in Wall B capacity for different opening positions using a load-based analysis procedure, contour plots of the wall capacity were created based on the centre point of the opening, see Figure 4.16. Maximum base shear forces and the maximum forces of Wall B for an opening at different positions analysed using a load-based analysis procedure are shown. Similar plots for Wall B using a displacement-based analysis procedure are shown in Figure 4.17.

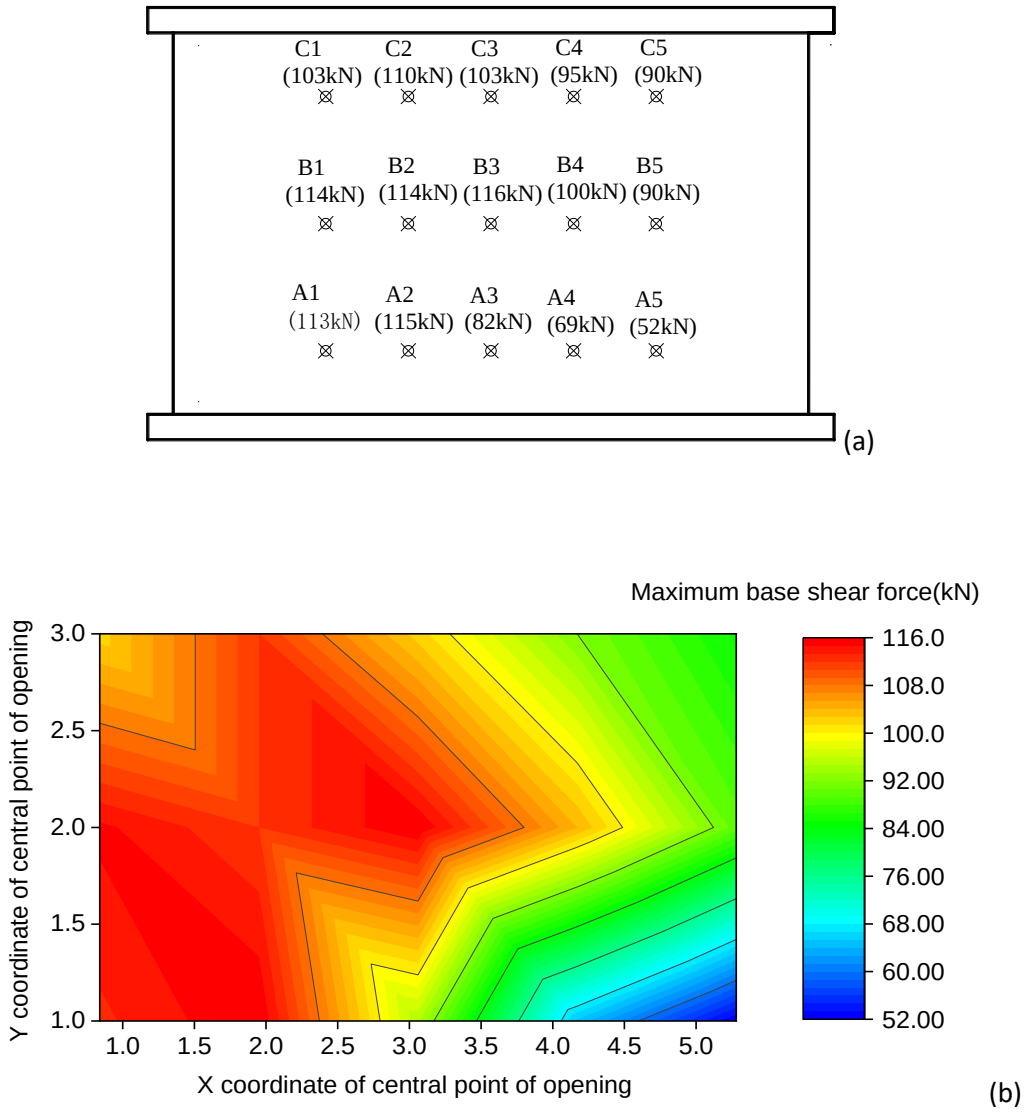

Figure 4.17 (a) Maximum base shear forces for the Wall B for the 15 different opening positions, (b) Contour plot of maximum in-plane strength capacity of the wall for different opening positions; analysed using a load-based analysis procedure

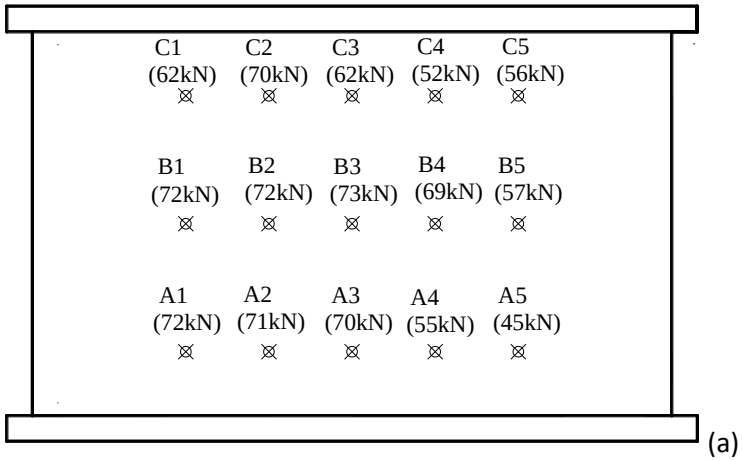

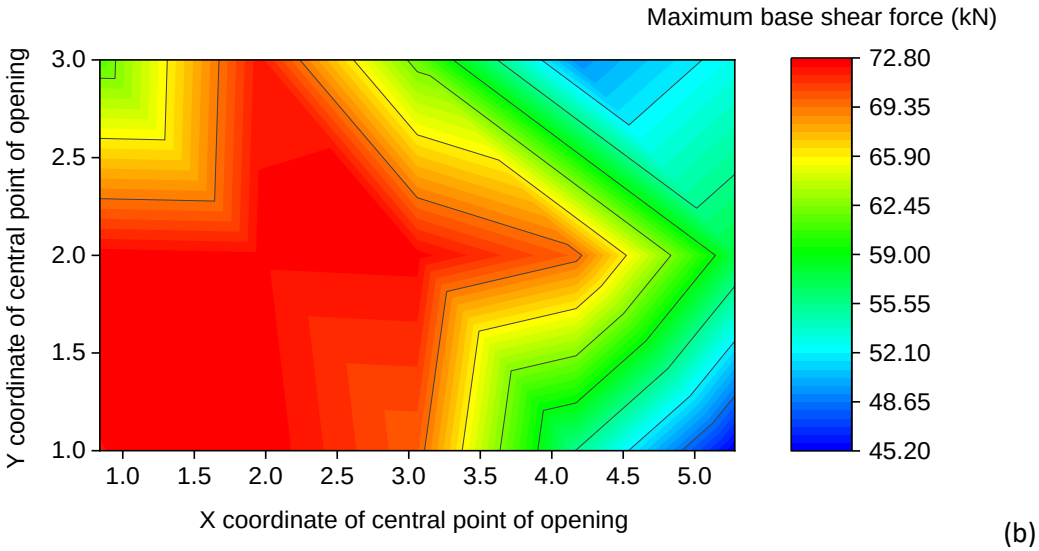

Figure 4.18 (a) Maximum base shear forces for the wall B for the 15 different opening positions, (b) Contour plot of maximum in-plane strength capacity of the wall for different opening positions; analysed using a displacement-based analysis procedure

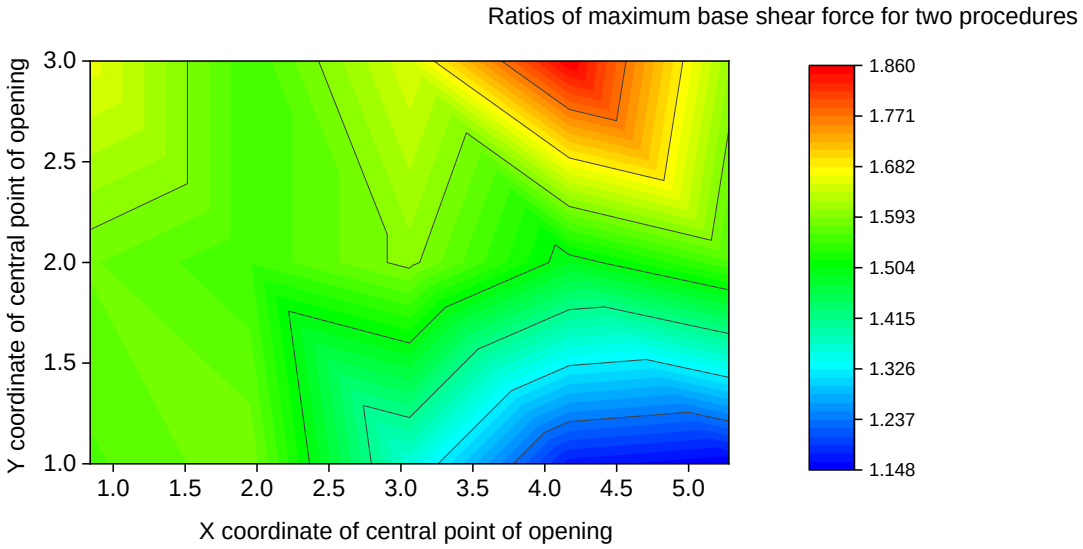

Figure 4.19 The comparison of maximum in-plane capacity for Wall B under a load-based analysis procedure and a displacement-based procedure

Figure 4.17 shows that the load-based analysis procedures result in slightly different distributions of in-plane capacity for the various opening positions in Wall B. For the maximum base shear force, the in-plane capacity of the wall with an opening in the left or middle is higher than when the opening is in the right-hand side of the wall. The value of the maximum base shear force of the wall is lowest when the opening is located at right end of the diagonal compression strut, and when the opening moves toward the upper right side of the wall, the wall carries a higher force.

Figure 4.18 shows that the displacement-based analysis procedure results in different distributions of in-plane capacity for the various opening positions in Wall B. For the maximum base shear force, the in-plane strength capacity of Wall B follows a similar pattern to the load-based analysis procedure where an opening positioned at the left or middle side has less impact on the wall. The lowest base shear force occurs when the opening is located at the bottom right end of the diagonal compression strut.

The maximum base shear force for an opening located at different positions in Wall B using load-based procedure generally shows a higher value than for a displacement-based analysis procedure. In order to compare how the differences in in-plane strength capacity change with different opening positions for the two analysis approaches more efficiently, for both walls the ratios of the normalised in-plane capacity calculated using the load and the displacement-based methods are shown in Figure 4.19. This figure shows that the different analysis approaches result in similar differences in both walls. The

ratios range from 1.1 to 1.8 and most positions the ratio is about 1.6. It can be seen that the results from both analysis procedures follow similar trends and the ratios of maximum base shear are similar.

Combining the results from wall A and wall B, both walls show a similar trend as the opening position moves and there are few differences between the two wall shapes. Therefore, the varying shape of walls appears to have little impact on the in-plane capacity of the wall for opening positions, although the opening position clearly does impact the wall strength.

4.6.3 The crack patterns in masonry walls for different opening positions

Looking at Figures 4.17 and 4.18 which give the maximum in-plane capacity for Wall B under both loading patterns it is clear that while some opening locations produce very similar results there are a few opening locations that result in distinct differences in the maximum in-plane capacity. The biggest difference between the two load patterns appears at the top-right corner where the in-plane capacity of the masonry wall using the load-based analysis procedure is close to its highest value while for same wall and opening analysed with the displacement-based procedure the capacity is less than 75% of maximum capacity recorded for all opening positions. The masonry wall with the opening located at bottom left show similar in-plane performance for both load patterns. For most opening positions the difference in capacity ranges from ~40% - ~60%. However when the opening is located in a critical location the difference in results varies by up to ~85%. It is clear that that the pushover procedure under the different load patterns significantly affects the in-plane behaviour of walls with different opening positions and so the differences between the methods need to be explored further. To explore the reasons for the differences, the crack patterns for different opening positions when the displacement of the top of the wall is 0.15m (4% drift) for both loading patterns are given in Table 4.10.

Table 4.10 In-plane crack patterns for Wall B with different opening locations when wall drift reaches 4% (0.15m)

	Load-based procedure	Displacement-based procedure
Opening position A1	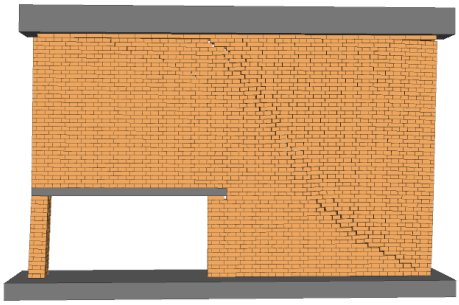	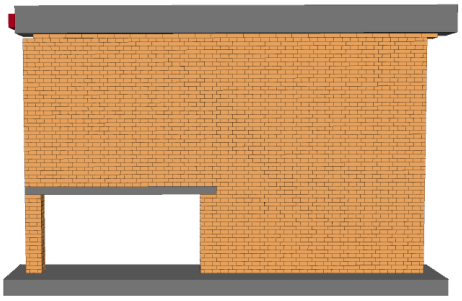
Opening position B1	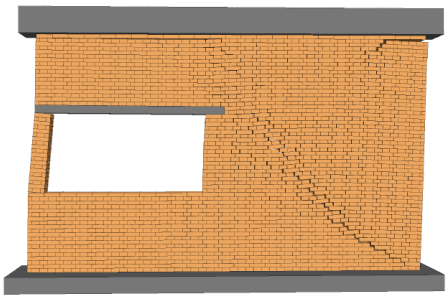	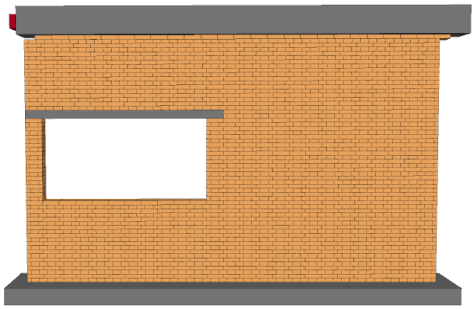
Opening position C1	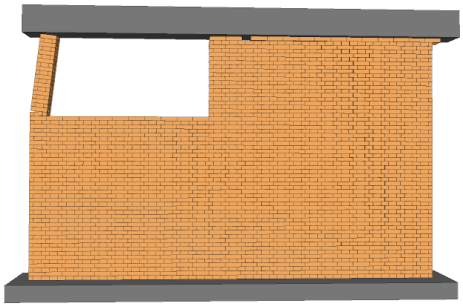	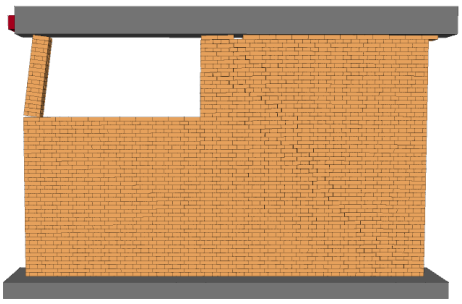
Opening position A2	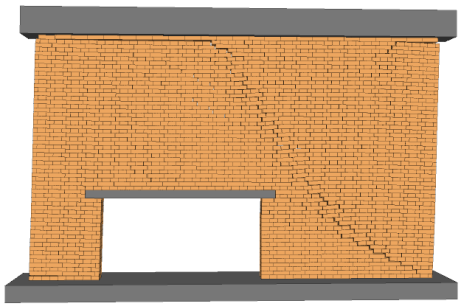	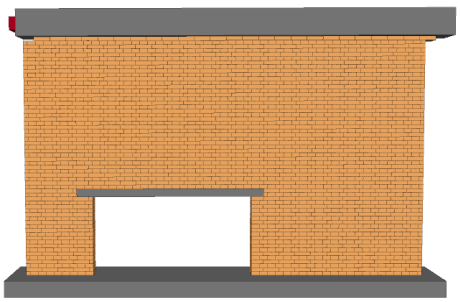

Opening position B2	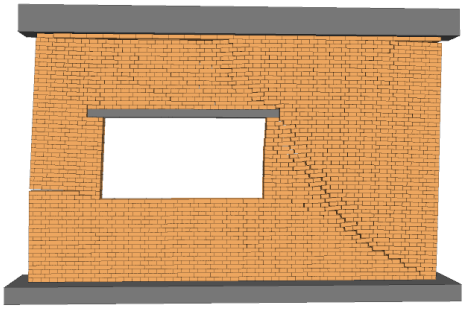	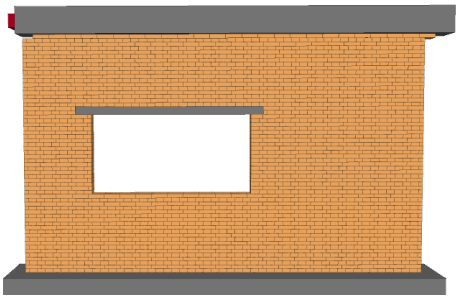
Opening position C2	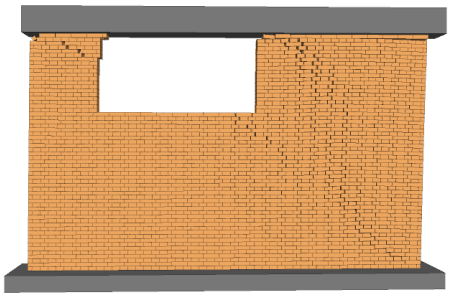	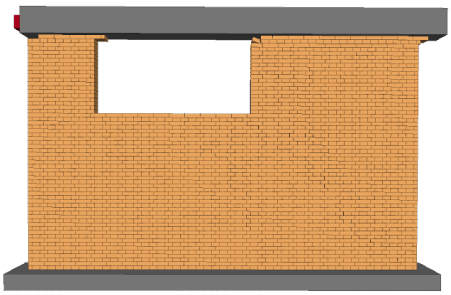
Opening position A3	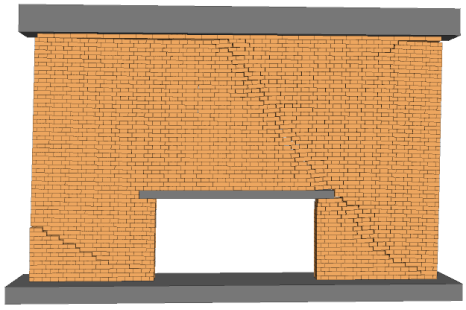	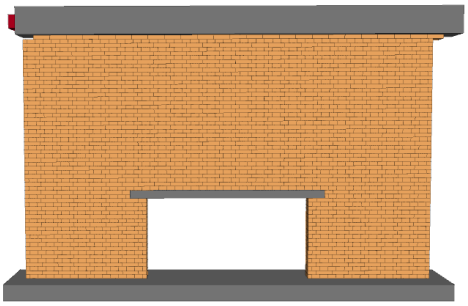
Opening position B3	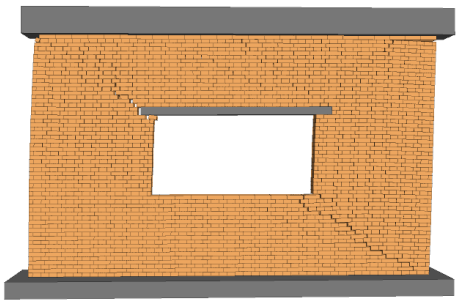	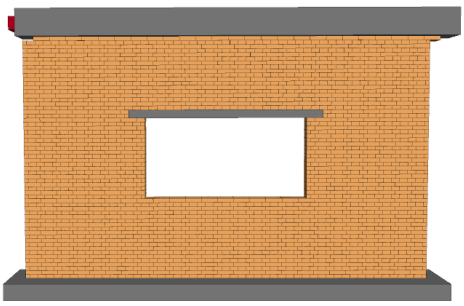
Opening position C3	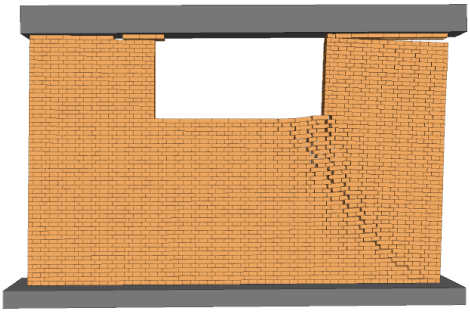	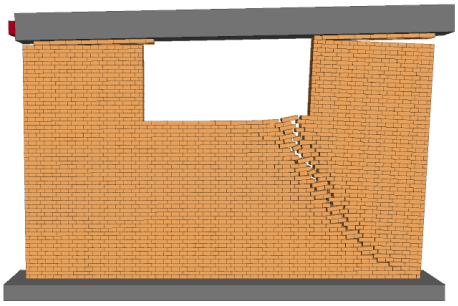

Opening position A4	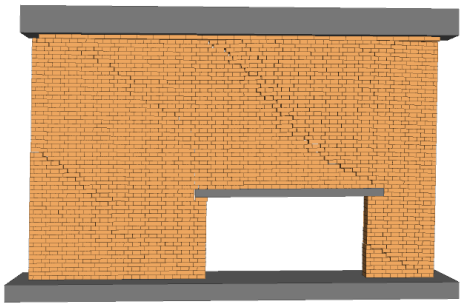	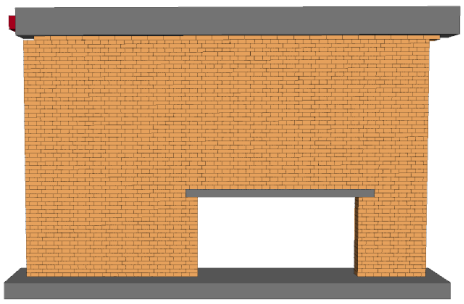
Opening position B4	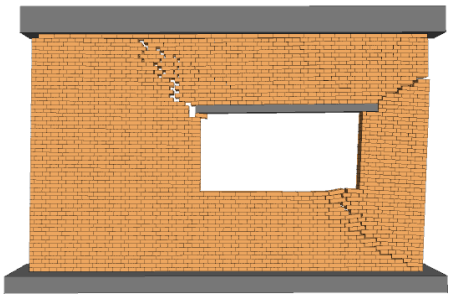	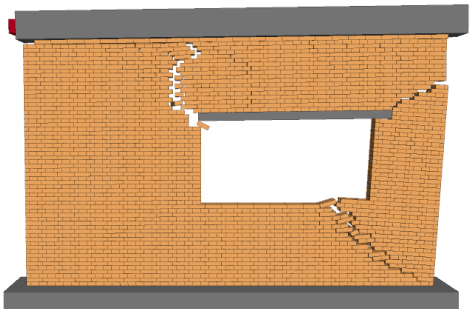
Opening position C4	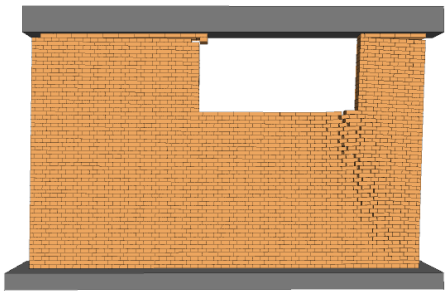	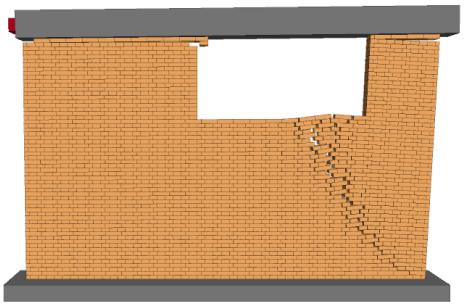
Opening position A5	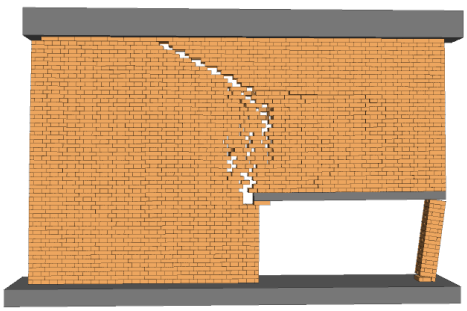	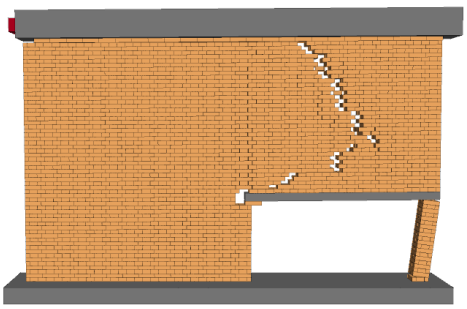
Opening position B5	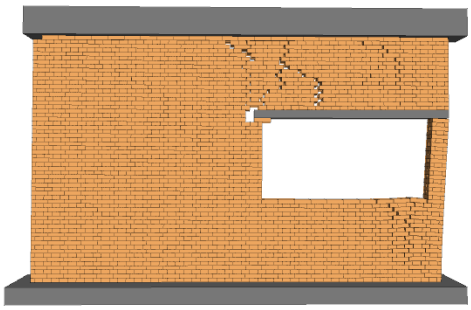	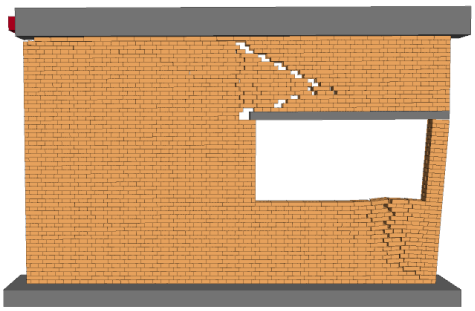

Opening position C5	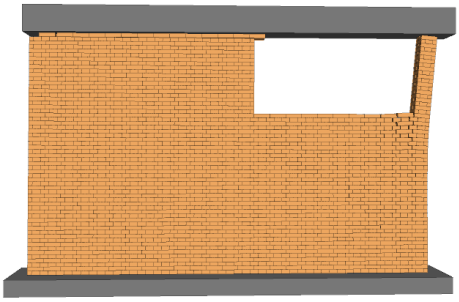	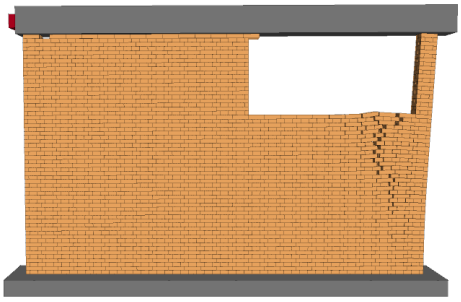

The variations in crack patterns shown in Table 4.10 help to explain the differences in the in-plane capacity calculated by the two methods and also show why locating the opening near the top left or at the bottom right of the wall has such a large effect on the wall capacity.

For the load-based analysis procedure, more distributed failures occur and the diagonal cracks are apparent in the figures. However, for the displacement-based analysis procedure, more shear failure occurs and some walls e.g. A1, B1, A2, B2, A3 and B3 show a sliding failure of the top block and relatively few cracks develop in the walls. For most opening positions, a visible difference in cracking pattern appears between the two analysis methods. For the masonry wall analysed with a load-based analysis procedure there are generally several distributed cracks and diagonal cracks in the wall. This compares with a much more localized failure for displacement-based analysis procedure.

These results again highlight the importance of accounting for the way the loading is applied to the walls. For the load-based analysis where each brick is subjected to a force proportional to its mass, the distributed loading applied the whole wall results in more distributed cracking. However, for the displacement-based analysis method where the loading is applied across the wall as a whole this results in fewer larger localised cracks. These differences are emphasised when the opening is moved closer to the edges of the wall as any change to a local failure pattern leads to a significant change in wall capacity.

4.7 Summary

This chapter presents the impact of opening size and position on the in-plane capacity of URM walls. A DEM micro modelling approach was used to parametrically analyse several URM walls containing openings. The wall capacities have been calculated using pushover analyses following both load-based and displacement-based procedures. The key conclusions from this part of the research are:

1. DEM (using 3DEC) can successfully simulate the quasi-static response of URM walls. This modelling approach allows observation of the progression of the failure patterns up to, and beyond, collapse of the walls.
2. The relationships between opening size and the capacity of a URM wall have been evaluated. The in-plane capacity of masonry walls decreases as the opening size increases. However, URM walls analysed using a load-based analysis procedure consistently have a lower base shear force than walls analysed using a displacement-based procedure when the opening percentage is under 40%. When the opening size exceeds 40%, both base shear forces are similar.
3. A variation in the number and shape of the opening(s) often changes the failure mechanism in URM (even when the % area of the opening remains constant) and may lead to soft storey type failures, significantly reducing the wall strength.
4. For walls with a central opening, when the % opening is less than ~10% the wall retains >80% of the intact wall capacity, which is more conservative than the provisions of Chinese code. Once the opening exceeds ~50%, only about 10% residual wall capacity remains.
5. DE modelling allows the crack patterns in masonry walls to be observed clearly and there is a clear link between the failure mechanism and the in-plane capacity of the masonry walls. The differences in the pushover curves developed for different opening percentages directly reflect differences in the crack propagation within the walls. Diagonal cracking and rocking are the major failure mechanisms for URM wall under in-plane loading. In general, the masonry walls analysed using a load-based analysis procedure show more localised cracking than those analysed using a displacement-based procedure and the maximum base shear force from load-based analysis procedure is also lower than from a displacement-based procedure.
6. For simple pushover analyses the direction of applied loading needs to be considered when evaluating failure patterns for in-plane loading. When using a displacement-based analysis procedure, the in-plane wall capacity is reduced when the openings are located along in the line of the diagonal compression strut compared to when the opening is the location along the other diagonal.
7. The difference in the performance of URM walls (with the opening in different positions) calculated using load and displacement-based procedures comes from the fact that under the displacement-based procedure a uniform force is applied across the whole wall, whereas for a load-based analysis, the load is applied at every single block, which tends to lead to more distributed failures.

8. For this work the masonry bricks were modelled as rigid blocks and the possibility of any crushing of the bricks was ignored because for most URM walls the behaviour is controlled by the properties of joints. However, the behaviour of masonry walls is sensitive to joint properties so further sensitivity studies may be needed.
9. This research shows that the size and location of openings in URM walls can have a significant effect on the in-plane capacity of the wall. Pushover analyses are useful tools for the assessment of URM wall capacities, but it is worth noting that load-based procedures and displacement-based procedures produce different results and load-based procedures reflect the real response of structures and suitable to be applied in the next chapters.

Chapter 5 EFFECT OF OPENINGS ON OUT-OF-PLANE BEHAVIOUR OF URM WALLS

5.1 Introduction

It is important to identify the out-of-plane behaviour of URM walls because it is common during earthquakes and lead to serious damage. Previous research has proved that the out-of-plane capacity of walls is highly dependent on the thickness of the walls, but the research considering the effects of openings under out-of-plane behaviour need further investigation. Therefore, this chapter focuses on the impacts of opening sizes and positions on the out-of-plane capacity of URM walls. A series of 3DEC quasi-static analyses have been used to evaluate the relationships between size and position of openings and out-of-plane capacity. The same methodology is used as in the chapters above, but it should nevertheless be noted that for the following analyses a quasi-static loading procedure has still been applied. For these simulations, the horizontal forces are applied in increments until failure occurs. The reaction forces are calculated during the analysis and a few monitor points are used to record the maximum displacements of the wall to create the load-displacement curves. For the boundary conditions, and in particular for the four-side supported boundary condition, some freedom of rotation had to be allowed because arching would occur if all the rotational degrees of freedom were fixed, leading to unrealistically high capacities for the walls. To develop the load-displacement curves and replicate the out-of-plane loads applied in an earthquake, the loading was applied as a pressure on the face of the wall which is equivalent to applying acceleration directly. This loading approach was adopted because the model analysis time for applied pressure loading was significantly quicker than for when a lateral acceleration was applied. Crack patterns could be observed clearly in 3DEC during the progress of the simulation. To identify the crack propagation patterns in the walls, the out-of-plane displacements of joints were calculated and were then plotted to infer the crack patterns.

5.2. URM walls modelling in 3DEC

5.2.1 Geometry

The geometric models of the masonry walls were built in 3DEC. To replicate the response of realistic masonry walls, the walls were built as double skin walls using a Flemish bond, the size of each masonry block was set as 0.06m x 0.24m x 0.12m (height x span x breadth), and the dimensions of masonry walls were 3.9m x 0.24m x 3.6m (length x width x height). The support wall was set as 1.08m x 0.24m x 3.6m (length x width x height). The detailed geometry of the models is shown in Figure 5.1.

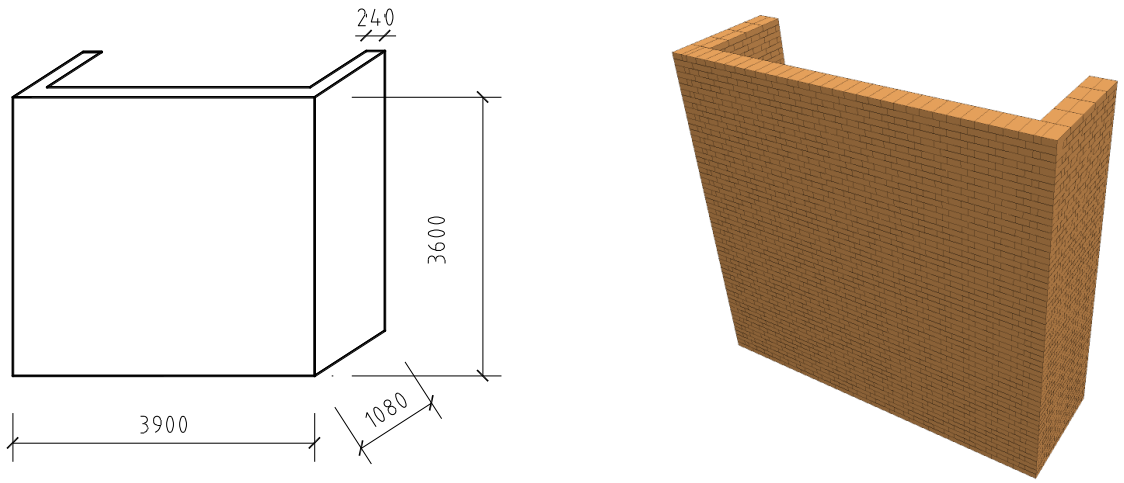

Figure 5.1. Geometry and numerical model of the masonry wall in 3DEC for out-of-plane loading

5.2.1 Material properties of blocks and joints

To improve the efficiency of the analytical process, the bricks were modelled using rigid blocks. For this type of rigid block model, the joint stiffness must represent the deformability of both block and joint. If E and G are the Young's and Shear moduli of the material respectively, then the calculated joint stiffnesses are given in Table 5.1.

The cohesion of joints in 3DEC was determined based on Equation 3.11, and τ_{max} and $\sigma_{n(max)}$ can be calculated when the compressive strength and tensile strength of bricks have been obtained based on information in design codes or from experimental results. The tensile strength of joints was taken as half of the cohesion strength (Lemos and Costa, 2017). The compressive strength of brick in this

research was taken as 1.83MPa, the average tensile strength of brick as 0.13MPa and the shear strength of brick as 0.11MPa as mentioned in 4.2. The friction angle was assumed to be 35 degrees, which is consistent with the values given in (Sarhosis and Sheng, 2014) for other 3DEC analyses. The final calculated properties used in the 3DEC model are given in Table 5.1 below:

Table 5.1 Properties of masonry blocks and joints

Density of blocks [kg/m³]		Joint normal stiffness [MPa/m]	Joint shear stiffness [MPa/m]	Joint friction angle [Degrees]	Joint tensile strength [MPa]	Joint cohesion [MPa]
1800	Vertical joints 1	35600	14240	35	0.1	0.2
	Vertical joints 2	17800	7120	35	0.1	0.2
	Horizontal joints	71200	28480	35	0.1	0.2

To consider the impact of different boundary support conditions on the behaviour of the walls both three-side and four-side supported walls have been analysed, in both cases identifying the effects of openings on their performance.

5.3 Effect of openings and lintels on masonry walls under out-of-plane behaviour (three-side supported boundary condition)

5.3.1 Effect of opening size for masonry walls under out-of-plane behaviour

The opening percentage is important for masonry walls under out-of-plane behaviour, with a poor opening not only affecting the strength of the masonry wall but the opening could also lead to local

failure and even collapse. Thus, it is necessary to identify the impacts of opening percentage on out-of-plane wall response and develop the relationship between out-of-plane performance and the opening size. Therefore, seven cases with different opening percentages have been considered. Opening sizes ranging from 0 to 31% were selected and the relevant numerical models were built-in 3DEC. Note that a 31% opening is realistically the largest opening to be still representative of a wall in a URM structure as larger openings could lead to a masonry wall becoming more like a frame rather than a wall. The pre-compression load on the wall was 0.1MPa and consistent. Then an out-of-plane pressure increment was applied until failure occurred. Although the wall boundaries were rigid the walls were connected to the boundaries in such a way that rotational degrees of freedom were still allowed. The detailed model information is shown in Figure 5.2.

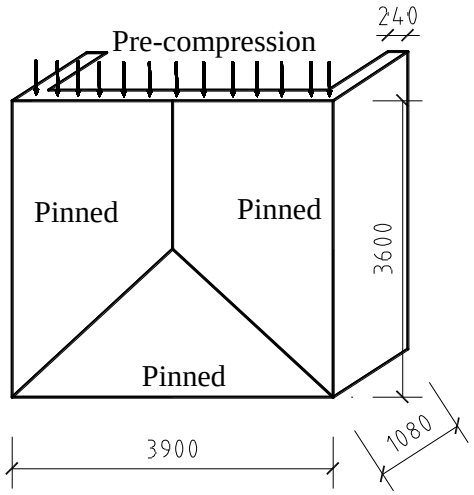

(a) wall geometry and boundary information

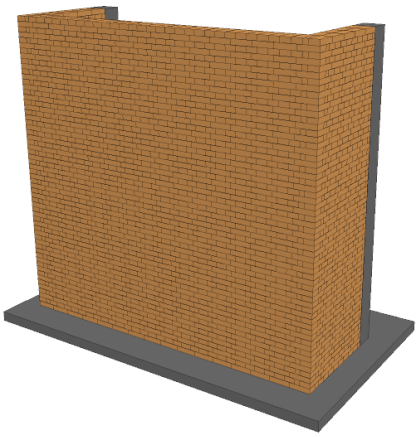

(b) view 1 of masonry wall in 3DEC

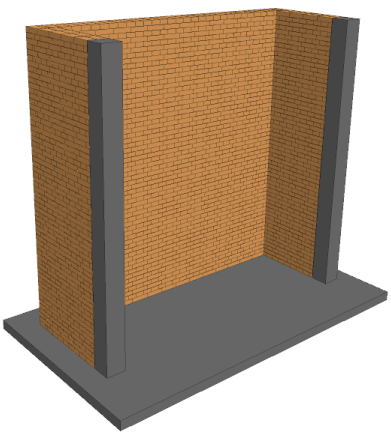

(c) view 2 of masonry wall in 3DEC

Figure 5.2 Wall information and numerical model in 3DEC for the three-side supported boundary condition

Using the material properties given above and by applying out-of-plane loads in 3DEC, the effects of opening percentage have been identified and load-displacement curves, as well as crack patterns, are given below. Inspection of the pressure-displacement curves in Figure 5.3(a) shows that the peak values of applied pressure (that cause failure) increase as the opening percentage increases. The masonry wall without opening carries the lowest applied pressure (9kPa) compared with other cases. When the opening percentage is over 10%, the peak value of applied pressure increases significantly, and the maximum applied pressure occurs for the opening percentage of 31% at 24.2kPa. The load-displacement curves in Figure 5.3(b) show that the wall without an opening carries the lowest applied load (135kN) and the wall with the opening percentage of 31% carries the highest value (230kN). Looking at the results from both the pressure-displacement and load-displacement figures, the relationships between opening percentage and out-of-plane performance follow similar trends.

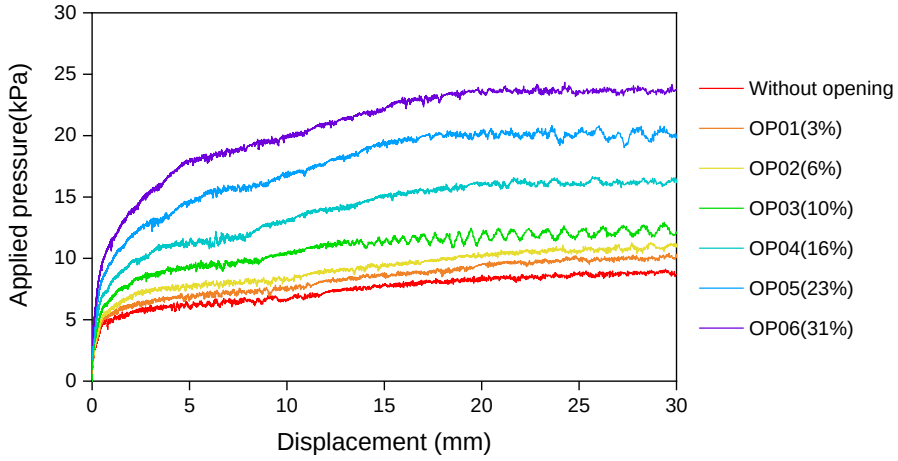

(a) Pressure-displacement curves for masonry wall with different opening percentage

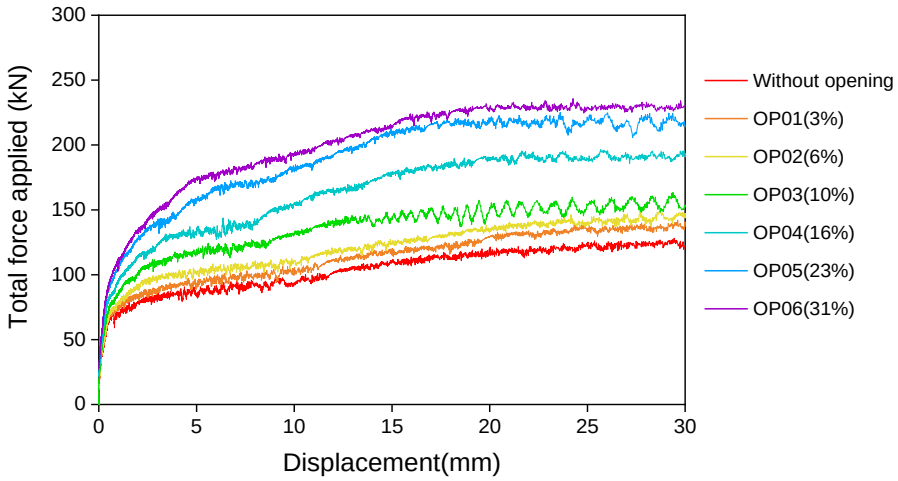

(b) Load-displacement curves for masonry wall with the different opening percentage

Figure 5.3 Results of masonry wall with different opening percentage

The crack patterns for the masonry walls with different opening percentages under out-of-plane loading are also presented in Table 5.2. In the analysis, to identify the crack pattern clearly, the maximum allowed crack length is 0.05m and once the crack length is over the value, the coulour is marked as red. From this table it is clear that the opening has a significant effect on the crack patterns as the opening percentage increases. When the opening percentage is over 10%, more localised failure occurred around the sides of the opening. When the opening percentage reached 30%, the bricks located at the bottom of the masonry wall suffered significant damage. Moreover, the bottom part of masonry walls tended to fail more quickly than the top part. This can be explained as an effect of the lintels which are always located in the top part of the wall and which increase the strength of that part of the wall. These results suggest that the region below openings is particularly vulnerable in URM walls subjected to seismic loading.

Table 5.2 Crack patterns in masonry walls with different opening percentages under out-of-plane loading (Maximum allowed crack length is 0.05m)

Peak Value of applied pressure	Crack pattern
without opening (9kPa)	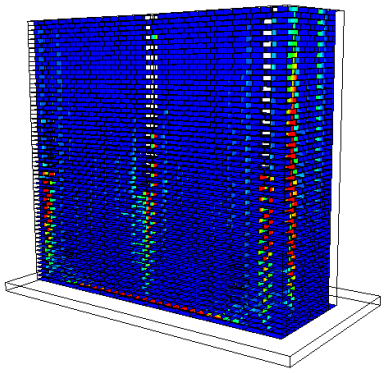

OP3% (10kPa)	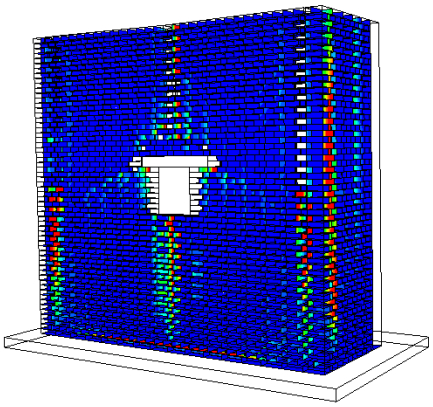
OP6% (11.5kPa)	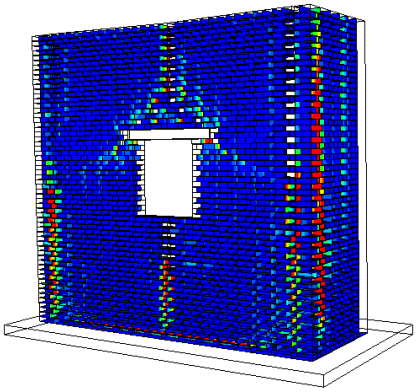
OP10% (13kPa)	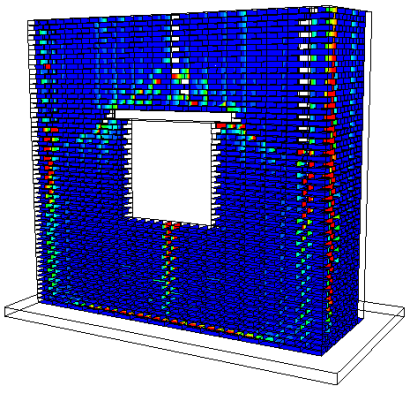

OP16% (16.5 kPa)	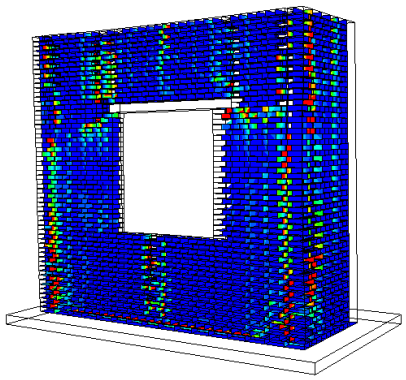
OP23% (20kPa)	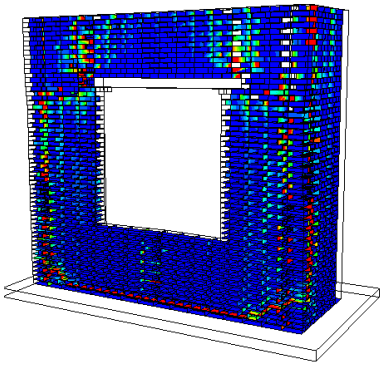
OP31% (24.2kPa)	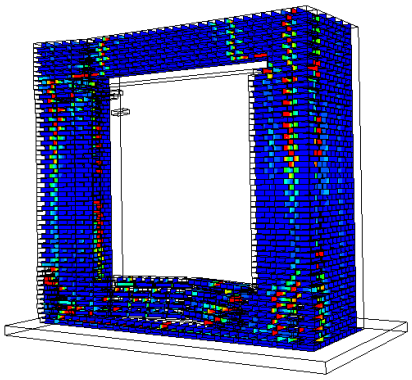

The reason that larger openings in three-side supported masonry walls leads to increased out-of-plane performance can be explained by observing that walls with this type of boundary condition lack support along their top surface but when the masonry walls include openings then lintels need to be added into the walls. The lintel then increases the stiffness and limits the displacement of the wall, which increases the capacity of the wall against out-of-plane behaviour to some extent. Therefore, it is necessary to identify the effects of the lintel on the out-of-plane behaviour of walls supported on only three sides.

5.3.2 Effect of lintels in masonry walls under out-of-plane loading

To evaluate the effects of just the lintels (and not the openings), a number of analysis cases were considered. The masonry walls did not contain openings but a lintel was included as if an opening were present. A lintel sized a 1680mm×240mm×120mm was used and the locations of lintel were varied to explore the impact of lintel position on the out-of-plane capacity.

The results of out-of-plane analyses, including load-displacement curves and crack patterns of masonry walls are given below. Inspection of curves in Figure 5.4 shows that all the masonry walls that included lintels carried higher peak values of applied pressure compared to the wall with no lintel, the maximum difference being an increase of around 57%. Of the analyses, masonry wall cases 01 and 02 showed the best performance and carried similar peak applied pressures of 11.2kPa while the other three walls were similar and carried a pressure of 9.8kPa.

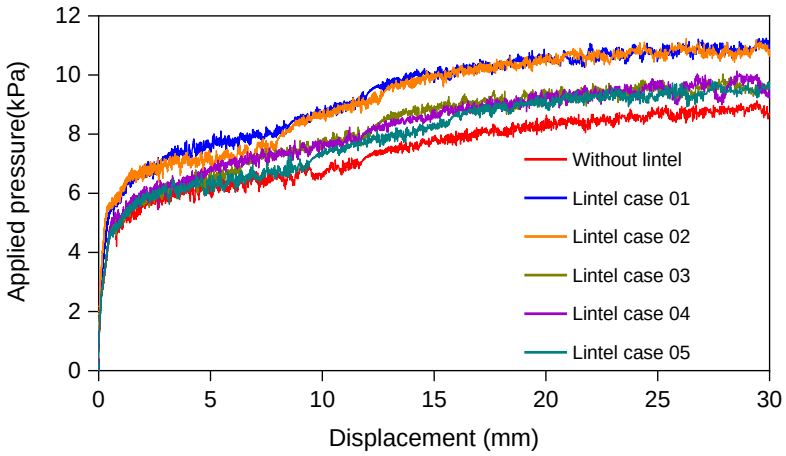

Figure 5.4 Pressure-displacement curves for masonry walls with different lintel positions under out-of-plane loading

The crack patterns in Table 5.3 illustrate the impact of the position of a lintel on the out-of-plane behaviour of the masonry wall. For masonry walls 01 and 02, the lintel restricts the displacement of the bricks located in the top part of the wall and significantly increases the strength of the wall. The stepped vertical cracks also possess a reserve of post-cracking moment capacity due to torsional resistance from the friction in the joints. Even though some local failure occurs around the lintel, the global behaviour still shows the best performance compared to other situations. For masonry walls 03, 04 and 05, the lintels are not located directly in the path of the main failure mechanism and provide less restriction to the wall displacement, so the improvement of post-cracking capacity is less obvious.

Table 5.3 Crack patterns in masonry walls with different lintel positions under out-of-plane loading (Maximum allowed crack length is 0.05m)

Peak Value of applied pressure	Crack pattern
Masonry wall 01 (11.2kPa)	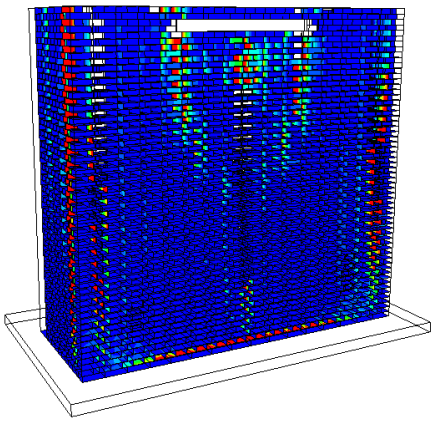
Masonry wall 02 (11.2kPa)	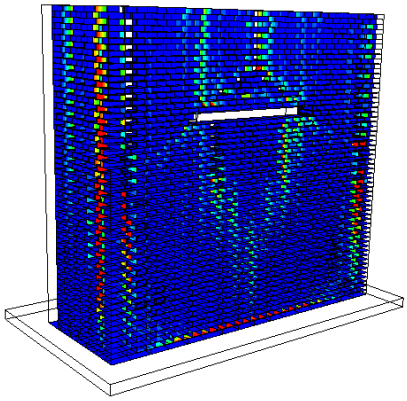
Masonry wall 03 (9.8kPa)	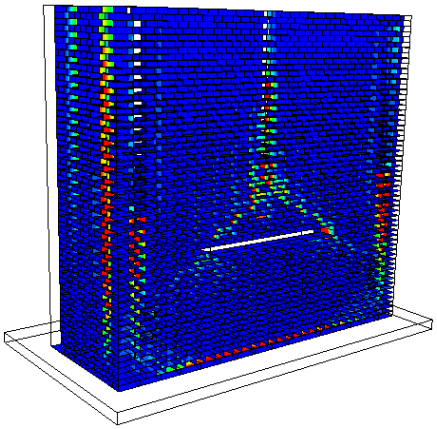

Masonry wall 04 (9.8kPa)	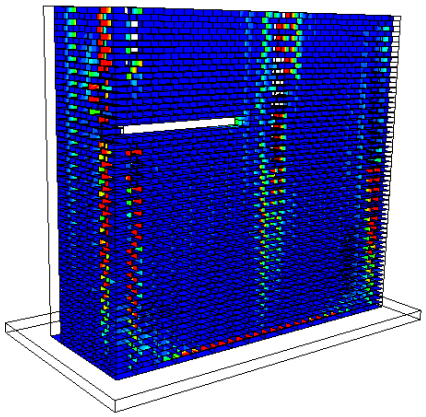
Masonry wall 05 (9.8kPa)	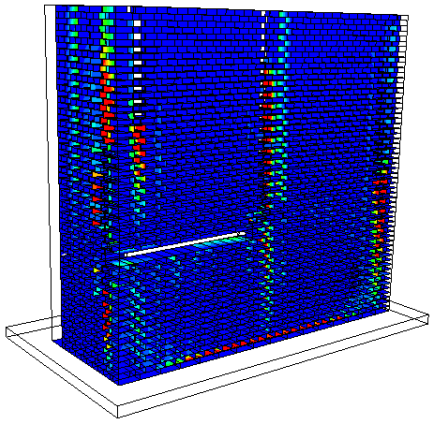

The results show that the lintels above openings can take the role of a ring beam, especially when the lintel is located at the top of the wall. If the lintel lies towards the sides or bottom of the wall, the improvement in out-of-plane performance is less obvious but there is still an improvement in capacity over a wall without a lintel. To observe the effects of lintels more clearly, a wall with a two-side supported boundary condition (contact interfaces located at the bottom boundary were set to have zero cohesion, tensile strength and friction angle) was built. Results for the intact wall and the wall with a lintel and opening are compared in Figure 5.5. The load-displacement curves and crack patterns in walls illustrate that the wall with the opening and lintel carries a higher total horizontal force than an intact wall. Even though the opening reduces the stiffness of wall, the lintel interrupts the failure mechanism at the top of the wall and restricts the displacements of bricks, which improves the out-of-plane capacity. The “ring beam” effect of the lintel is clear from the change in the failure mode of the wall.

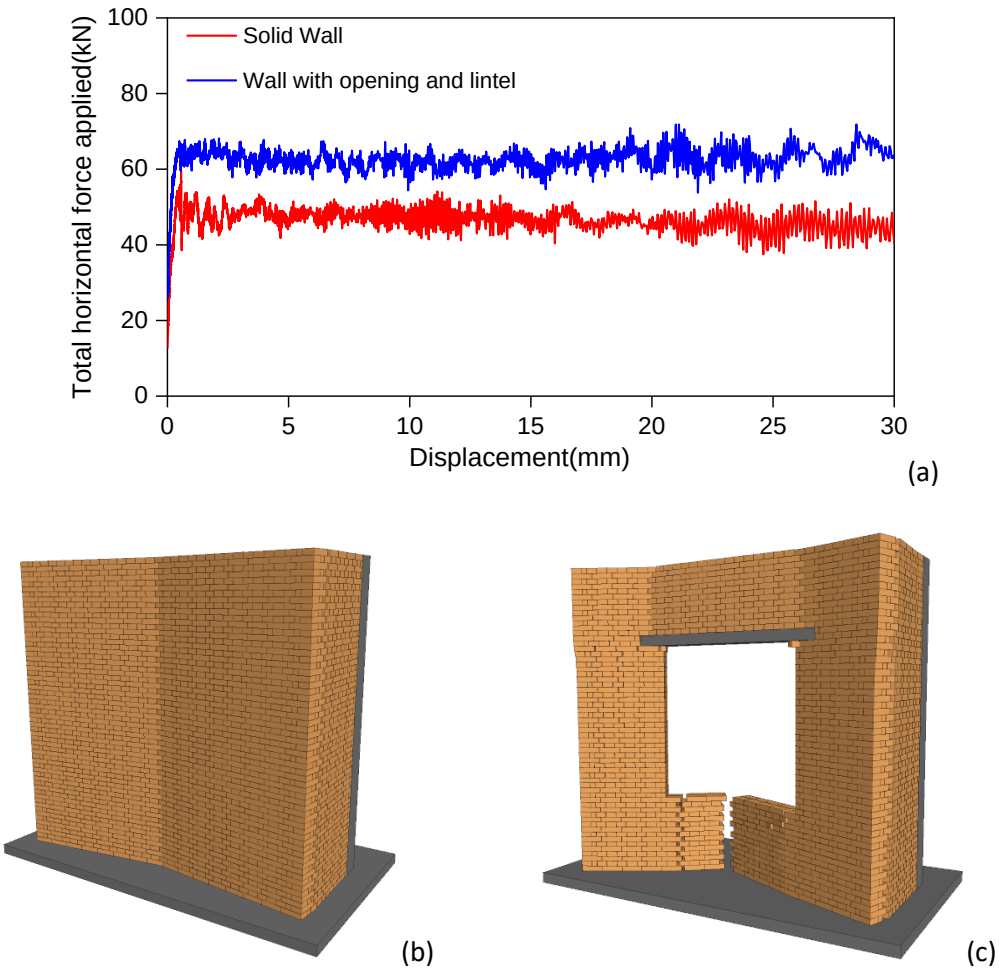

(a) Load-displacement curves; (b) crack patterns for solid wall; (c) crack patterns for solid wall with lintel and opening

Figure 5.5 Results of solid wall and wall with lintel and opening

When considering walls with supports on four sides, because the top edge is supported, as shown in Figure 5.8, the walls are similar to a URM wall with a ring beam, where the displacements at the top of the wall are restricted and out-of-plane capacity is improved. Another comparison was made for the out-of-plane behaviour of a solid wall with three-side supported with a similar wall, but now containing a large opening and a lintel, and a solid wall supported on four-side. Out-of-plane pressures were applied to all three walls and the pressure-displacement curves and crack patterns are shown in Figure 5.6. The intact wall with three-side supported carried the lowest total horizontal force, the wall with three-side supported and a 31% opening carried a slightly higher load but the intact wall with four-side supported carries the highest load. The results demonstrate that the lintels can be regarded as part of ring beams even the wall contains a large opening. As the opening size becomes bigger, the size of the lintel also becomes larger and the masonry wall becomes closer to a four-sided supported boundary condition, and the effects of lintels become more obvious. Even though the wall has a large opening, the total out-of-plane capacity is still improved.

In conclusion, lintels restrict the displacement of the wall and improve the out-of-plane capacity significantly. Especially for walls with a three-side supported boundary condition, lintels can effectively be regarded as part of a “ring beam” and they therefore offset the negative impacts of openings. Therefore, when considering the effects of openings on out-of-plane behaviour, the lintels should be considered carefully, and the out-of-plane capacity can be improved if suitable lintels are used.

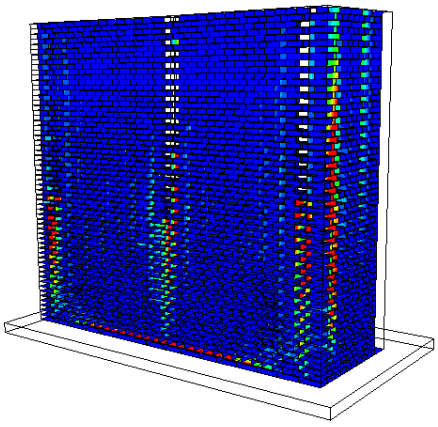

(a)

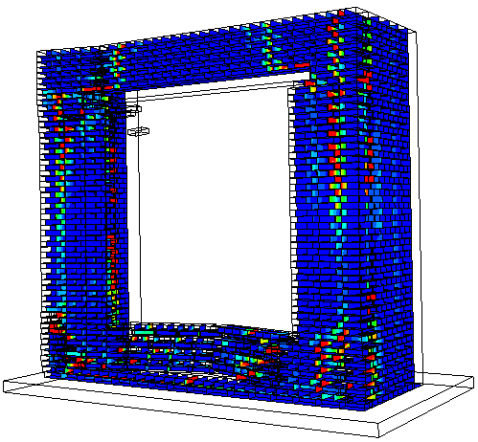

(b)

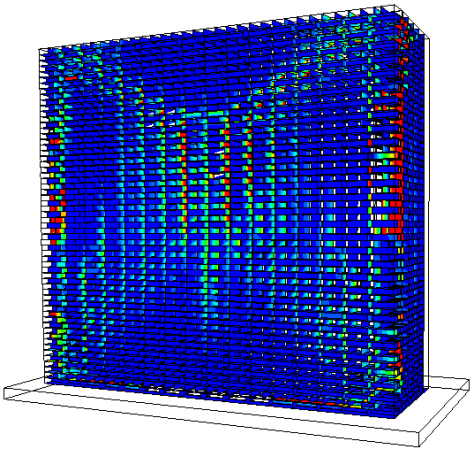

(c)

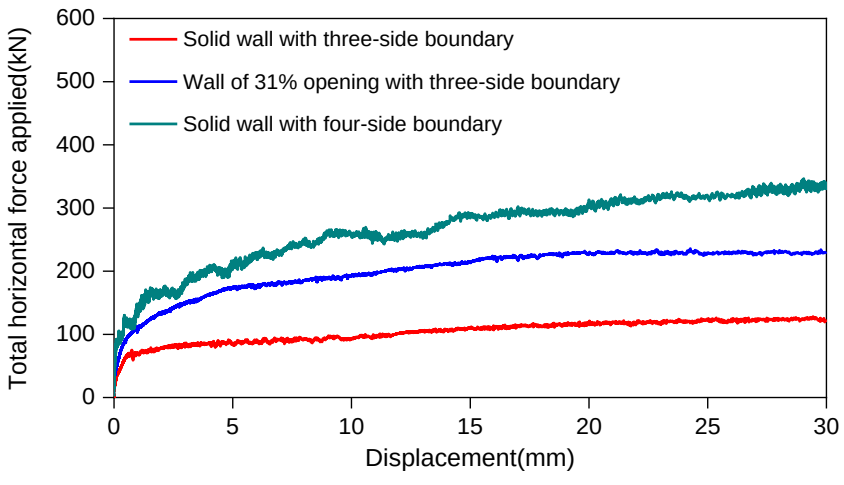

(d)

(a) Crack patterns of solid wall with three-side supported boundary (Maximum allowed crack length is 0.05m); (b) Crack patterns in masonry wall with 31% opening with three-side supported boundary(Maximum allowed crack length is 0.05m); (c) Crack patterns of solid wall with four-side supported boundary(Maximum allowed crack length is 0.05m); (d) horizontal force applied and displacement curves of the different walls

Figure 5.6 Results of different URM walls subjected to out-of-plane loading

5.2.3 The effect of opening position on out-of-plane behaviour of walls

Variation in the position of an opening in a URM wall can result in a change to the wall failure mechanism, creating more local failures and less wall integrity. To further evaluate the effect of opening position on the out-of-plane capacity of masonry walls, Wall A was built in 3DEC and many different opening positions (A1 to C2) were considered, see Figure 5.7.

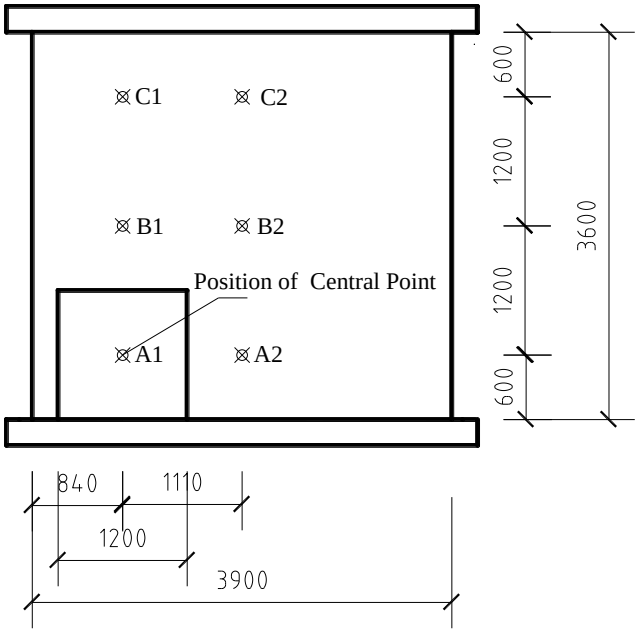

(a)

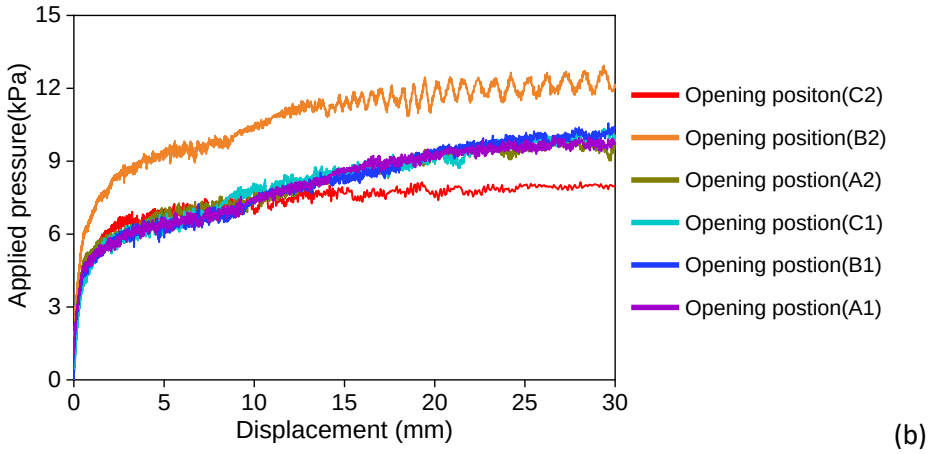

(a) Different opening positions considered of URM wall; (b) Pressure-displacement curves for masonry walls with different opening positions

Figure 5.7 Geometry information of different opening positions for case A and associated pressure-displacement curves

Looking at the load-displacement curves in Figure 5.7, the masonry walls with the opening located at the centre carry a maximum peak value of applied pressure of 13kPa, while when the opening position is central-top the wall only carries 7.8kPa. The difference between these peak values is around 60%, which is significant. The other three opening locations show a more similar performance with the capacities ranges from 9kPa to 11kPa peak applied pressure. It is worth noting that the elastic stiffness of the wall with the central opening is still higher than in other cases. Thus, the masonry wall with the central opening shows best out-of-plane performance with a three-side supported boundary condition.

The crack patterns in these masonry walls under out-of-plane loading are shown in Table 5.4 which also shows that the masonry wall with a central-top opening position does not have lintel as the location of the opening is so high. In this case there is a significant local failure around opening and it can be seen that some bricks have also fallen out of the wall. However, the top-left opening location shows much better performance which can be explained in that the central-top opening position is located in the main cracking area affected by failure mechanism for the three-side supported wall which leads to the significant drop in capacity. However when the opening is in the top-left position it is now not located in the main failure zone so the opening does not have such an impact on the overall capacity of the wall. For masonry wall with a central opening, the force is applied in a more uniform way across the wall and the lintel also gives additional support to the wall, increasing the out-of-plane strength. For masonry walls with the opening located at one side, the openings are not in the path of the main failure mechanism, so the lintel provides no significant support to resist the deformation.

Overall, for masonry walls with three supported sides, the location of lintels has a significant impact on the out-of-plane behaviour and lintels can start to behave as a ring beam if the lintel is located at the top of the wall and spans across enough of the wall.

Table 5.4 Crack patterns and Pressure-displacement curves of masonry walls with the different opening position under out-of-plane behaviour (Maximum allowed crack length is 0.05m)

Peak Value of applied pressure	Crack pattern
Opening position A1 (10.4 kPa)	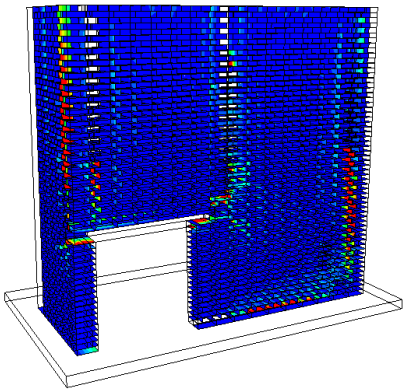
Opening position A2 (9.5 kPa)	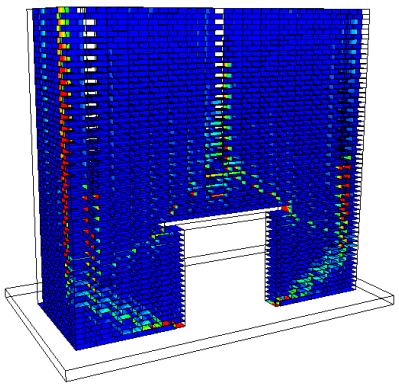

Opening position B1 (11 kPa)	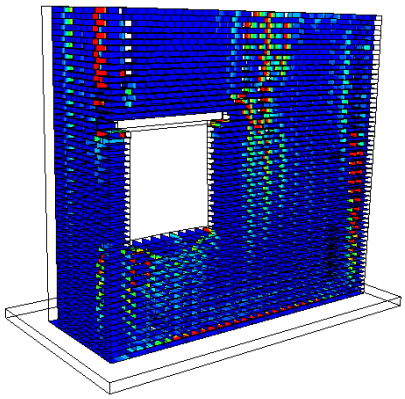
Opening position B2 (13 kPa)	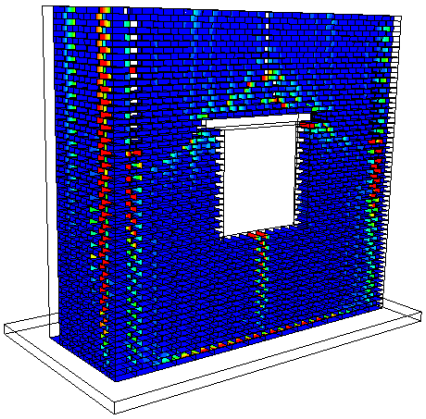
Opening position C1 (10.2 kPa)	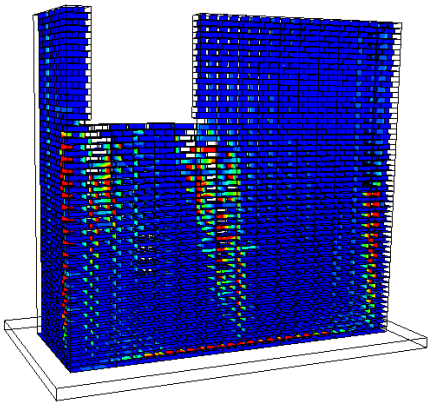

Opening position C2 (7.8 kPa)	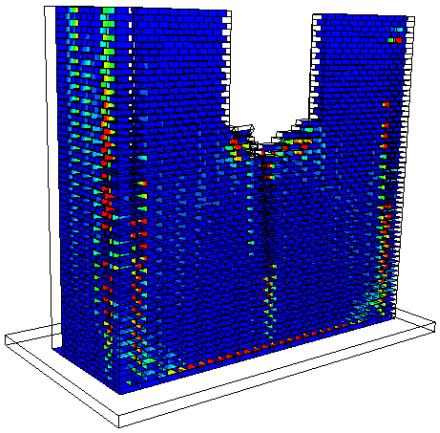

5.4 Effect of openings and lintels on masonry walls under out-of-plane loading (four-side supported boundary condition)

While a three-side supported boundary condition has been discussed above, a four-side supported boundary condition is more normal in the real world so the effects of opening on this type of wall also need to be considered.

5.4.1 Four-side supported boundary condition in 3DEC

Before considering the opening and lintel issues, it should be noted that modelling this type of URM wall in 3DEC is quite challenging because, when fixing the location of a bounding blocks in space, 3DEC sets the block as being fixed in all directions. This, unfortunately, restricts the motion of blocks in the wall as, when they begin to fail, an arching action can build up between the fixed boundary blocks. The leads to peak forces being carried by the walls that are unrealistic. In order to deal with this issue the top block of the wall has to be constrained such that lateral displacement is stopped but vertical displacement is not. In this way arching is avoided and the wall will behave in the same way as a real wall bounded by elements that have some flexibility.

To build the wall boundary the contacts between the frame and masonry walls were given very high joint stiffness so that the boundary could be regarded as rigid. Using this approach, a certain amount of rotational degree of freedom was still allowed. Besides, a consistent pre-compression is applied

and then the out-of-plane pressure is used until the failure of the wall. The detailed information about wall geometry and boundary conditions in 3DEC can be seen in Figure 5.8.

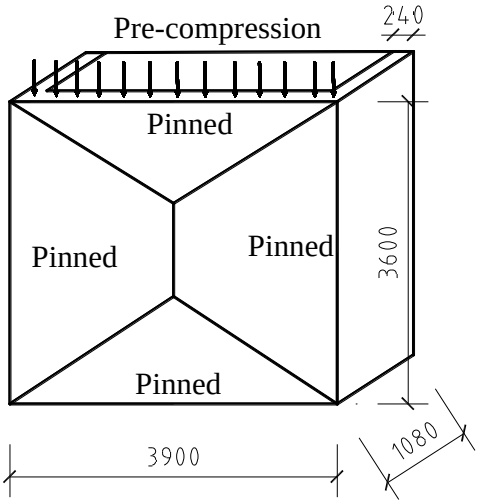

(a) Wall geometry and boundary information

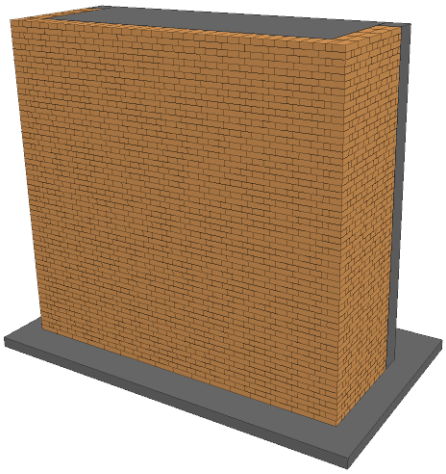

(b) View 1 of masonry wall in 3DEC

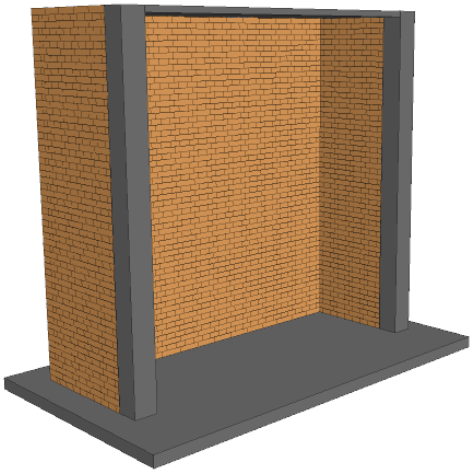

(c) View 2 of masonry wall in 3DEC

Figure 5.8 Wall information and numerical model in 3DEC under four side fixed boundary condition

5.4.2 Effect of lintels for masonry walls under out-of-plane behaviour

Lintels in a masonry wall with three supported sides have previously been shown to have a significant impact on the wall capacity as they improve the wall stiffness and restrain deformations. It is

interesting to investigate the lintel effects for four-side supported boundary condition. To assess this a comparison has been made between masonry walls with and without lintels subjected to out-of-plane loading.

Based on the results shown in Figure 5.9, both walls carry a similar peak applied pressure of 27.9kPa and 26.4kPa, respectively. Comparing these results to those for the three-side supported walls in section 5.3.1, a lintel in masonry wall with a four-side fixed boundary condition only increases the wall capacity by 6%. The crack patterns for the four-side supported walls with and without lintels both show a similar failure mechanisms (Figure 5.10) suggesting that, for this boundary condition, the lintel does not have a significant effect on the out-of-plane behaviour of the wall. In this case the four-side supported boundary condition masonry walls have enough supports and the load can readily be transferred to all the edges so the lintel does not resist the deformation significantly. The effects of the lintel are only to increase the out-of-plane strength of the wall slightly. Thus, compared with the three-side supported boundary condition, a lintels in a masonry wall with four sides supported has a much lower impact on the out-of-plane wall behaviour.

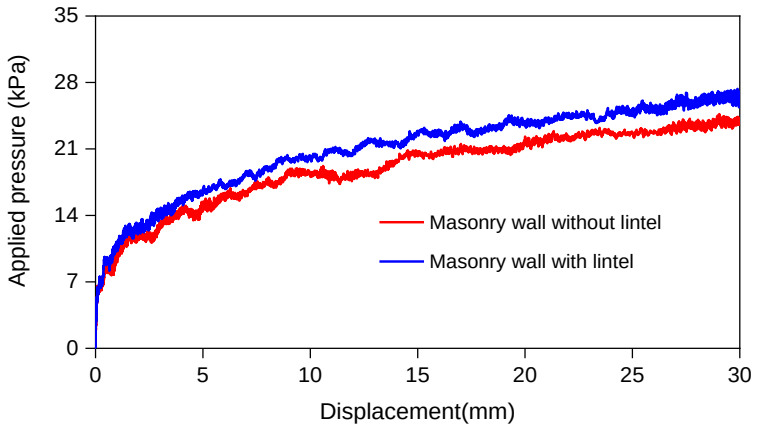

Figure 5.9 Pressure-displacement curves for masonry walls with and without lintels

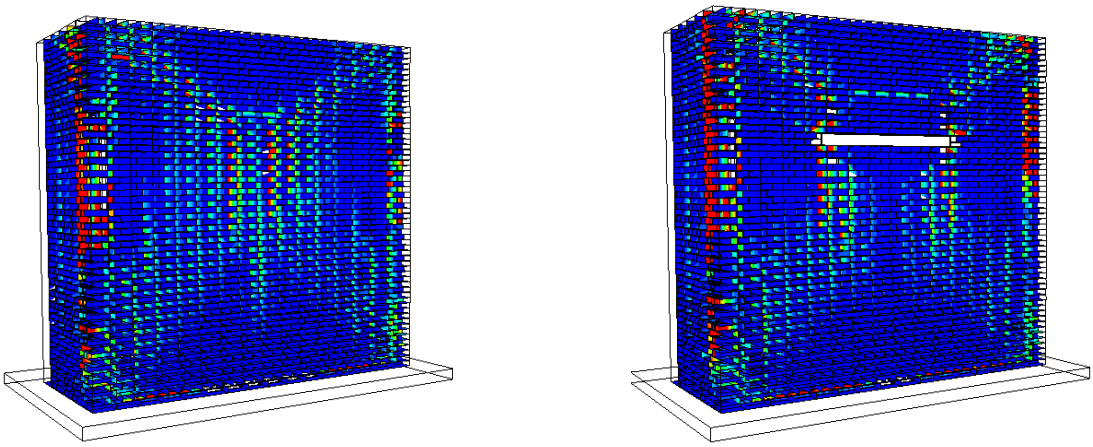

(a) Crack patterns for masonry wall without lintel (b) Crack patterns for masonry wall with lintel

Figure 5.10 Results for masonry walls with and without lintels under out-of-plane loading

5.4.3 Effect of opening percentage on masonry walls subjected to out-of-plane loading

The effect of the opening percentage on masonry walls with a four-side supported boundary condition under out-of-plane loading is now considered. Seven cases have been considered under out-of-plane loading in 3DEC. The pressure-displacement curves for masonry walls for different opening percentages are shown in Figure 5.11(a). Looking at the pressure-displacement curves, it is clear that as the opening size increase, the pressure resistance capacity becomes greater, again following a similar trend to the three-side supported boundary condition discussed previously. The masonry wall without any opening shows the worst out-of-plane performance with a peak value of pressure of 25.2kPa (at a displacement of 40mm). For masonry walls with opening percentages ranging from 3% to 16%, the difference of maximum pressure varies between 29.8kPa and 35kPa. When the opening size reaches 23% and 31%, the peak values of the applied pressure are 37kPa and 42kPa, respectively. The results show that for masonry walls with a four-side supported boundary condition, the peak out-of-plane pressure resistance increases as the opening size increases. However when converting the applied pressures to total loads on the wall the difference in capacity reduces. These load-displacement curves are shown in Figure 5.11(b). The masonry wall without an opening has the lowest value of load at 350kN. The other cases are quite similar to maximum values of around 420kN. This illustrates that, due to lintel having less effect on the out-of-plane performance for four-side supported masonry wall, the relationship between opening size and total load applied does not follow

a clear trend. Again this shows that the out-of-plane performance of a masonry wall with openings is mainly related to the effects of the lintel rather than the opening size.

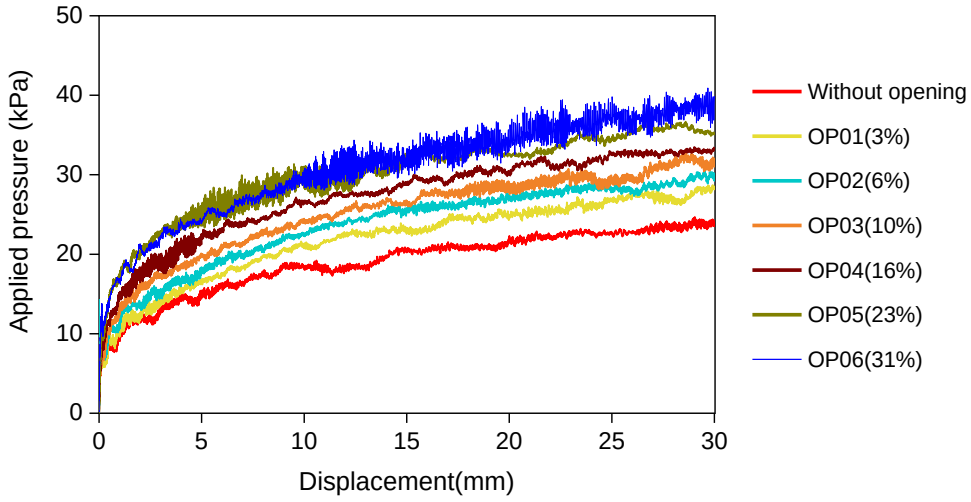

(a) Pressure-displacement curves for masonry walls with different opening percentage

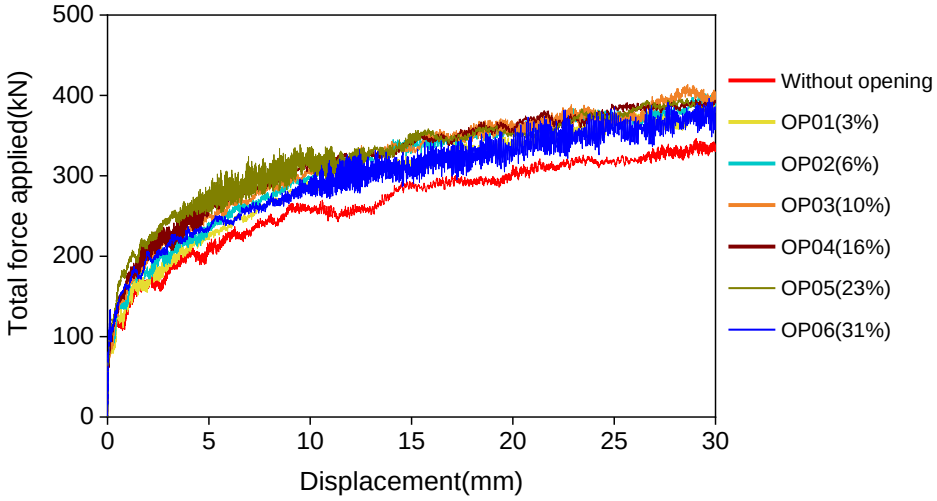

(b) Load-displacement curves for masonry walls with different opening percentage

Figure 5.11 Results of masonry walls with different opening percentage

The crack patterns for the masonry walls with different opening percentages are given in Table 5.5 and show that all the masonry walls with different opening percentages display similar crack patterns. As the opening size increases, the areas of remaining wall reduce and fewer cracks occur but the failure mechanism is similar. It is interesting to note that a 31% opening percentage does not occupy half of the wall area yet as an opening it still looks very large. It is therefore debatable whether this

should be considered as a wall with an opening or just as a set of brick columns and beams. Overall, the crack patterns are consistent with the results from the pressure-displacement curves.

Table 5.5 Results of masonry walls with different opening percentages under out-of-plane behaviour (Maximum allowed crack length is 0.05m)

Peak Value of applied pressure	Crack pattern
without opening (25.2 kPa)	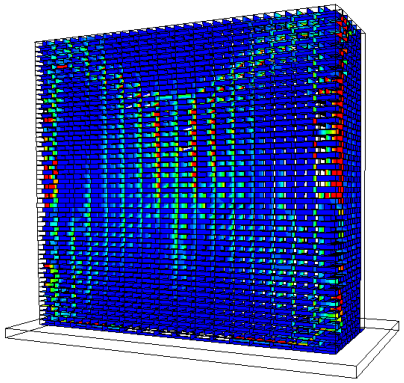
OP3% (29.8 kPa)	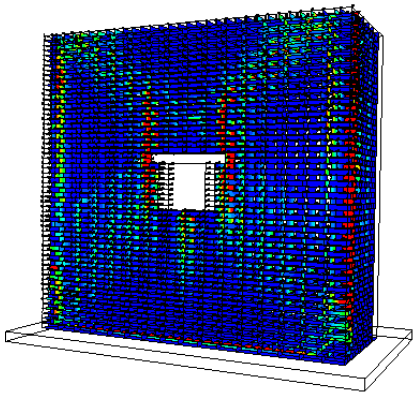

OP6% (32 kPa)	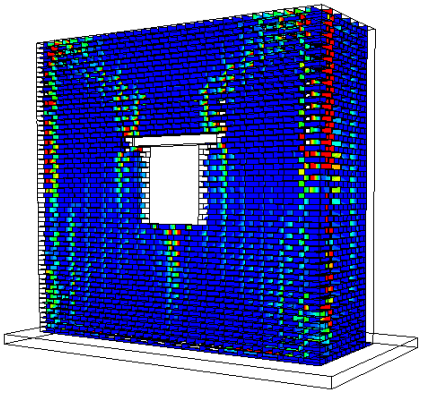
OP10% (33.5 kPa)	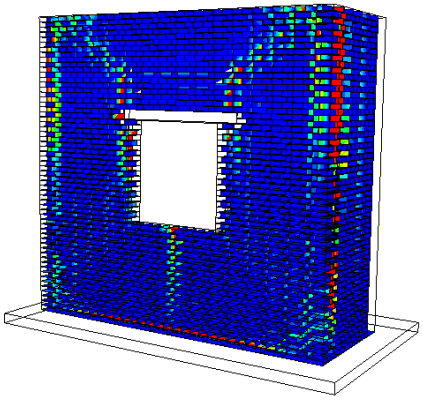
OP16% (35 kPa)	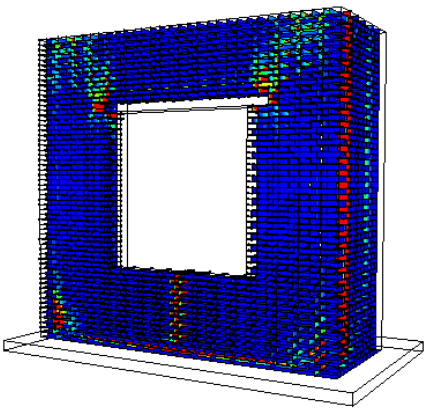

OP23% (37 kPa)	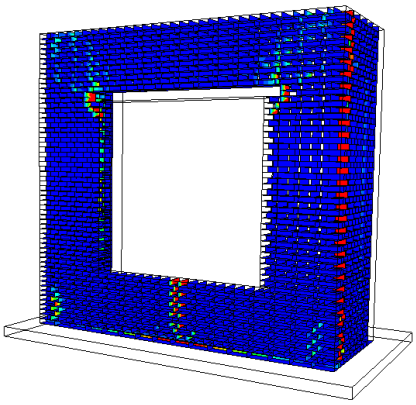
OP31% (42 kPa)	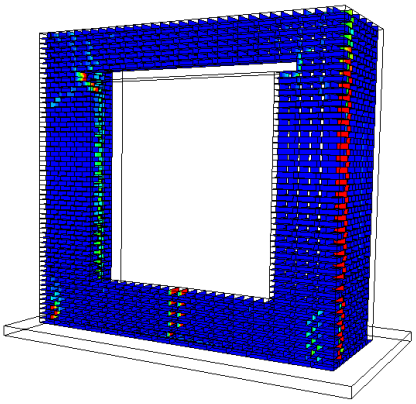

5.4.4 Effect of opening position on masonry walls under out-of-plane behaviour

The effects of opening positions for masonry walls with four-side supported boundary condition are now evaluated. The six opening cases (with a 10% opening percentage) shown in Figure 5.7 were considered and out-of-plane loading was applied. The pressure-displacement curves for these cases are shown in Figure 5.12, and the crack patterns and peak applied forces for the masonry walls with different opening positions are given in Table 5.6. For the peak values of applied pressure, the masonry wall with a central opening has the highest capacity carrying 33.5kPa. The wall with a central-top opening shows the worst capacity at 24.5kPa, this general behaviour is similar to that seen in the three-side supported boundary condition. The walls with the other two top openings show similar poor out-of-plane performances of 25kPa and 26kPa, respectively. The URM walls with other opening positions have similar peak values of applied pressure ranging from 26kPa to 30kPa. The difference in out-of-plane performance between the URM walls with a central opening and central top opening is

about 37% and all the walls with top openings show lower out-of-plane capacities than any other opening cases.

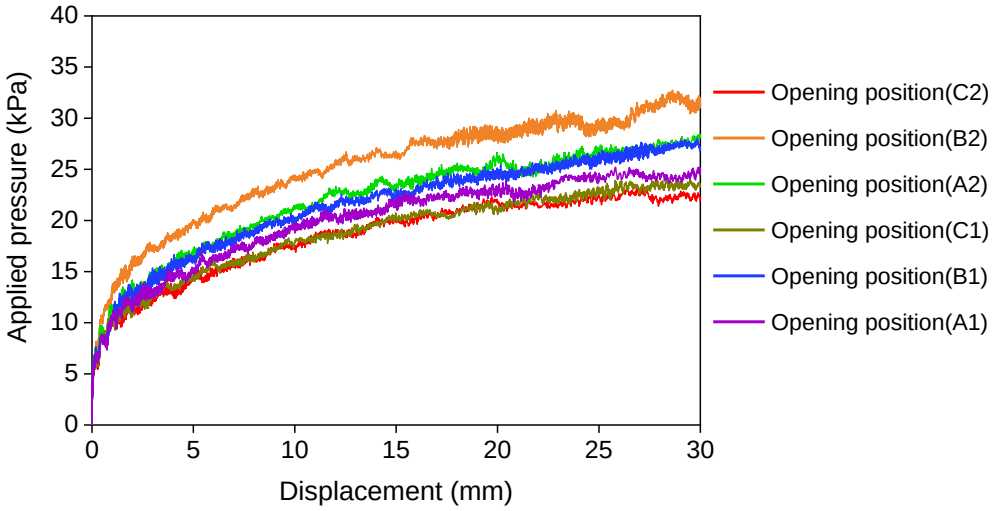

Figure 5.12 Pressure-displacement curves for masonry walls with different opening positions

Table 5.6 Results for masonry walls with different opening position under out-of-plane loading (Maximum allowed crack length is 0.05m)

Peak Value of applied pressure	Crack pattern
Opening position A1 (26 kPa)	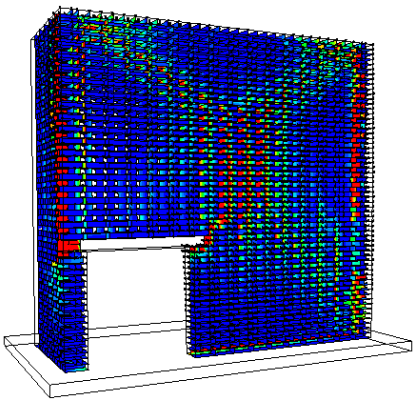

Opening position A2 (30 kPa)	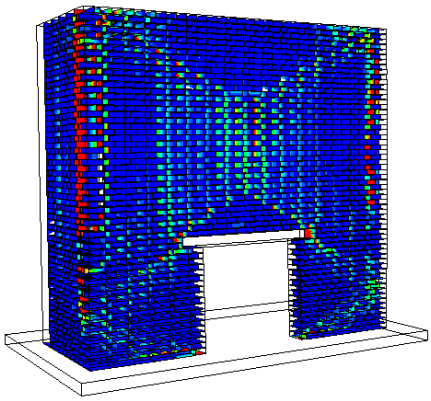
Opening position B1 (30 kPa)	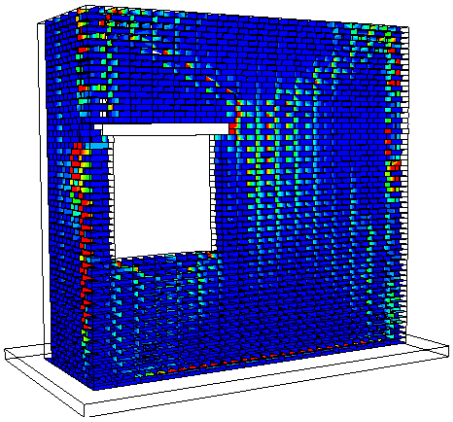
Opening position B2 (33.5 kPa)	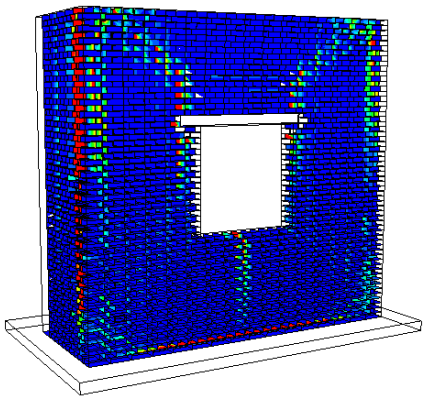

Opening position C1 (25 kPa)	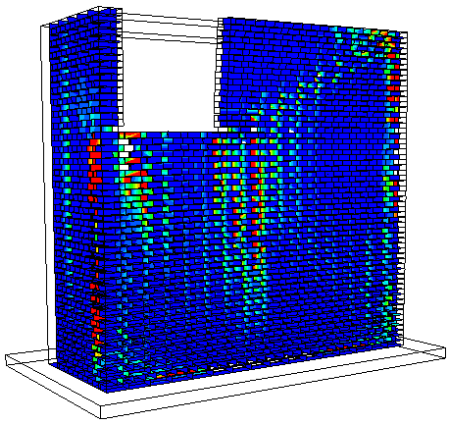
Opening position C2 (24.5 kPa)	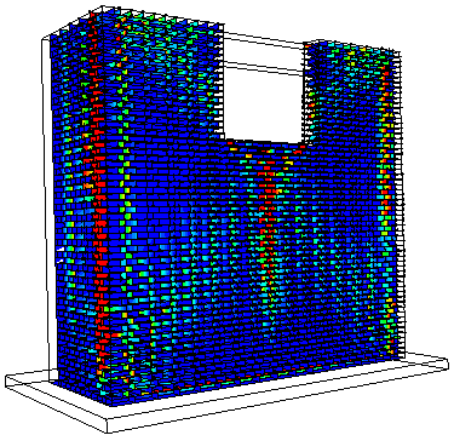

Looking at the crack patterns in the masonry walls shown in Table 5.6, it is clear that the different opening positions result in quite different crack patterns in the walls. The masonry wall with a central-top opening shows the worst out-of-plane performance and shows more cracks compared with other cases. The reason for the low out-of-plane capacity is that the wall did not have a lintel, and this lead to reduced stiffness and will have affected the wall capacity. The masonry wall with a left-top opening also showed the second-worst out-of-plane performance due to lack of lintel. The wall with the central opening carries the highest peak value of horizontal pressure, as the opening is located symmetrically in the wall, and the load can be transferred uniformly to the boundaries. It is worth noting that the masonry wall with the lowest peak horizontal capacity is similar to the capacity of the wall without an opening. This suggests that a 10% opening could be assumed to have little effect on the out-of-plane resistance capacity of a wall even if the location is not symmetrical in the wall.

5.5. Comparison of out-of-plane performance between three-side and four-side supported boundaries

Both masonry walls with three-side and four-side boundary conditions have been presented above and it is clear that the failure mechanisms are quite different. To evaluate the differences in opening effects, including opening size and opening position on out-of-plane performance, a comparison between both boundary conditions is given in Figure 5.13. The difference in masonry wall results between with three-side and four-side boundary conditions indicate that the masonry walls with four-side boundary condition show a significantly better out-of-plane resistance capacity and that the peak values of applied pressure and load with four-side boundary condition are three times higher than for the three-side boundary condition as shown in Figure 5.13(a). With the peak values of pressure normalised, the same curves are shown in Figure 5.13(b), which shows that the impact of openings on the out-of-plane performance of four-side boundary condition masonry walls is smaller than for the three-side boundary condition. Figure 5.13(c) then shows that the peak values of the applied load for masonry walls with a four-side supported boundary condition are very much higher than the three-side supported boundary condition for the different opening percentages. Again, the normalised peak load factor for different opening percentages shows that walls with a three-sided boundary condition are affected by openings much more significantly than the four-side supported walls. All the figures show that lintels play an important role in the three-side boundary condition with the lintel providing additional stiffness and resistant to deformation in the walls. However, for the four-side boundary condition, where all the boundaries are already supported the lintel has less of a role to play so its effects are less noticeable. Thus, opening percentage effects under three-side boundary condition are more sensitive than for the four-side boundary condition.

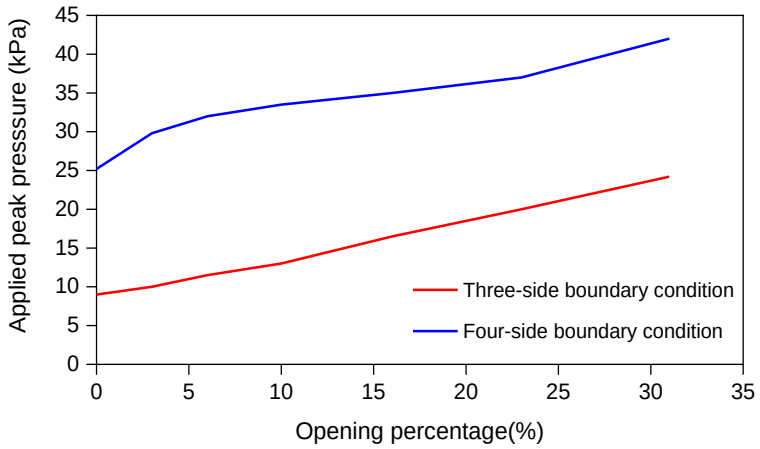

(a) Comparison between applied peak pressure and opening percentage effects for both boundary conditions

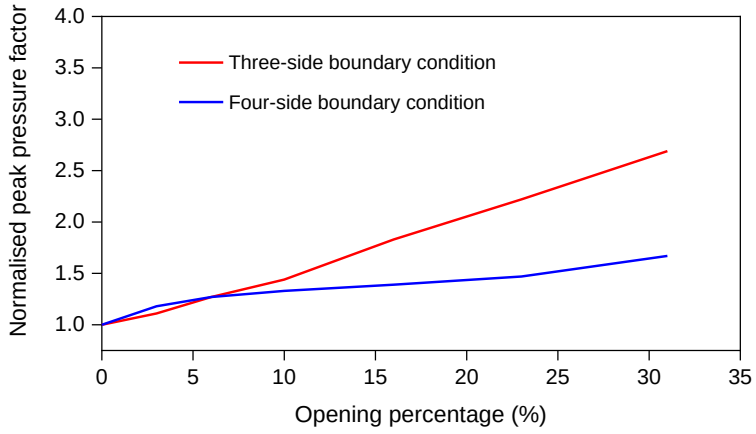

(b) Comparison between normalised peak pressure factor and opening percentage effects for both boundary conditions

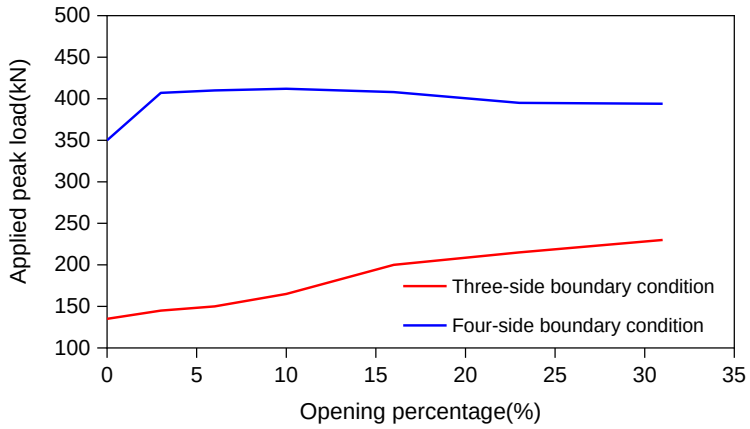

(c) Comparison between applied peak load and opening percentage effects for both boundary conditions

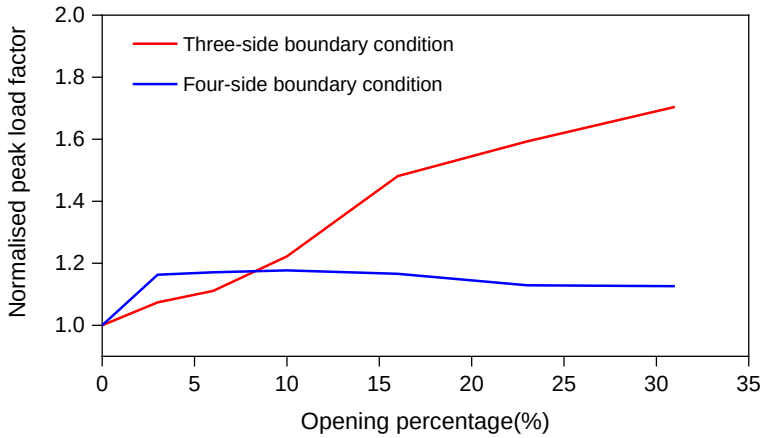

(d) Comparison between normalised peak load factor and opening percentage effects for both boundary conditions

Figure 5.13 Comparison of opening percentage effects for masonry walls with three-side and four-side boundary conditions

Another key objective is the comparison of opening position effects between three-side and four-side boundary conditions as shown in Figure 5.14. It can be seen that the walls with both boundary conditions generally display a similar out-of-plane performance with respect to the different opening positions. Central openings have the best out-of-plane capacity for both boundary conditions and top openings display the worst out-of-plane performance. However, some differences need to be discussed. For URM walls with a three-side supported boundary condition, the lowest value of peak pressure factor occurs when the opening is located in the central of the top of the wall with a residual strength 58% of the maximum, while for the four-side supported boundary condition masonry wall an opening anywhere along the top face leads to the wall having a residual strength 73% of the maximum. For the three-side supported boundary condition masonry walls, due to lack of lintel to provide extra support to the wall, the central top open location leads to particularly poor wall behaviour. However, for the four-side supported boundary condition, the lintel does not play such an essential role in the out-of-plane behaviour. An opening in the top of the wall still reduces the wall strength, but the value of the peak pressure factor only decreases by 30%.

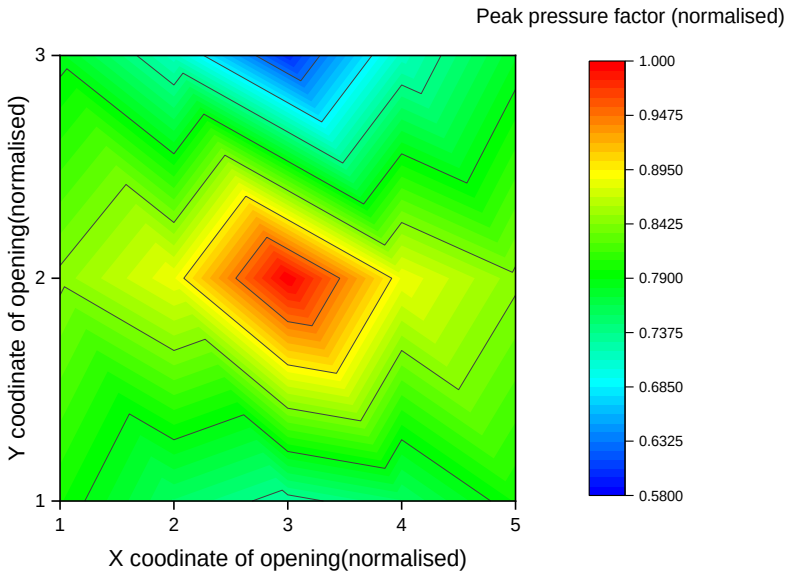

(a) Comparison between horizontal pressure and opening position effects for three-side fixed boundary conditions

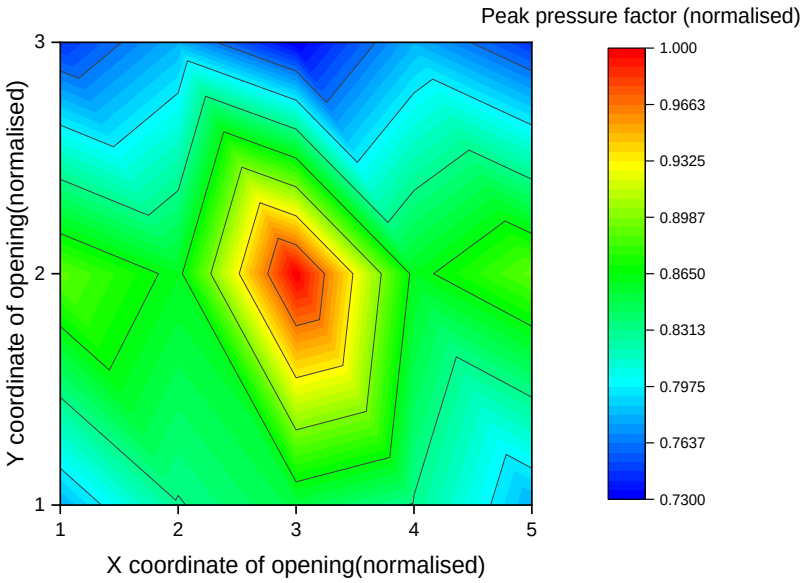

(b) Comparison between out-of-plane capacity and opening position effects for four-side fixed boundary conditions

Figure 5.14 Comparison of opening position effects for masonry walls with three-side and four-side supported boundary conditions

5.6. Effect of openings on rectangular URM walls (four-side supported boundary condition)

In the sections above the effects of openings on square URM walls have been considered. However rectangular walls are common in real masonry structures so the out-of-plane performance of rectangular walls is considered below and then the results for rectangular walls are compared with those for square walls. Focusing on rectangular URM walls with a four-side supported boundary condition, both the impacts of opening size and position on the out-of-plane capacity are evaluated. The comparison between the two geometries of URM walls is then discussed.

5.6.1 Effect of opening sizes for masonry walls under out-of-plane behaviour

The geometrical information for the rectangular URM walls and numerical models in 3DEC is shown in Figure 5.15. Four sides of the wall are supported out-of-plane and a pre-compressive pressure of 0.10MPa is applied. To look at the impact of opening sizes, a total of eight opening percentages with the openings located at the centre of the URM wall are considered ranging from 0 to 41% of the wall area. Compared to square shape masonry walls, the rectangular walls with four-side supported boundary conditions display a slightly different failure mechanism. This can be observed from the crack patterns of both types of URM walls. The creation of the boundary conditions and out-of-plane loading procedure in 3DEC was the same as that discussed in section 5.4.2 and the results for the pressure-displacement relationships and crack patterns are shown below:

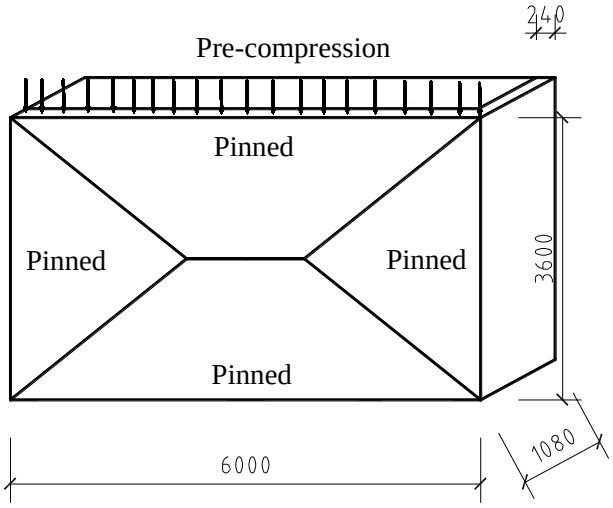

(a) Wall geometry and boundary condition information

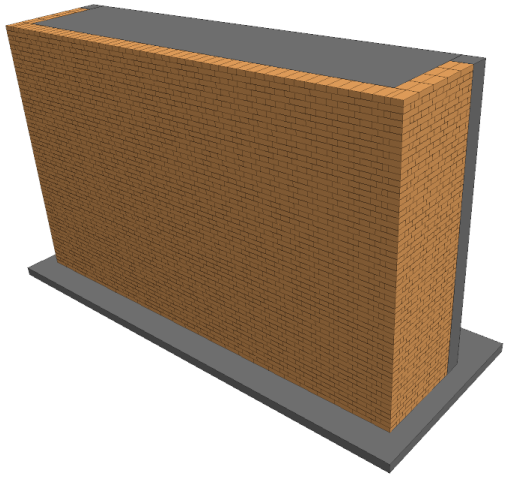

(b) View 1 of masonry wall in 3DEC

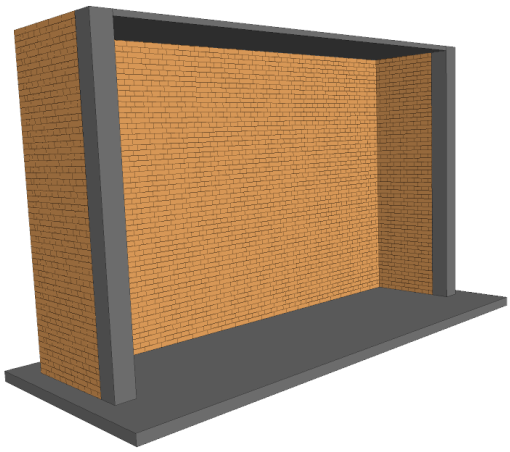

(c) View 2 of masonry wall in 3DEC

Figure 5.15 Rectangular wall information and numerical model in 3DEC for four-side supported boundary condition

The pressure-displacement plots shown in Figure 5.16(a) indicate that the peak values of applied pressure increase as the opening size grows. The peak horizontal pressure that the URM wall without openings can carry is the smallest at 24.6kPa, while the URM wall with a 41% opening shows the best out-of-plane performance carrying 38kPa peak applied pressure. The URM walls with opening sizes ranging from 3% to 23% carry a uniformly growing pressure as the opening size increases. When the opening reaches 31%, the peak value of pressure carried rises significantly. However when converting the applied pressure to a total applied load it is clear from Figure 5.16(b) that there is no significant difference in total load applied for masonry wall with different opening percentages. The wall without an opening does have the smallest capacity at 420kN but the other masonry walls are quite similar. Again, as in section 5.4.3, because the lintel has little effect on the out-of-plane performance of a four-side supported masonry wall, the relationship between opening size and total applied load is not clear. In other words, this variation in capacities is similar to the previous research about square walls with a four-side supported boundary, which illustrates that the opening percentage effects are not dramatically affected by the wall shape.

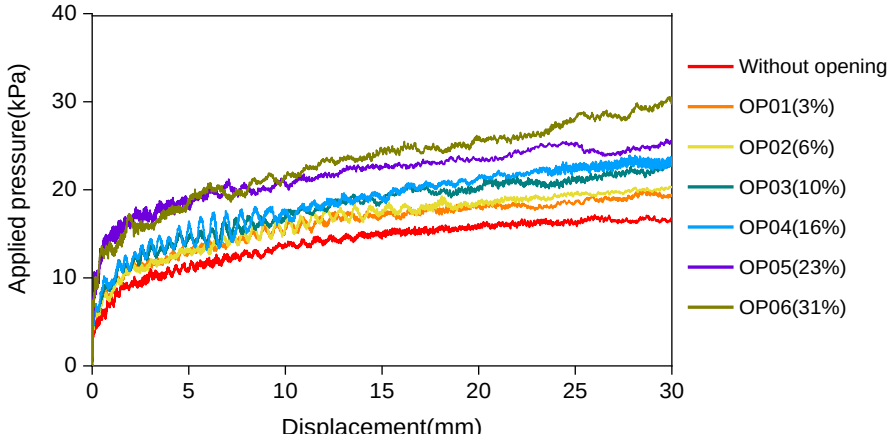

(a) Pressure-displacement curves for masonry wall with different opening percentage

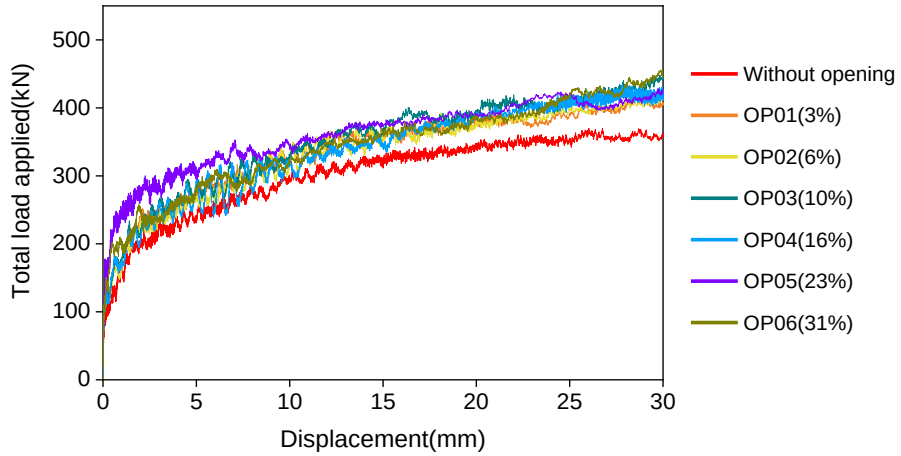

(b) Load-displacement curves for masonry wall with different opening percentage

Figure 5.16 Results of masonry wall with different opening percentage

The crack patterns for the rectangular URM walls with the different opening percentages subjected to out-of-plane loading are shown in Table 5.7. The failure mechanisms of the URM walls remain similar until the opening percentage exceeds 30%. For opening percentages ranging from 0 to 23%, all masonry walls follow similar failure patterns with two diagonal cracks running through the whole structure. Some local failures occur at the bottom of the opening, but the two diagonal cracks are still clear to see. Once the opening is greater than 30%, a sliding failure located under the lower half of central opening starts to dominate the failure mode and the diagonal cracks can only be easily identified in the upper half of the wall.

Table 5.7 Results of masonry walls with different opening percentages under out-of-plane loading (Maximum allowed crack length is 0.05m)

Peak Value of applied pressure	Crack pattern
without opening (19 kPa)	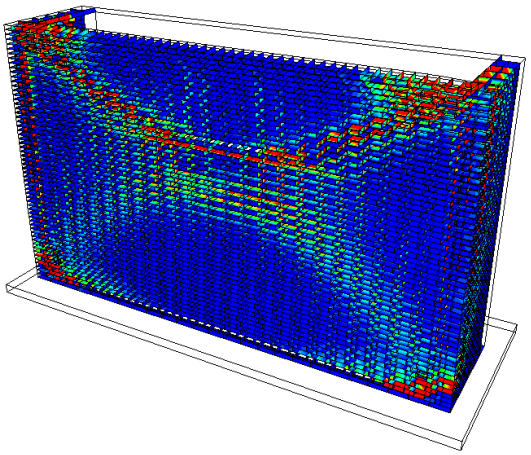
OP3% (22 kPa)	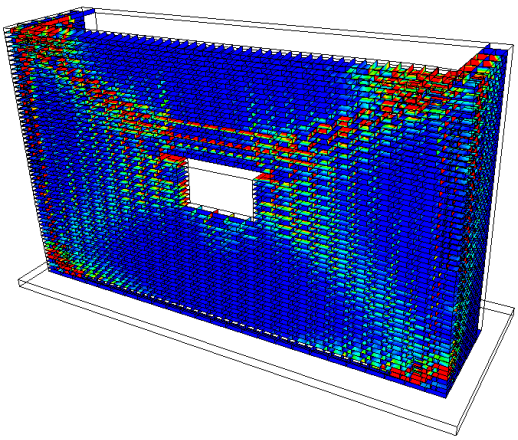

OP6% (23 kPa)	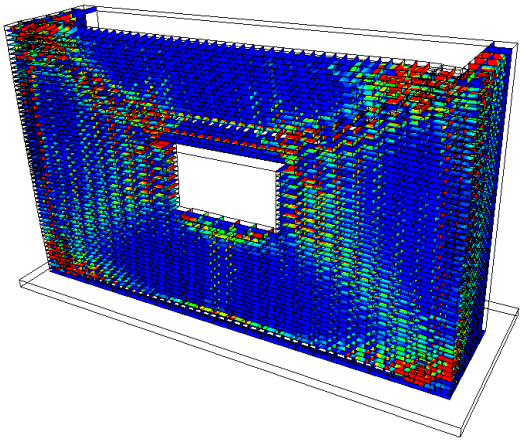
OP10% (25.5 kPa)	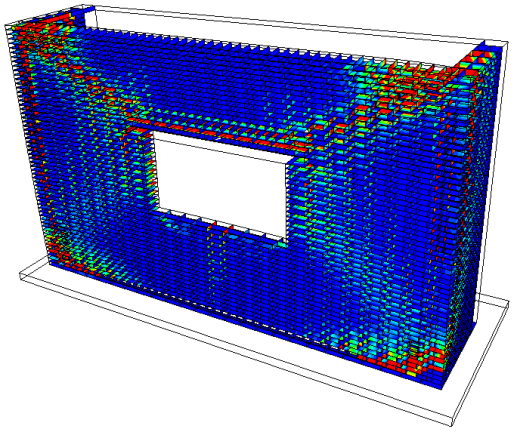
OP16% (27.5 kPa)	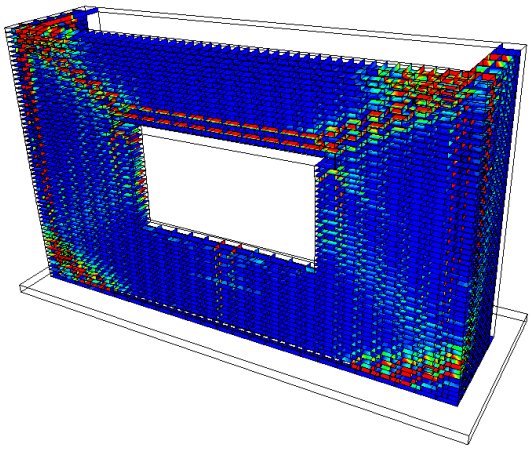

OP23% (29.2 kPa)	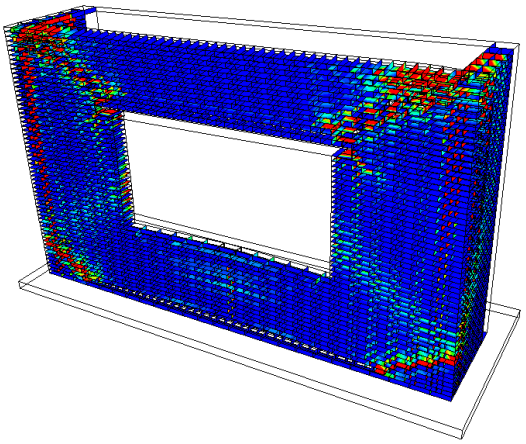
OP31% (32.5 kPa)	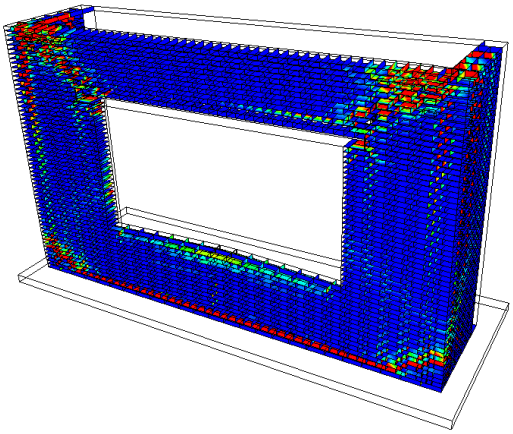
OP41% (38kPa)	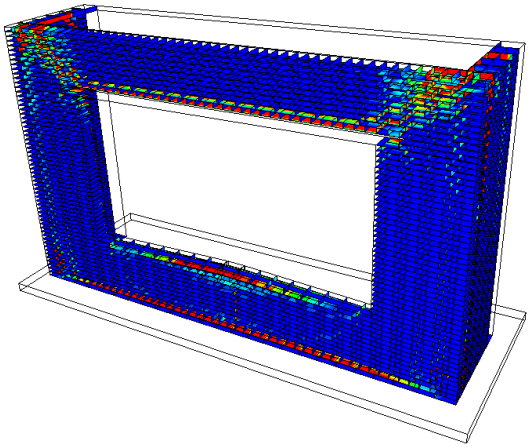

5.6.2 Effect of opening positions for masonry walls under out-of-plane behaviour

Impacts of opening positions on the out-of-plane performance of rectangular masonry walls on have been identified above and in this section the impact of the opening position on these walls is considered. A total of nine opening positions are studied as shown in Figure 5.17. The opening percentage is kept at 10% which is typical of opening sizes in walls in real structures. The boundary conditions for the numerical model and the out-of-plane loading procedure in 3DEC is as described in section 5.4.3. The pressure-displacement curves and crack patterns for the URM walls with different opening positions are shown below.

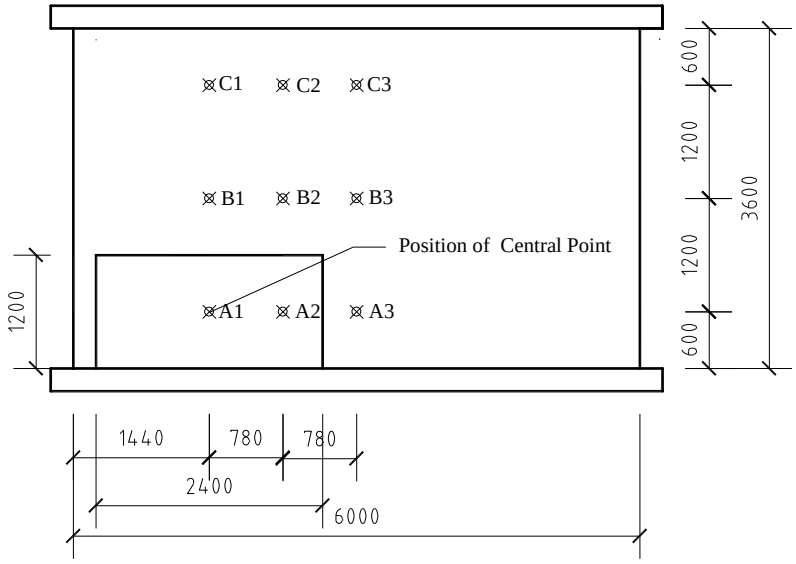

Figure 5.17 Different opening position cases for URM wall

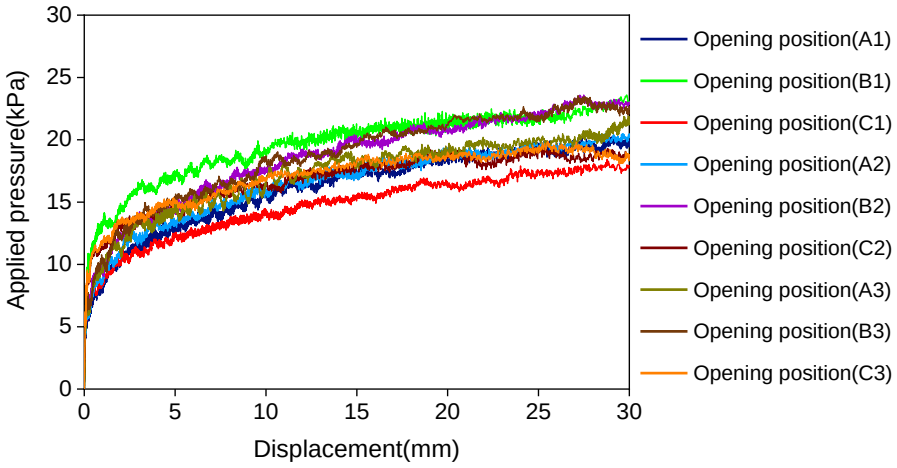

Figure 5.18 Pressure-displacement curves for masonry wall with different opening positions

As seen in Figure 5.18, the horizontal pressure-displacement curves indicate that the out-of-plane performance of URM walls varies with the opening position. An opening in the leftmost-top edge leads

to the worst out-of-plane performance with a peak applied pressure of 20kPa. The other two top edge openings also carry small peak applied pressures of 22.5kPa and 22kPa. The peak values of horizontal pressure for a central opening, a left-centre opening and a left-centre edge opening are similar and carry the highest pressures ranging from 25kPa to 27kPa. The other opening cases such as central-bottom opening, left-bottom opening and left-bottom edge opening all carry similar peak applied pressures of around 23kPa. The difference between the highest and lowest values is almost 35% which means that different opening positions do have a significant impact on the out-of-plane wall performance. The openings located at the centre along the horizontal axis of the URM wall lead to the best out-of-plane performance while the openings located on the top edge of the panel are the worst. The main reason for this is again that the top openings do not have lintels which reduce the stiffness of the whole wall to some extent and lead to poor out-of-plane performance.

The crack patterns for these walls are given in Table 5.8 and show that two diagonal cracks running through the whole URM wall are the dominant failure mechanism although some local failures still occur depending on the positions of the openings. It can be clearly seen that the openings located at the top positions lead to more local failures than the other situations. Due to lack of lintels, larger displacements appear near the openings leading to the poor out-of-plane capacity compared with other opening locations. The crack patterns for the URM walls also identify certain local failures that are not obvious from the pressure-displacement curves, in particular, local failure and cracks propagating from the corners of the openings.

Table 5.8 Crack patterns for masonry walls with different opening positions under out-of-plane loading (Maximum allowed crack length is 0.05m)

Peak Value of applied pressure	Crack pattern

Opening position A1 (22.5 kPa)	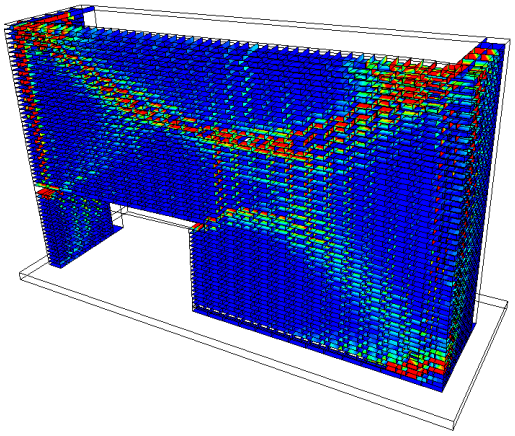
Opening position B1 (25 kPa)	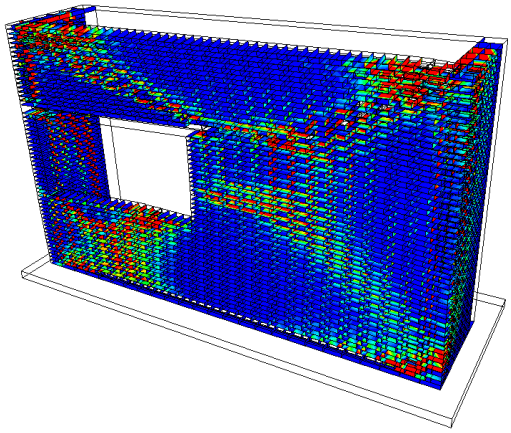
Opening position C1 (20 kPa)	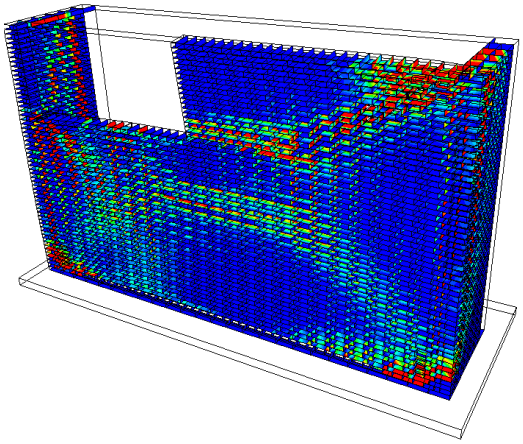

Opening position A2 (22.5 kPa)	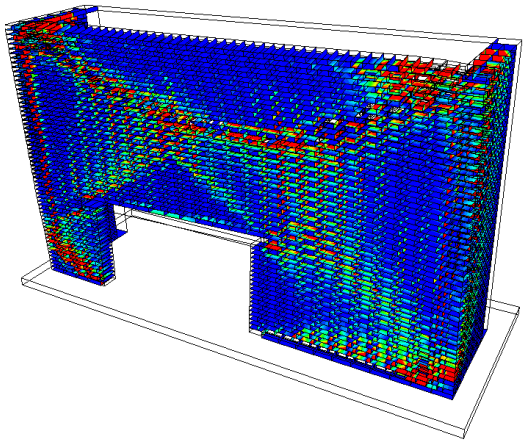
Opening position B2 (27 kPa)	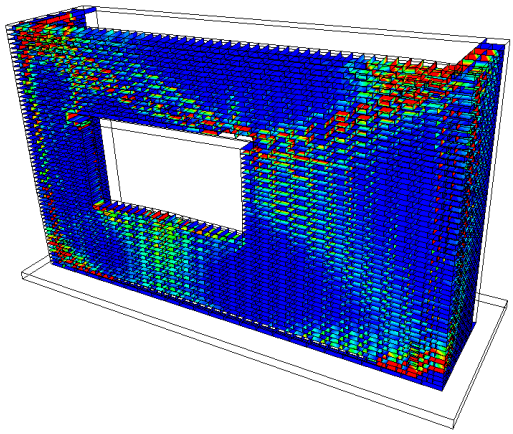
Opening position C2 (22.5 kPa)	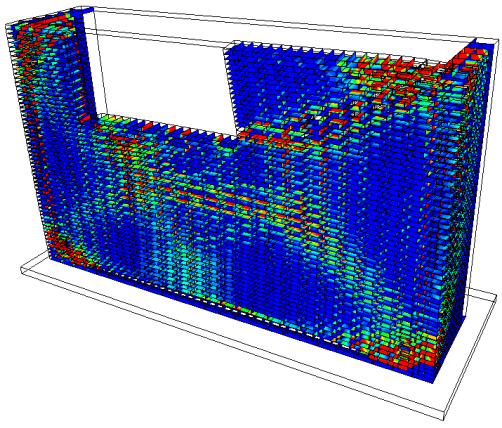

Opening position A3 (24 kPa)	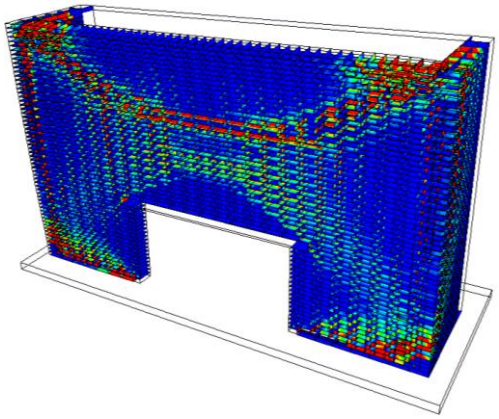
Opening position B3 (27kPa)	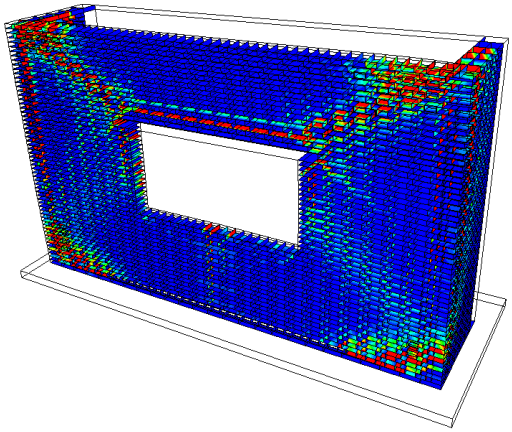
Opening position C3 (22 kPa)	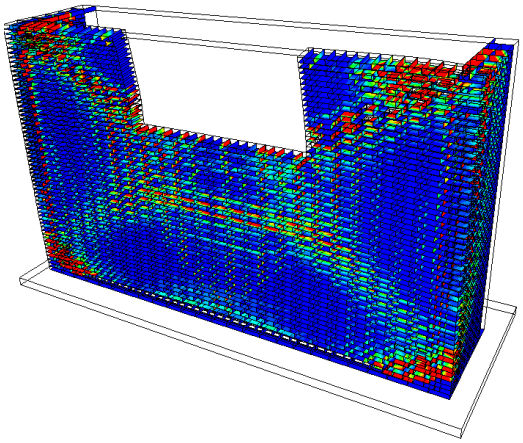

The out-of-plane performance of URM walls with different opening positions is shown in Figure 5.19. When the opening is in the centre of the wall the wall carries the highest peak pressure while the walls

with openings at the top only carry 74% of that peak pressure factor. For other opening positions, the out-of-plane performance is fairly similar and the peak pressure factor is 80% of the highest value.

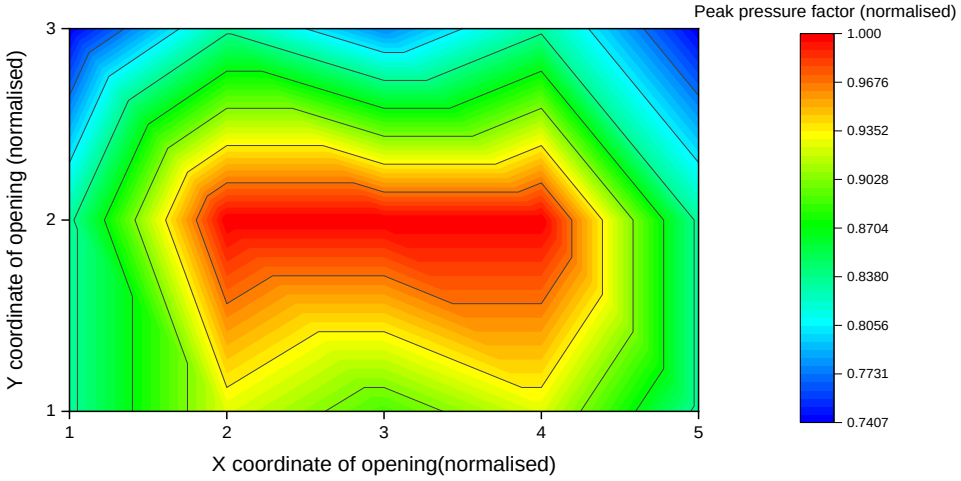

Figure 5.19 Results of masonry walls with different opening positions under out-of-plane behaviour

Again these results show that the opening positions have a significant impact on the out-of-plane wall capacity. Central openings show the best performance while top openings perform worst. It is therefore important when designing or assessing openings in URM structures that any openings located at the top of a wall should be considered carefully to avoid possible failures.

5.6.3 Comparison of out-of-plane performance between square and rectangular URM walls with a four-side supported boundary

Both square and rectangular URM walls have been analysed above and it is worth comparing the results to identify any similarities and differences. Based on the results in sections 5.4.1 and 5.6.1, a comparison of opening percentage effects on out-of-plane performance is summarised in Figure 5.20. The curves in Figure 5.20(a) indicate that square URM walls can carry higher peak applied pressures than rectangular URM walls for the same opening percentages and the difference in peak values remaining constant at about 44%. The curves in Figure 5.20(b) show that the applied peak load for both types of URM walls also follow a similar trend and difference in peak values between square URM wall and Rectangular URM wall is around 20%. Based on these figures, it is clear that even though

the peak values for the two shapes of walls are different, they both follow a similar trend as the opening percentage rises.

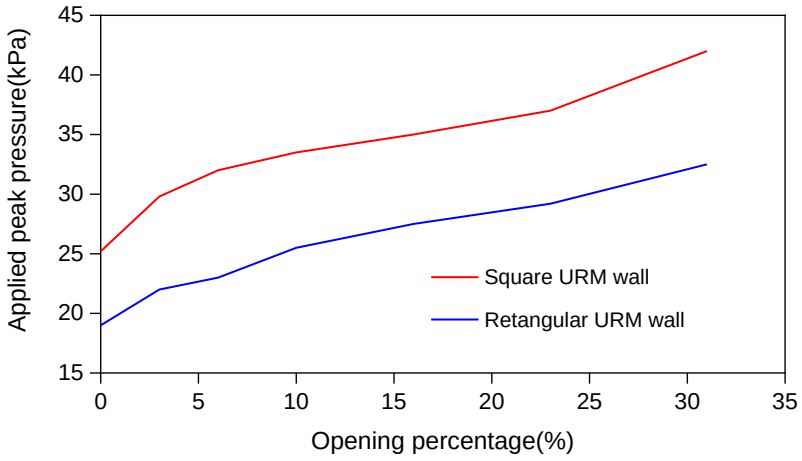

(a) Comparison between applied peak pressure and opening percentage effects for both types of URM walls

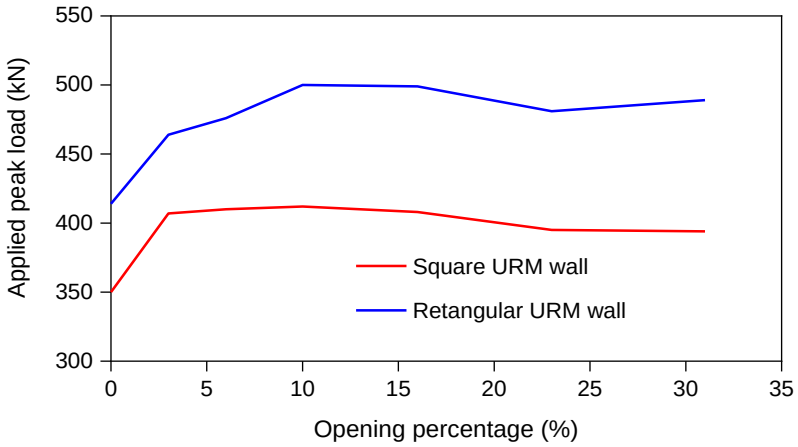

(b) Comparison between applied peak load and opening percentage effects for both types of URM walls

Figure 5.20 Comparison of opening percentage effects for both square and rectangular URM walls

Looking at the relationships between opening position and peak load capacity in Figure 5.14(b) and Figure 5.19, it is clear that whether for square URM walls or rectangular URM walls, similar behaviour can be observed. Central openings lead to the best out-of-plane performance while the top openings lead to the worst performance. The maximum difference between the highest and lowest loads for both types of walls are about 37% and 36%, respectively. Little difference occurs for URM walls when the openings are located at the bottom or sides of the walls and the square walls have a little lower capacity than rectangular ones. However, the differences between the differently shaped walls is

minimal suggesting that the impact of opening position does not depend on the shape of the URM wall.

5.7. Summary

Quasi-static push over tests of URM masonry walls under out-of-plane behaviour has been presented in this chapter. To consider the effects of openings including opening percentage and opening position, a number of 3DEC models have been designed and the same pushover procedure has been applied to each. The effect of changing in the boundary conditions (including three-side and four-side boundary conditions) has been discussed and the relationships between opening effects and out-of-plane performance have been identified. The conclusions from this work are given below:

1. For masonry walls with three-side supported boundary conditions, as the opening size increases, the peak value of horizontal pressure carried rises. The main reason for this is that lintel over the opening increases the stiffness and restricts the displacement of the masonry walls, which significantly improves the strength of the masonry wall.
2. An opening position in the central-top of a three-side supported wall has the greatest impact on the wall performance because there is no lintel above the window and some local failure also occurs around the opening.
3. For masonry walls with four-side supported conditions, as the opening size increases, the peak value of horizontal pressure carried rises, but due to lintel having limited effects on masonry wall, the differences between the highest and lowest capacities are not as apparent as for the three-sided supported walls. The total load capacities for various opening percentages in four-side supported walls do not follow a clear trend, which is different from the three-side supported wall case. Another significant difference in performance occurs at the top edge due to a different failure mechanism.
4. Comparing the two different boundary conditions, the opening size does not reduce the out-of-plane behaviour, rather, the opening and associated lintel improve the out-of-plane performance in most cases. When looking at the opening position, it is vital to consider the failure mechanism of masonry walls because the load needs to be transferred evenly to the supporting structure. A symmetrical opening allows loads to distribute evenly around the wall leading to a better performance than for edge or asymmetrically placed openings.
5. Comparing the results for the square and rectangular walls, there are no distinct differences in the out-of-plane performance. The peak values of loading showing only minor differences.

This chapter has presented the effects of openings on the out-of-plane behaviour of masonry walls. It is really important to note the positive effect of lintels, the importance of a four-side supported boundary condition and to try to avoid asymmetrical openings or openings near the edges of the walls. Nevertheless, openings do not really impact the out-of-plane capacity of URM walls, as is the case for the in-plane behaviour of URM walls. This does however mean that URM walls subjected to combined in and out-of-plane walls need careful consideration as it is not necessarily obvious which loading direction will be more critical when there are openings.

Chapter 6 DYNAMIC ANALYSIS OF MASONRY WALLS

6.1 Introduction

In previous chapters, both the static in-plane and out-of-plane behaviour of URM walls have been discussed and the relationships between opening effects and relevant capacity have been developed. However, the response of URM structures under dynamic analysis (time-history analysis) is also important because this type of analysis closer reflects the actual behaviour of URM buildings under real earthquakes. To study the dynamic behaviour of URM walls, a time history analysis procedure has also been applied using 3DEC. The results are compared to static analyses for both in-plane and out-of-plane behaviours. Before running dynamic analyses using earthquake records, simpler tests of URM walls subjected to harmonic excitation were performed to identify the impact of effects such as frequency, vertical load and amplitude. The effects of openings are then considered under dynamic loading. Compared with the static loading procedures in 3DEC, dynamic analysis is applied by creating a dynamic input, and Rayleigh damping is used. It should be noted that in 3DEC as the input data has to be in the form of either a prescribed velocity history or a stress history, if only acceleration histories are available, these need to be integrated numerically to generate a velocity history for use in 3DEC.

6.2 Dynamic modelling of a URM wall in 3DEC

6.2.1 Dynamic input of harmonic and artificial earthquake waves in 3DEC

Before running dynamic tests of URM walls with earthquake waves, it is necessary to investigate the performance of the URM walls from some simple dynamic analysis in 3DEC. Therefore, a set of simpler harmonic excitation singles was used to consider how some single factors like frequency, vertical load and amplitude affect the dynamic behaviour of URM walls in 3DEC. The displacements and acceleration records for these inputs, with frequencies from 0.5Hz to 2Hz, are shown in Figure 6.1. All these input time-history records are simple and easy to control the variable, which is easy to identify and observe how these factors affect the behaviour of URM walls.

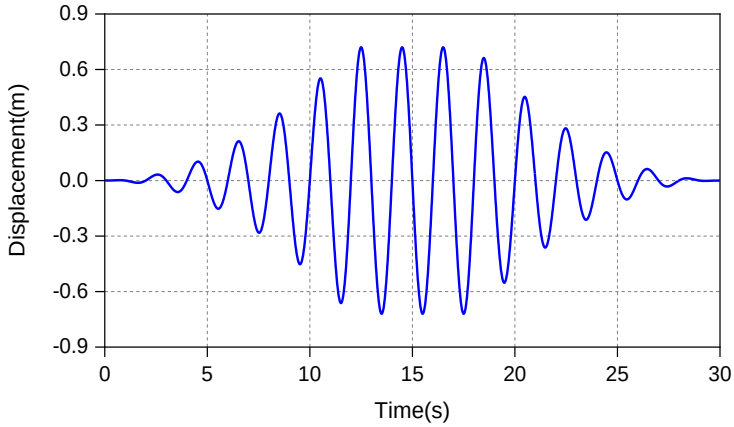

(a) Input time-displacement history at frequency=0.5Hz

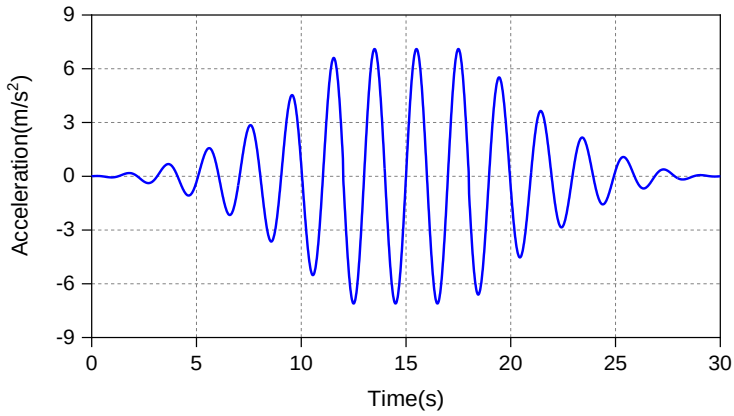

(b) Input time-acceleration history frequency=0.5Hz

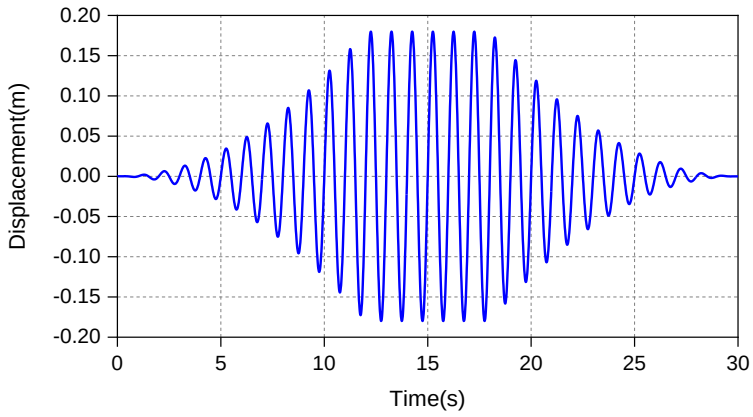

(c) Input time-displacement history at frequency=1Hz

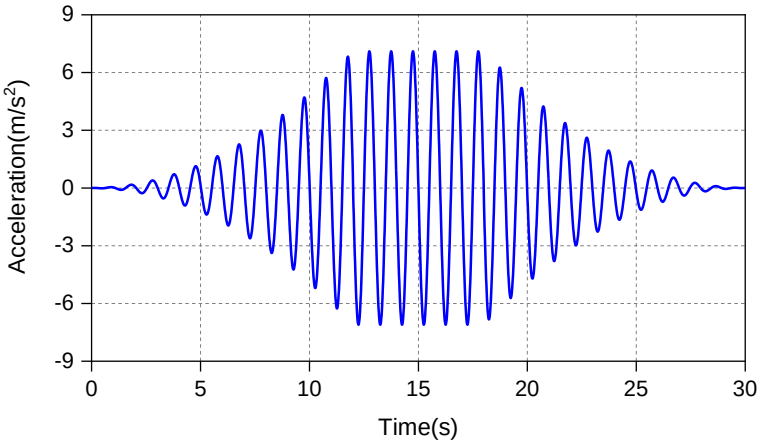

(d) Input time-acceleration history at frequency=1Hz

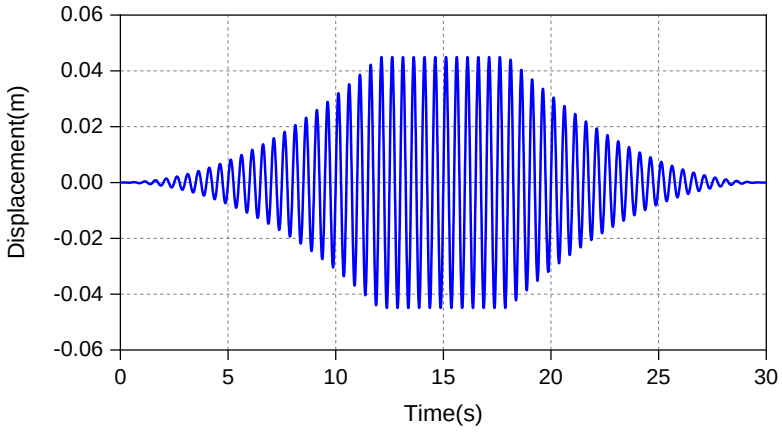

(e) Input time-displacement history at frequency=2Hz

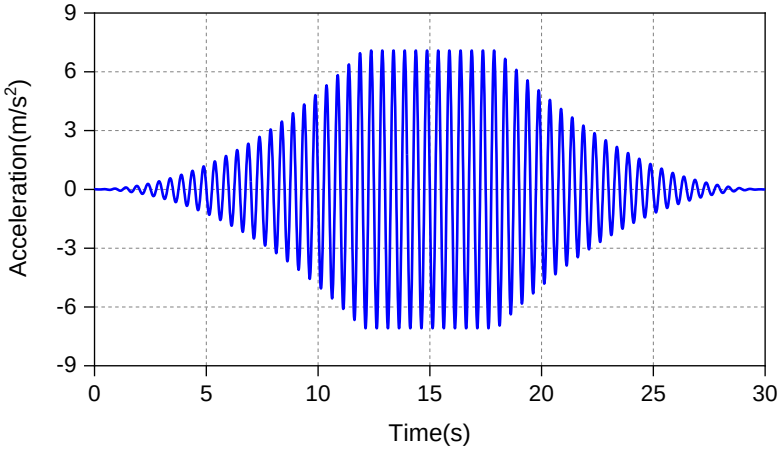

(f) Input time-acceleration history at frequency=2Hz

Figure 6.1 Input time histories of displacement, velocity and acceleration with different frequencies

After these tests, an artificial earthquake-generated to match a defined spectrum was used. The target spectra were taken from the elastic spectrum of Eurocode 8, Part-3. The damping ratio was 5%, the duration of the motion was 22 seconds, and a ground type was B and importance Class II was selected. Based on the requirements of Eurocode 8, a total of six artificial earthquake waves were generated to represent the range of the ground motions and the spectral matches these six histories are shown in Figure 6.2. The six equivalent displacements, velocity and acceleration time histories are shown in Figure 6.3. The matching process was done using the function of MATLAB code written by (Crewe A, 2020).

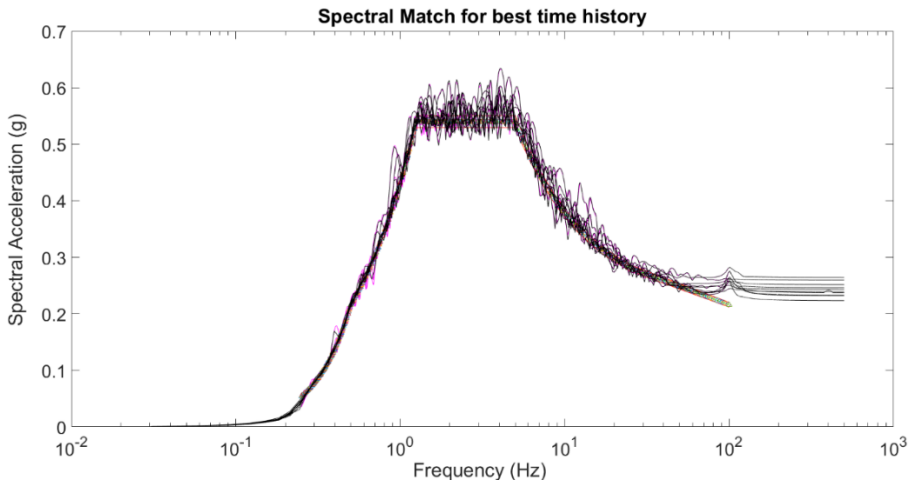

Figure 6.2 Spectral match for six artificial ground motions

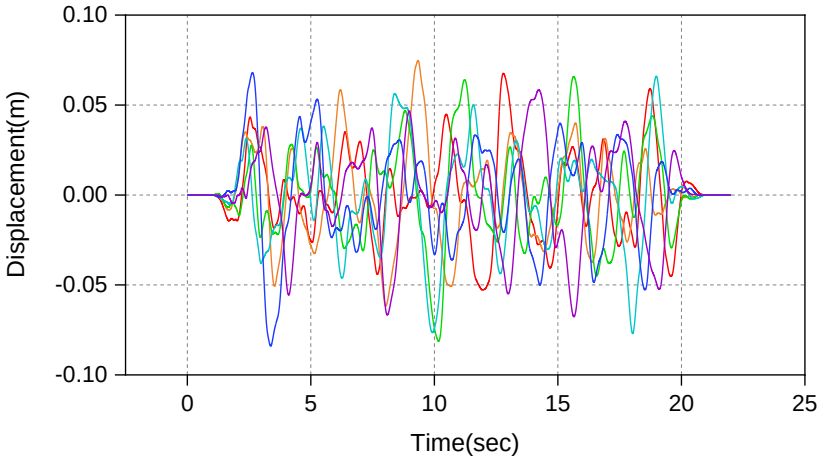

(a) Six input displacement time histories

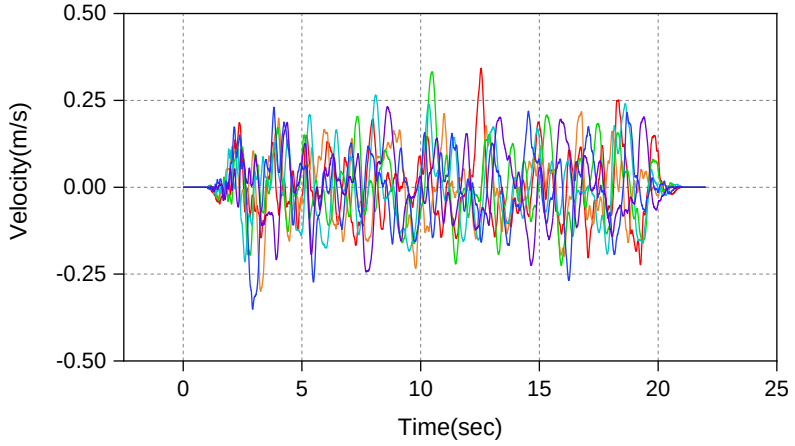

(b) Six input velocity time histories

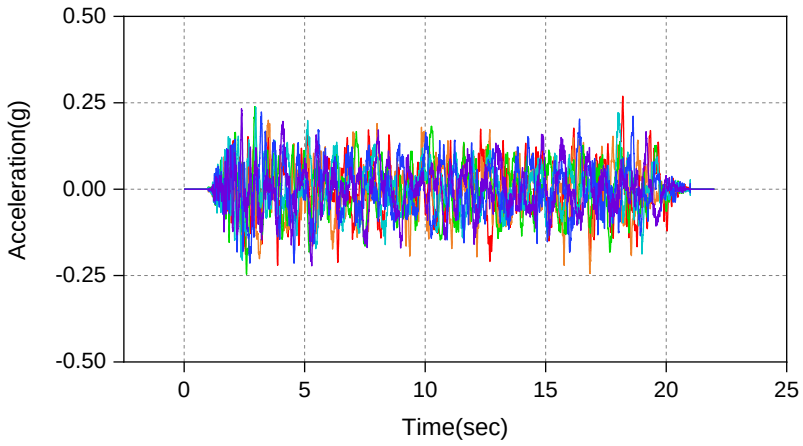

(c) Six Input acceleration time histories

Figure 6.3 Six input time histories for the numerical models

6.2.2 Boundary condition and damping

As only velocities (or stresses which are not applicable in this case) are recognized as input motions in 3DEC, the velocity inputs (shown in Figure 6.3) were used as the input motions in 3DEC. Once the dynamic input was determined, it was applied to the bottom block of the numerical model in 3DEC to apply the ground input motion into the URM wall. Two main parts are needed in the 3DEC analysis to produce a dynamic simulation of the structure properly. Initially the base block was fixed and gravity load was applied till the wall was elastic equilibrium. In this stage the boundary conditions of the top block were set as free but a large density was given to this block to allow simulation of the vertical prestresses in the URM walls. The relevant dynamic input was then applied to the base block and the time-domain dynamic analysis was performed.

Mass-proportional Rayleigh damping was applied during the analyses, with a value of 5% critical damping at a fundamental frequency of 1.5Hz. To improve the efficiency of the numerical analyses, only mass damping was employed and the relevant damping parameters of critical damping ratio and frequency were taken as 0.05 and 1.5Hz in 3DEC. For the numerical stability of the explicit algorithm and efficiency, the time step used was 0.001 sec (default).

6.2.3 Failure criterion for dynamic analysis of URM walls

It was necessary to define a failure criterion for the dynamic analysis when observing the URM wall responses and to identify changes in behaviour. However, for dynamic analysis, it is hard to define what failure of a structure is in a simple way. For static pushover analyses a simple peak capacity value can be determined directly from pushover curves. However, failure in a dynamic analysis can be defined in many ways, such as length of cracks, maximum allowed displacement, the collapse of a single brick or collapse of the entire wall, with every option leading to different peak acceleration. It is difficult to determine where the worst cracks or displacement will be without checking every possible location, which is impractical, and the dynamic behaviour of URM structures is also quite sensitive to the input accelerations. Even small changes in acceleration can lead to the sudden collapse of a URM wall. However, the collapse of the wall is relatively easy to define and this is also a limiting condition for URM walls as it leads to the risk of death. Therefore, in this chapter, the peak acceleration for collapse is used as the indicator of URM wall performance. For the harmonic input time-histories, the results are described as the relationships between the base shear force and displacement of the

top of the wall. For the artificial ground motions, the peak accelerations for the collapse are determined from the inputs levels and the drift ratio was calculated by looking at the relative displacements across the walls. To help identify the progress of damage and failure mechanisms, the crack patterns of URM under seismic excitation are also considered.

6.3 Dynamic tests of URM walls subjected to in-plane loading with harmonic input waves

Frequency, vertical load and amplitude are basic factors that might influence the dynamic response of URM walls, so these were studied before applying earthquake-like excitation to the walls. To do this, the harmonic input velocities shown in Figure 6.1 were used and the 3DEC model was set up as described in section 6.2.4. After running the numerical analyses in 3DEC, the load-displacement curves and crack patterns of masonry walls were obtained. Detailed information about the model setup is given below.

The properties of blocks and joints for the URM wall models were as discussed in sections 4.2.2 and 5.2.1. For the dynamic analysis with harmonic input, the displacements and velocities at the monitoring points were recorded and then the base shear force was obtained by creating a function to calculate the sum of the contact forces between the wall and the base block. For the dynamic analyses with earthquake-like inputs, accelerations were also recorded at the monitoring points. The key outputs from the dynamics analyses were the peak accelerations that caused failure, storey drifts ratios, and crack patterns of URM walls.

Detailed information about the loading points can be seen in Figure 6.4 with the input velocities being harmonic motions of artificial earthquake waves.

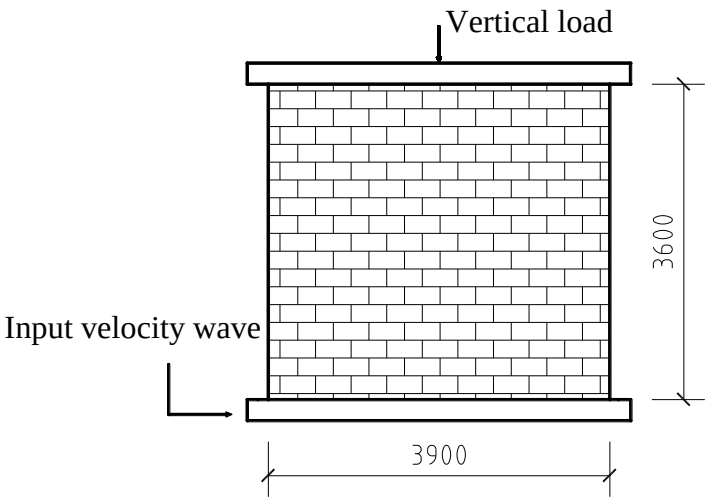

Figure 6.4 Set of loading blocks with input velocity

6.3.1 Frequency effects of seismic performance on URM walls in 3DEC

To identify the impacts of the frequency of the input velocity waves on the URM wall, the relationship between base shear and absolute displacement of the top of the wall is given in Figure 6.5. While the different frequencies appear to produce different responses it should be noted that the peak base shears are the same for all three velocities and that the displacement shown is the absolute wall displacement. Because the peak acceleration was kept constant (see Figure 6.1) the peak velocity (and displacements) for the three inputs varied and it is this variation that is being seen in the different peak displacements in Figure 6.5. If this effect is ignored that it can be seen that there is no significant difference in the wall response for the three frequencies suggesting that this wall is not particularly sensitive to different input frequencies.

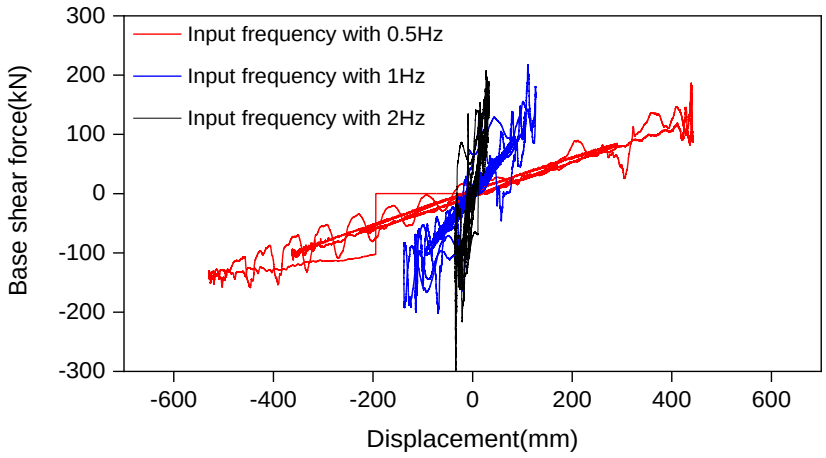

Figure 6.5 Load-displacement curves with different input frequencies for shaking table tests at analysis time 12s

The crack patterns for these tests can be seen in Table 6.1. The main crack pattern in all cases is diagonal cracking and the only real difference between the walls is that wall shaken at 2Hz shows more damage as more cycles of loading have been applied by the snapshot time of 12 sec.

Table 6.1 Crack patterns of masonry walls with different frequencies (Maximum allowed crack length is 0.05m) at 12s

Frequency	Crack pattern
Crack patterns with 0.5Hz frequency	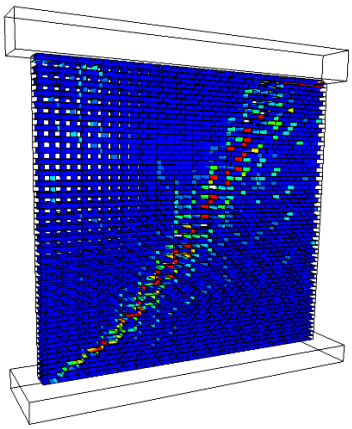

Crack patterns with 1Hz frequency	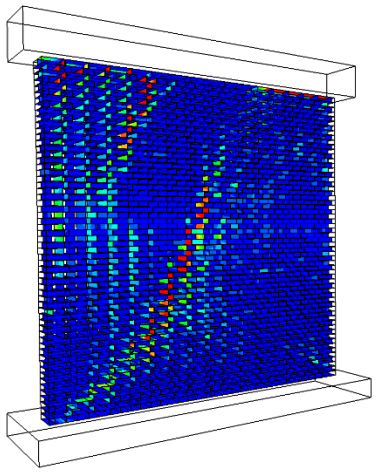
Crack patterns with 2Hz frequency	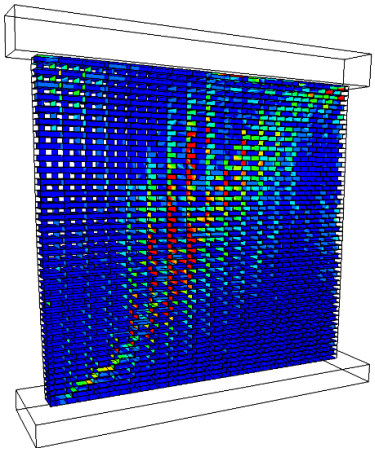

6.3.2 Effect of vertical load on the seismic performance of URM walls in 3DEC

Similar to static pushover tests discussed previously, the vertical load is another factor to be considered when looking at the dynamic performance of URM walls. Three different vertical loads i.e. 200kN, 100kN and 25kN were chosen and otherwise identical analyses were done. A 1 Hz singe dwell input time-history motion was applied as shown in Figure 6.1(c) and Figure 6.1(d). Looking at the load-displacement curves in Figure 6.6, the maximum base shear force recorded in the three dynamic tests clearly varies depending on the vertical load. However, the maximum wall displacements in all the three tests are similar, especially for the tests with 100kN and 25kN vertical loads. The maximum base shear force for the masonry wall with the 200kN vertical load is about 2.5 times higher than for the wall with the 100kN vertical load and is more than ten times higher than for the wall with the 25kN

vertical load. It can be seen that the URM wall is very sensitive to a change of vertical load, and the increase of maximum base shear force is directly related to the increase in vertical load.

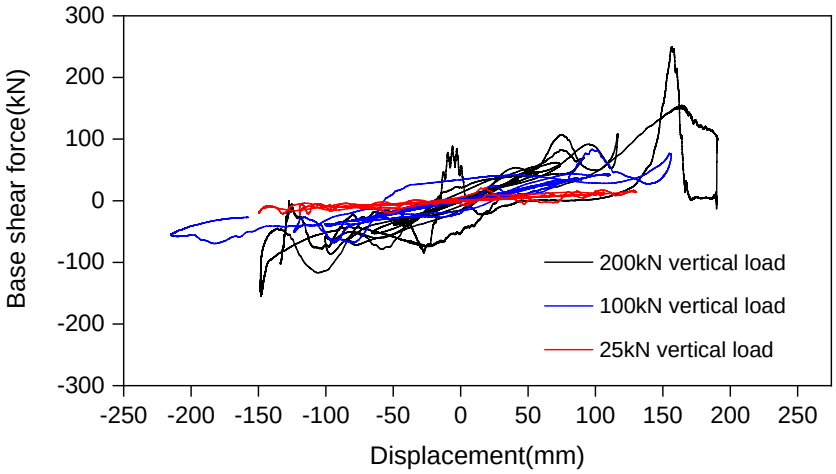

Figure 6.6 Load-displacement curves with different vertical loads for shaking table tests at analysis time 12s

The impact of changes in the vertical load can also be seen in the crack patterns in the masonry walls. Looking at the crack patterns for these analyses in Table 6.2, the different vertical loads lead to distinct cracking patterns. For the masonry wall with a 25kN vertical load, the cracks mainly occur along one diagonal direction and a few local cracks appear at the top-left corner of the wall. For masonry wall with a 100kN vertical load, more cracks appeared with an obvious rocking failure, and for the wall with a 200kN vertical load, cracks were generated along with both diagonal directions and local failure appears at the wall corners. Clearly the vertical load has a significant impact on the dynamic performance of the masonry wall. The change in vertical load not only affects the dynamic capacity of the structure but also changes the crack propagation in the wall. The reason for this can be explained that different vertical load would lead to the bricks of the wall having different vertical acceleration and when the dynamic input was applied, the walls with different vertical loads could generate distinct total force, which could affect the cracks of the URM walls.

Table 6.2 Crack patterns for masonry walls with different vertical loads (Maximum allowed crack length is 0.05m) at 12s

Vertical load	Crack pattern
Crack patterns with 25kN vertical loads	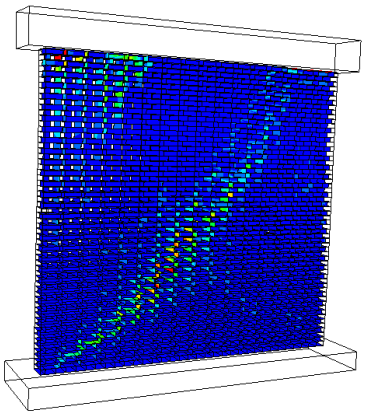
Crack patterns with 100kN vertical loads	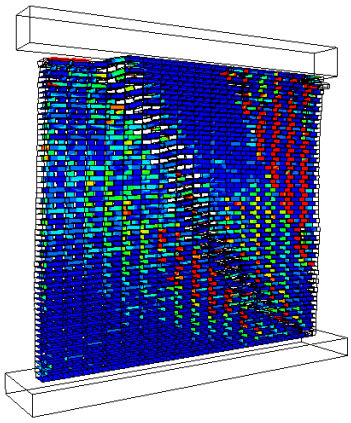
Crack patterns with 200kN vertical loads	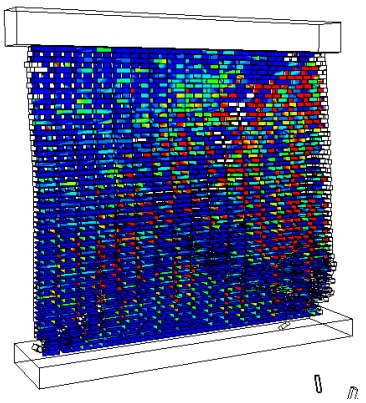

6.3.3 Amplitude effects of seismic performance on URM walls in 3DEC

The amplitude of the input motion is clearly going to affect the response of a masonry wall. However to confirm the influence of amplitude, three different amplitude factors i.e. 0.25, 0.5 and 1 were selected and the results of these dynamic tests are shown in Figure 6.7 and Table 6.3.

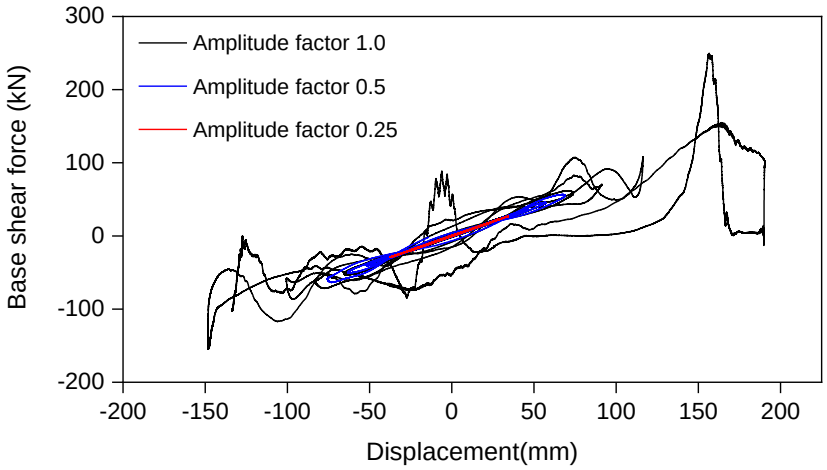

Figure 6.7 load-displacement curves with different amplitude factors for shaking table tests at analysis time 12s

Looking at the load-displacement curves in Figure 6.7, it is clear that the maximum base shear force is directly related to the amplitude factor. For the masonry walls subjected to motions with amplitudes of 0.25 and 0.5, the walls remain elastic range and curves are almost linear. For the masonry wall with an amplitude factor of 1.0, the wall starts to fail and the maximum base shear force increases more significantly compared with another two cases. The effect of the different amplitude factors is also reflected in the crack patterns in the masonry walls. For masonry walls with 0.25 and 0.5 amplitude factors, there is no cracking as the walls remain in their elastic range. For the wall with an amplitude factor of 1.0, obvious cracks occur along both diagonals, and local failure is seen at the bottom corner of the wall.

Table 6.3 Crack patterns for masonry walls with different amplitude factors (Maximum allowed crack length is 0.05m) at 12s

Amplitude factor	Crack pattern
Crack patterns with 0.25 amplitude factor	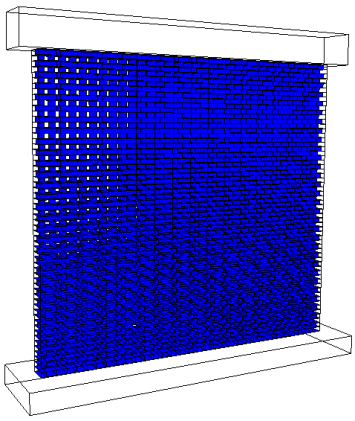
Crack patterns with 0.5 amplitude factor	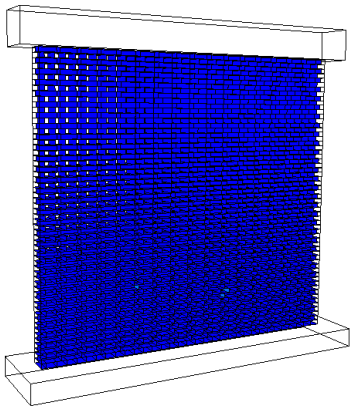
Crack patterns with 1 amplitude factor	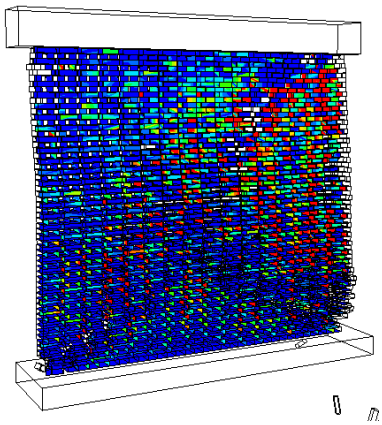

Of the three factors studied only the vertical load and amplitude of input have a significant effect on the dynamic behaviour of the masonry wall. Due to the more random nature of a dynamic test, the load-displacement curves all tend to display some variation but it is still helpful to now evaluate the effects of opening factors on the dynamic performance of URM walls in 3DEC.

6.4 Dynamic analysis of opening effects on URM walls under in-plane behaviour

6.4.1 Sensitivity of dynamic analysis for URM walls in 3DEC

Before identifying the impact of openings on URM walls for dynamic loading, the sensitivity of the wall response to the input motion needed to be assessed. The six input motions described in section 6.2.1, were scaled to have the same peak acceleration and were then used to analyse a single example URM wall. The range of responses recorded were then used to calculate some envelopes of response and this envelope of response was compared the responses previously obtained from the static analyses. As there is no restrain for the top block, the displacement of monitoring point located at the top block is recorded. All the results are based on one identical URM wall with 3% opening as shown in Figure 6.8, all the properties are similar to that described in section 6.3 and the results are given in Figure 6.9 and Figure 6.10. In the results, the displacement over 5% drift ration is defined as failure.

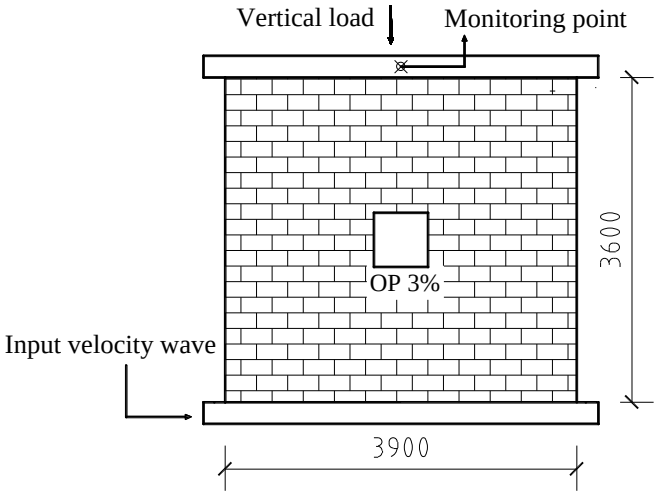

Figure 6.8 Detail information for the URM wall for considering the stability of the dynamic analysis

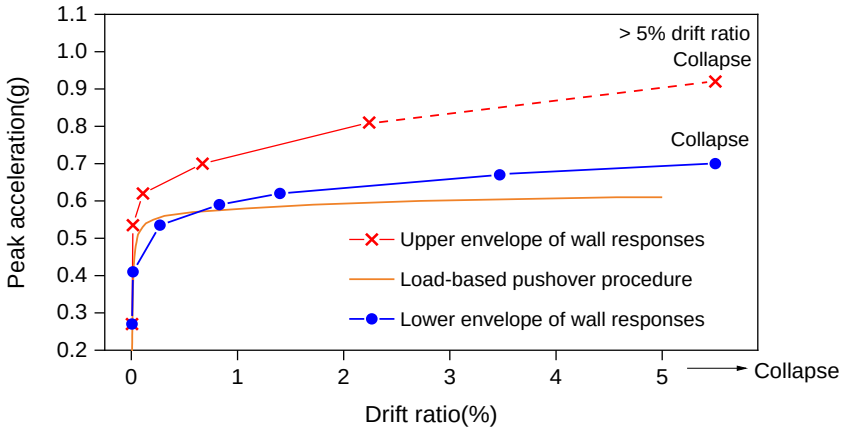

Figure 6.9 Comparison of results between the envelope of dynamic analyses and the pushover test results for a URM wall with a 3% opening

Looking at Figure 6.9 it is clear that the envelope of results from the dynamic analyses of the URM wall almost always display higher peak accelerations than for the static load-based analysis procedure pushover test. In other words, the dynamic response of the walls is generally better than the quasi-static response. For the upper envelope the highest peak acceleration is 0.92g for a 5% drift and for the lower envelope the lowest peak acceleration is 0.7g for a 5% drift. These two values are 53% and 16.7% higher than the peak pushover value of 0.6g, respectively. For dynamic analyses, the input time-histories include cyclic motions, and even though the acceleration in one direction has led to the onset of failure when the direction of the acceleration reverses this tends to limit the progress of wall deformations. This then increases the time needed for the wall to reach a critical failure drift, leading to an increase in the value of peak acceleration needed to cause significant displacement across the wall. For a static pushover test, the peak acceleration capacity is achieved as soon as the structure starts to fail. Therefore, a static pushover test will record a more conservative value of peak acceleration capacity for a wall, and for the assessment of the in-plane capacity of URM walls, this is a safer value to use.

Table 6.4 Crack patterns in the URM for a single time history scaled to different peak acceleration levels at 12s

Failure description	Crack patterns of URM
Initial small cracks	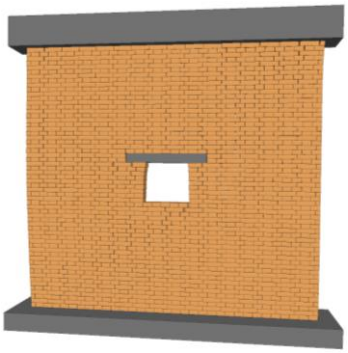
Crack propagation	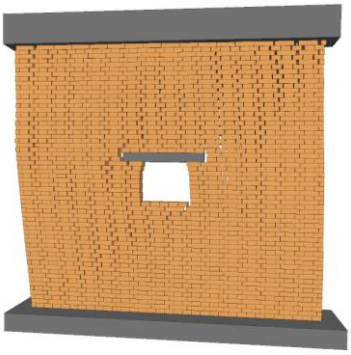
Large diagonal cracks forming through wall	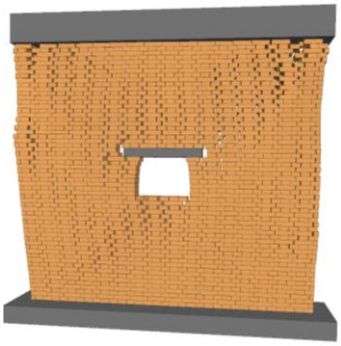
Total collapse	

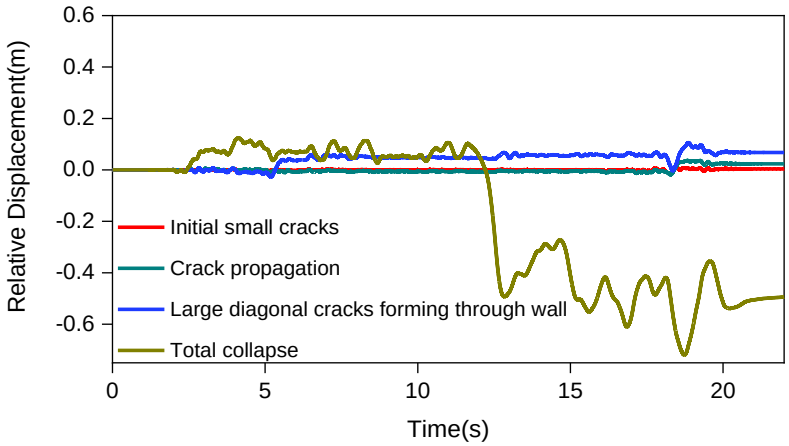

Figure 6.10 Relative displacement histories of monitoring points scaled to different peak acceleration levels

The development of crack patterns in the URM wall for one of the artificial ground input motions scaled to different acceleration levels is shown in Table 6.4. To compare the crack patterns with different peak accelerations, the cracks of walls at the same time of the analysis (12s) with different peak values of accelerations are recorded. For the smallest shakes the wall remains in its the elastic range, and there are no cracks and deformation of the wall occurs. As the acceleration increases, more cracking occurs through the wall and the deformations are more visible. When the structure reaches its plastic range, some large cracks are generated along both diagonal directions and the deformation of walls exceeds the allowed maximum drift ratio, which has been defined as failure. Finally, the URM walls collapse, and the deformation cannot be recorded. The development of cracking illustrates the failure mechanisms and the progress of the seismic response of the wall. Compared to the static pushover test it is clear that for a dynamic analysis the cracks occur on both sides and diagonals of the wall and there is also a more localised failure as a result of the number of reversing cycles of loading. Figure 6.10 presents the relative displacement histories of the monitoring point for the acceleration levels leading to different failure types. The displacements time histories match the crack patterns, which shows the consistency of the dynamic analysis of URM walls in 3DEC.

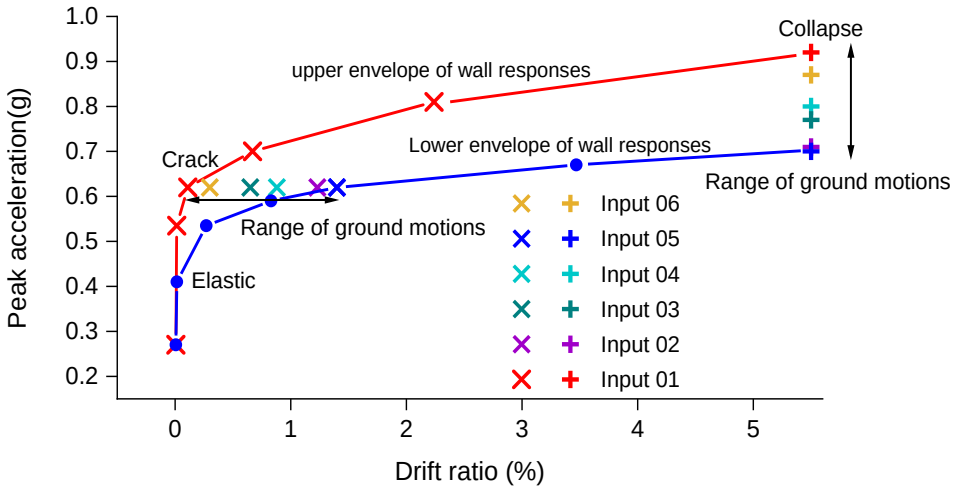

Figure 6.11 Range of peak acceleration-drift ratio curves for different input ground motion of URM walls with 3% opening

Figure 6.11 shows in more detail for the six different input artificial ground motions used in the analysis of the wall. The two motions producing the highest and lowest acceleration-drift ratio curves are shown and a few specific points from the rest of the motions are also included. While the wall remains in its elastic range (i.e. the peak input acceleration is less than 0.4g), the results for all the motions are similar, but after 0.4g, the curves begin to vary as cracking occurs. As the peak acceleration increases, the drift ratios for the motions start to show larger variances. Taking the points with an acceleration of 0.62g for instance, the range of drift ratio varies from 0.11% to 1.4% and the difference in drift ratio between the six input artificial ground motions is 1.29%. However, when looking at the peak accelerations at collapse (i.e. 5.5% drift), the maximum and minimum values of acceleration are 0.89g and 0.7g, i.e. a difference of around 31.4%. Whether looking at drift ratio for a particular acceleration or the peak acceleration at collapse, the results are consistent between the input ground motions with input motion 01 resulting in the best seismic performance for the wall, while the wall performs quite badly when subjected to input motion 05. These outcomes reveal that the behaviour of the wall is quite sensitive to the input motion, so a range of motions should be used if it is important to determine the likely range of wall behaviours for an earthquake that matches a particular response spectrum. Even for artificial ground motions that were all a good match to a single demand spectrum, the shape of time-histories and the time of peak accelerations are distinct, which could lead to a local structural failure occurring at different times, thus affecting the whole seismic performance of the URM walls.

Table 6.5 Crack patterns of the URM wall for the different input ground motions at 6s

Input ground motion	Crack pattern
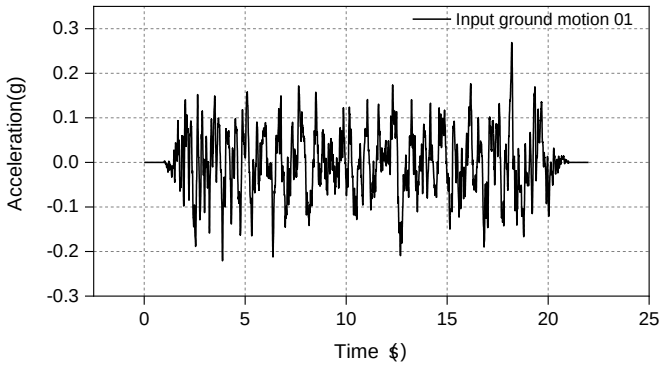	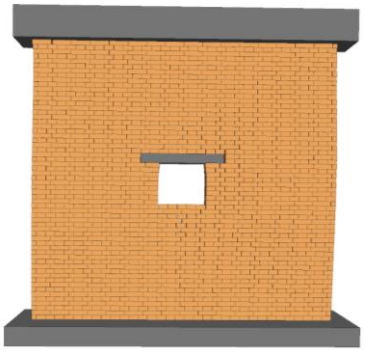
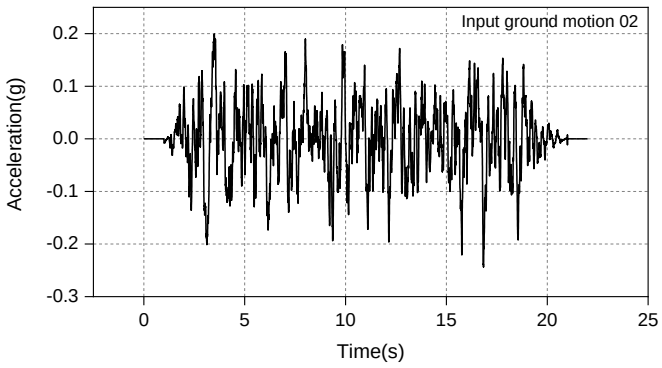	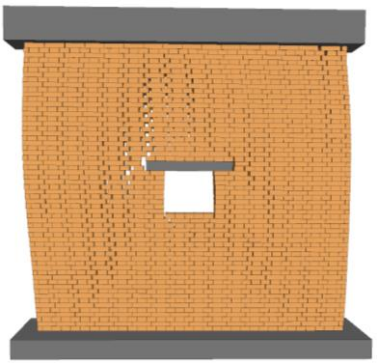
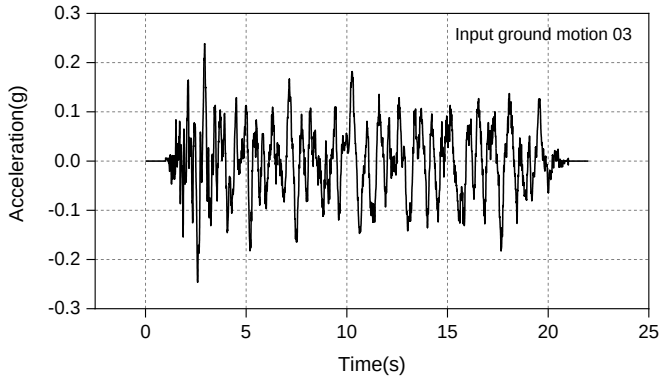	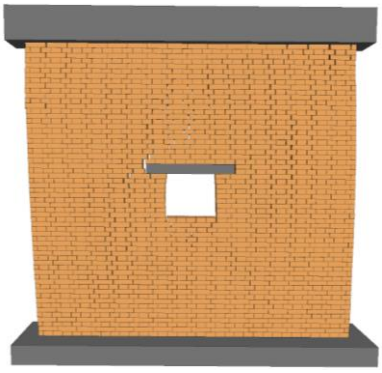

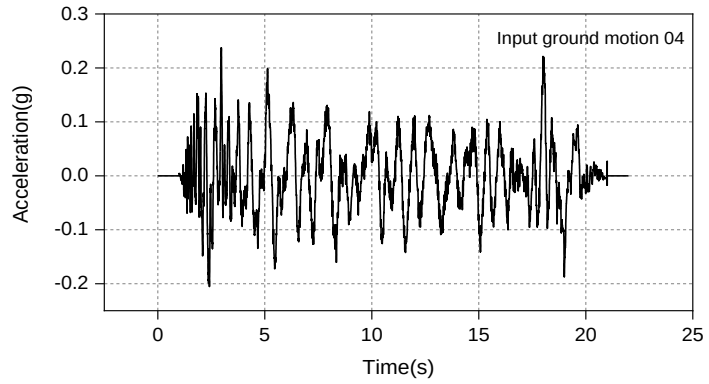

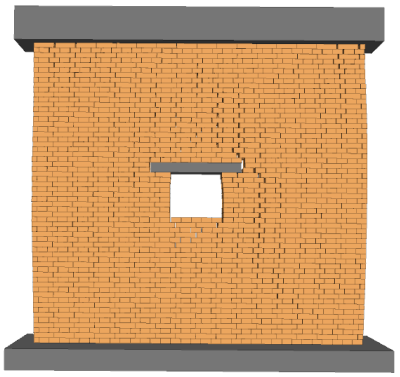

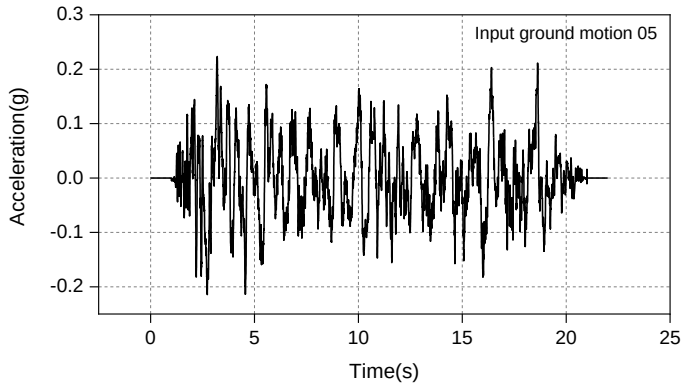

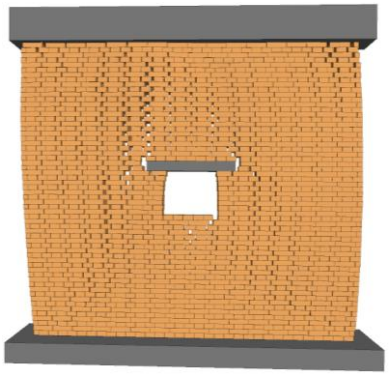

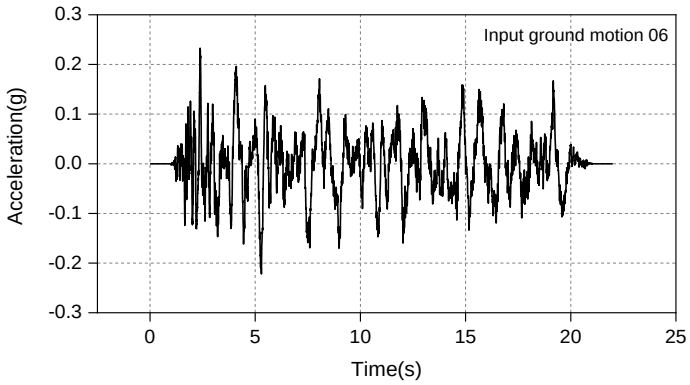

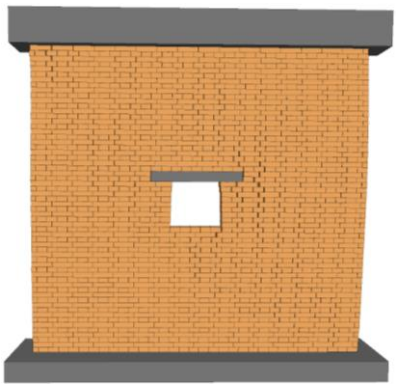

The crack patterns for the URM wall for the six different input ground motions, scaled to the same peak acceleration, are shown in Table 6.5. The table shows that six input artificial input ground motions generate different crack patterns in the URM wall, due to the differences in the phasing of the cycles and the location of the peak acceleration. Of the input ground motions, the walls subjected to input 02 and input 05 display the worst crack patterns with large cracks and lots of local failures. The wall subjected to input 01 shows the best performance and only a few small cracks can be seen. This can be explained in that input 01 has a lower acceleration for most of its duration and only hits the target peak acceleration value at the end of the time history, so there is not adequate time for the

progression of significant failure. However, for the walls with input 02 and 05, the peak target acceleration occurs at the beginning of the time history and there are a number of further high acceleration peaks, which leads to the walls failing quickly and then continuing to experience high forces which generates further cracking.

This section has identified that the dynamic behaviour of URM walls is sensitive to the exact time history motion applied. Even so the range of responses only varied by about 30% which can be considered acceptable for most non-linear dynamic analyses based on time histories generated to match a single response spectra. Therefore, as long as a number of time histories are used to determine the range of possible responses, it can be assumed that 3DEC is a potent tool for the dynamic analyses of URM walls. The next section looks at the impact of openings on the dynamic behaviour of URM walls.

6.4.2 Opening percentage effects on URM wall under dynamic analysis

A similar set of opening sizes, as discussed in section 4.3, are now considered under dynamic loading. Seven different opening percentages from OS1 (without openings) to OS7 (31%) are defined in Figure 6.12. The peak accelerations at collapse, and the equivalent results from the static analyses, are shown in Figure 6.13.

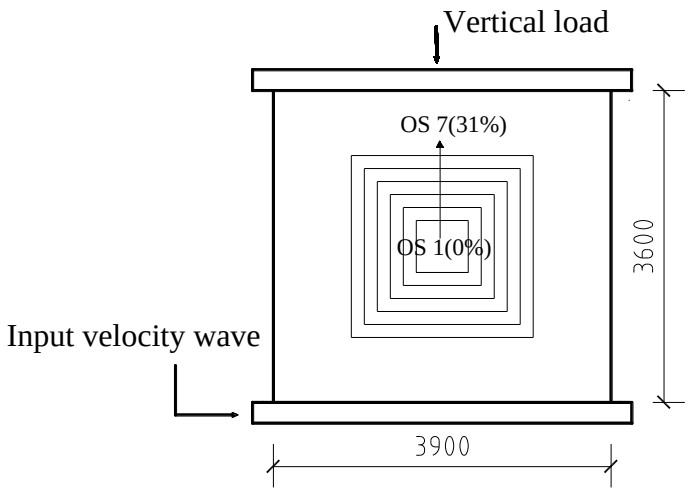

Figure 6.12 Cases considering different opening percentages of URM walls for dynamic testing

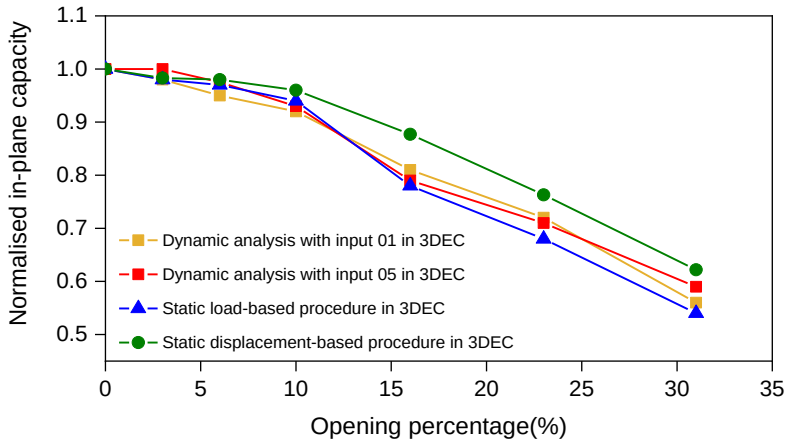

Figure 6.13 Normalised comparison of relationship for opening percentage effects between static pushover test and dynamic analysis

Figure 6.13 shows that the three analysis procedures produce slightly different curves for the relationship between opening percentage and in-plane capacity. In general, the results from the dynamic analyses give lower in-plane capacities than the static load-based analysis procedure but they are little better than those from the displacement-based analysis procedure. Nevertheless, the curves for all the analysis procedures are similar and follow a similar trend. Taking a 31% opening percentage, for example, the normalised in-plane capacities from the four analyses are 0.56, 0.6, 0.54 and 0.64, respectively. When the opening percentage is less than 10%, both static analyses show better in-plane performance than the dynamic analyses, which means that the results of a dynamic analysis of URM walls are more sensitive small openings compared to the results from the static analyses. This is probably because a dynamic analysis is cyclic and generally results in lots of local failures which propagate more readily under cyclic loading. When URM walls have even small sized openings, the local failures generated by cyclic loading can lead to an imbalance in loading that can affect the global seismic behaviour of structures. It can also be observed that the curves from the dynamic analyses are closer to the static load-based analysis procedure possibly because the load-based approach also leads to more localised failures.

Table 6.6 Typical crack patterns for URM with different opening percentages under seismic loading at 12s

Opening percentage	Crack patterns
0%	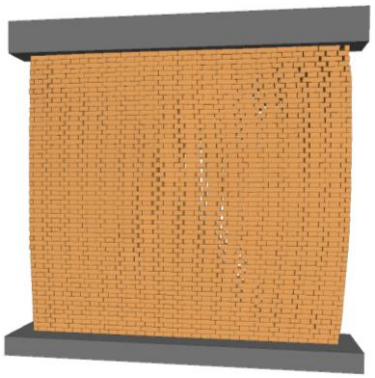
3%	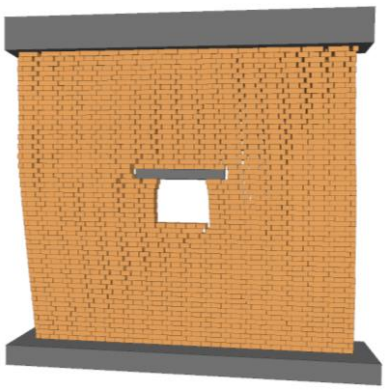
6%	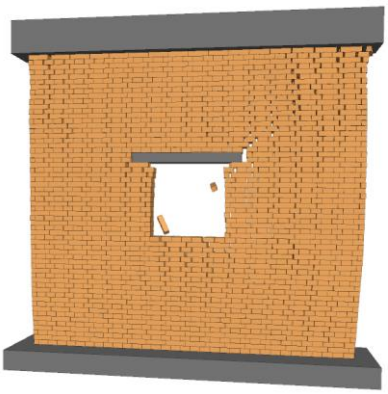

10%	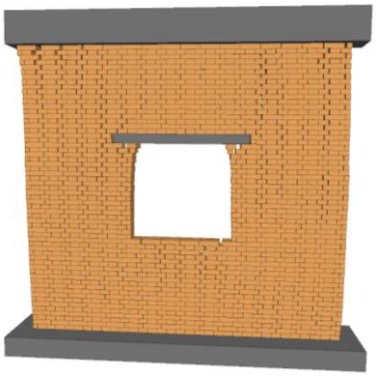
16%	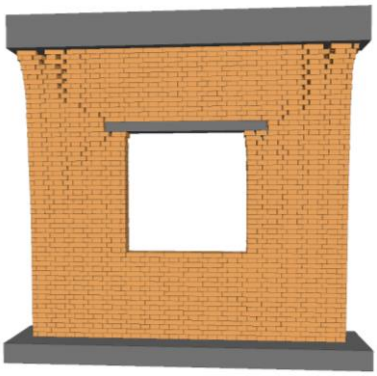
23%	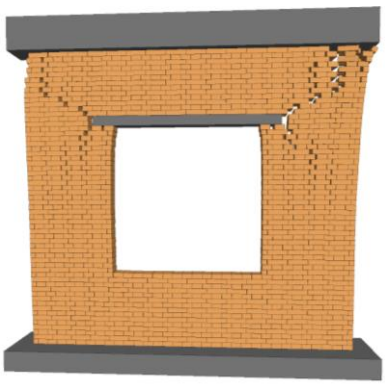
31%	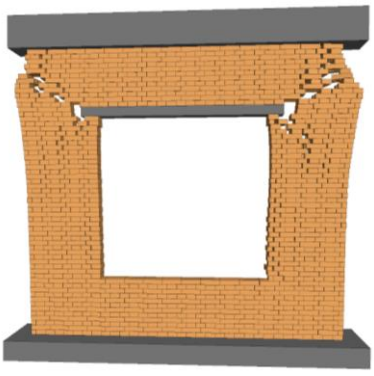

Some typical crack patterns in the URM walls for seismic loading with different opening sizes can be seen in Table 6.6. The images show that the failure pattern in the walls remains similar as the opening percentage increases. This is different from the results from the static analyses because loads in the static pushover tests are only applied in one direction and initially cracks are generated only along one diagonal. For static analyses, as the opening size increases the failure mechanism changes and then diagonal cracks appear on both diagonals. However, the input accelerations for a dynamic analysis occur in both directions in the loading axis and therefore the walls show two diagonal cracks for all sizes of opening. The crack patterns from the time history analyses are also far more distributed than those in the static analyses and for the dynamic analyses the diagonal cracks cannot be observed clearly. It can also be seen that when the URM walls analysed using dynamic and static procedures have same opening percentages, the one subjected to dynamic loading shows more localised cracking and these cracks reduce the in-plane strength of the wall sometimes causing local collapse which seriously affects the global performance. It is crucial to consider the possibility of local failure of walls as this can impact the global performance of the wall and in addition local failures can still be dangerous to the lives of people even if the walls do not collapse completely.

The effects opening percentage on the in-plane performance of URM walls under dynamic loading have been investigated. The fact that static and dynamics analyses produce similar results for the in-plane behaviour for URM structures is useful and this can allow development of simpler assessment methods, as will be seen in the next chapter. Nevertheless, it is still important to consider the possibilities of local failures that can affect the in-plane behaviour of masonry walls significantly under dynamic loading.

6.4.3 Opening position effects on URM wall under dynamic analysis

In addition to considering the effect of opening size on the seismic behaviour of URM, the impact of opening position also needs to be considered because unbalanced forces can be generated in the walls because of the asymmetrical layout of the sections of wall left by the openings. This could reduce the in-plane strength of walls and lead to collapse under seismic loading. The set-up of the wall model and the dynamic analysis procedure were as described in section 6.3.2 and six opening positions (A1 to C2) were considered, as shown in Figure 6.14. Using one seismic input, ground motion 05 based on Table 6.5 as an example, the performance of the wall and the equivalent crack patterns are shown in Figure 6.15 and Table 6.6.

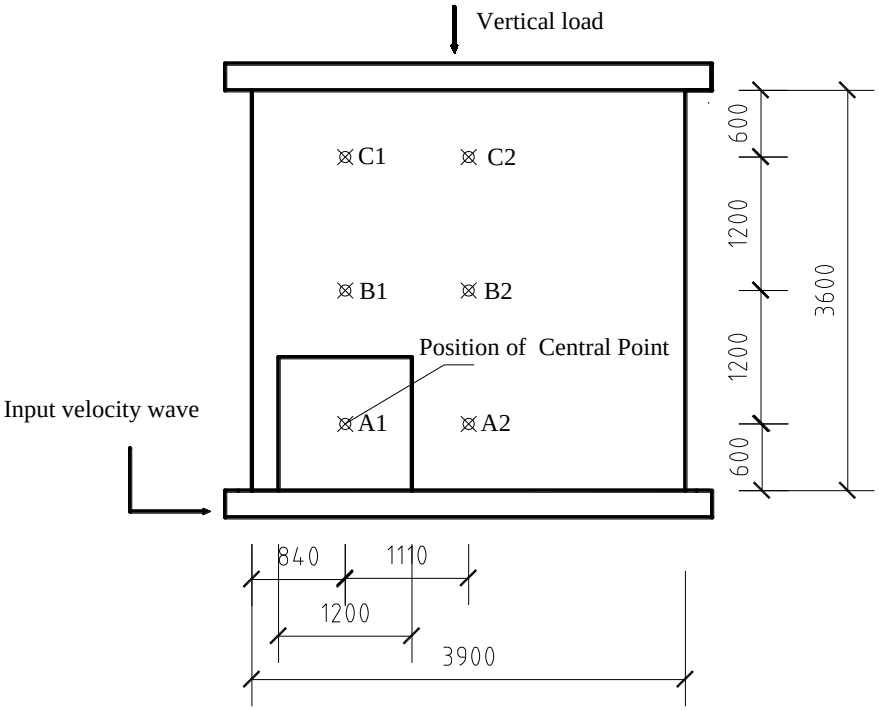

Figure 6.14 Arrangement of the opening position under the shaking table test

It is clear from Figure 6.15(a) that the in-plane capacities of URM walls with different opening positions are different. The walls with the opening located at central show better in-plane performance than those with the top openings, and walls with bottom openings have higher in-plane capacity than those with edge openings. Specifically, the wall with an opening at position B1 shows the worst seismic performance with peak acceleration capacity of 0.52g while the wall with an opening at B2 has the highest peak acceleration capacity of 0.68g, the difference between these values being 30%. The wall with an opening at A2 has the second-best seismic capacity of 0.65g and the seismic capacities of walls with the other three opening positions (C1, C2 and A1) are similar carrying 0.58g, 0.62g and 0.6g, respectively. The results are also shown in Figure 6.15(b) which shows how the capacity of the wall varies for different opening positions. This figure shows that URM walls with central openings have the best in-plane seismic capacity while those with holes at the edges are the worst.

Compared with the results from the static pushover tests shown in Figure 4.17(a) (b), there are a few differences that are worth noting. For both types of static analysis procedure, the walls with the maximum in-plane capacity had the openings located at B2 and the same is true for the walls subjected to dynamic analysis. The most significant differences occur for the wall with an opening at location A1. In this case both static analyses showed the wall performed worst of all opening positions while for a dynamic analysis this was the third-worst case. It is also clear that for the single direction pushover

tests there is asymmetry in in-plane capacity distribution, which leads walls with holes in one side have the highest capacities and holes in the other side producing the lowest capacities. However, because of the cyclic nature of the seismic motions, dynamic analysis can almost be considered to be a symmetrical loading cases and therefore holes in either edge lead to effectively the same result. That can explain the differences between the static pushover tests and dynamic seismic tests for openings located at the borders of the wall. However, when the opening is in the centre of the wall both the static and dynamic analyses produce follow the similar pattern that wall capacity is larger than when the opening is at the edge of the wall.

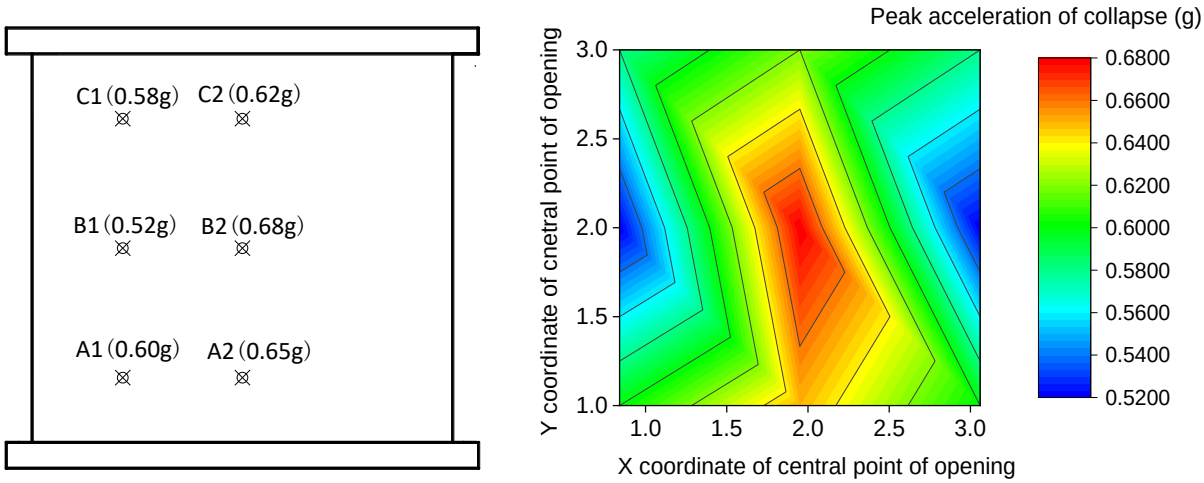

(a) Peak accelerations for URM walls with different opening positions; (b) Normalised in-plane capacities of URM walls with different opening positions

Figure 6.15 Dynamic results for URM walls with different opening positions under in-plane seismic loading

The crack patterns for the seismic test with the different opening positions are shown in Table 6.7. The images showed that the different opening positions result in quite different crack patterns. When the openings are located in the central part of the wall, the cracks are generated symmetrically and cracks appear on both diagonals. For walls with openings at edges, some asymmetrical cracks occur and severe localised cracking can be seen. This is also reflected in the results, where the accelerations that the walls can carry in-plane, when the holes are at the edge, are lower. The asymmetry of the opening location can cause a localised failure of the walls especially in the bricks located below the openings, which significantly reduces the seismic performance of the walls.

Table 6.7 Typical crack patterns of URM walls with different opening positions under seismic loading at 12s

Opening positions	Crack patterns
A1	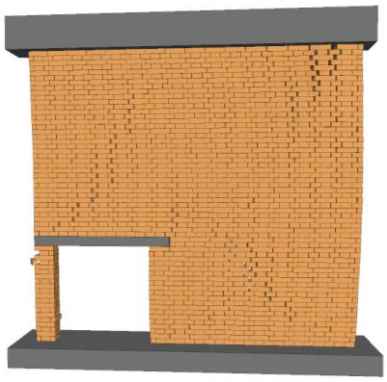
A2	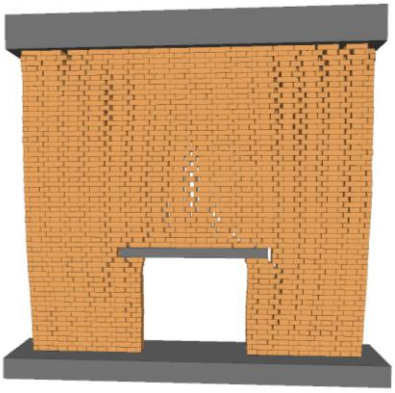
B1	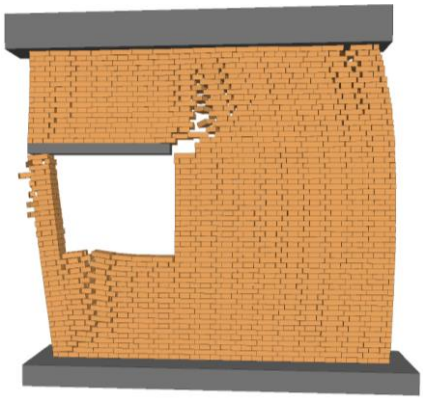

B2	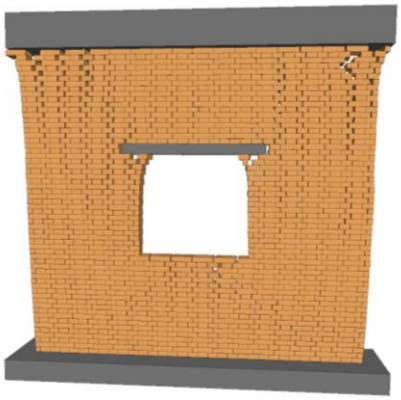
C1	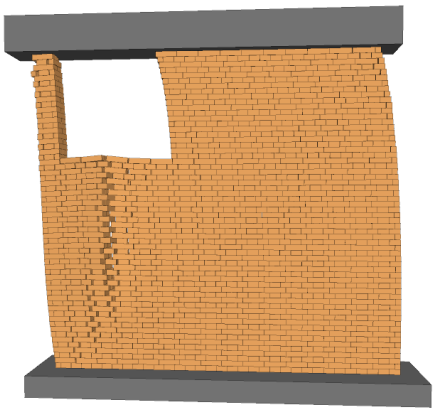
C2	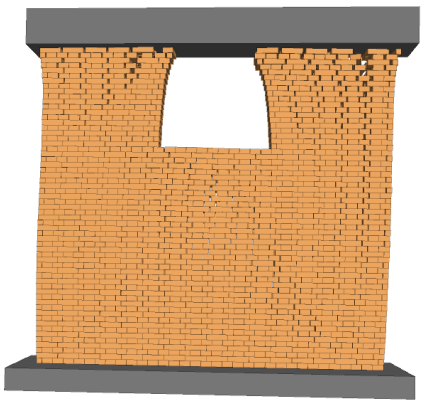

The dynamic analyses of the effect of opening position on the capacity of URM walls subjected to in-plane excitation show that walls with different opening locations have different seismic performances. However, the overall in-plane capacities for the different opening positions follow the same trends as for the static analyses which suggest that the dynamic results can be effectively represented by the simpler static analysis procedures.

6.5 Dynamic analysis of the effect of openings on URM walls subjected to out-of-plane dynamic loading

Out-of-plane behaviour is another important aspect of the performance of URM walls so it is essential to identify the effects of the openings under this type of dynamic loading. It is important to note that for dynamic analysis of URM walls under out-of-plane loading the computational time was far longer than that for the static loading cases discussed previously. Therefore, only one type of boundary condition (three-side supported) was considered in this research, particularly as walls with these boundary conditions faired worst under the static pushover tests.

6.5.1 Modelling of URM walls subjected to out-of-plane seismic loading

Before running dynamic analysis of walls in the out-of-plane direction, appropriate numerical models of URM walls had to be built that could reproduce the correct boundary conditions under dynamic conditions in 3DEC. The geometry of such models can be seen in Figure 6.16(a) where the supporting walls are set as long as possible to make a wall under test effectively supported on three sides. The vertical loads are applied by adding a top block with a high density and the bottom block has the dynamic input applied to it. The size of each masonry brick was set as 0.06m x 0.24m x 0.12m (height x span x breadth), and the dimensions of masonry wall under test was 3.9m x 0.24m x 3.6m (length x width x height). The support walls were set as 2.24m x 0.24m x 3.6m (length x width x height). The boundary conditions of the out-of-plane wall are supported by in-plane walls and two extra blocks are fixed to at the end of these walls to remove any shear motion at the ends of the supporting walls. The final arrangement of the numerical model in 3DEC can be seen in Figure 6.16(b). The properties of all bricks and joints are as defined in section 5.2.1.

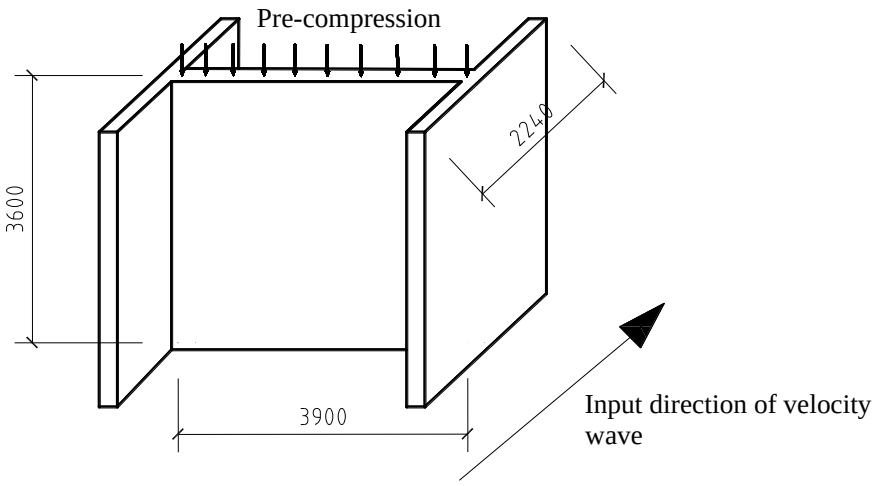

(a) Geometry information of the numerical model

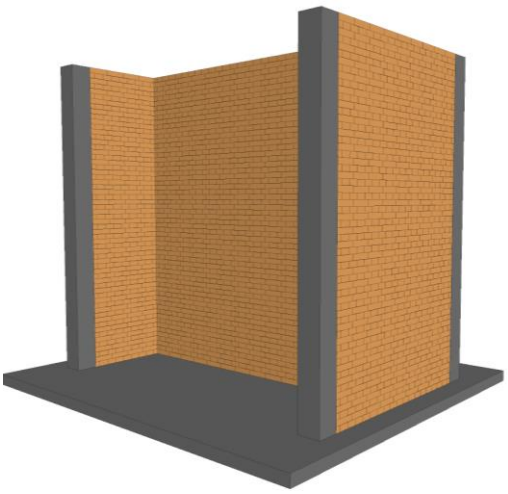

(b) Numerical model in 3DEC

Figure 6.16 Geometry information of URM walls under out-of-plane seismic loading

Based on the static tests described in section 5.3 and 5.4, the out-of-plane behaviour of URM walls is much more related to the effects of lintels than opening size. In other words, there is no clear direct relationship between opening percentage and the out-of-plane performance of a URM wall. Therefore, for dynamic analysis of the effect of openings on URM walls under out-of-behaviour, only opening position effect was considered.

6.5.2 Opening position effects on URM wall under dynamic analysis

The effect of the opening position on the out-of-plane performance of the URM wall under dynamic loading was considered by looking at a total of six different opening positions. The location of the opening cases is shown in Figure 6.17(a). The dynamic analysis follows that described in section 6.5.1 (but changing the loading direction) and the relationships between the opening position and the out-of-plane capacity are shown below in Figure 6.17(a) and Figure 6.17(b).

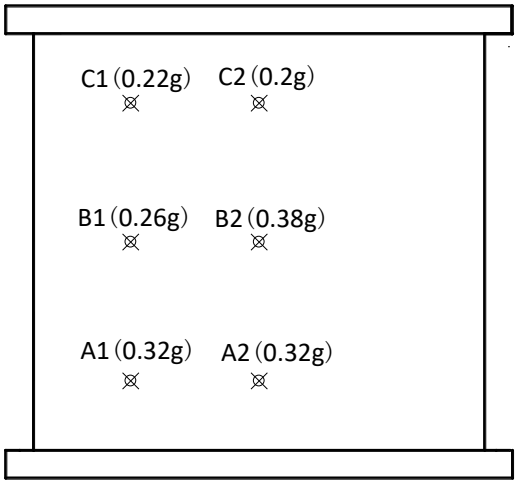

(a)

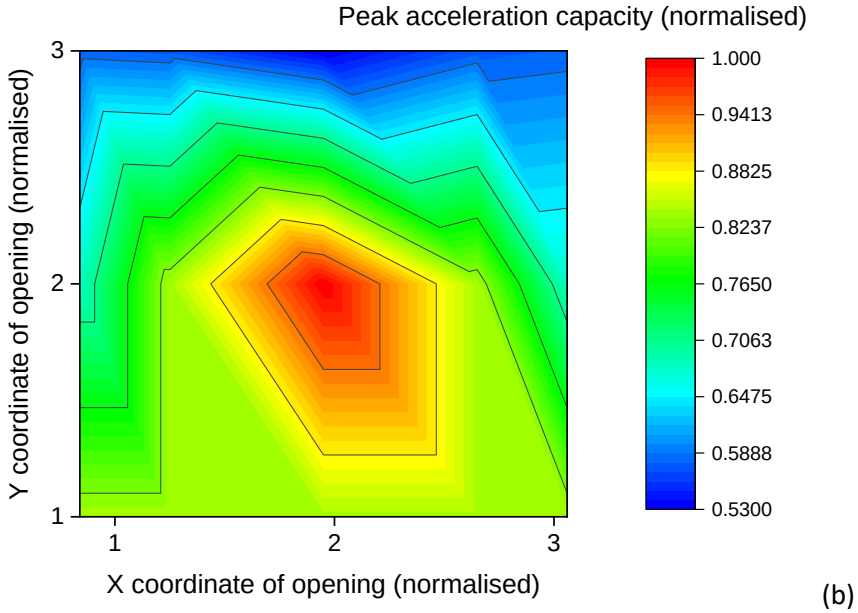

(b)

(a) Peak acceleration of the URM wall with different opening positions; (b) Normalised in-plane capacities of the URM wall with different opening positions

Figure 6.17 Dynamic results for URM walls with different opening positions under dynamic out-of-plane loading

The results in Figure 6.17(a) indicate that the normalised out-of-plane peak acceleration capacities vary significantly as the openings change locations. It is clear that the opening located at the centre of the wall results in the best out-of-plane performance, carrying 0.38g, compared with the other opening cases. Openings in the top of the wall result in a particularly poor wall performance and if the opening is top centre then the wall has the lowest acceleration capacity at only 0.2g. Figure 6.17(b) shows the variation of peak acceleration capacities for the different opening positions. The minimum normalised peak acceleration capacities when the opening is at the top of the wall are 53% of the maximum capacity. The reason why top openings are weak is that there are no lintels and therefore no restraint at the top edges of these openings. Therefore, under seismic loading, the bricks are easy to displace quickly leading to large displacements and wall failure at these points.

The crack patterns of the URM walls with openings in different positions subjected to dynamic out-of-plane loading are shown in Table 6.8. The figures indicate that as the opening moves, the failure pattern changes as well. It is seen that the opening at location C2 shows much more serious cracking compared to other cases and the failure mechanism is driven by the three-side boundary condition. It is interesting that the bricks located below the openings suffer significant damage no matter the location of the openings. However, the area above the openings, where it exists, shows fewer cracks (e.g. cases A1 to B2). An explanation for this is that the areas above the openings are also located just above the top of the lintels. As lintels can play the role of a ring beam (as described in section 5.3.2), the wall displacements in the areas above the lintels tend to be restricted.

Table 6.8 Typical crack patterns of URM with different opening positions under the shaking table test at 12s

Opening positions	Crack patterns
A1	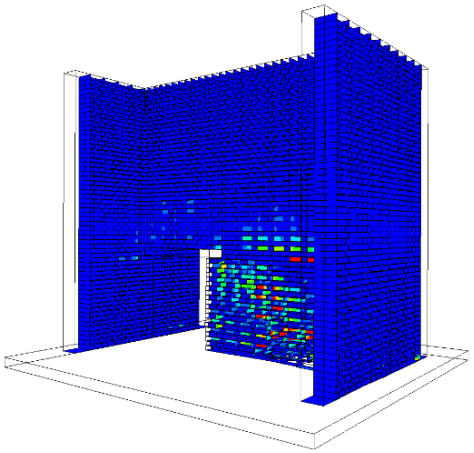

A2	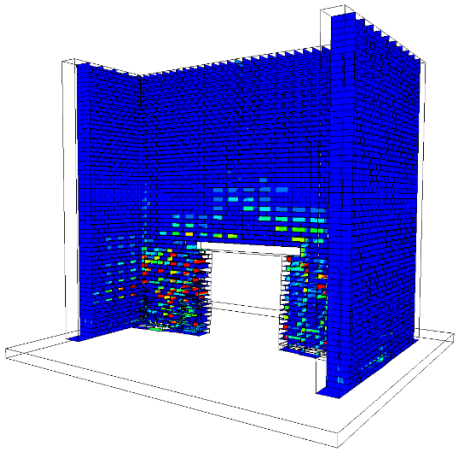
B1	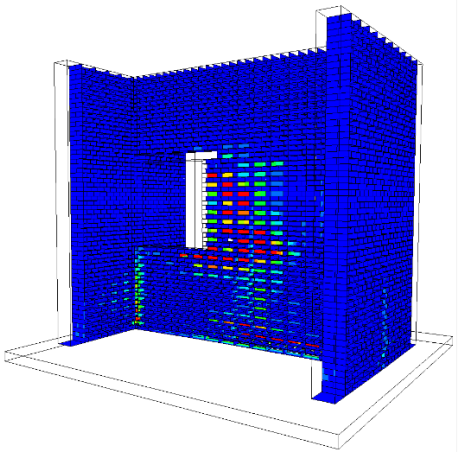
B2	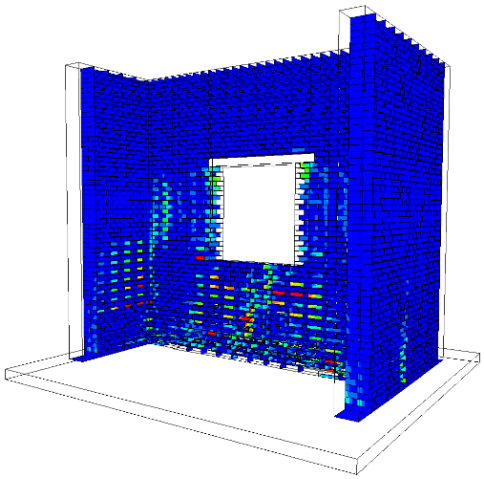

C1	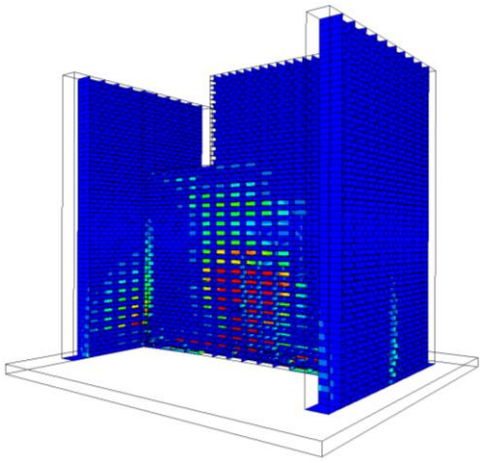
C2	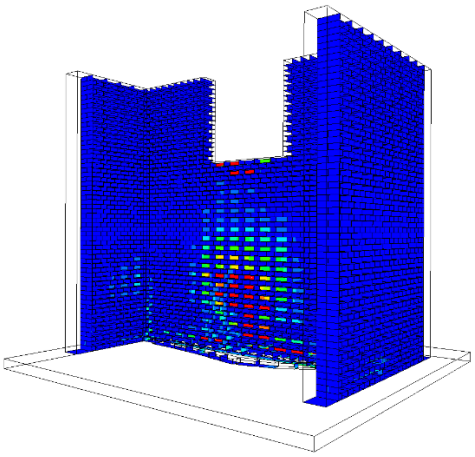

Comparing these dynamic results with the results from the static analyses discussed in section 5.5 and in Figure 5.17 and Figure 6.17, it can be seen that both the static and the dynamic analyses generally follow similar trends for the capacities under different opening positions. However, for the dynamic analyses, an opening in the central top location results in a worse performance than for the static cases and openings in the sides of the walls also result in poor wall performance. Therefore, the out-of-plane behaviour of walls needs to be considered carefully when proposing the wall capacity reduction factors.

6.6 Summary

The dynamic behaviour of URM walls is discussed in this chapter. Similar to the earlier static analyses, the dynamic analysis procedure considers the wall properties, boundary conditions, dynamic loading

input cases and the definition of the failure criteria. The sensitivity of the dynamic analyses was considered by comparing results from six different artificial earthquake motions and building acceleration-drift ratio curves to identify the sensitivity of the results to the input motion. Numerical models considering both in-plane and out-of-plane behaviours have been used and the relationships between the seismic excitation and the opening sizes and positions are developed. The key results from the dynamic analyses are summarised below:

1. 3DEC can simulate the dynamic analysis of URM structures successfully and present the failure patterns accurately. The impact of basic dynamic factors such as frequency effects, vertical loading and amplitude are discussed, respectively and vertical loading and amplitude have an impact on the dynamic capacity of URM walls.
2. To identify the sensitivity of the dynamic analyses in 3DEC, six different artificial earthquake inputs were tested and the seismic performance of the wall varied with the different input motions. Although the artificial ground motions were matched to the same demand spectrum, the shape of time-histories and the time of peak acceleration was different, which lead to the onset of failure in the walls at different times which affected the overall seismic performance of the URM walls. However, the range of wall capacities was quite small showing that the analysis was not particularly sensitive to the excitation input used.
3. The relationship between opening size and location for dynamic in-plane capacities has been evaluated. The effect of opening size follows a similar trend to the results from static analyses in that as the opening size increases, the in-plane capacity decreases, which indicate that the results of static analysis of opening effects for URM walls are reliable. However, there are some differences between the dynamic and the static analyses when considering the effect of opening position on the wall performance. The reason for these differences is that the dynamic loading results in cyclic loading of the wall whereas the static loading is only applied in a single direction.
4. The opening position as the significant impact on the dynamic out-of-plane behaviour of URM masonry walls. Of the possible opening position cases, an opening in a central location maintains the best dynamic performance for the wall while an opening in the top centre of the wall results in the worst wall performance.
5. There are still a few limitations for the dynamic analysis of URM structures in 3DEC which need to be discussed. For the input earthquake waves, only six artificial-generated ground motion waves which match the spectra from Eurocode 8 are considered. The natural earthquake waves especially for high frequency cases are ignored. As the results of dynamic analysis in the research are mainly used by comparing with static analysis and calibrate the reliability of

the outcomes for static analysis, the simplified earthquake input is determined. However, it is still interesting and important to consider specific dynamic input for a comprehensive investigation of dynamic issues.

Chapter 7 THE APPLICATION OF A QUICK ASSESSMENT PROCEDURE FOR URM WALLS

7.1 Introduction

Previous chapters present the effects of openings, including opening size and opening position, on the in-plane and out-of-plane behaviour for URM walls. Behaviour under both static and dynamic loading has been considered and comparisons have been made between structural capacity and opening size and position. This chapter considers the results from these analyses and then proposes some methods for the quick assessment of URM structures based on opening size and position and tests the proposed method against a specific case study. This chapter starts by summarising the previous work and then proposes some specific relationships that deal with a combination of opening size and position on the strength of a URM wall. Then a quick assessment procedure for the seismic capacity of URM walls with openings is proposed. A real URM building in China is modelled in detail in 3DEC and the results of this analysis are compared with the seismic capacity predicted by the quick assessment method that is developed. The comparison between the methods shows that the quick assessment method works well but is slightly conservative.

7.2 Relationships for in-plane performance of URM walls considering opening effects

The results of the relationships between in-plane capacity and openings (size and position) have been presented in previous chapters. Many factors have been discussed previously but they need to be summarised and then converted into some simple relationships to represent the in-plane behaviour of walls with openings. These relationships for in-plane URM wall performance considering the effects of openings are presented below.

7.2.1 The summary of the relationship between in-plane capacity and opening percentage

In general, a central opening is taken as the focus for consideration of URM structures, the other opening cases will be discussed as part of the simple assessment approach for walls with openings. In Figure 6.12, the results of a load-based analysis procedure, a displacement-based analysis procedure and dynamic analysis are compared. As the load-based analysis procedure results are similar to those form the dynamic analyses and also give lower capacities values compared to the displacement-based analysis procedure, the relationships between the normalised in-plane capacity and the opening percentage are derived based on the curve from the load-based analysis procedure. The data and the curve fitting is shown in Figure 7.1. Two alternative equations that fit the data are presented.

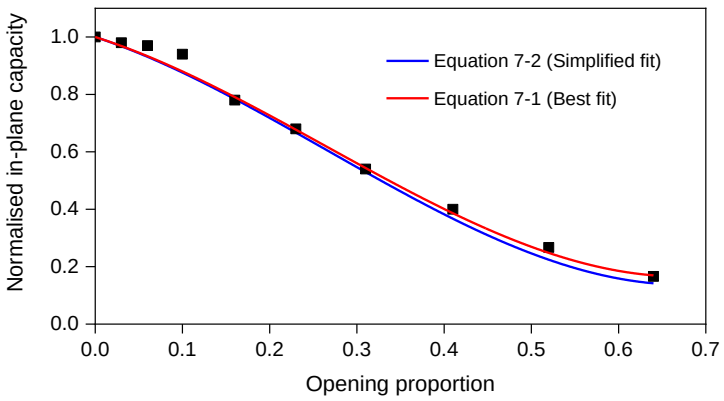

Figure 7.1 The relationship between opening percentage and normalised in-plane capacity of URM wall (central opening)

The best fit to the data in Figure 7.1 is a third order polynomial, expressed by Equation 7-1 below:

$$y = 1 - 0.983x - 2.738x^2 + 3.45033x^3 \quad 7\text{-}1$$

In which y is the in-plane capacity of URM wall, the maximum value is limited to 1 (i.e. no reduction in strength for the wall) and x is the opening proportion, the range of x is $0 \leq x < 0.7$. It should be noted that once the opening percentage exceeds 70%, the walls behave more like a frame structure and it is no longer appropriate to consider the structure like a wall. Furthermore, Equation 7-1 should only be applied to a wall with a regular central opening, and for other forms of openings mentioned in section 4.3.4, different equations need to be considered.

As Equation 7-1 is quite complex, to aid simple assessment of wall capacities, a simplified version of Equation 7-1, i.e. Equation 7-2 is also considered below.

$$y = 1 - x - 2.74x^2 + 3.45x^3 \quad 7\text{-}2$$

Both equations are plotted in Figure 7.1 for comparison and show that by simplifying the equation the curve fit is not significantly different.

For a wall with both door and window openings, the in-plane capacity of wall drops significantly when the opening size is small (Figure 7.2) and the relationship is given in Equation 7-3.

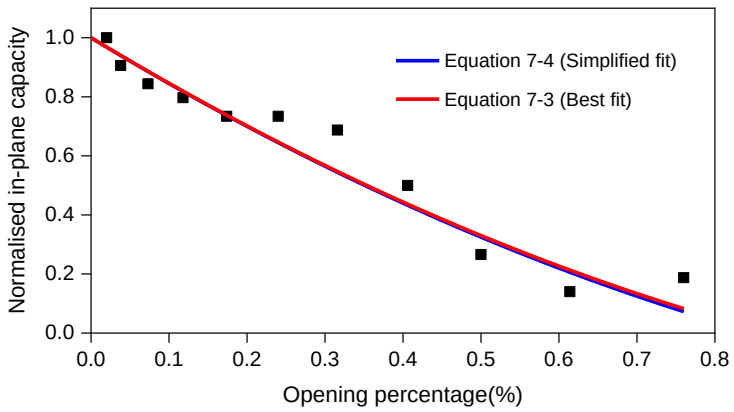

Figure 7.2 The relationship between opening percentage and normalised in-plane capacity of URM wall (both door and window openings)

$$y = 1 - 1.5948x + 0.5105x^2 \quad 7\text{-}3$$

This equation can be simplified as shown below (Equation 7-4) without having a significant effect on the quality of the curve fit:

$$y = 1 - 1.6x + 0.5x^2 \quad 7\text{-}4$$

For the door openings, the effect of doors is somewhat different to that for central openings (Figure 7.3), and the in-plane capacity does not reduce much until quite a large opening percentage has been reached. The equation for the fitted data is shown in Equation 7.5 as followed:

$$y = 1 - 0.13483x - 1.29511x^2 \quad 7\text{-}5$$

This equation can be simplified as shown below (Equation 7-6) without having a significant effect on the quality of the curve fit:

$$y = 1 - 0.135x - 1.3x^2 \quad 7\text{-}6$$

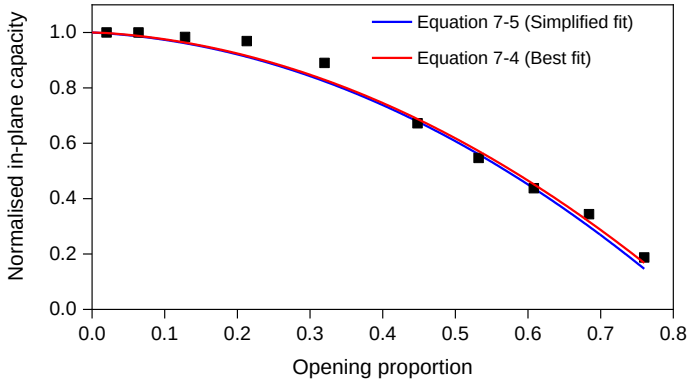

Figure 7.3 The relationship between opening percentage and normalised in-plane capacity of URM wall (door opening)

For weak openings (as shown in Figure 4.6(b)) the in-plane performance decreases dramatically as soon as any opening is introduced (Figure 7.4), due to an inherent weakness in this opening arrangement. The relationship between opening percentage and in-plane capacity can be expressed as in Equation 7-7:

$$y = 1 - 1.9033x - 1.4461x^2 + 3.1389x^3 \quad 7\text{-}7$$

When the opening proportion x is about 0.6, the value of y tends to 0 based on this equation curve, however the when opening proportion x is greater than 0.6, the value of y starts to increase (because the equation is cubic) and this is not appropriate for real walls. Therefore, once the opening percentage is over 60%, the capacity of the walls should be taken as 0, so the range of x for Equation 7-8 has to be limited between 0 and 0.6.

The simplified version of this equation can be expressed as:

$$y = 1 - 1.9x - 1.45x^2 + 3.14x^3 \qquad 7\text{-}8$$

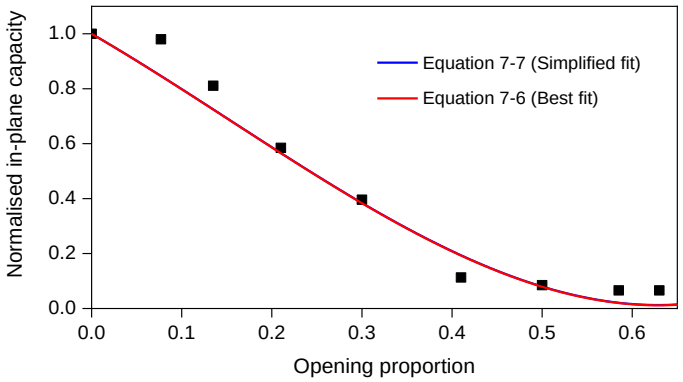

Figure 7.4 The relationship between opening percentage and normalised in-plane capacity of URM wall (weak openings)

Overall, the relationships between opening percentage and in-plane capacity of URM walls have been obtained by curve fitting the data from the 3DEC analyses for a variety of opening cases in the walls. It should be noted that the different opening cases should use the corresponding equations and that there will be some error between the actual response of the walls and the curve fitted predictions. In the case of real buildings, door openings and window openings are common and Equations 7-2, 7-4, 7-6 and 7-8 will be the most useful. When assessing walls with windows, Equation 7-2 will generally be used, however, if there are weak openings (as in Figure 4.6(b)) then Equation 7-8 should be used.

As an alternative to considering the size of the opening as a percentage of the wall area, the curves in Figure 4.10(b), show the relationships between the residual in-plane capacity and total percentage (%) width of wall removed for all opening cases. As all the curves in Figure 4.10(b) follow a similar trend, these can be fitted to the single Equation 7-9 below:

$$y = 1 - 0.0180848x - 1.4483x^2 \quad 7\text{-}9$$

The simplified version of Equation 7-8 is given below in Equation 7-9:

$$y = 1 - 0.018x - 1.45x^2 \quad 7\text{-}10$$

The fitted curves (Equation 7-9 and Equation 7-10) are shown in Figure 7.5 and it is clear that the simplified equation is as accurate as the full equation. Equation 7-10 considers the worst case for all the opening types and is simpler to use compared with the set of curves needed to deal with the different types of opening percentage effects. Therefore, this equation is used as the capacity predictor for the case study in the next section.

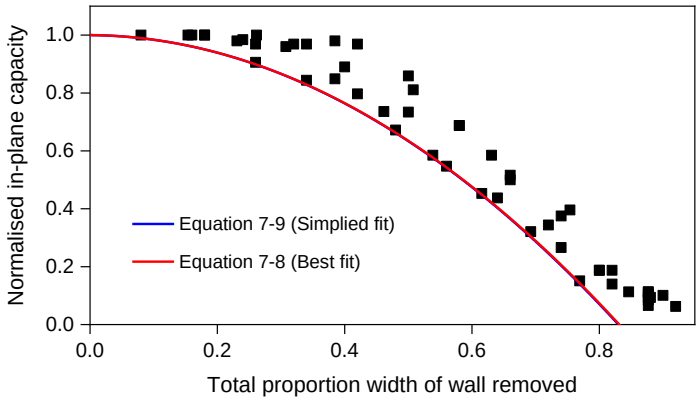

Figure 7.5 The relationship between total percentage (%) width of wall removed for various opening cases and normalised in-plane capacity of URM wall

7.2.2 Summary of the relationship between in-plane capacity and opening position

The relationships between in-plane capacity and opening position have been discussed in sections 4.4 and 6.4.3. However, it is hard to define a simple factor that deals with the in-plane capacity of a URM wall with respect to the opening position because the analysis looking at the effect of opening position was limited to a single opening percentage and it is therefore not simple to extrapolate the impact of other opening sizes on the in-plane response of URM walls. Also, if the opening size is large enough, the opening can only move to a small number of locations and there is effectively no difference

between these opening positions. Within the scope of this work it was not possible to test every combination of opening size and position so this research focussed on a wall with a single realistic sized opening and develops some predictor equations to deal with this realistic case. Therefore, this section looks at an opening size of 10% and develops the equations to predict the in-plane performance of the wall as this opening moves.

Considering the worst cases for all pushover tests, and to allow some symmetry in the equations being derived the worst values for either of the two sides of the panel are chosen and the base shear forces are normalized and shown in Figure 7.6(a). From this figure it can be seen that the in-plane capacity of the URM walls with different opening positions follows a principle that the bottom openings have worse in-plane performance than the top and the central openings and the centre locations have higher capacity than the side openings.

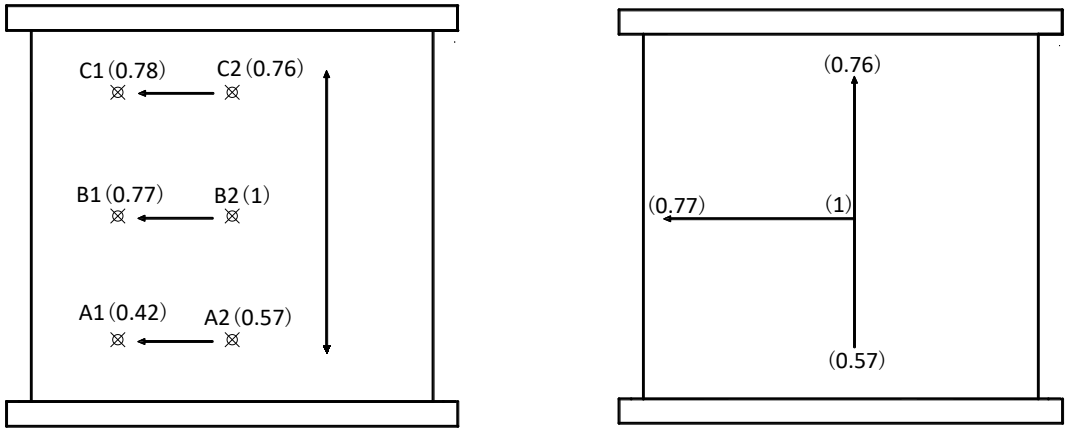

(a) The relationship between opening position and in-plane capacity; (b) The relationship between opening position and in-plane capacity (Simplification)

Figure 7.6 The schematic diagram of opening position effects

Based on this observation from Figure 7.6(a) a simplified relationship between central and edge positions and top and bottom positions can be defined by a few unique values as illustrated in Figure 7.6(b). The central point of a URM wall is then defined as the zero point of the axes and the length and height of URM wall as L and H respectively. The coordinates of the central point of opening are taken as x_1, y_1, therefore the equations of the relationship between opening positions and in-plane performance capacity C are expressed by Equation 7-11 and Equation 7-12 as below:

Opening above the horizontal centre line $$c_u = \left(1 - \frac{|x_1|}{\frac{L}{2}} * 0.23\right) \times \left(1 - \frac{y_1}{\frac{H}{2}} * 0.24\right) \quad 7\text{-}11$$

Opening below the horizontal centre line $$c_b = \left(1 - \frac{|x_1|}{\frac{L}{2}} * 0.23\right) \times \left(1 - \frac{y_1}{\frac{H}{2}} * 0.43\right) \quad 7\text{-}12$$

The equations are divided into two parts by horizontal centre line and the values of y_1 are positive. Using the coordinates of the central point of openings, the corresponding in-plane capacity can be calculated using these expressions.

As the equations are based on a simplified assumption for the impact of opening position, they cannot accurately reflect the values of in-plane capacity for every opening location. These expressions are also specific to a specific opening percentage (10% in this case), and other types of opening case may not follow exactly the same relationship. However, Equations 7-11 and 7-12 still replicate the basic trend of in-plane performance as openings move to different positions and it is helpful to combine them with the effects of the opening percentage to obtain some equations for considering the opening effects including both opening size and position.

7.2.3 Proposed predicted equations for in-plane capacity of walls with openings

The individual relationships between the in-plane capacity and size and position of openings have been discussed above. However, it is important to combine two results to build up the equations that can reflect the change of in-plane performance based on both opening size and position. In this section, considering the features of Equations 7-1 to 7-10 and the shape of openings (rectangular or square), the values of the opening percentages and positions can be calculated from the coordinates of two points of the openings, O_1 and O_2. A URM wall with an opening defined by these points is shown in Figure 7.7, which also shows the plane coordinate system.

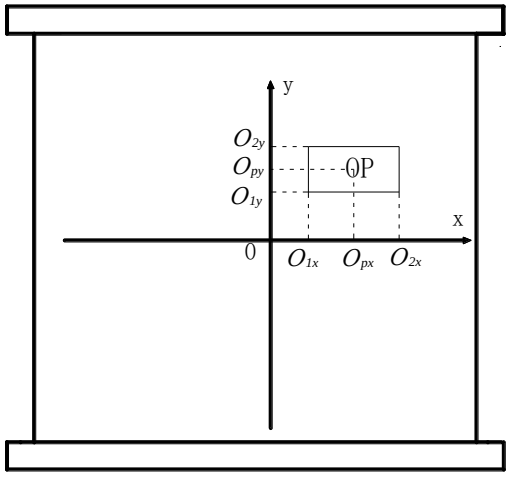

Figure 7.7 The coordinate system of openings for URM wall

Therefore, the opening percentages and positions can then be defined by Equations 7-13, 7-14 and 7-15 as shown below:

Opening size OS $$\mathrm{OS} = (|O_{2x}| - |O_{1x}|) \times \left(\left|O_{2y}\right| - \left|O_{1y}\right|\right)/L * H \quad \text{7-13}$$

Opening position OP (coordinate of central point of opening)

$$OP_x = (O_{2x} - O_{1x})/2 \quad \text{7-14}$$

$$OP_y = \left(O_{2y} - O_{1y}\right)/2 \quad \text{7-15}$$

The relationship F_{in} between the in-plane capacity and the opening effects is therefore given by Equation 7-16 and Equation 7-17 below:

For an opening above the horizontal centre line:

$$F_{in} = [1 - 0.01OS - 3e^{-4}OS^2] \times \left[\left(1 - \frac{|OP_x|}{L} * 0.46\right) * \left(1 - \frac{OP_y}{H} * 0.48\right)\right] \quad \text{7-16}$$

and for an opening below the horizontal centre line:

$$F_{in} = [1. - 0.01OS - 3e^{-4}OS^2] \times \left[\left(1 - \frac{|OP_x|}{L} * 0.46\right) * \left(1 - \frac{OP_y}{H} * 0.86\right)\right] \quad \text{7-17}$$

Equations 7-13 to 7-17 express the relationships between the in-plane capacity and the sizes and positions for central openings (window openings) including square openings and rectangular openings, but the size should be limited to a reasonable range because when the opening is large, there is little space to accommodate any movement of the opening. However, when there are two or more central openings in a single URM wall these equations are not suitable as the opening sizes and the opening positions need to be calculated in other (more complex) ways. Therefore, the relationships for the in-plane performance dealing with a combination of size and position effects in Equations 7-16 and 7-17 are only suitable for single window openings.

For door openings, as door openings are limited to being at the bottom of URM walls, fewer coordinate points for the opening are needed, the relationship between opening position and in-plane capacity can be simplified and the relevant expression is shown as below in Equation 7-18:

$$F_{in} = [1 - 0.135OS - 1.3OS^2] \times \left[\left(1 - \frac{|OP_x|}{L} * 0.46\right)\right] \quad 7\text{-}18$$

For weak openings (as in Figure 4.6(b)), Equations 7-19 and 7-20 present the relationships between in-plane performance and opening effects:

For an opening above the horizontal centre line:

$$F_{in} = [1 - 0.08OS - 16.4OS^2 + 35.46OS^3 - 21.33OS^4] \times \left[\left(1 - \frac{|OP_x|}{L} * 0.46\right) * \left(1 - \frac{OP_y}{H} * 0.48\right)\right] \quad 7\text{-}19$$

And for an opening below the horizontal centre line:

$$F_{in} = [1 - 0.08OS - 16.4OS^2 + 35.46OS^3 - 21.33OS^4] \times \left[\left(1 - \frac{|OP_x|}{L} * 0.46\right) * \left(1 - \frac{OP_y}{H} * 0.86\right)\right] \quad 7\text{-}20$$

For this type of opening case, the sizes of opening cannot follow the full range of sizes defined by Equations 7-16 and 7-17 because the weak openings are already closer to the edges of the wall and therefore there are a limited number of positions that they can be moved to.

For the case of where there are both window and door openings in the walls, as the two opening positions are hard to identify in a simple way, it is suggested that the relationships between in-plane capacity and total opening effects are only considered opening size impacts.

All the different opening cases have been discussed above to develop relationships between opening sizes and position and the in-plane capacities of URM walls. The above equations deal with the impacts of both opening percentages and positions with the exception of a few special opening cases. These equations will be used as the theoretical basis for the simple assessment protocol for real buildings in the next sections.

7.3 The relationships of out-of-plane performance considering opening effects on URM walls

The out-of-plane performance of URM walls considering opening effects is considered in this section. Differently from in-plane behaviour, the out-of-plane behaviour depends mainly on the boundary conditions and the opening location. From the results of the static out-of-plane loading and dynamic loading, the wall capacity is only reduced by the position of the opening. The impact of the opening size is not as important as the influence of lintels leads to an increase in the strength of the walls. Therefore, the relationships for the out-of-plane performance of URM walls considering the effects of openings focus solely on the position of the opening.

Based on sections 5.6 and 6.5, combining the static results for the effect of opening position for three-side supported walls, four-side supported walls and the dynamic responses for three-side supported walls, the worst cases are considered below. The relationship between the opening position and the out-of-plane capacity of a URM wall is shown in Figure 7.8 and Figure 7.9.

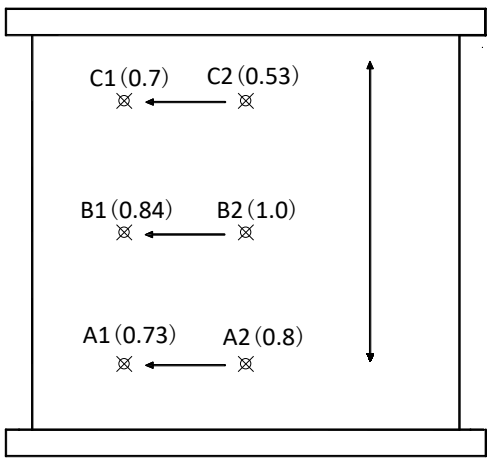

Figure 7.8 The relationship between opening position and out-of-plane capacity

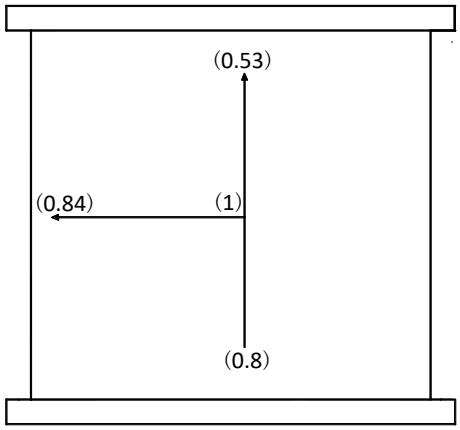

Figure 7.9 The relationship between opening position and out-of-plane capacity (Simplification)

The central point of URM walls is taken as the zero point of the axes, and the length and height of URM wall as L and H respectively. The coordinates of the central point of opening are taken as x_1, y_1, therefore the Equations 7-21 and 7-22 give relationships between the opening position and the out-of-plane performance capacity of the wall:

Opening above the horizontal centre line $$F_{out} = \left(1 - \frac{|x_1|}{\frac{L}{2}} * 0.2\right) \times \left(1 - \frac{y_1}{\frac{H}{2}} * 0.47\right) \quad 7\text{-}21$$

Opening below the horizontal centre line $$F_{out} = \left(1 - \frac{|x_1|}{\frac{L}{2}} * 0.2\right) \times \left(1 - \frac{y_1}{\frac{H}{2}} * 0.16\right) \quad 7\text{-}22$$

The equations are split into two parts by the horizontal centre line and the values of y_1 are positive. Using the coordinates of the central point of the opening, the corresponding out-of-plane capacity can be calculated using the above expressions.

These equations are also based on a simplified set of relationships for the impact of the opening position on the wall capacity. There are some limitations in that the equations do not reflect the in-plane capacity of walls with the opening in every possible location. The capacity of the wall with openings in some locations may be better than predicted by the equations derived above (as they are based on worst case values). The expressions are also based on a specific opening percentage (10% in this case) and then relationships for other sizes opening may be slightly different. Nevertheless, it is reasonable to assume that moving other sizes openings would follow a similar pattern.

7.4 Summary of proposed opening reduction factors for identifying seismic capacity of URM structures

The behaviour capacity factor for openings to identify the seismic capacity of URM structures is summarised in Table 7.1 below. The tables show the detailed relationships between the openings and the capacity of the wall. When assessing the capacity of URM structures, the positive or negative effects of openings can be expressed using these equations.

It should be noted that the capacity of URM walls with openings subjected to out-of-plane behaviour is largely related to the presence of lintels and these lintels lead to an increase in capacity, even when the openings are large. Therefore, the walls should be identified carefully and the reduction of out-of-plane capacity should focus on the opening positions. Generally, URM walls are weaker when subjected to out-of-plane loading than in-plane loading and out-of-plane failure occurs typically first in real buildings. If there are no openings in walls subjected to out-of-plane loading, the behaviour capacity factor should be related to the walls with in-plane loading; if there are some openings in walls with out-of-plane loading, it is important to identify both the in-plane and out-of-plane behaviour capacities and then take the weakest value to determine the reduction in a structural capacity.

Table 7.1 Behaviour capacity factor of openings for identifying seismic capacity of URM structures

	In-plane behaviour capacity factor (F_{in})	**Out-of-plane behaviour capacity factor (F_{out})**
Equations	(1) Central opening Above the horizontal centre line $F_{in} = [1 - OS - 2.74OS^2 + 3.45OS^3] \times \left[\left(1 - \frac{\lvert OP_x \rvert}{L} * 0.46\right) * \left(1 - \frac{OP_y}{H} * 0.48\right)\right]$ Below the horizontal centre line $F_{in} = [1 - OS - 2.74OS^2 + 3.45OS^3] \times \left[\left(1 - \frac{\lvert OP_x \rvert}{L} * 0.46\right) * \left(1 - \frac{OP_y}{H} * 0.86\right)\right]$ (2) The door opening $F_{in} = [1 - 0.135OS - 1.3OS^2] \times \left[\left(1 - \frac{\lvert OP_x \rvert}{L} * 0.46\right)\right]$ (3) Weak opening Above the horizontal centre line $F_{in} = [1 - 1.9OS - 1.45OS^2 + 3.14OS^3] \times \left[\left(1 - \frac{\lvert OP_x \rvert}{L} * 0.46\right) * \left(1 - \frac{OP_y}{H} * 0.48\right)\right]$	Above the horizontal centre line $F_{out} = \left(1 - \frac{\lvert x_1 \rvert}{L} * 0.4\right) \times \left(1 - \frac{y_1}{H} * 0.94\right)$ Below the horizontal centre line $F_{out} = \left(1 - \frac{\lvert x_1 \rvert}{L} * 0.4\right) \times \left(1 - \frac{y_1}{H} * 0.32\right)$

	Below the horizontal centre line $F_{in} = [1 - 1.9OS - 1.45OS^2 + 3.14OS^3] \times \left[\left(1 - \frac{\lvert OP_x \rvert}{L} * 0.46\right) * \left(1 - \frac{OP_y}{H} * 0.86\right)\right]$ (4) wall with both door and window openings $F_{in} = 1 - 1.6OS + 0.5OS^2$ (5) Total width of wall removed Above the horizontal centre line $F_{in} = [1 - 0.018OS - 1.45OS^2] \times \left[\left(1 - \frac{\lvert OP_x \rvert}{L} * 0.46\right) * \left(1 - \frac{OP_y}{H} * 0.48\right)\right]$ Below the horizontal centre line $F_{in} = [1 - 0.018OS - 1.45OS^2] \times \left[\left(1 - \frac{\lvert OP_x \rvert}{L} * 0.46\right) * \left(1 - \frac{OP_y}{H} * 0.86\right)\right]$	

A simple set of equations for identifying the seismic capacity of URM structures, based on the size and position of the opening has been presented. In the next sections these relationships will be used to predict the behaviour of an unreinforced masonry structure modelling in 3DEC.

7.5 Proposed simple quick assessment procedure for case study building

The first step of calculating the capacity of a URM building with openings is to calculate the capacity of the structure without openings. This can be done using current design codes or based on previous research. Once the design earthquake is obtained, the safety of the building is calculated by comparing the capacity of the walls without openings to the input loading. If the design loading is more than capacity of the walls without any openings, it indicates that the building will fail and there is no need to calculate the reduced capacities of the walls with openings. If the walls (without openings) are strong enough then, the capacity of walls with any openings needs to be calculated. By identifying the cases of the opening, the reduction factors can be determined. Based on the proposed opening reduction factors, the capacity of walls with openings are then known. The safety of building is then justified by comparing the capacity of structures with openings against the design loading. This process is shown in more detail in Figure 7.10.

Figure 7.10 shows the complete proposed assessment method. To justify the safety of buildings with openings, if design loading is smaller than capacity, the buildings are safe. If not, a safety factor could be considered. However, it is hard to propose an accurate value directly so this needs to be obtained from a specific case study, and a method for determining an appropriate safety factor is discussed in the next section.

In summary, a simple quick assessment procedure is proposed and the next step is to validate the reliability of this method through a specific case study.

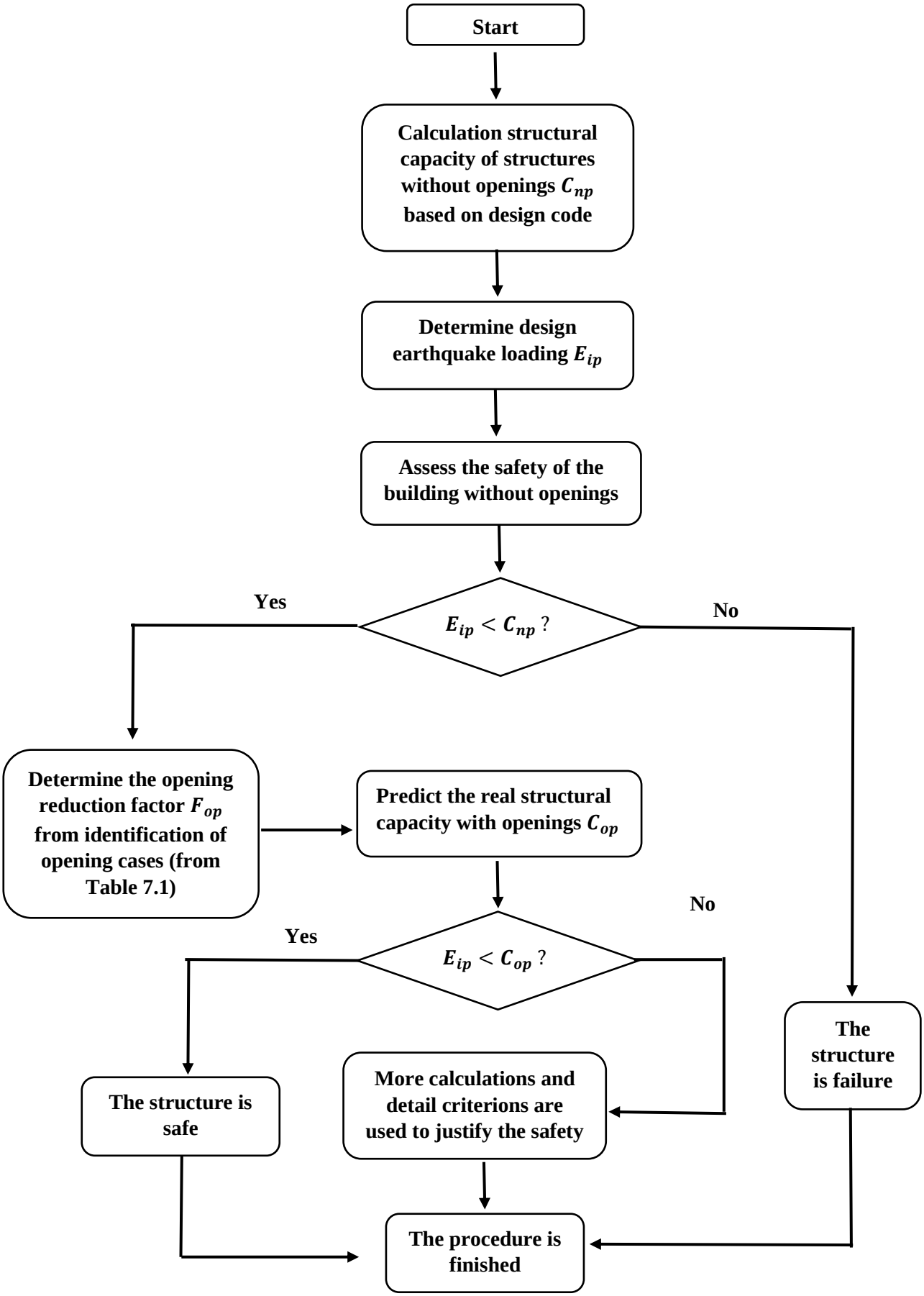
Start
Calculation structural capacity of structures without openings C_{np} based on design code
Determine design earthquake loading E_{ip}
Assess the safety of the building without openings
$E_{ip} < C_{np}$?
Yes
No
Determine the opening reduction factor F_{op} from identification of opening cases (from Table 7.1)
Predict the real structural capacity with openings C_{op}
$E_{ip} < C_{op}$?
Yes
No
The structure is safe
More calculations and detail criterions are used to justify the safety
The structure is failure
The procedure is finished

Figure 7.10 Flowchart of the simple assessment procedure for buildings

7.6 Case study of a real unreinforced masonry structure in 3DEC

7.6.1 The geometry of case study building

To test the proposed simple quick assessment procedure for real buildings, a 3DEC analysis of a real building is needed. Looking at typical unreinforced masonry housing in China, a typical unreinforced masonry building in the rural area of China can be seen in Figure 7.11.

Figure 7.11 View of typical unreinforced masonry structure in the rural area of China

For this same structure, a detailed plan view and vertical view of the structure can be seen in Figure 7.12. The size of the house is 15.9m × 6m, the height of the floor is 3.6m and the height of the roof is 1.6m. To compare the behaviour of the masonry walls with and without openings with the numerical results, the walls are classified into two types i.e. without openings and with openings, the arrangements of the walls in the building are divided into 4 types and the specific sizes and characteristics of the walls are given in Figure 7.12.

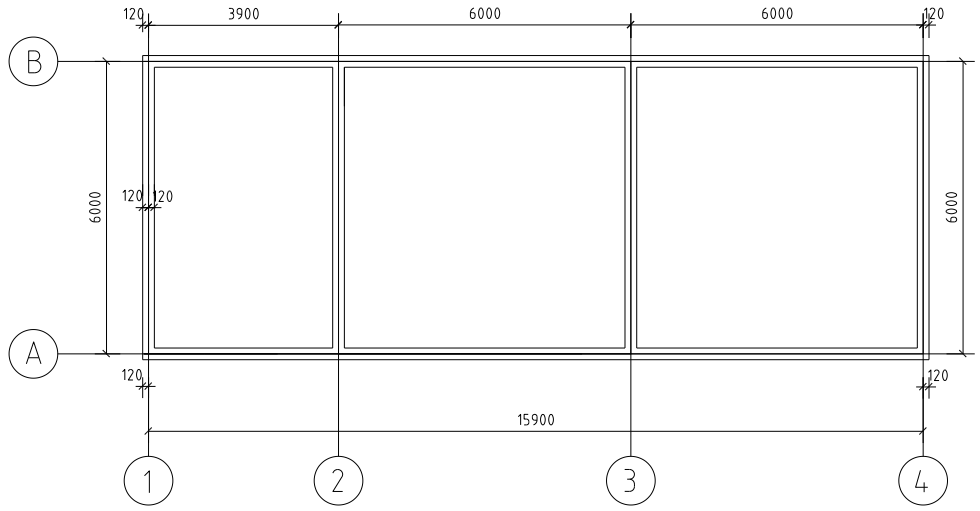

(a) Plan view of typical unreinforced masonry housing without openings

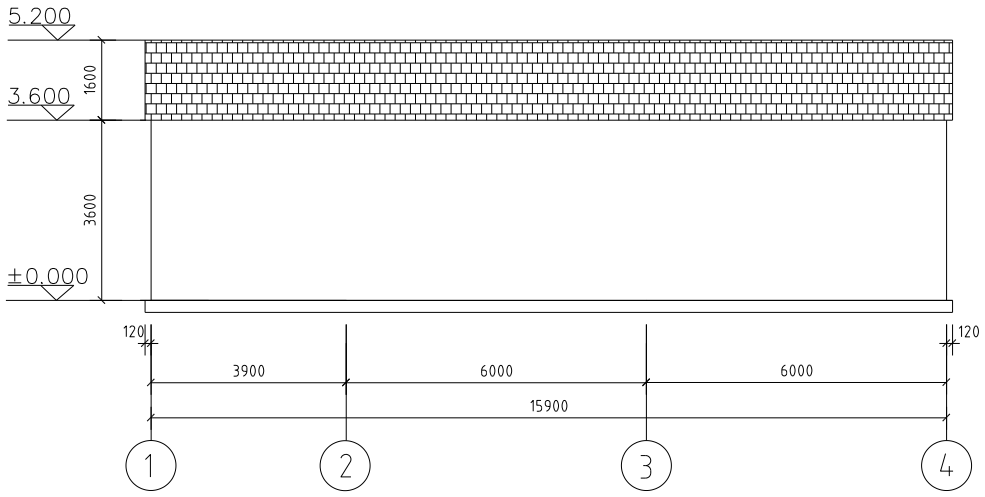

(b) Vertical view of typical unreinforced masonry housing without openings

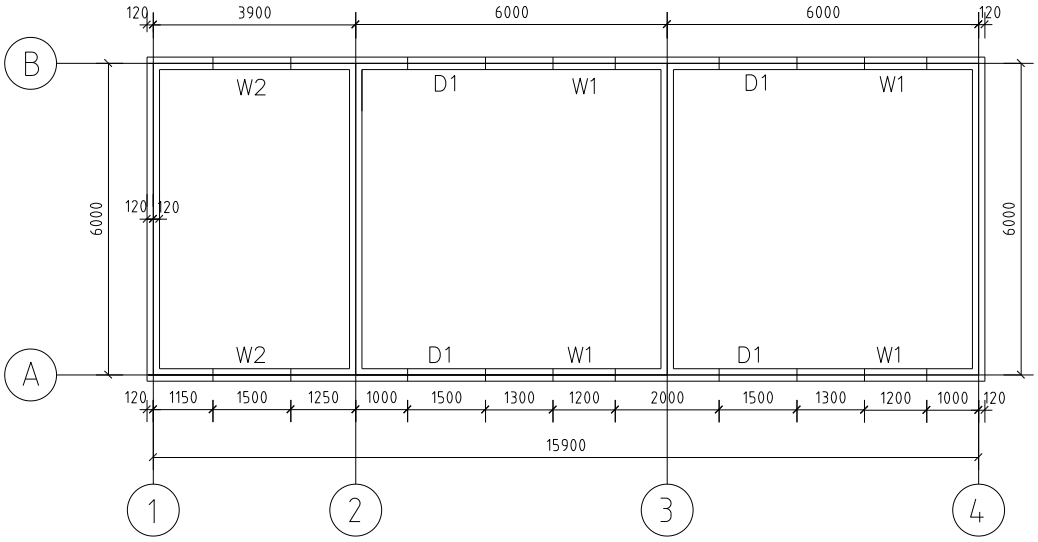

(c) Plan view of typical unreinforced masonry housing with openings

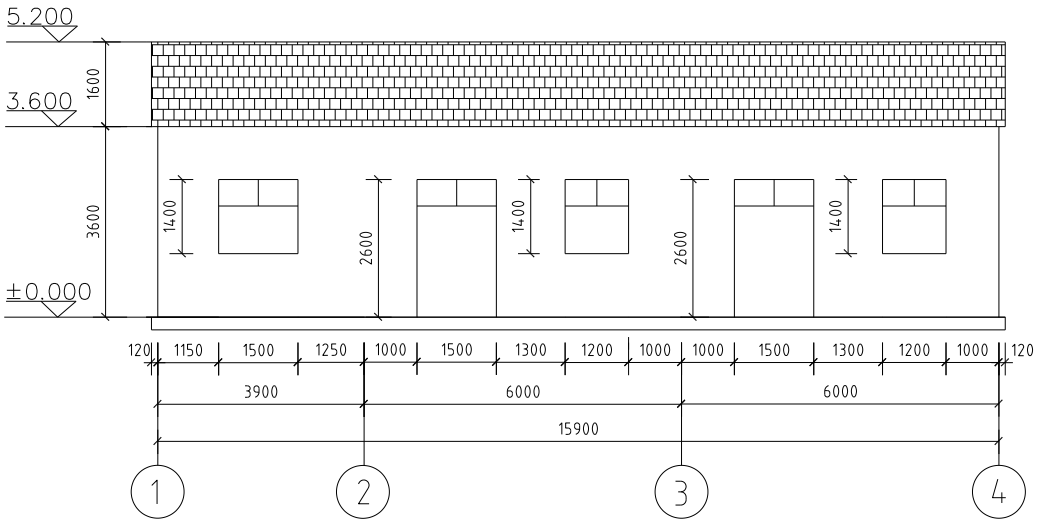

(d) Vertical view of typical unreinforced masonry housing with openings

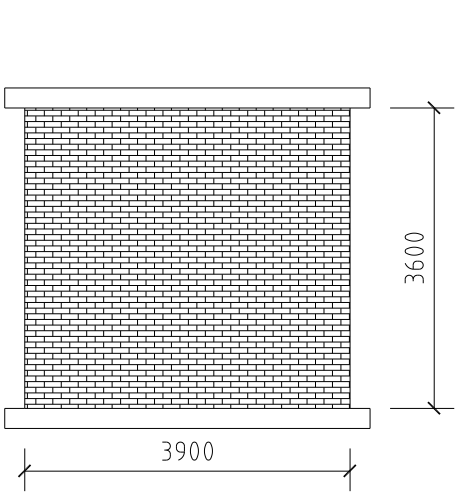

(e) Wall section I

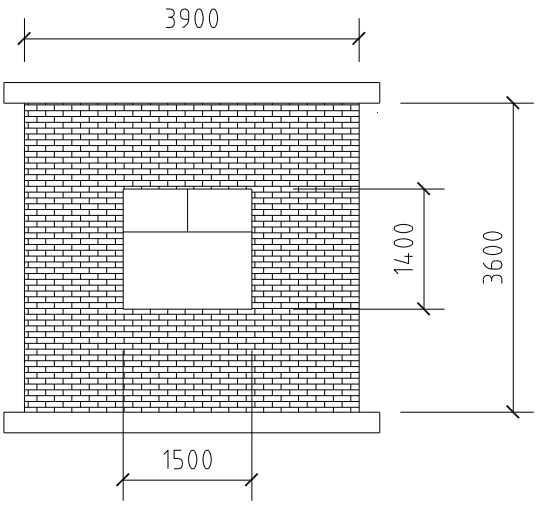

(f) Wall section II

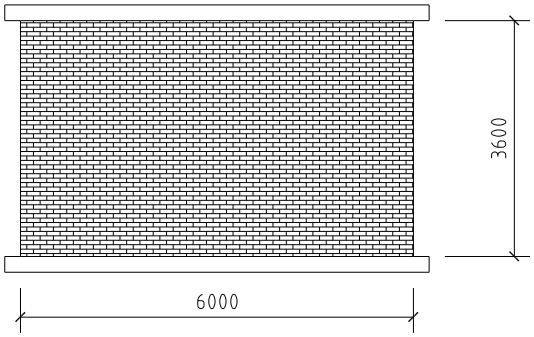

(g) Wall section III

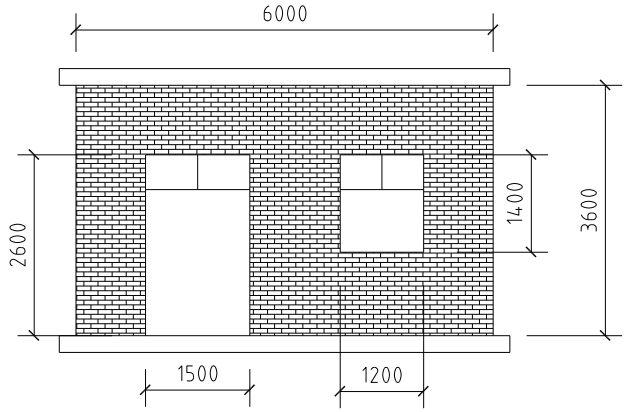

(h) Wall section IV

Figure 7.12 View of simplified typical unreinforced masonry housing in the rural area of China

The size of the wall section I is 3.9m×3.6m without any openings, the size of wall section II is the same as wall section I with a window sized 1.5m×1.4m. Wall section III is a rectangle-shaped wall sized 6.0m×3.6m and there is no opening. Wall section IV is 6.0m×3.6m and contains both door and window openings whose sizes are 1.5m×2.6m and 1.2m×1.4m, respectively.

7.6.2 Assumed material properties for case study building

According to (GB50003-2011, 2012), the material properties of regular brick masonry in China are given in Table 7.2, Table 7.3 and Table 7.4.

Table 7.2 The compressive strength design value of normal sintering bricks (MPa) [From (GB50003-2011, 2012)]

The strength levels of brick	The strength levels of mortar					
	M15	M10	M7.5	M5	M2.5	0
MU30	3.94	3.27	2.93	2.59	2.26	1.15
MU25	3.60	2.98	2.68	2.37	2.06	1.05
MU20	3.22	2.67	2.39	2.12	1.84	0.94
MU15	2.79	2.31	2.07	1.83	1.60	0.82
MU10	-	1.89	1.69	1.50	1.30	0.67

Table 7.3 The design value of axial tensile strength, bending tensile strength and shear strength for normal sintering brick masonry (MPa) [From (GB50003-2011, 2012)]

Strength type	Illustration of failure	The strength levels of mortar			
		≥M10	M7.5	M5	M2.5
Axial tensile strength	Failure along the footage 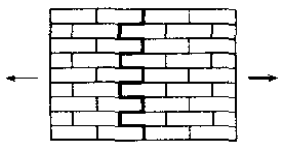	0.19	0.16	0.13	0.09

Bending tensile strength	Failure along the footage	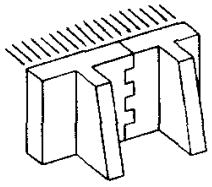	0.33	0.29	0.23	0.17
Shear strength	Failure throng the seam	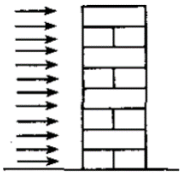	0.17	0.14	0.11	0.08

Table 7.4 The elastic modulus (E) of masonry blocks (MPa) [From (GB50003-2011, 2012)]

The normal sintering brick	The strength levels of mortar			
	≥M10	M7.5	M5	M2.5
	1600 *f*	1600 *f*	1600 *f*	1390 *f*

Note: *f* refers to the design value of compressive strength.

7.6.3 Prediction of strength of the case study building in 3DEC

The strength of each of the four wall cases was calculated using two design codes to predict the structural performance of building and these results are then compared with the results from numerical analyses. Looking at the example building, Figure 7.12(c) is used to identify the intact walls to calculate in-plane and out-of-plane capacities. The calculation progress is shown below.

7.6.3.1. In-plane capacities without openings

Chinese code

Based on the regulations 5.2.6 and 7.2.3 of (GB50011, 2010), the assignment of lateral shear force is as follows:

The horizontal earthquake shear force $V_{im}$with respect to the rigid floor system is calculated using Equation 7-23:

$$V_{im} = \frac{K_{im}}{\sum_{k=1}^{n} K_{ik}} V_i \quad 7\text{-}23$$

In which, K_{im} and K_{ik} are the equivalent stiffness of storey i, m and k piece of wall, V_i refers to the horizontal earthquake shear of storey i.

The lateral stiffness of walls

Assuming that there is no rotation and only lateral sway in the two directions up and down the walls, then the bending deformation and shear deformation, caused by horizontal force, are represented by Equations 7-24 and 7-25 as follows:

Bending deformation: $$\delta_b = \frac{h^3}{12EI} = \frac{1}{Et}\rho^3 \quad 7\text{-}24$$

Shear deformation: $$\delta_s = \frac{\xi h}{AG} = \frac{3\rho}{Et} \quad 7\text{-}25$$

Where h refers to the height of the bearing walls, the walls between windows and then walls between the door, A refers to the area of bearing walls, walls between window and walls between door, $\mathrm{A} = \mathrm{b} * \mathrm{t}$, I is the horizontal second moment of area, $\mathrm{I} = (b\text{^}3\ t)/12$, ξ refers to the non-even coefficient of distribution of shear stress, for the rectangular section, the value is $\xi = 1.2$, E is the elasticity modulus of masonry, G refers to the shear modulus of masonry, take $\mathrm{G} = 0.4\ \mathrm{E}$, $\rho = h/b$.

The total deformation at the top of the walls under the lateral force is defined by Equation 7-26:

$$\delta = \frac{\rho^3}{Et} + \frac{3\rho}{Et} \quad 7\text{-}26$$

The lateral stiffness K_{bs} which considers both bending and shear deformation is expressed by Equation 7-27:

$$K_{bs} = \frac{1}{\delta} = \frac{Et}{\rho^3 + 3\rho} \quad 7\text{-}27$$

The lateral stiffness K_{bs} which ignores the bending deformation is expressed by Equation 7-28:

$$K_{bs} = \frac{1}{\delta_s} = \frac{Et}{3\rho} \quad 7\text{-}28$$

When h/b < 1, you only consider the shear deformation, and h/b > 4, you ignore the lateral stiffness of the relevant piece of wall, and when 4≥h/b≥1, consider the effects of both deformations.

Besides, there are also some cases where the distribution of shear forces can be simplified. For the cross brick walls without windows and doors, when satisfying the requirements such as no staggered floors, the strength of the brick and mortar can be considered to be the same. As the aspect ratio of every piece of wall is in the same range, the ratio of lateral stiffness of every piece of wall to the floor lateral stiffness can also be simplified. As most walls have an aspect ratio of less than 1.0, the bending deformation can be ignored, and only the shear deformation needs to be considered when calculating the lateral stiffness.

Then the relevant equation is Equation 7-29 as follows:

$$K_{im} = \frac{A_{im} G_{im}}{\xi h_{im}} \quad 7\text{-}29$$

In which, G_{im} refers to the shear modulus of storey i and piece m of the walls; A_{im} is the cross-section area of storey i and piece m of walls; h_{im} is the height of walls for storey i and piece m.

When the height and material of walls are same, the above equation can be simplified to Equation 7-30 below:

$$V_{im} = \frac{A_{im}}{\sum_{m=1}^{s} V_i} = \frac{A_{im}}{A_i} V_i \quad 7\text{-}30$$

Where A_i is the sum of the cross-section area of every seismic resistant cross wall at storey i.

It is worth noting that the distribution of lateral shear force is related to stiffness of the roof. The roof mainly comprises one of two types of structure, i.e. a flexible timber roof or semi-rigid precast reinforced concrete hollow slabs. For housing with a flexible timber roof, the lateral shear force can be assigned according to a representative proportion of the gravity load from the tributary area of all lateral load resisting members. The tributary area can be calculated from the spacing between the adjacent shear walls. For the semi-rigid precast reinforced concrete hollow slab, the lateral earthquake shear force can be calculated as the average of two outcomes: (a) It is calculated as the representative proportion of gravity load from the tributary area of all lateral load resisting members; (b) It is calculated in proportion to the equivalent stiffness of lateral load resisting members.

Vertical load of wall

When calculating the vertical load in the wall, this can be regarded as the average value of the sum of the gravity load or the wall and vertical load from the roof as shown in Equation 7-31 below:

$$L_{\text{vertical}} = \frac{G_{wall}}{2} + L_{roof} \quad 7\text{-}31$$

Where G_{wall} is the gravity load of wall, L_{roof} is the vertical load of roof.

The strength of materials

According to (JGJ161-2008, 2008), the strength value is taken as the mean of shear force, $f_{v,m}$. The calculation of the strength and the relationships between the mean shear force and design value of shear force is given below:

The mean shear strength of masonry including bricks, blocks and stone is given by Equation 7-32:

$$f_{v,k} = f_{v,m}\left(1 - 1.645\delta_f\right) \quad 7\text{-}32$$

Where $f_{v,k}$ is the standard value of shear resistance for masonry without seismic design;

$f_{v,m}$ refers to the mean of shear resistance for masonry without seismic design;

δ_f is the variability coefficient of masonry strength for all types of masonry, δ_f can be taken as 0.2, (for stone, δ_f is 0.3).

Based on (GB50003-2011, 2012), $f_v = f_{v.k}/r_f$, r_f is the material partial factor for masonry with $r_f = 1.6$, and f_v , which is design value of shear resistance for masonry, can be obtained from (GB50003-2011, 2012). So $f_{v,m}$ can be calculated using Equation 7-33 below:

$$f_{v,m} = 2.38 f_v \quad 7\text{-}33$$

Average shear strength of masonry

The shear strength of masonry is decided by the strength of the mortar, and the masonry code uses Equation 7-34 as follow:

$$f_{v,m} = k_5\sqrt{f_2} \quad 7\text{-}34$$

In which, f_2 is the average value of the mortar compressive strength from experimental tests, i.e. the strength class of the mortar. For the brick masonry, k_5 is 0.125; for rubble masonry, k_5 is 0.188.

The method above should be used to calculate the mean shear strength of the masonry, but because the quality of mortar in rural areas is not good and the strength generally does not reach the design value of shear resistance, which is 0.08Mpa, f_v can be multiplied by two factors, β and δ. β is the adjustment coefficient for the masonry mortar type used, for clay it is 0.15; for lime earth it is 0.35; for cement mortar it is 0.5 and for mixed mortar it is 0.7. δ is 1.0 when joints are full of mortar, and δ is 0.7 when joints are only partially fully mortar due to rain.

The sectional seismic shear capacity method for masonry walls

According to (JGJ161-2008, 2008), the sectional seismic shear capacity for masonry walls is as shown in Equation 7-35 below:

$$V_b \leq \mu r_{bE} \xi_n f_{v,m} A \quad 7\text{-}35$$

In which, μ is the adjustment coefficient of seismic capacity. When there are no confined columns and ring beams, μ is 0.75; when there are confined columns and ring beams but the structural measures are not good, μ is 0.85. V_b refers to the standard value of masonry wall shear strength under basic seismic intensity. r_{bE} is the adjustment coefficient of ultimate seismic bearing capacity; for bearing walls it is 0.95; for non-bearing walls it is 0.85. $f_{v,m}$ refers to the mean of shear resistance of masonry without seismic design. A is the cross sectional area of shear walls. ξ_n is an impact factor of normal stress for the masonry shear strength. From (GB50011, 2010) this can be derived via Equation 7-36 below:

$$\xi_n = \frac{1}{1.2}\sqrt{1 + 0.45\sigma_0/f_v} \quad 7\text{-}36$$

Where σ_0 is the average stress in the masonry corresponding to the representative value of gravity load and f_v is the design value of shear resistance for masonry structures.

Besides, according to (GB50011, 2010), the sectional seismic shear resistance capacity, Equation 7-37 and 7-38, for masonry wall are as given below:

$$\mathrm{V} \leq f_{vE} A/\gamma_{RE} \quad 7\text{-}37$$

$$f_{vE} = \xi_n f_v \quad 7\text{-}38$$

In which, f_v is the non-seismic design value of shear resistance for masonry, f_{vE} refers to the seismic design value of shear resistance for masonry, γ_{RE} is the seismic capacity adjustment factor, usually equal to 1 for general bearing walls, 0.09 for walls with confined columns, and 0.75 for a simple wall.

It can be seen that the shear value derived from the seismic design code is better than that from the regulations of rural housing, so for the rest of this work the more pessimistic method from the regulations will be used to calculate the seismic performance of buildings.

In addition, based on (GB50011, 2010), the shear resistance can also be obtained from Equations 7-39 to 7-41 as follows:

For unreinforced masonry:

$$V \leq f_{VE}A/\gamma_{RE} \quad 7\text{-}39$$

$$f_E = \xi_N f_v \quad 7\text{-}40$$

For the composite walls constructed of brick masonry and reinforced concrete structural columns:

$$V \leq [\eta_c f_{VE}(A - A_c) + \zeta f_t A_c + 0.08 f_y A_s]/\gamma_{RE} \quad 7\text{-}41$$

Where V is the seismic load-bearing shear capacity of the section, f_{VE} refers to the design masonry shear strength for diagonal tension, A is the cross-sectional area of the wall, η_c is the restrained correction of the column (for transverse walls and internal longitudinal walls, $A_c \leq 0.25A$), f_t is the design value of the concrete tensile strength for the column, A_s refers to the total area of the vertical column reinforcement, and ζ is the factor taking into account the column participation.

The ratio of force resistance and seismic effect

The lateral earthquake shear of each piece of wall through the distribution of seismic shear is defined as $r_{RE}S$, the design value of shear resistance for masonry walls is $\mathrm{R} \leq \mu r_{bE}\,\xi_n f_v\,A$. According to section 5.4.2 of (GB50011, 2010), the walls meet the design requirements when $\frac{R}{r_{RE}S} \geq 1$.

The calculation for the force resistance of the walls in the example structure is as follows:

If there are no confined columns and ring beams, μ is taken as 0.75; but if the longitudinal wall belongs to bearing wall, the adjustment coefficient of ultimate seismic bearing capacity, γ_{bE}, is taken as 0.85. According to (GB50011, 2010), the impact factor of normal stress for the masonry shear strength calculated using Equation 7-42 as below:

$$\zeta_N = \frac{1}{1.2}\sqrt{1 + 0.45\sigma_0/f_v} \quad 7\text{-}42$$

In which σ_0 is taken as the ratio of the vertical load and the sectional area of the longitudinal wall.

To calculate σ_0, the vertical load and sectional area of the longitudinal wall need to be determined.

For a single masonry wall, the vertical load should be distributed based on the ratios of sectional areas of walls, the vertical load can be determined using Equation 7-28, combined with the load distribution in Equation 7-27. In this case there are two different types of in-plane URM walls, the sizes of walls are 6.0m×3.6m and 3.9m×3.6m, respectively. As the effective height of the URM walls is the same, the differences only depend on the lengths of walls and the load distribution can also be simplified by the ratios of lengths.

The vertical loads for both types of walls are shown below:

$$L_{\text{vertical1}} = \frac{6 \times 3.6 \times 0.24 \times 18}{2} + \frac{6}{6 \times 8 + 3.9 \times 2} \times 500 = 101.7kN$$

$$L_{\text{vertical2}} = \frac{3.9 \times 3.6 \times 0.24 \times 18}{2} + \frac{3.9}{6 \times 8 + 3.9 \times 2} \times 500 = 65.33kN$$

The sectional areas of two types of wall are 1.44m^2 and 0.936m^2

Thus, according to Equation 7-39, the impact factors of normal stress for the masonry shear strength are expressed below:

$\sigma_1 = 101.7 \div 1.44 = 70.625\text{kPa}$

$\sigma_2 = 65.33 \div 0.936 = 69.8\text{kPa}$

In order to calculate the material strength, based on Equation 7-30, values of $f_v = 0.08MPa$ and $\beta = 0.5$ are taken based on the use of clay bricks and mortar pointing joints. Therefore

$f_{v,m} = 2.38 f_v \beta = 2.38 * 0.08 * 0.5 = 0.0952\text{MPa}.$

Based on Equation 7-39, then the impact factor of normal stress for the masonry shear strength can be calculated:

$$\xi_{N1} = \frac{1}{1.2}\sqrt{1 + \frac{0.45\sigma_1}{f_v}} = \frac{1}{1.2}\sqrt{1 + 0.45 \times 70.6251/(0.08 \times 1000)} = 0.985$$

$$\xi_{N2} = \frac{1}{1.2}\sqrt{1 + \frac{0.45\sigma_2}{f_v}} = \frac{1}{1.2}\sqrt{1 + 0.45 \times 69.8/(0.08 \times 1000)} = 0.983$$

Finally, the force resistance of the longitudinal walls can be calculated from Equation 7-32 as

$\mu r_{bE} \xi_{N1} f_{v,m} A_1 = 0.75 \times 0.85 \times 0.985 \times 0.0952 \times 1.44 \times 1000 = 86.1kN$

$\mu r_{bE} \xi_{N2} f_{v,m} A_2 = 0.75 \times 0.85 \times 0.983 \times 0.0952 \times 0.936 \times 1000 = 55.8kN$

Based on $\frac{R}{r_{RE} S} \geq 1$, and there is no confined columns, r_{RE} = 1.0

$S_1 \leq R_1 = 86.1kN$

$S_2 \leq R_2 = 55.8kN$

Therefore, the overall seismic force $S = S_1 \times 4 + S_2 \times 2 = 465\text{kN}$

The equivalent of gravity load: $G = 858.5/2 + 500 = 929.3\text{kN}$

The failure acceleration can be obtained by: $\alpha_{n-intact} = S/G = 0.5\ g$

Eurocode 6

As an alternative to using the Chinese code Eurocode 6 could also be used. For in-plane behaviour, according to part 1-1 of (EN1996-1-1, 2005) the shear resistance force can be calculated using Equations 7-43 to 7-45 as below:

Filled head joints:

$$f_{vk} = f_{vk0} + 0.4 \cdot \sigma_d \leq \begin{cases} 0.065 \cdot f_b \\ f_{vlt} \end{cases} \quad \text{7-43}$$

Unfilled head joints:

$$f_{vk} = 0.5 \cdot f_{vk0} + 0.4 \cdot \sigma_d \leq \begin{cases} 0.045 \cdot f_b \\ f_{vlt} \end{cases} \quad \text{7-44}$$

Shell bedded masonry:

$$f_{vk} = \frac{g}{t} \cdot f_{vk0} + 0.4 \cdot \sigma_d \leq \begin{cases} 0.045 \cdot f_b \\ f_{vlt} \end{cases} \quad \text{7-45}$$

where f_{vk0} is the characteristic initial shear strength, under zero compressive stress, f_{vlt} is a limit to the value of f_{vk}, σ_d is the design compressive stress perpendicular to the shear in the member at the level under consideration, using the appropriate load combination based on the average vertical stress over the compressed part of the wall that is providing shear resistance, f_b is the normalised compressive strength of the masonry units, when the direction of application of the load on the test specimens is perpendicular to the bed face.

The resistance shear force is expressed by Equation 7-46 below:

$$V_{Rd} = f_{vd} \cdot t \cdot l_c \quad \text{7-46}$$

where f_{vd} is the design value of the shear strength of masonry, obtained from Equations 7-41, 7-42 and 7-43, based on the average of the vertical stress over the compressed part of the wall that is providing the shear resistance, t is the thickness of the wall resisting the shear, l_c is the length of the compressed part of the wall, ignoring any part of wall that is in tension.

Taking the case of the intact URM walls shown in Figure 7.12(c) and assuming the loading direction is in the longitudinal direction. Similar to Chinese code, the shear resistance force for a single URM wall is based on the stiffness of walls and for walls without openings, this simplifies to the distribution of sectional areas of walls. Therefore, for the building without openings, there are two different types of

in-plane URM walls, being 6.0m×3.6m and 3.9m×3.6m, respectively. According to the shear resistance force, the predicted failure force can be obtained. The specific calculation progress is shown below.

Based on Equation 7-41, f_{vk} is determined as 0.06 N/mm^2

Therefore the $V_{Rd} = f_{vd} \cdot t \cdot l_c = (0.06 \times 0.24 \times 6 \times 4 + 0.06 \times 0.24 \times 3.9 \times 2) \times 1000 = 468\text{kN}$

The failure acceleration can be obtained by $\alpha_{in-intact} = S/G = 0.51g$

Based on the above results, the in-plane failure acceleration is 0.5g

7.6.3.2. In-plane loading with openings

Based on (GB50011, 2010), the shear force distribution considering openings is determined below.

For the small opening wall section, first the stiffness should be considered as for a wall without opening, then multiplied by the factor for opening effects; for the wall section with a large opening (the height of the opening is over 50% of the storey height), the wall should be divided based on the window and door. Importantly, due to the weakness of the walls between the windows or between windows and doors, the height of wall should be taken as the height of the windows or doors.

Table 7.5 The opening effects factor from (GB50011, 2010)

Opening percentage	0.10	0.20	0.30
Effects factor	0.98	0.94	0.88

Based on this the building can be divided into three types of URM walls, the sizes of walls being 3.9m×3.6m, 1.0m×2.6m and 1.3m×2.6m, respectively. Therefore, the calculation progress is similar to in-plane loading without openings.

$$L_{\text{vertical1}} = \frac{3.9 \times 3.6 \times 0.24 \times 18}{2} + \frac{3.6}{13.8} \times 500 = 160.3kN$$

$$L_{\text{vertical2}} = \frac{1.0 \times 3.6 \times 0.24 \times 18}{2} + \frac{1}{13.8} \times 500 = 42.78kN$$

$$L_{\text{vertical3}} = \frac{1.3 \times 3.6 \times 0.24 \times 18}{2} + \frac{1.3}{13.8} \times 500 = 55.1kN$$

The sectional areas of three types of wall are $0.936m^2$, $0.24m^2$ and $0.312m^2$, then according to Equation 7-39, the impact factors of normal stress for the masonry shear strength are expressed as:

$\sigma_1 = 160.3 \div 0.936 = 171.3\text{kPa}$

$\sigma_2 = 42.78 \div 0.24 = 178.25\text{kPa}$

$\sigma_3 = 39.6 \div 0.312 = 176.63\text{kPa}$

Using Equation 7-39, the impact factor of normal stress for the masonry shear strength is calculated as:

$$\xi_{N1} = \frac{1}{1.2}\sqrt{1 + \frac{0.45\sigma_1}{f_v}} = \frac{1}{1.2}\sqrt{1 + 0.45 \times 171.3/(0.08 \times 1000)} = 1.17$$

$$\xi_{N2} = \frac{1}{1.2}\sqrt{1 + \frac{0.45\sigma_2}{f_v}} = \frac{1}{1.2}\sqrt{1 + 0.45 \times 178.25/(0.08 \times 1000)} = 1.18$$

$$\xi_{N3} = \frac{1}{1.2}\sqrt{1 + \frac{0.45\sigma_2}{f_v}} = \frac{1}{1.2}\sqrt{1 + 0.45 \times 176.63/(0.08 \times 1000)} = 1.177$$

The force resistance of longitudinal walls from Equation 7-32 is:

$\mu r_{bE}\xi_{N1}f_{v,m}A_1 = 0.75 \times 0.85 \times 1.17 \times 0.0952 \times 0.936 \times 1000 = 66.46kN$

$\mu r_{bE}\xi_{N2}f_{v,m}A_2 = 0.75 \times 0.85 \times 1.18 \times 0.0952 \times 0.24 \times 1000 = 17.19kN$

$\mu r_{bE}\xi_{N3}f_{v,m}A_3 = 0.75 \times 0.85 \times 1.177 \times 0.0952 \times 0.312 \times 1000 = 22.29kN$

Based on $\frac{R}{r_{RE}S} \geq 1$, and there is no confined columns, so the r_{RE} = 1.0

$S_1 \leq R_1 = 66.46kN$

$S_2 \leq R_2 = 17.19kN$

$S_3 \leq R_3 = 22.29kN$

Therefore, the failure acceleration of each pier is shown below:

$$\alpha_1 = \frac{S_1}{L_{\text{vertical1}}} = 0.42g$$

$$\alpha_2 = \frac{S_2}{L_{\text{vertical2}}} = 0.39g$$

$$\alpha_3 = \frac{S_3}{L_{\text{vertical3}}} = 0.41g$$

The failure acceleration can be obtained by: $\alpha_{in-opening} = S/G = 0.39\ g$

7.6.3.3. Out-of-plane loading

(Doherty, 2000) suggested a quasi-static linear elastic design methodology from Australia (AS3700-1998) for vertical one-way bending URM walls (described in Figure 7.13). The moment is expressed by Equation 7-47 as follows:

$$M_e = \frac{t^2 l}{6}\left[\frac{O+\frac{W}{2}}{tl} + f_t'\right] \quad \text{7-47}$$

And the predicted cracking acceleration is shown by Equation 7-48 below:

$$a = \left[\frac{4t}{3\gamma g h^2}\left(\frac{O+\frac{W}{2}}{t} + f_t'\right)\right] \quad \text{7-48}$$

Where W is the self-weight of the URM wall; w is the earthquake inertia load; γ is the specific weight of the URM wall; f_t' is the flexural tensile strength; O is the superimposed load (from a concrete slab for instance).

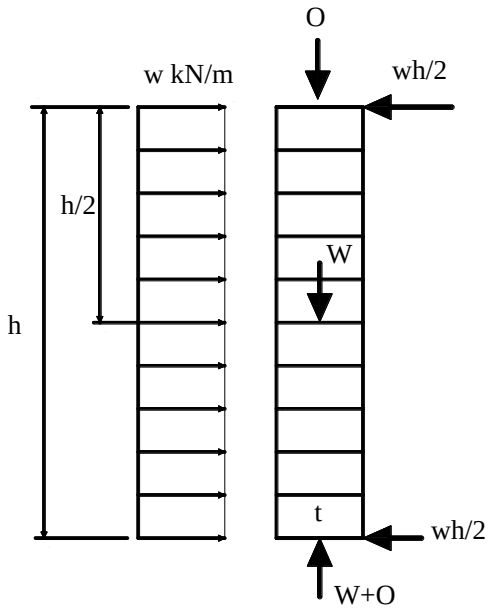

Figure 7.13 Quasi-Static Linear Elastic Design Methodology [Adapted from (Doherty, 2000)]

Based on Equation 7-46, the predicted failure acceleration leading to cracking is given by

$$\alpha_{out} = \left[\frac{4t}{3\gamma g h^2}\left(\frac{O+\frac{W}{2}}{t} + f_t'\right)\right] = \frac{712.6}{1511.6544} g = 0.47g$$

7.6.3.4. The predictions of seismic capacity of specific cases

Based on the results of in-plane loading and out-of-plane loading considering buildings with and without openings, the predictions of seismic capacity of specific cases are shown below.

For comparing the in-plane and out-of-plane capacity, based on the results that $\alpha_{out} < \alpha_{in}$, it is indicated that the out-of-plane capacity is weaker than the in-plane capacity so the wall fails out-of-plane first.

To compare the walls with and without openings, based on the results that $\alpha_{in-opening} < \alpha_{in-intact}$, it is clear that the opening reduction factor from the design code obtained using $\frac{\alpha_{in-opening}}{\alpha_{in-intact}} = 0.78$. For the failure acceleration of whole building without openings, as $\alpha_{in-intact}$ is 0.5g and $\alpha_{out}$is 0.47g, the failure acceleration should be taken as 0.47g. For the building with openings, as $\alpha_{in-intact}$ is 0.39g and $\alpha_{out}$is 0.47g, the failure acceleration should be taken as 0.39g.

7.6.4 Results of case study from proposed simple quick assessment procedure

The simplified procedure shown in section 7.5 is now applied to the case study building. The design earthquake is obtained from Table 2.3 and is equal to 0.36g. The details of the quick assessment method are shown in Figure 7.14.

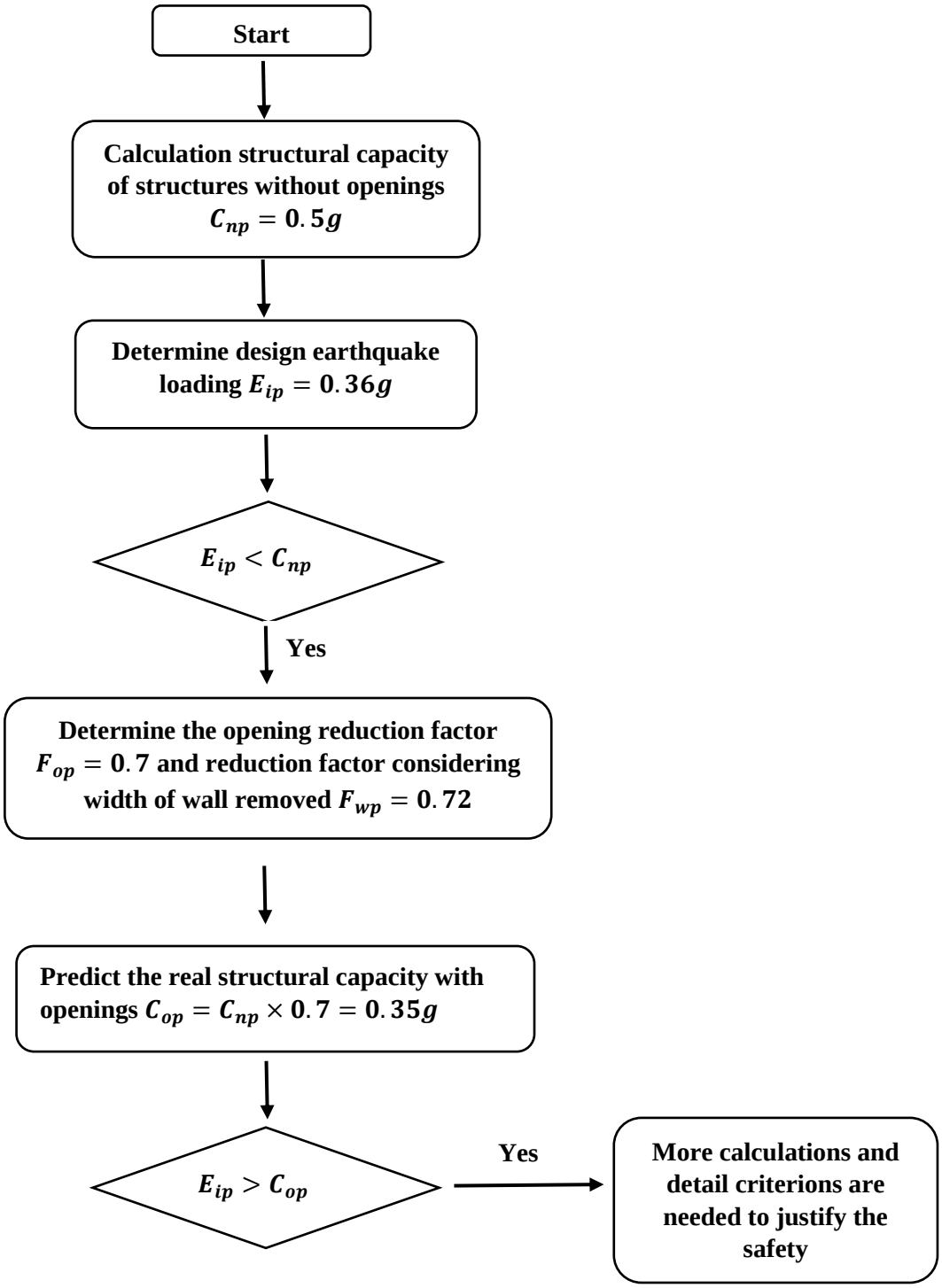

Figure 7.14 The proposed simple assessment procedure for case study building

Following the flow chart in Figure 7.14 the in-plane capacity of the wall without openings is 0.5g. To obtaining the opening reduction factor, as the opening can be classified as central openings, the opening reduction factor is determined using Equation 7-2 as 0.7. Therefore, the structural in-plane capacity with the opening is equal to 0.35g. If the alternative method of calculating the reduction factor (based on the total width of wall removed is used) Equation 7-9 is applied and the reduction factor is 0.72. Therefore, when calculating the reduced in-plane capacity, the smaller value of 0.7 is applied.

As there are no openings for out-of-plane walls in this case, the out-of-plane capacity is calculated as 0.47g from Equation 7-45, so the overall capacity of the building C_{op} is taken as 0.35g. It should be noted that, even though $\boldsymbol{E_{ip} > C_{op}}$, the building might be OK because a safety factor could be considered. An appropriate safety factor is suggested based on the results of the numerical modelling in the next section.

7.6.5 Numerical analysis of case study building in 3DEC

7.6.5.1 Numerical 3D model and material properties in 3DEC

Following the procedures in Chapter 3, the several models of the case study building were developed, as shown in Figure 7.15. To aid identification of the effects of openings and avoid adding in torsional effects, the models are built (a) without openings and (b) with a symmetrical set of openings in both walls. For the roof of building, usually there are two possible types, one is a timber roof (based on the case of a typical unreinforced masonry structure), while another assumed a flat concrete roof (which is also common). Because the two types of roofs display different failure mechanisms both would ideally be considered. However, as it is hard to model a flexible timber roof in 3DEC. To simplify the numerical modelling for this case study two buildings, one with a rigid roof and one with no roof are considered. The vertical load is applied via the density of the top block. The detailed layout of models is illustrated in Figure 7.15.

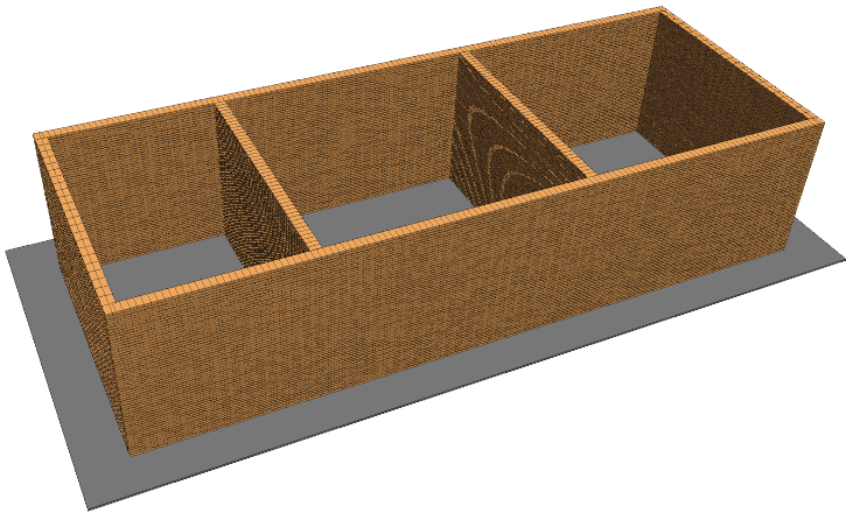

(a) 3D model of building without openings in 3DEC

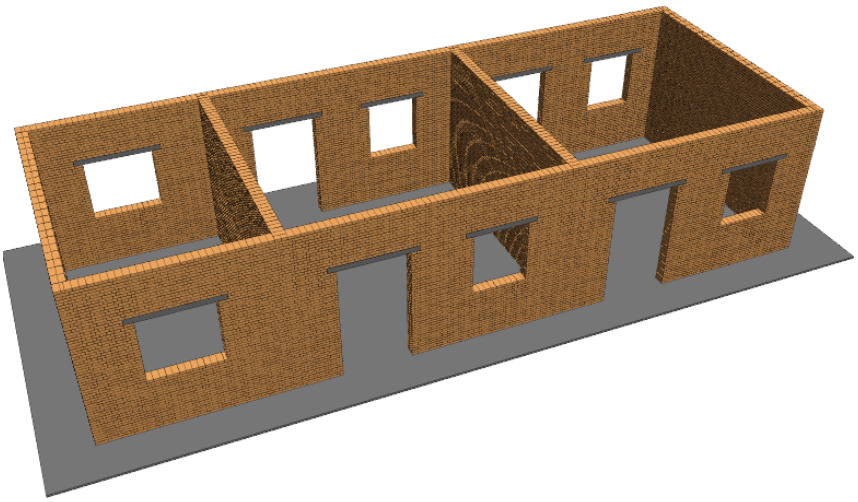

(b) 3D model of building with openings in 3DEC

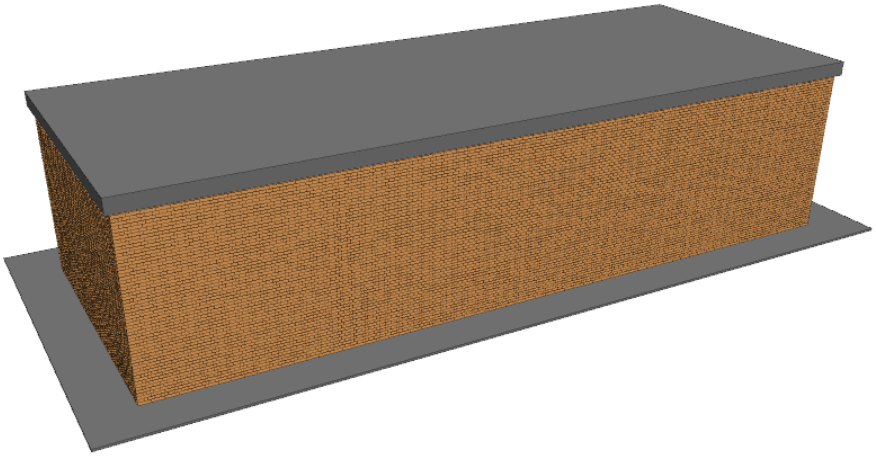

(c) 3D model of building without openings and with roof block in 3DEC

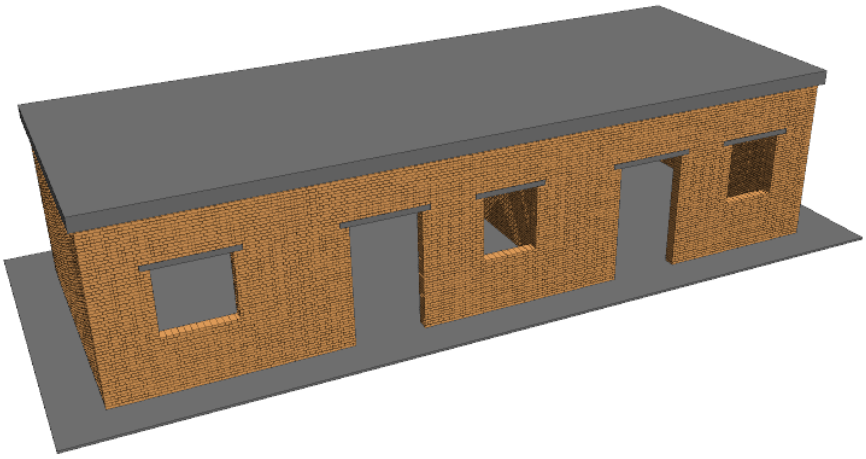

(d) 3D model of building with openings and with roof block in 3DEC

Figure 7.15 Numerical model for 3D real buildings in 3DEC

The cohesion properties of the joints in 3DEC were determined based on Equation 3-11 and were calculated from the compressive strength and tensile strength of the bricks which was obtained from the design code in this case. The tensile strength of joints was taken as half of the cohesion (Lemos and Costa, 2017). The compressive strength of bricks in the model was taken as 1.83MPa, the average tensile strength of bricks as 0.13MPa and the shear strength of the bricks as 0.11MPa (GB50003-2011, 2012). The friction angle was assumed to be 35 degrees. The properties of blocks and joints in 3DEC are summarised in Table 7.6 and Table 7.7.

Table 7.6 Properties of masonry blocks [From (GB50003-2011, 2012)]

Density [kg/m³]	Young modulus [GPa]	Poisson's ratio [-]
1800	4.272	0.15

Table 7.7 Properties of joints

	Joint normal stiffness [MPa/m]	Joint shear stiffness [MPa/m]	Joint friction angle [Degrees]	Joint tensile strength [MPa]	Joint cohesion [MPa]
Vertical joints 1	35600	14240	35	0.1	0.2
Vertical joints 2	17800	7120	35	0.1	0.2
Horizontal joints	71200	28480	35	0.1	0.2

7.6.5.2 Loading and failure criterion

To identify the structural capacity of the whole building considering the effect of the openings, a pseudo-static pushover procedure was applied. Increasing horizontal accelerations were used to observe the changes in the displacements of the walls and the failure mechanisms. A vertical load equal to 500kN was applied in one of two different ways. For one model the vertical load was applied as vertical stress without a top block (representative of a timber roof), for the other model the loading was applied by top block (representative of a concrete roof). To monitor the effect of the pushover analyses of the buildings in 3DEC, a total six points labelled A, B, C, D, E and F were selected to record the displacements as these points are possible to have maximum displacements of the structures. Detailed information for models is shown in Figure 7.16 and Figure 7.17.

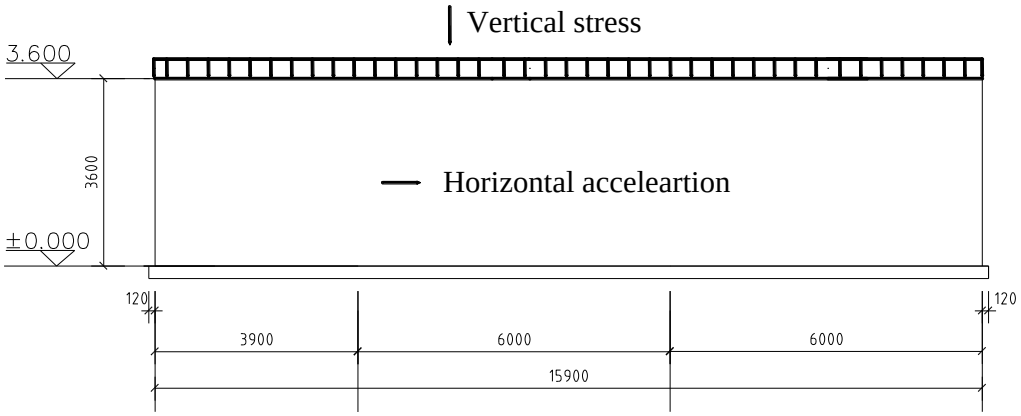

(a) Load application with vertical stress

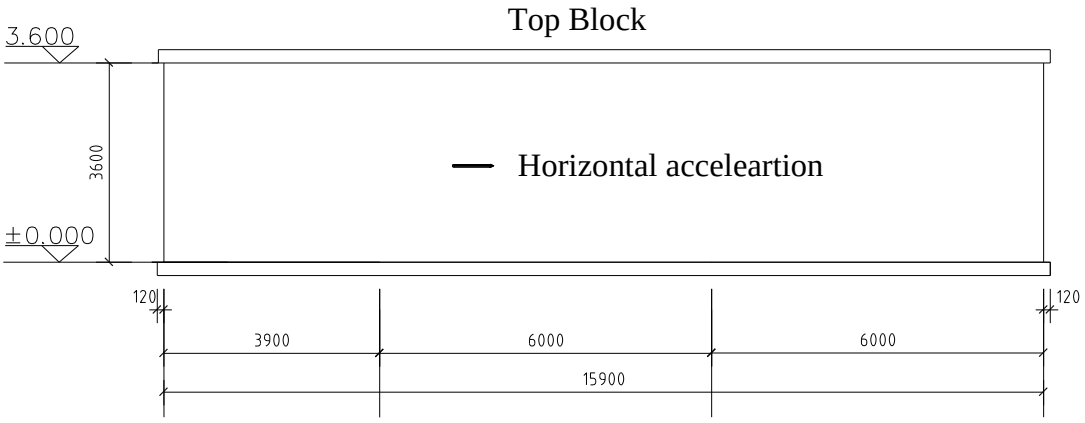

(b) Load application with top block

Figure 7.16 Different loading methods for the numerical models in 3DEC

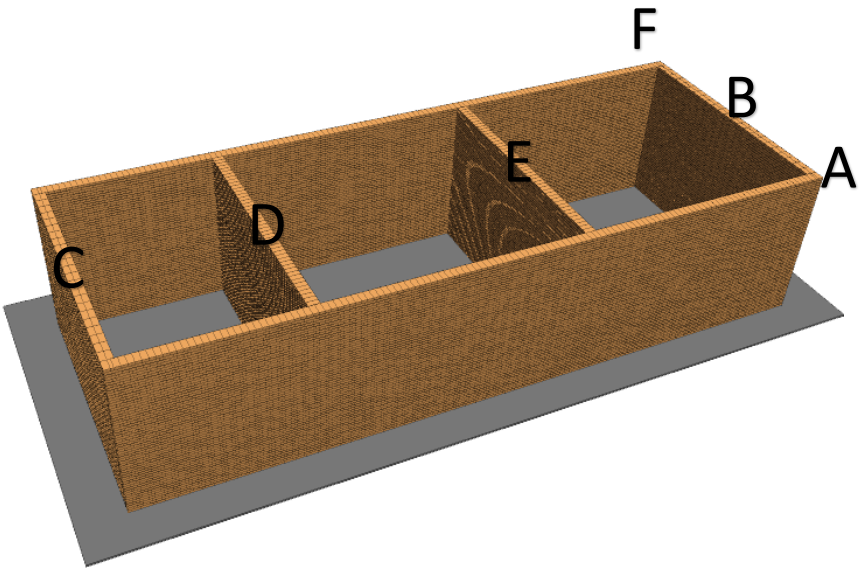

Figure 7.17 Monitor points on the building for the pushover analyses in 3DEC

Once the displacements increased significantly and reached a 4% drift, this was assumed to equate to failure of the structure. If the displacements only increased slightly and the structure remained stable, this meant the structure remained safe. However, because a load based calculation method was used (so that all the walls experienced appropriate loading), it was hard to accurately determine the peak acceleration values for failure and instead failure could only be determined to take place within a range of values.

7.6.5.3 Results of pushover curves and crack patterns

Using the models, material properties and loading procedure described above, the results for each model under different horizontal accelerations were obtained and are shown in Figure 7.18.

For buildings without openings under vertical stress:

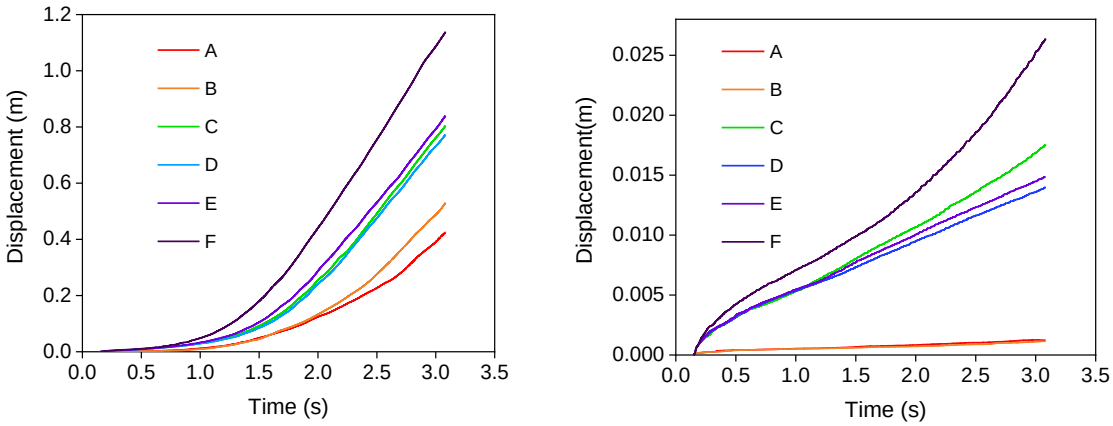

(a) Curves of time-displacement for different points under 2g; (b) Curves of time-displacement for different points under 1.2g

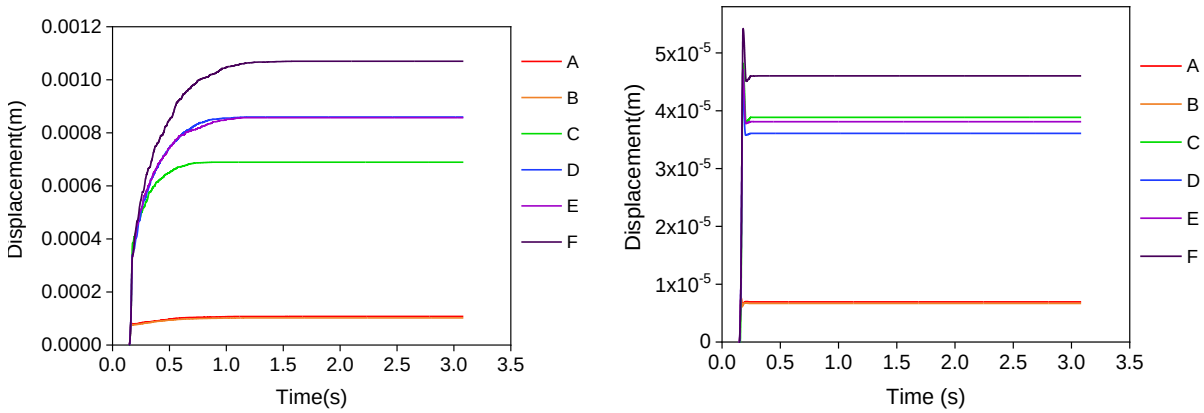

(c) Curves of time-displacement for different points under 0.5g; (d) Curves of time-displacement for different points under 0.1g

Figure 7.18 Curves of time-displacement with different points under different horizontal accelerations

Looking at the responses in Figure 7.18, the displacements of point F have the highest values and are taken as the peak values for the analysis. If the structure remains safe under the loading, the displacements will increase a little as the analysis starts and then remain stable (e.g. Figure 7.18 (c)), while if the structures fail, the displacements keep rising until they exceed the maximum drift ratio (e.g. Figure 7.18(a)). Taking the displacement results from the complete set of analyses, the failure accelerations were determined to be in the range of 0.9g to 1.0g, i.e. around 0.95g. More detail of the set of analyses is shown in Figure 7.19(a).

Because the number of calculation cycles for the model was limited (to reduce calculation time), the difference between the displacements being safe and failure occurring was not clear. Taking two points (0.9g and 1g) for example, and allowing three times more analysis cycles resulted in a slightly

different set of displacements as shown in Figure 7.19(b). From this it is clear that failure is occurring (albeit slowly) under a pushover acceleration of 1g.

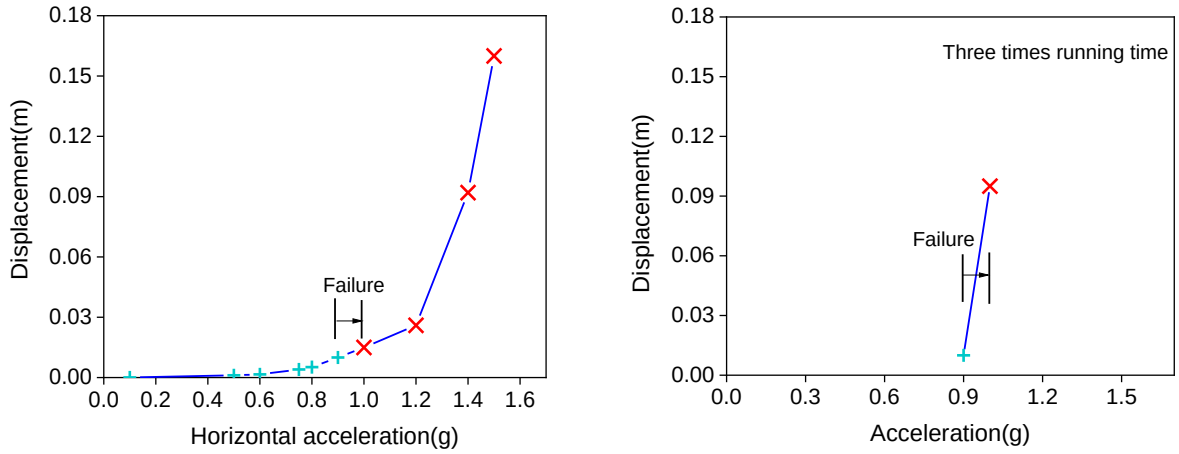

(a) Acceleration-displacement curve (b) Detail information of failure range

Figure 7.19 Curves of acceleration-displacement for URM structures without opening under vertical stress

For buildings with openings under vertical stress, the curves for time-displacement of the different monitoring points are shown in Figure 7.20. Point F still has the largest displacements at any specific time. For horizontal accelerations under 0.6g, the displacements remain stable as time increases which means the building is safe.

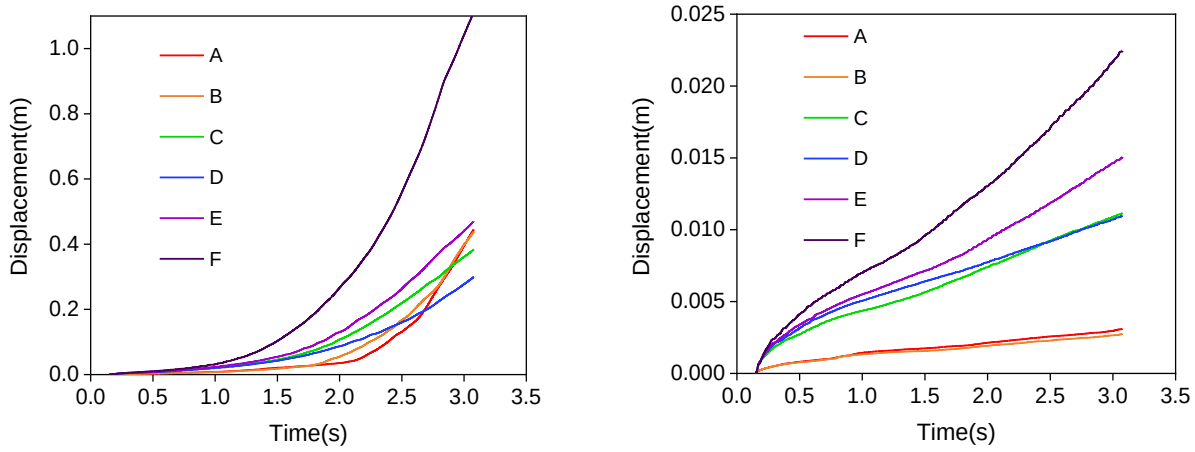

(a) Curves of time-displacement for different points under 1.8g; (b) Curves of time-displacement for different points under 1.1g

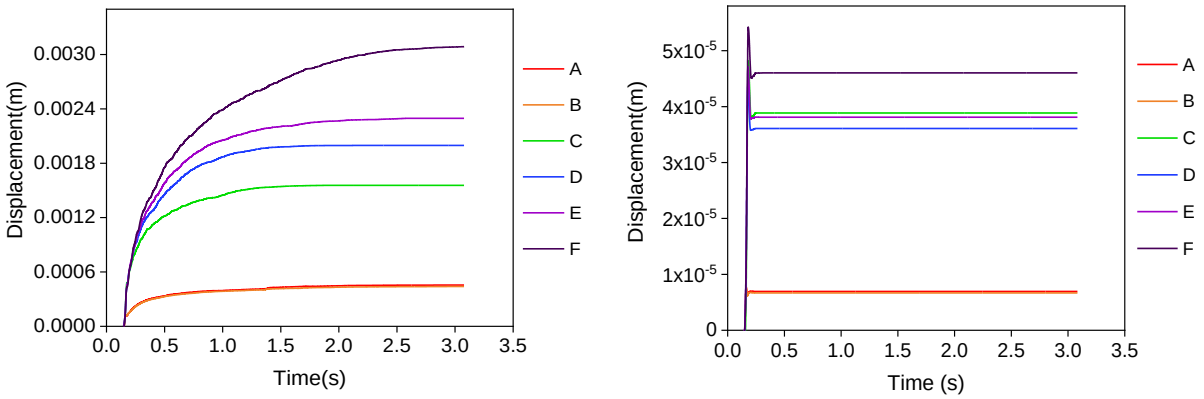

(c) Curves of time-displacement for different points under 0.6g; (d) Curves of time-displacement for different points under 0.1g

Figure 7.20 Curves of time-displacement with different points under different horizontal accelerations

More detailed information for point F is shown in Figure 7.21, the failure acceleration can be determined to be in the range from 0.75g to 0.85g, i.e. around 0.8g. Therefore, when the building was loaded with vertical stress (i.e. timber roof), with no openings it failed at 0.95g, and with openings it failed at 0.8g.

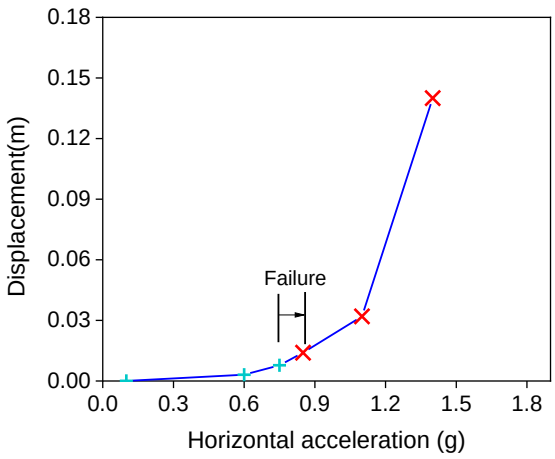

Figure 7.21 Curve of acceleration-displacement for URM structures with openings under vertical stress

For the building model without openings, but with a top block (i.e. concrete roof), the models were more sensitive to a change in horizontal acceleration. It can be seen in Figure 7.22 that when the horizontal accelerations changed from 0.4g to 0.55g, the displacement increased dramatically and at 0.6g significant displacement occurred occur failure. Point F still showed the largest displacements at

any fixed time. Figure 7.23 shows that within a range of accelerations from 0.56g to 0.58g, the displacements increase clearly and it is easy to identify that the failure acceleration is around 0.56g. Compared with the models with applied vertical stress, the failure accelerations were much easier to identify with the top block on the model.

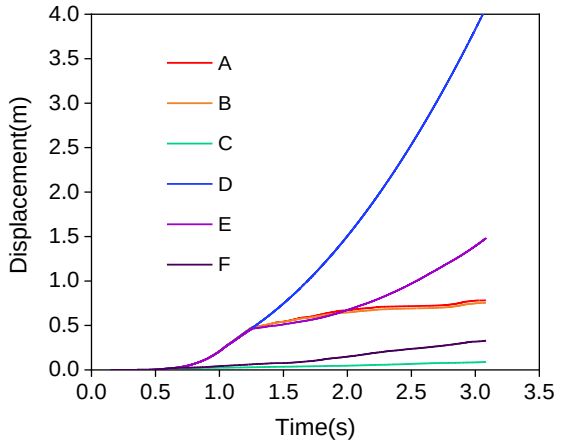

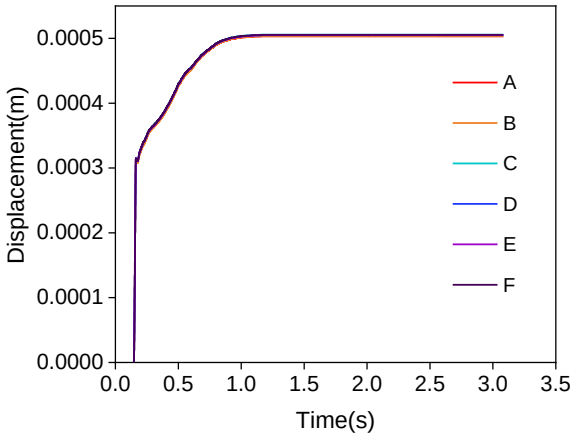

(a) Curves of time-displacement for different points under 0.6g; (b) Curves of time-displacement for different points under 0.5g

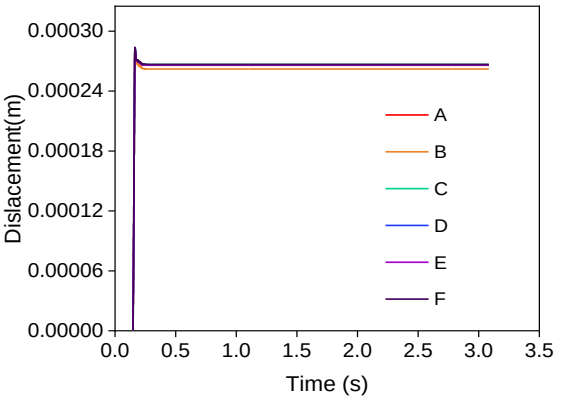

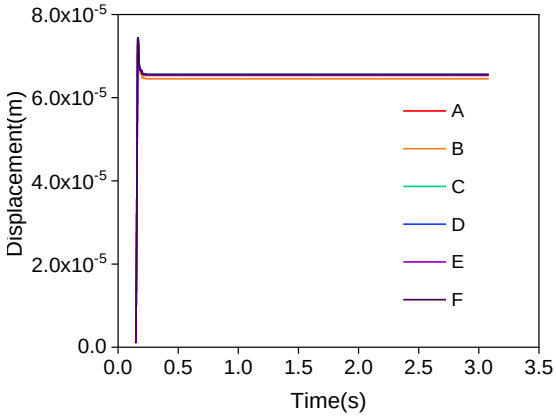

(c) Curves of time-displacement for different points under 0.4g; (d) Curves of time-displacement for different points under 0.1g

Figure 7.22 Curves of time-displacement with different points under different horizontal accelerations

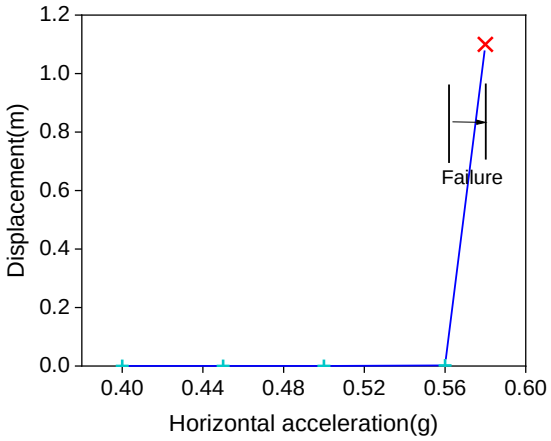

Figure 7.23 Curve of acceleration-displacement for URM structures without openings under top block

For the building with openings and loading applied by a top block, the displacements were still sensitive to a change in accelerations. Point F still had the largest displacements. Figure 7.24 shows that the displacement of point F changes from 0.0027m at 0.4g to 0.015m at 0.5g. When the acceleration is 0.49g the displacement of F is small but the shape of the curve suggests it is continuing to increase and if enough time is allowed, the structure will continue to displace and eventually the maximum displacement tolerance will be reached. Therefore 0.49g could be taken as the failure acceleration. Further investigation around this acceleration value in Figure 7.25 indicates that the failure acceleration is in the range from 0.485g to 0.5g. Therefore, the failure acceleration was taken as 0.49g.

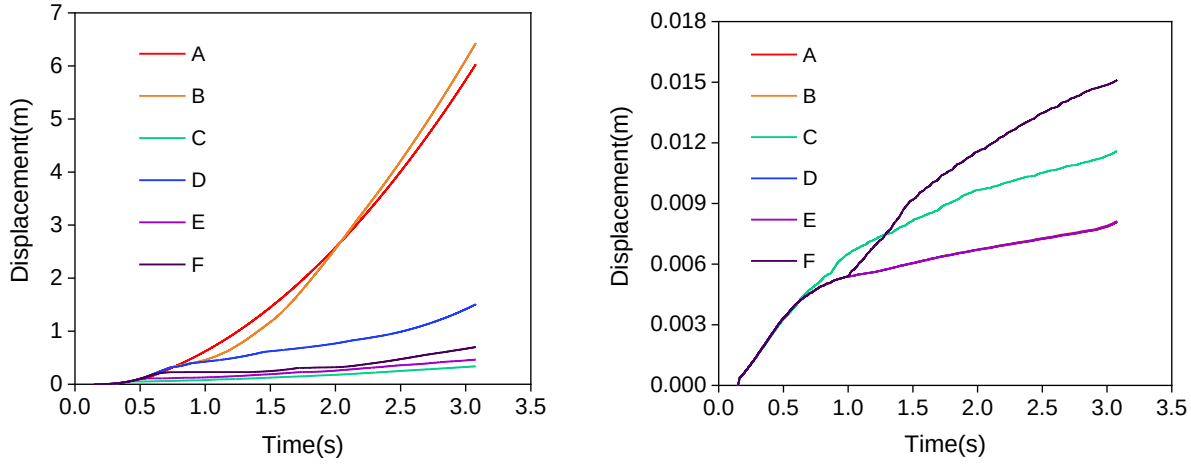

(a) Curves of time-displacement for different points under 0.6g; (b) Curves of time-displacement for different points under 0.49g

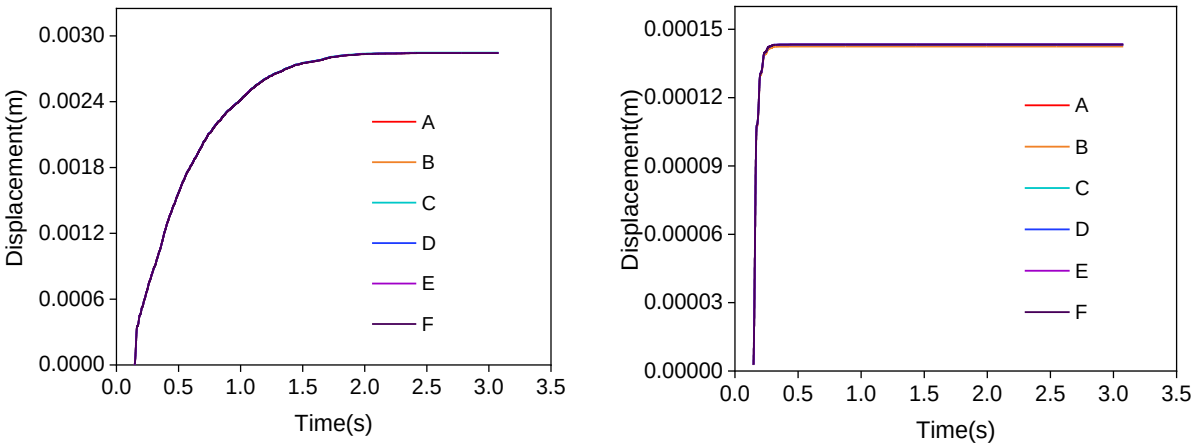

(c) Curves of time-displacement for different points under 0.4g; (d) Curves of time-displacement for different points under 0.1g

Figure 7.24 Curves of time-displacement with different points under different horizontal Accelerations

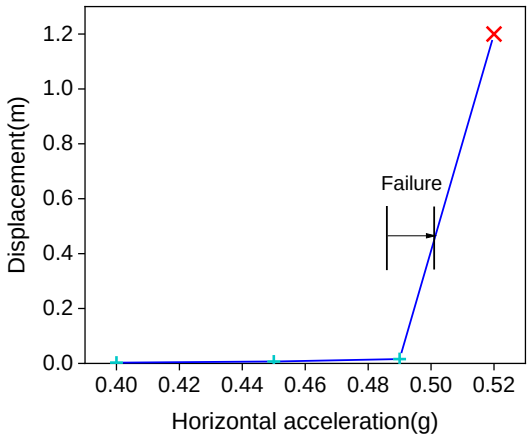

Figure 7.25 Curve of acceleration-displacement for URM structures with openings under top block

The typical crack patterns for the buildings in 3DEC are also worth investigating. For all the models a large horizontal acceleration was applied to observe the obvious crack patterns. Based on the crack propagations, the failure mechanisms of different cases were identified. Figure 7.26(a) shows the crack patterns in the building without openings (and applied vertical stress). It is clear that the out-of-plane walls suffer significant failure and then collapse. The in-plane walls also display visible diagonal cracks especially at the right part of the structure. Figure 7.26(b) shows that the out-of-plane walls also failure first even when there are openings in the in-plane walls. The failure mechanisms of both structures are similar.

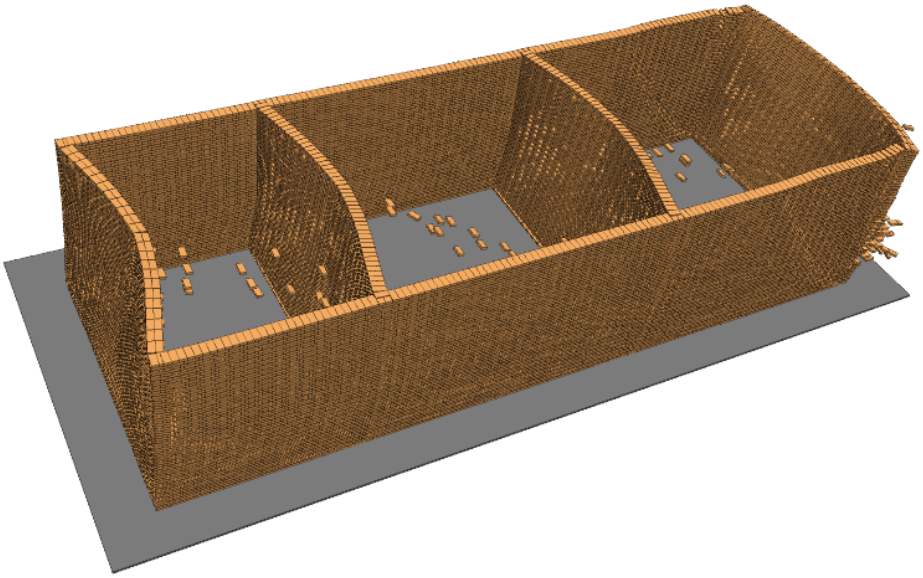

(a) Crack patterns without openings under 2g

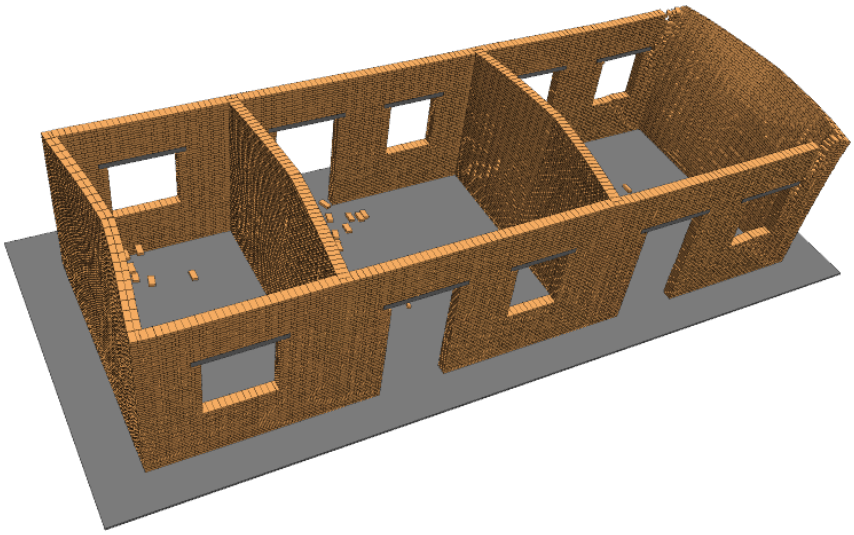

(b) Crack patterns with opening under 1.8g

Figure 7.26 Typical crack patterns for the URM structure under vertical stress

The crack patterns of buildings with vertical loading applied via a top block are shown below. Figure 7.27(a) shows that there are clear diagonal cracks located in the right part of the structure. The out-of-plane walls fail first and are close to complete collapse. Figure 7.27(b) indicates that the in-plane walls fail totally when they contain openings. Diagonal cracks occur in all the masonry walls and out-of-plane walls also appear to collapse. Observing the crack patterns in all the 3DEC models, it is obvious

that the out-of-plane walls are weaker than in-plane walls and these fail first even when the in-plane walls contain openings. All in-plane walls have diagonal cracks and the right part of the building is the first to crack.

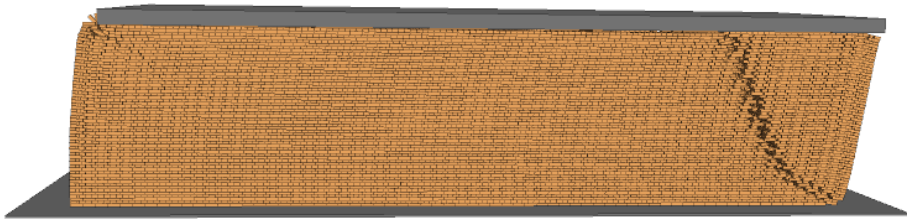

(a) Crack patterns Without opening under 0.58g

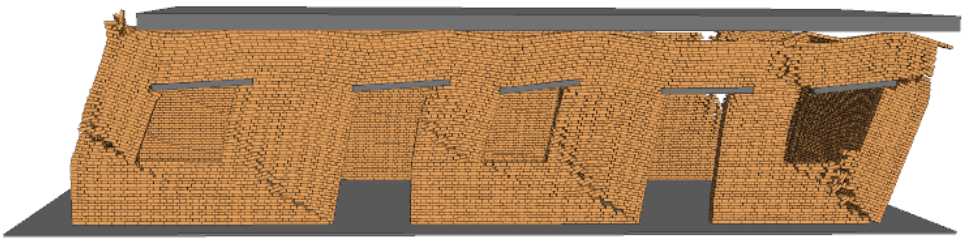

(b) Crack patterns with opening under 0.52g

Figure 7.27 Typical crack patterns for URM structure with a top block

Overall, the numerical analyses show that the failure acceleration for this structure without openings is 0.57g and the failure acceleration for structure with openings is 0.49g. Considering the design earthquake acceleration is 0.36g, the numerical model suggests this structure is safe.

7.7 Comparison of the predictions, proposed procedure and numerical analysis in 3DEC

A comparison between the results for the building capacity from the design code, from the proposed simplified assessment method and from the numerical modelling for the building with loading applied via a top block is shown in Table 7.8.

Table 7.8 Comparison of results between design code and numerical analysis

	Design code and previous research			Proposed assessment procedure			Numerical results	
	In-plane		Out-of-plane	In-plane		Out-of-plane	Without opening	With opening
	Without opening	With opening		Without opening	With opening			
Failure acceleration	0.5g	0.39g	0.47g	0.5g	0.35g	0.47g	0.57g	0.49g

The reduction factor taking into account the openings based on the design code calculations, the simplified method proposed in this thesis and the 3D numerical modelling are also compared in Table 7.9.

Table 7.9 Comparison of opening reduction factor for different methods (Opening percentage 22% and total percentage 43% width of wall removed)

	Design code and previous research	Proposed assessment procedure	Numerical results
Reduction factor	0.78	0.70 and 0.72	0.86

Based on the results in Table 7.8, it is clear that the numerical analysis predicts a better building performance when the openings are added than the results calculated by the design codes or proposed assessment procedure. This can be explained in that the numerical model reflects the whole failure progress considering 3D effects and includes the interaction between in-plane behaviour and out-of-plane behaviour. The out-of-plane walls show the worst performance for the building without openings and they fail first. For building with openings, the failure acceleration is limited by the failure

of the in-plane walls. The numerical models show the best building response and the proposed simplified assessment procedure is the most pessimistic.

The comparisons of three methods reveal that the proposed assessment procedure in this thesis gives a conservative value for the failure acceleration and for the opening reduction factor. This is acceptable because the simplified assessment procedure is meant to be quick and simple, allowing a quick and safe assessment of the safety for buildings. If this simplified method suggests the building safely, the results are reliable because the method is conservative. However, if the method suggests the buildings are slightly unsafe then more detailed calculations may be needed to assess the risk of failure more accurately.

In addition, the comparison of the analytical time between masonry wall and entire building is interesting to investigate. For the standard analysis of URM walls in 3DEC, the computational time is normally one hour while for an entire building, the computational time is over 10 hours. Therefore, it is nor real to run amounts of analysis for whole buildings and it is still suitable to mainly investigate the effects of openings through masonry walls.

In summary, all three methods have been compared as methods to predict the failure accelerations and opening reduction factors for a real building. The proposed assessment procedure has been shown to be a quick and reliable method that would be useful for identifying the seismic performance of real buildings quickly in the future.

7.8 Possible implementation

Based on the comparison of results, a proposed simple assessment procedure has been proposed. If the building layout and material properties are available, the safety of the building can be quickly assessed. However, to check the safety of the building more accurately, some boundaries for different conditions should be determined. A possible implementation is proposed below to support the simplified assessment procedure. The detailed information is described in Figure 7.28.

The design capacity of a building with openings C_{dop} is obtained from a detailed code-based design analysis. Based on Table 7.6, the capacity C_{op} from the proposed assessment method will be smaller than that from the design code, therefore C_{op} could be multiplied by a safety factor to describe the failure condition of structure accurately. The safety factor is calculated by the comparison between

the value of the design code and proposed assessment procedure. From the work above a safety factor of 1.2 was determined.

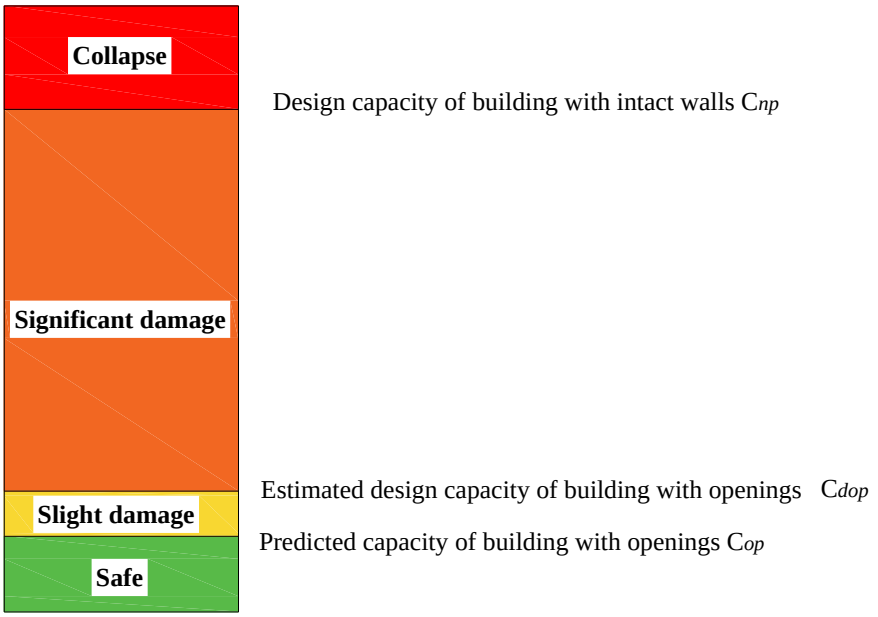

Figure 7.28 Proposed criterion for safety check of building

Figure 7.28 also shows that an additional criterion on the safety can then be applied. Based on the assessment procedure mentioned in section 7.5, when the input properties and design earthquake loading E_{ip} are determined, the safety of building can be checked. If $E_{ip} > C_{np}$ the structure will collapse, if $E_{ip} < C_{op}$ the structure is safe, if $C_{op} < E_{ip} < C_{dop}$ the structure is likely to experience slight damage, and if $C_{dop} < E_{ip} < C_{np}$, the structure is likely to experience significant damage. Using the simplified assessment method and the set of criteria above, URM buildings at risk of damage would be relatively easy to identify and this method could be applied to more buildings in the future.

7.9 Summary

This chapter has defined some relationships for the impact of openings on the in-plane performance and out-of-plane performance of URM walls. An opening reduction factor has been proposed based on this research and a specific test case has been studied. By comparing the numerical results with design codes, it has been shown that a 3DEC numerical analysis can reflect the behaviour of URM structures successfully and a simple assessment procedure for buildings is then suggested. The key points from this chapter are summarised below:

1. Relationships for the in-plane and out-of-plane performance of URM walls considering the effects of openings are proposed. For in-plane behaviour, different opening cases are considered including central openings, door openings and weak openings. For all opening cases relationships have been derived and have been summarised. For the out-of-plane behaviour of URM walls, the wall capacity increases due to the strength of the lintel, therefore only the effect of the opening position needs to be considered for out-of-plane loading.
2. Based on the relationships for the effect of openings on URM walls, an opening reduction factor is proposed. All opening cases have been considered and the results are listed in Table 7.1. The equations in Table 7.1 combine the effects of opening size and position, and for some more common cases, e.g. central openings simple relationships for just the opening percentage are presented. Based on these equations a simple assessment procedure for URM buildings is proposed.
3. A specific test case of a real building in China is studied. To simplify the numerical analysis, the building model was symmetrical so that torsion effects were avoided. Before running the numerical analyses, the capacity of the building was predicted by calculating the failure acceleration from design codes and using the proposed simplified assessment procedure.
4. The numerical model was built using material properties from the Chinese design codes and the values are obtained from Chinese masonry design code. It was important to decide the appropriate failure criterion and the monitor the building accordingly. In order to limit the calculation time, the calculation of the failure acceleration was only determined within a range of values by looking at whether the numerical model still kept a stable position under the applied acceleration.
5. A comparison between the numerical analyses, design codes, and simplified assessment procedures is discussed. The numerical results suggested the building had a better performance than the other methods and the simple assessment procedure predicted a sensible but slightly conservative performance. The simplified method is therefore a suitable way to deal with the impact of openings in real buildings and a possible implementation has been discussed.
6. There are still a few limitations of the relationships between openings and both in-plane and out-of-plane performance for URM structures. As all the results are derived from curve fitting, which means some errors are ignored. Besides, to come up with equations to reflect all the cases, some results are taken as the most dangerous values, while in fact, the real response

may be safer than the proposed outcomes. In the future, more case studies and experimental tests can be applied to calibrate the reliability of the proposed procedure.

Chapter 8 CONCLUSIONS

8.1 Summary and conclusions

This thesis has studied the effects of openings on URM walls and has identified strategies for identifying the impact of openings on the seismic performance of the walls, with the aim of reducing the damage to low-rise masonry structures in China in earthquakes. To investigate this problem, numerical models of URM walls were built in 3DEC and the effects of openings on both the in-plane and out-of-plane behaviour of the walls have been considered. Using static and dynamic analyses of URM walls with a variety of openings, opening reduction factors for different opening cases are proposed and a simple quick assessment procedure is suggested. To test the proposed simplified assessment method, a specific case study has been analysed using three different methods, and the results from the three methods (design code, proposed assessment procedure and numerical analysis) have been compared. The innovation of the research mainly include identifying the opening effects of URM structures under both in-plane and out-of-plane behaviour by DEM in 3DEC, obtaining a detailed relationship between all kinds of opening effects and seismic performance of URM buildings through numerical analysis and proposing a simple assessment method for safety check of URM housing targeting opening situations and would be potential to apply the procedure to URM housing in rural area of China to reduce the seismic damage.

The main conclusions from this research are shown below.

1. A comprehensive literature review of modelling methods for masonry structures, seismic analysis procedures, seismic performance and seismic assessment for unreinforced masonry structures shows that there has been little research to date dealing with the effects of openings in URM structures. There is also little in the way of guidelines for dealing with the relationships between sizes and locations of openings and the seismic capacity of URM walls. While some seismic assessment procedures have been developed for URM walls, but mostly are quite complicated and lots of calculation are needed, which may not be suitable in rural

area, therefore a simple rapid method is still needed. Based on the review, there is no simple assessment procedure in China and it is interesting to develop and could apply the method in rural area widely.

2. This thesis presents a methodology for using the Discrete Element Code 3DEC to model URM walls and buildings. Sensitivity studies have been done on the analysis method along with validation of the numerical models by comparison with experimental data. It has been shown that numerical models in 3DEC can reflect the behaviour of masonry structures successfully and accurately. Through sensitivity studies, some factors like cycle numbers, values of velocities and block types could affect the results of numerical analysis, these factors should be considered carefully when running analysis in 3DEC.
3. For in-plane behaviour, the relationships between opening size and the capacity of a URM wall have been evaluated. For walls with a central opening, when the opening percentage is less than ~10% the wall retains >80% of the solid wall capacity. Once the opening exceeds ~50%, only about 10% residual wall capacity remains. DE modelling approach allows the crack patterns in masonry walls to be observed clearly and there is a clear link between the failure mechanism and the in-plane capacity of the masonry walls. The differences in the pushover curves developed for different opening percentages directly reflect differences in the crack propagation within the walls. Diagonal cracking and rocking are the dominant failure mechanisms for URM walls under in-plane loading. In general, the masonry walls analysed using a load-based analysis procedure show more localized cracking than those analysed using a displacement-based procedure and the maximum base shear force for the load-based analysis procedure is also lower than for the displacement-based procedure. For simple pushover analyses the direction of applied loading needs to be considered when evaluating failure patterns for in-plane loading. The in-plane wall capacity is reduced when the openings are located along in the line of the compression diagonal strut compared to when the opening is the location along the other diagonal.
4. This thesis has studied the impact of opening size and position on the out-of-plane capacity of URM walls. For masonry walls with three side support conditions, the relationship between opening percentage effects and out-of-plane performance is developed. As the opening size increases, unexpectedly, the peak value of horizontal pressure that the wall can withstand increases. The main reason for this is the influence of the lintel which increases the stiffness of the wall and restricts the displacement of the wall like ring beam. This significantly improves the strength of URM walls especially for three-side boundary condition wall. For four-side

boundary condition wall, as the top side is restrained, the effect of lintel is not obvious. Combined with the results of two different boundary conditions, the opening size was not found to have a significant negative effect on the out-of-plane behaviour of the wall, rather the inclusion of an opening (with its lintel) often improved the out-of-plane performance of the wall. When considering the effect of the opening position on the out-of-plane performance of the walls, the failure mechanism is the key factor because it can explain why some walls carry much lower loads than might be expected. A wall with a central opening can carry the load uniformly and has a better performance than walls with the edge or asymmetrical openings.

5. The dynamic behaviour of URM walls is also discussed in this thesis. The relationships between opening effects and the dynamic in-plane capacities of URM walls are evaluated. The opening size effects follow a similar trend to the static analyses, in that as the opening size increases the in-plane capacity decreases. However, there are some differences in the effect of the opening position, and in particular the failure mechanisms. The reason for these differences is that the dynamic analysis procedure applies cyclic loading to the wall whereas the static pushover test only produces loading in one direction.
6. This thesis derives relationships for the in-plane performance and out-of-plane performance of URM walls taking onto account the effect of openings. An opening reduction factor is proposed based on this research and was applied to a test case URM building. Using the relationships for the effects of openings, a simple assessment procedure for URM buildings is proposed as shown in Figure 8.1. This new method is compared to 3DEC modelling of the structure and design code rules, and the comparison between the three different methods is discussed. The results indicated that the building of numerical model in 3DEC had better performance than the results calculated by design code, and the design code suggested the building was stronger than the capacity predicted by the simple assessment method. The simple assessment method was the most conservative of the three methods and could therefore be safely used as a quick assessment method for URM buildings. The thesis finishes with the outline of a possible implementation procedure for this new assessment method.

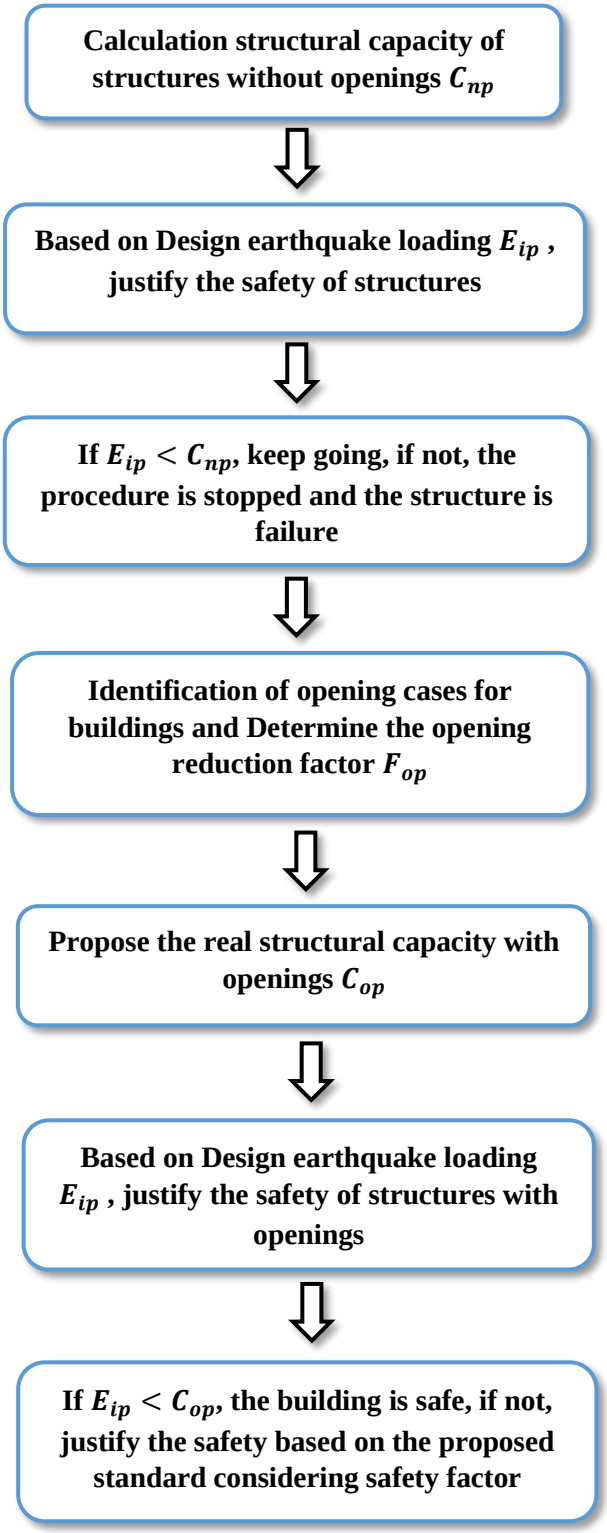

Figure 8.1 The Simple assessment procedure for buildings with opening

8.2 Limitations and recommendations for future works

It is worth noting that there are some limitations to this research.

1. The numbers of opening cases considered for both in-plane and out-of-plane behaviours was limited. Using 3DEC the analysis time for even one case was costing which at least one hour and therefore only a few key cases could be considered within the scope of this research.
2. For the dynamic analysis, the aim of the seismic analysis in the thesis was to calibrate the reliability of the static procedure. The research has been mostly limited to static pushover analyses rather than full dynamic analyses. Therefore, the simplified earthquake input is determined and only artificial ground motion is considered.
3. The case study ignores torsion effects to simplify the calculation progress. Therefore the interactions between in-plane and out-of-plane behaviours are ignored and the numerical analysis thus suggests better structural performance than the design codes.

Considering the limitations of research, some suggestions for future research are given below:

1. Develop a method that can build up more opening cases but running the analysis efficiently to verify the relationship between opening percentage and structural capacity.
2. More analysis is needed to allow consideration of all dynamic issues. It is also necessary to consider specific dynamic input for a comprehensive investigation of dynamic issues. Besides, there are also some interesting topics about the dynamic problems like different sizes of bricks or different bonding patterns.
3. More case studies can be applied. Especially for some complicated structures, it is worth identifying the reliability of the proposed procedure against more buildings.

REFERENCES

ABRAMS, D. P. & SHAH, N. 1992. *Cyclic load testing of unreinforced masonry walls.* Illinois univeristy at urbana advanced construction technology center.

ACHS, G. & ADAM, C. 2012. Rapid seismic evaluation of historic brick-masonry buildings in Vienna (Austria) based on visual screening. *Bulletin of Earthquake Engineering,* 10**,** 1833-1856.

AKHAVEISSY, A. & MILANI, G. 2013. A numerical model for the analysis of masonry walls in-plane loaded and strengthened with steel bars. *International Journal of Mechanical Sciences,* 72**,** 13-27.

AKHAVEISSY, A., MILANI, G. J. C. & MATERIALS, B. 2013. Pushover analysis of large scale unreinforced masonry structures by means of a fully 2D non-linear model. 41**,** 276-295.

AKHAVEISSY, A. H. & DESAI, C. S. 2011. Unreinforced masonry walls: nonlinear finite element analysis with a unified constitutive model. *Archives of Computational Methods in Engineering,* 18**,** 485-502.

AL-CHAAR, G., LAMB, G. E. & ISSA, M. 2003. Effect of openings on structural performance of unreinforced masonry infilled frames. *ACI Special Publications* 211**,** 247-262.

ALBANESI, T., BIONDI, S. & PETRANGELI, M. Pushover analysis: An energy based approach. Proc. of the Twelfth European Conference on Earthquake Engineering, London, United Kingdom, Paper, 2002.

ALEXANDRIS, A., PROTOPAPA, E. & PSYCHARIS, I. Collapse mechanisms of masonry buildings derived by the distinct element method. Proceedings of the 13th world conference on earthquake engineering, 2004. Citeseer, 1-6.

ANDREAUS, U. 1996. Failure Criteria for Masonry Panels under In-Plane Loading. *Journal of Structural Engineering* [Online], 122.

ASCE 2007. Seismic rehabilitation of existing buildings. Reston, VA.

ASTERIS, P. 2003. Lateral stiffness of brick masonry infilled plane frames. *Journal of Structural Engineering,* 129**,** 1071-1079.

ASTERIS, P. G., CAVALERI, L., DI TRAPANI, F. & SARHOSIS, V. 2016. A macro-modelling approach for the analysis of infilled frame structures considering the effects of openings and vertical loads. *Structure and Infrastructure Engineering,* 12**,** 551-566.

ATC 1996. Seismic evaluation and retrofit of concrete buildings. Applied Technology Council, report ATC-40. Redwood City.

ATC 1997a. NEHRP commentary on the guidelines for the seismic rehabilitation of buildings. Federal Emergency Management Agency , Washington, DC. (FEMA-274).

ATC 1997b. NEHRP guidelines for the seismic rehabilitation of buildings. Federal Emergency Management Agency, Washington, D.C. (FEMA-273).

ATC 1999. *Evaluation of Earthquake Damaged Concrete and Masonry Wall Buildings: Basic Procedures Manual*, FEMA-306.

ATC 2000. Prestandard and commentary for the seismic rehabilitation of buildings. Federal Emergency Management Agency , Washington, DC. (FEMA-356).

ATC 2005. Improvement of nonlinear static seismic analysis procedures. Federal Emergency Management Agency , Washington, DC. (FEMA-400).

AUGENTI, N. & PARISI, F. Non-linear static analysis of masonry structures. Proceedings of the 13th Italian national conference on earthquake engineering, paper no. S4, 2009.

AUGENTI, N., PARISI, F., PROTA, A. & MANFREDI, G. 2010. In-plane lateral response of a full-scale masonry subassemblage with and without an inorganic matrix-grid strengthening system. *Journal of Composites for Construction,* 15**,** 578-590.

AVOSSA, A. M. & MALANGONE, P. 2015. Seismic performance assessment of masonry structures with a modified "concrete" model. *Bulletin of Earthquake Engineering,* 13**,** 2693-2718.

BAGGIO, C. & TROVALUSCI, P. 1998. Limit analysis for no-tension and frictional three-dimensional discrete systems. *Journal of Structural Mechanics,* 26**,** 287-304.

BELMOUDEN, Y. & LESTUZZI, P. 2009. An equivalent frame model for seismic analysis of masonry and reinforced concrete buildings. *Construction and Building Materials,* 23**,** 40-53.

BIĆANIĆ, N., STIRLING, C. & PEARCE, C. 2003. Discontinuous modelling of masonry bridges. *Computational Mechanics,* 31**,** 60-68.

BOBET, A., FAKHIMI, A., JOHNSON, S., MORRIS, J., TONON, F. & YEUNG, M. R. 2009. Numerical models in discontinuous media: review of advances for rock mechanics applications. *Journal of Geotechnical and Geoenvironmental Engineering,* 135**,** 1547-1561.

BOTHARA, J. K., DHAKAL, R. P. & MANDER, J. B. 2010. Seismic performance of an unreinforced masonry building: An experimental investigation. *Earthquake Engineering & Structural Dynamics,* 39**,** 45-68.

BRASILE, S., CASCIARO, R. & FORMICA, G. 2010. Finite element formulation for nonlinear analysis of masonry walls. *Computers & structures,* 88**,** 135-143.

BRUNEAU, M. J. C. J. O. C. E. 1994a. Seismic evaluation of unreinforced masonry buildings—A state-of-the-art report. 21**,** 512-539.

BRUNEAU, M. J. J. O. S. E. 1994b. State-of-the-art report on seismic performance of unreinforced masonry buildings. 120**,** 230-251.

BUI, T.-T., LIMAM, A. & SARHOSIS, V. 2019. Failure analysis of masonry wall panels subjected to in-plane and out-of-plane loading using the discrete element method. *European Journal of Environmental and Civil Engineering***,** 1-17.

BUI, T., LIMAM, A., SARHOSIS, V. & HJIAJ, M. 2017. Discrete element modelling of the in-plane and out-of-plane behaviour of dry-joint masonry wall constructions. *Engineering Structures,* 136**,** 277-294.

ÇAKTı, E., SAYGıLı, Ö., LEMOS, J. V. & OLIVEIRA, C. S. 2016. Discrete element modeling of a scaled masonry structure and its validation. *Engineering Structures,* 126**,** 224-236.

CALDERINI, C., CATTARI, S. & LAGOMARSINO, S. 2009. In-plane strength of unreinforced masonry piers. *Earthquake Engineering & Structural Dynamics,* 38**,** 243-267.

CALIò, I., MARLETTA, M. & PANTò, B. J. E. S. 2012. A new discrete element model for the evaluation of the seismic behaviour of unreinforced masonry buildings. 40**,** 327-338.

CALVI, G. M., KINGSLEY, G. R. & MAGENES, G. J. E. S. 1996. Testing of masonry structures for seismic assessment. 12**,** 145-162.

CASAPULLA, C., CASCINI, L., PORTIOLI, F. & LANDOLFO, R. J. M. 2014. 3D macro and micro-block models for limit analysis of out-of-plane loaded masonry walls with non-associative Coulomb friction. 49**,** 1653-1678.

CASOLO, S. 2000. Modelling the out‐of‐plane seismic behaviour of masonry walls by rigid elements. *Earthquake Engineering & Structural Dynamics,* 29**,** 1797-1813.

CASOLO, S. J. C. I. N. M. I. E. 1999. Rigid element model for non‐linear analysis of masonry façades subjected to out‐of‐plane loading. 15**,** 457-468.

CHAIMOON, K. & ATTARD, M. M. 2007. Modeling of unreinforced masonry walls under shear and compression. *Engineering structures,* 29**,** 2056-2068.

CHOPRA, A. K. & GOEL, R. K. 2000. Evaluation of NSP to estimate seismic deformation: SDF systems. *Journal of Structural Engineering,* 126**,** 482-490.

COSTA, A. A., AREDE, A., COSTA, A. C., PENNA, A. & COSTA, A. 2013. Out-of-plane behaviour of a full scale stone masonry façade. Part 2: Shaking table tests. *Earthquake Engineering and Structural Dynamics,* 42**,** 2097-2111.

COSTA, A. A., ARÊDE, A. N., COSTA, A. B. & OLIVEIRA, C. S. 2012. Out-of-plane behaviour of existing stone masonry buildings: experimental evaluation. *Bulletin of Earthquake Engineering : Official Publication of the European Association for Earthquake Engineering,* 10**,** 93-111.

COSTLEY, A. C. & ABRAMS, D. P. 1996. Dynamic response of unreinforced masonry buildings with flexible diaphragms.

CREWE A 2020. Time history generation software [Matlab code] (In-house software-University of Bristol).

CUNDALL, P. 1987. Distinct element models of rock and soil structure. *Analytical and computational methods in engineering rock mechanics***,** 129-163.

CUNDALL, P. A. A computer model for simulating progressive, large scale movement in blocky rock systems. Symp. ISRM, Nancy, France, Proc., 1971. 129-136.

D'AYALA, D. & SPERANZA, E. J. D. 2002. An integrated procedure for the assessment of seismic vulnerability of historic buildings. 3**,** 3-3.

DAZIO, A. The effect of the boundary conditions on the out-of-plane behaviour of unreinforced masonry walls. 14th World Conference on Earthquake Engineering, 2008. 12-17.

DE FELICE, G. 2011. Out-of-plane seismic capacity of masonry depending on wall section morphology. *International Journal of Architectural Heritage,* 5**,** 466-482.

DERAKHSHAN, H. 2011. *Seismic assessment of out of plane loaded unreinforced masonry walls.*

DERAKHSHAN, H. & INGHAM, J. M. 2008. Out-of-Plane testing of an unreinforced masonry wall subjected to one-way bending.

DHANASEKAR, M. & HAIDER, W. 2008. Explicit finite element analysis of lightly reinforced masonry shear walls. *Computers & structures,* 86**,** 15-26.

DIALER, C. P. 2002. Typical masonry failures and repairs: a German Engineer's view. *Progress in Structural Engineering and Materials,* 4**,** 332-339.

DIHROU L, CREWE AJ, LIU Z & TAYLOR CA 2018. Shaking table studies of FRP-reinforced masonry: experimental and numerical results. *Proceedings of the 16th European Conference on Earthquake Engineering.* Thessaloniki, Greece: Springer.

DIMITRI, R., DE LORENZIS, L. & ZAVARISE, G. 2011. Numerical study on the dynamic behavior of masonry columns and arches on buttresses with the discrete element method. *Engineering Structures,* 33**,** 3172-3188.

DOHERTY, K., GRIFFITH, M. C., LAM, N. & WILSON, J. 2002. Displacement-based seismic analysis for out-of-plane bending of unreinforced masonry walls. *Earthquake Engineering & Structural Dynamics,* 31**,** 833.

DOHERTY, K. T. 2000. *An investigation of the weak links in the seismic load path of unreinforced masonary buildings.*

DUMOVA-JOVANOSLA, E. & CHURILOW, S. 2009. Calibration of a numerical model for masonry with application to experimental results. *Protection of historical Buildings, Mazzolani***,** 1139-1145.

EN1996-1-1 2005. Eurocode 6: Design of masonry structures–Part 1–1: Common rules for reinforced and unreinforced masonry structures. ENV 1996-1-1: 2004: E, CEN Brussels.

EN1996-3 2006. Eurocode 6 - Design of masonry structures - Part 3: Simplified calculation methods for unreinforced masonry structures. ENV 1996-3: 2006: E, CEN Brussels.

EN1998-1 2004. Eurocode 8: Design of structures for earthquake resistance-part 1: general rules, seismic actions and rules for buildings.

FEMA-154 1988. *Rapid Visual Screening of Buildings for Potential Seismic Hazards: A Handbook*, FEMA.

FEMA-154 2002. *Rapid Visual Screening of Buildings for Potential Seismic Hazards: A Handbook*, FEMA.

FEMA-154 2015. *Rapid Visual Screening of Buildings for Potential Seismic Hazards: A Handbook*, FEMA.

FERREIRA, T. M., COSTA, A. A. & COSTA, A. J. I. J. O. A. H. 2015. Analysis of the out-of-plane seismic behavior of unreinforced masonry: A literature review. 9**,** 949-972.

GALASCO, A., LAGOMARSINO, S. & PENNA, A. On the use of pushover analysis for existing masonry buildings. Proceedings of the 1st European conference on earthquake engineering and seismology, 2006. Geneva Switzerland, 3-8.

GALASCO, A., LAGOMARSINO, S., PENNA, A. & RESEMINI, S. Non-linear seismic analysis of masonry structures. 13th world conference on earthquake engineering, 2004. 1-6.

GáLVEZ, F., IP, K., VACULIK, J., GRIFFITH, M., SORRENTINO, L., DIZHUR, D. & INGHAM, J. Discrete Element Modelling to Predict Failure Strength of Unreinforced Masonry Walls. Proceedings of the Australian Earthquake Engineering Society 2017 Conference, 2017.

GALVEZ, F., SEGATTA, S., GIARETTON, M., WALSH, K., GIONGO, I. & DIZHUR, D. FE and DE modelling of out-of-plane two way bending behaviour of unreinforced masonry walls. 16th European Conference on Earthquake Engineering, Thessaloniki, Greece, 2018.

GAMBAROTTA, L. & LAGOMARSINO, S. 1997. Damage models for the seismic response of brick masonry shear walls. Part I: the mortar joint model and its applications. *Earthquake engineering & structural dynamics,* 26**,** 423-439.

GARBIN, E. P. D. 2010. In-Plane Behavior of Clay Masonry Walls: Experimental Testing and Finite-Element Modeling. *Journal of Structural Engineering* [Online], 136.

GARRITY, S., ASHOUR, A. & CHEN, Y. 2010. An experimental investigation of retro-reinforced clay brick arches. *International Masonry Society Proceedings,* 1**,** 733-742.

GB50003-2011 2012. *The national standard of the People's Republic of China; Code for design of masonry structures:* , Chinese building and industry press. (in Chinese).

GB50011 2010. The national standard of the People's Republic of China; Code for seismic design of buildings [S]. . Chinese building and industry press. (in Chinese).

GB50023. 2009. *Standard for earthquake-resistant evaluation of buildings [S].*

GHABOUSSI, J. & BARBOSA, R. 1990. Three‐dimensional discrete element method for granular materials. *International Journal for Numerical and Analytical Methods in Geomechanics,* 14**,** 451-472.

GHIASSI, B., SOLTANI, M. & TASNIMI, A. A. 2012a. A simplified model for analysis of unreinforced masonry shear walls under combined axial, shear and flexural loading. *Engineering Structures,* 42**,** 396-409.

GHIASSI, B., SOLTANI, M. & TASNIMI, A. A. J. E. S. 2012b. A simplified model for analysis of unreinforced masonry shear walls under combined axial, shear and flexural loading. 42**,** 396-409.

GIAMUNDO, V., SARHOSIS, V., LIGNOLA, G., SHENG, Y. & MANFREDI, G. 2014. Evaluation of different computational modelling strategies for the analysis of low strength masonry structures. *Engineering Structures,* 73**,** 160-169.

GIANNAKAS, A., PATRONIS, D. & FARDIS, M. 'The influence of the position and the size of openings to the elastic rigidity of infill walls. Proc., 8th Hellenic Concrete Conf, 1987. 49-56.

GILBERT, M. Limit analysis applied to masonry arch bridges: state-of-the-art and recent developments. Proceedings of 5th International Conference on Arch Bridges (ARCH'07), PB Lourenço, DB Oliveira, and A. Portela, eds., Funchal, Madeira, Portugal, 2007. 13-28.

GILBERT, M., CASAPULLA, C. & AHMED, H. 2006. Limit analysis of masonry block structures with non-associative frictional joints using linear programming. *Computers & structures,* 84**,** 873-887.

GOODMAN, R. E. Discontinuous deformation analysis-a new method forcomputing stress, strain and sliding of block systems. The 29th US Symposium on Rock Mechanics (USRMS), 1988. American Rock Mechanics Association.

GRIFFITH, M. C., MAGENES, G., MELIS, G. & PICCHI, L. 2003. Evaluation of out-of-plane stability of unreinforced masonry walls subjected to seismic excitation *Journal of Earthquake Engineering,* 7**,** 141-169.

GRIFFITH, M. C., VACULIK, J., LAM, N., WILSON, J., LUMANTARNA, E. J. E. E. & DYNAMICS, S. 2007. Cyclic testing of unreinforced masonry walls in two‐way bending. 36**,** 801-821.

GRIFFITH, M. V., JAROSLAV 2007. Out-of-Plane Flexural Strength of Unreinforced Clay Brick Masonry Walls. *TMS Journal,* 25. 53-68. .

GUPTA, B. & KUNNATH, S. K. 2000. Adaptive spectra-based pushover procedure for seismic evaluation of structures. *Earthquake spectra,* 16**,** 367-392.

HAIDER, S. 1995. *In-plane cyclic response of reinforced concrete frames with unreinforced masonry infills.* M. Sc. Thesis, Rice University, Houston, Texas, US.

HAMED, E. 2008. Nonlinear Dynamic Behavior of Unreinforced Masonry Walls Subjected to Out-of-Plane Loads. *Journal of Structural Engineering* [Online], 134.

INGHAM, J. & GRIFFITH, M. 2010. Performance of unreinforced masonry buildings during the 2010 Darfield (Christchurch, NZ) earthquake. *Australian Journal of Structural Engineering,* 11**,** 207-224.

INGHAM, J. M., DHANASEKAR, M., MASIA, M., KNOX, C. L. & MA, Q. T. 2011. Experimental testing to determine failure patterns in URM pier/spandrel sub-structures.

ITASCA 2012. 3DEC - Three-dimensional distinct element code. Version 5. Minneapolis, MN: Itasca Consulting Group.

JAIN, S. K., MITRA, K., KUMAR, M. & SHAH, M. 2010. A proposed rapid visual screening procedure for seismic evaluation of RC-frame buildings in India. *Earthquake Spectra,* 26**,** 709-729.

JGJ161-2008 2008. *Regulations of rural housing construction technique [S]* Chinese building and industry press. (in Chinese).

KAKALETSIS, D. & KARAYANNIS, C. 2007. Experimental investigation of infilled R/C frames with eccentric openings. *Structural Engineering and Mechanics,* 26**,** 231-250.

KAKALETSIS, D. & KARAYANNIS, C. 2008. Influence of masonry strength and openings on infilled R/C frames under cycling loading. *Journal of Earthquake Engineering,* 12**,** 197-221.

KAPPOS, A. J., PENELIS, G. G. & DRAKOPOULOS, C. G. 2002. Evaluation of simplified models for lateral load analysis of unreinforced masonry buildings. *Journal of structural Engineering,* 128**,** 890-897.

LAM, N. T.-K., GRIFFITH, M., WILSON, J. & DOHERTY, K. J. E. S. 2003. Time–history analysis of URM walls in out-of-plane flexure. 25**,** 743-754.

LEMOS, J. 1995. Assessment of the ultimate load of a masonry arch using discrete elements. *Computer methods in structural masonry,* 3**,** 294-302.

LEMOS, J. 1998. Discrete element modelling of the seismic behaviour of stone masonry arches. *Computer methods in structural masonry,* 4**,** 220-227.

LEMOS, J. 2001. Modelling the behaviour of a stone masonry arch structure under cyclic loads. *HughesT. G. PandeG. N.(Eds.), Computer Methods in Structural Masonry-5***,** 101-108.

LEMOS, J. Modelling stone masonry dynamics with 3DEC. Konietzky (eds): 1st International UDEC/3DEC Symposium: Numerical modelling of Discrete Materials in Geotechnical Engineering, Civil Engineering and Earth Sciences, 2004. 7-13.

LEMOS, J. & COSTA, A. 2017. Simulation of shake table tests on out-of-plane masonry buildings. Part (V): discrete element approach. *International Journal of Architectural Heritage,* 11**,** 117-124.

LEMOS, J. V. 2007. Discrete element modeling of masonry structures. *International Journal of Architectural Heritage,* 1**,** 190-213.

LIEPING, Y., XINZHENG, L., ZHE, Q. & PENG, F. Analysis on building seismic damage in the Wenchuan earthquake. The 14th World Conference on Earthquake Engineering. Beijing, China, 2008.

LIU Z & CREWE AJ 2018. Effect of position and size of openings on the seismic performance of masonry structures. *Proceedings of the 16th European Conference on Earthquake Engineering.* Thessaloniki, Greece: Springer.

LIU, Z. & CREWE, A. 2020. Effects of size and position of openings on in-plane capacity of unreinforced masonry walls. *Bulletin of Earthquake Engineering***,** 1-30.

LOTFI, H. & SHING, P. 1991. An appraisal of smeared crack models for masonry shear wall analysis. *Computers & structures,* 41**,** 413-425.

LOTFI, H. R. & SHING, P. B. 1994. Interface model applied to fracture of masonry structures. *Journal of structural engineering,* 120**,** 63-80.

LOURENCO, P., MENDES, N., RAMOS, L. & OLIVEIRA, D. 2011. Analysis of Masonry Structures Without Box Behavior. *International Journal of Architectural Heritage,* 5**,** 369-382.

LOURENCO, P. & ROTS, J. 1994. Analysis of masonry structures with interface elements. *Rep. No. 03-21-22-0,* 1.

LOURENCO, P. B. 1996. *Computational strategies for masonry structures.* TU Delft, Delft University of Technology.

LOURENçO, P. B., OLIVEIRA, D. V., ROCA, P. & ORDUñA, A. 2005a. Dry joint stone masonry walls subjected to in-plane combined loading. *Journal of Structural Engineering,* 131**,** 1665-1673.

LOURENçO, P. B., OLIVEIRA, D. V., ROCA, P. & ORDUñA, A. 2005b. Dry joint stone masonry walls subjected to in-plane combined loading. *Journal of Structural Engineering,* 131**,** 1665-1673.

LOURENçO, P. B., PINA-HENRIQUES, J. J. C. & STRUCTURES 2006. Validation of analytical and continuum numerical methods for estimating the compressive strength of masonry. 84**,** 1977-1989.

LOURENçO, P. B., ROTS, J. G. & BLAAUWENDRAAD, J. 1998. Continuum model for masonry: parameter estimation and validation. *Journal of Structural Engineering,* 124**,** 642-652.

MAGENES, G. A method for pushover analysis in seismic assessment of masonry buildings. Proceedings of the12th world conference on earthquake engineering, 2000.

MAGENES, G. & CALVI, G. M. 1997. In-plane seismic response of brick masonry walls. *Earthquake engineering & structural dynamics,* 26**,** 1091-1112.

MAMAGHANI, I. H., AYDAN, Ö. & KAJLKAWA, Y. 1999. Analysis of masonry structures under static and dynamic loading by discrete finite element method. *Doboku Gakkai Ronbunshu,* 1999**,** 1-12.

MILANI, V. S. K. B. J. V. L. G. 2016. *Computational Modeling of Masonry Structures Using the Discrete Element Method,* United States of America, Engineering Science Reference.

MOHAMMADI, M. & NIKFAR, F. 2012. Strength and stiffness of masonry-infilled frames with central openings based on experimental results. *Journal of Structural Engineering,* 139**,** 974-984.

MOHEBKHAH, A., TASNIMI, A. & MOGHADAM, H. 2008. Nonlinear analysis of masonry-infilled steel frames with openings using discrete element method. *Journal of Constructional Steel Research,* 64**,** 1463-1472.

MOLA, F. & VITALIANI, R. J. S. A. O. H. C. I. C., BARCELONA, SPAIN 1995. Analysis, diagnosis and preservation of ancient monuments: the St. Mark's Basilica in Venice. 166-188.

MOON, F. L. 2003. *Seismic strengthening of low-rise unreinforced masonry structures with flexible diaphragms.* Georgia Institute of Technology.

MORANDI, P. & MAGENES, G. 2008. Seismic design of masonry buildings: Current procedures and new perspectives. *Proc, of the 14th WCEE*.

MUNJIZA, A., OWEN, D. & BICANIC, N. 1995. A combined finite-discrete element method in transient dynamics of fracturing solids. *Engineering computations,* 12**,** 145-174.

MWAFY, A. & ELNASHAI, A. 2001. Static pushover versus dynamic collapse analysis of RC buildings. *Engineering structures,* 23**,** 407-424.

MWAFY, A. A. M. A.-R. 2001. Seismic performance of code designed RC buildings.

NETWORK, C. M. 2011. Seismic Design Guide for Low-Rise Confined Masonry Buildings. *Earthquake Engineering Research Institute (EERI)*.

NZSEE 2006. *Assessment and improvement of the structural performance of buildings in earthquakes : prioritisation, initial evaluation, detailed assessment, improvement measures : recommendations of a NZSEE study group on earthquake risk buildings,* [Wellington, N.Z.], New Zealand Society for Earthquake Engineering.

OLIVEIRA, D. V. 2003. Experimental and numerical analysis of blocky masonry structures under cyclic loading.

ORDUñA, A. ı. N. & LOURENçO, P. B. 2003. Cap model for limit analysis and strengthening of masonry structures. *Journal of Structural Engineering,* 129**,** 1367-1375.

OWEN, D., PERIC, D., PETRINIC, N., BROOKES, C. & JAMES, P. Finite/discrete element models for assessment and repair of masonry structures. Arch Bridges–History, analysis, assessment, maintenance and repair. Proc. Second Int. Arch Bridge Conf., AA Balkema, 1998. 173-180.

PAPA, E. J. C. M. O. M. B. & BLOCKWORK STRUCTURES", B. J., STIRLING, SCOTLAND, SAXE-COBURG PUBLICATION 2001. Damage and failure models. 1-26.

PARISI, F. 2010. *Non-linear seismic analysis of masonry buildings.* Università degli Studi di Napoli Federico II.

PARISI, F. & AUGENTI, N. 2013. Seismic capacity of irregular unreinforced masonry walls with openings. *Earthquake Engineering & Structural Dynamics,* 42**,** 101-121.

PARISI, F., AUGENTI, N. & PROTA, A. 2014. Implications of the spandrel type on the lateral behavior of unreinforced masonry walls. *Earthquake Engineering & Structural Dynamics,* 43**,** 1867-1887.

PEGON, P., PINTO, A. V. & GéRADIN, M. 2001. Numerical modelling of stone-block monumental structures. *Computers & Structures,* 79**,** 2165-2181.

PENAVA, D., SARHOSIS, V., KOŽAR, I. & GULJAŠ, I. 2018. Contribution of RC columns and masonry wall to the shear resistance of masonry infilled RC frames containing different in size window and door openings. *Engineering Structures,* 172**,** 105-130.

PENELIS, G. G. J. J. O. E. E. 2006. An efficient approach for pushover analysis of unreinforced masonry (URM) structures. 10**,** 359-379.

PENNA, A., LAGOMARSINO, S. & GALASCO, A. 2014. A nonlinear macroelement model for the seismic analysis of masonry buildings. *Earthquake Engineering & Structural Dynamics,* 43**,** 159-179.

RESTREPO-VELEZ, L. F. & MAGENES, G. Simplified procedure for the seismic risk assessment of unreinforced masonry buildings. Proceedings of the 13th world conference on earthquake engineering, 2004.

RESTREPO VéLEZ, L. F., MAGENES, G. & GRIFFITH, M. C. 2014. Dry stone masonry walls in bending—Part I: static tests. *International Journal of Architectural Heritage,* 8**,** 1-28.

ROCA, P., CERVERA, M. & GARIUP, G. 2010. Structural analysis of masonry historical constructions. Classical and advanced approaches. *Archives of Computational Methods in Engineering,* 17**,** 299-325.

RUSSO, S. J. E. S. 2013. Testing and modelling of dynamic out-of-plane behaviour of the historic masonry façade of Palazzo Ducale in Venice, Italy. 46**,** 130-139.

SARHOSIS, V., GARRITY, S. & SHENG, Y. 2015. Influence of brick–mortar interface on the mechanical behaviour of low bond strength masonry brickwork lintels. *Engineering Structures,* 88**,** 1-11.

SARHOSIS, V., OLIVEIRA, D. V., LEMOS, J. V. & LOURENçO, P. B. 2014a. The effect of skew angle on the mechanical behaviour of masonry arches. *Mechanics Research Communications,* 61**,** 53-59.

SARHOSIS, V. & SHENG, Y. 2014. Identification of material parameters for low bond strength masonry. *Engineering Structures,* 60**,** 100-110.

SARHOSIS, V., TSAVDARIDIS, K. & GIANNOPOULOS, I. 2014b. Discrete element modelling (DEM) for masonry infilled steel frames with multiple window openings subjected to lateral load variations. *Open Construction and Building Technology Journal,* 8**,** 93-103.

SCHLEGEL, R. & RAUTENSTRAUCH, K. 2004. Failure analysis of masonry shear walls. *Numer Model Discrete Mater***,** 15-18.

SHAWA, O. A., FELICE, G., MAURO, A. & SORRENTINO, L. 2012. Out-of-plane seismic behaviour of rocking masonry walls. *Earthquake Engineering & Structural Dynamics,* 41**,** 949-968.

SHI, Y., D'AYALA, D. & PRATEEK, J. Analysis of out-of-plane damage behaviour of unreinforced masonry walls. 14th international brick and block masonry conference, 2008. 02-17.

SHIEH-BEYGI, B. & PIETRUSZCZAK, S. 2008. Numerical analysis of structural masonry: mesoscale approach. *Computers & Structures,* 86**,** 1958-1973.

SIMSIR, C. C., ASCHHEIM, M. A. & ABRAMS, D. P. Out-of-plane dynamic response of unreinforced masonry bearing walls attached to flexible diaphragms. 13th World Conference on Earthquake Engineering, 2004. 1-6.

SINHA, R. & GOYAL, A. 2004. A national policy for seismic vulnerability assessment of buildings and procedure for rapid visual screening of buildings for potential seismic vulnerability. *Department of Civil Engineering, Indian Institute of Technology, Bombay, India*.

SUCUOĞLU, H., YAZGAN, U. & YAKUT, A. 2007. A screening procedure for seismic risk assessment in urban building stocks. *Earthquake Spectra,* 23**,** 441-458.

SUN, B. T. & ZHANG, G. X. Statistical Analysis of Seismic Vulnerability for Various Types of Building Structures in Wenchuan Earthquake. Key Engineering Materials, 2011. Trans Tech Publ, 461-464.

SUTCLIFFE, D., YU, H. & PAGE, A. 2001. Lower bound limit analysis of unreinforced masonry shear walls. *Computers & Structures,* 79**,** 1295-1312.

TAVAFI, E., MOHEBKHAH, A. & SARHOSIS, V. 2019. Seismic behavior of the cube of Zoroaster tower using the discrete element method. *International Journal of Architectural Heritage***,** 1-16.

THAVALINGAM, A., BICANIC, N., ROBINSON, J. & PONNIAH, D. 2001. Computational framework for discontinuous modelling of masonry arch bridges. *Computers & structures,* 79**,** 1821-1830.

THEMELIS, S. 2008. *Pushover analysis for seismic assessment and design of structures.* Heriot-Watt University.

TOMAZEVIC, M. 1999. *Earthquake-resistant design of masonry buildings*, World Scientific.

TOMAŽEVIČ, M., BOSILJKOV, V. & WEISS, P. Structural behaviour factor for masonry structures. 13th World Conference on Earthquake Engineering, 2004.

TóTH, A. R., ORBáN, Z. & BAGI, K. 2009. Discrete element analysis of a stone masonry arch. *Mechanics Research Communications,* 36**,** 469-480.

VACULIK, J. 2012. *Unreinforced masonry walls subjected to out-of-plane seismic actions [Phd].* The university of Adelaide.

VOON, K. & INGHAM, J. M. 2008. Experimental in-plane strength investigation of reinforced concrete masonry walls with openings. *Journal of structural engineering,* 134**,** 758-768.

WANG, Y., YAO, Y., CHENG, B. & WANG, L. The seismic damage characteristic and mechanism analysis of building structure in Wenchuan earthquake. Advanced Materials Research, 2011. Trans Tech Publ, 1892-1895.

WANG, Z. 2008. A preliminary report on the Great Wenchuan Earthquake. *Earthquake Engineering and Engineering Vibration,* 7**,** 225-234.

WANG, Z. 2015. *Shandong province villages and towns building aseismic capacity analysis and seismic measures research.* [MSc], ShandongJianzhu University. (in Chinese).

WANG, Z. & HAO, L. 2014. Masonry housing of rural area in Shandong Province.[Images]

WIJANTO, L. S. 2007. Seismic assessment of unreinforced masonry walls.

WILLIS, C. R. 2004. *Design of unreinforced masonry walls for out-of-plane loading.*

WU, Z., ZHOU, X., XIE, W. & AN, X. 2010. Statistics of Wenchuan Earthquake investigation and some ideas on seismic design of buildings [J]. *Building Structures,* 40**,** 144-144. (in chinese).

XIAO, J., XIE, H. & ZHANG, C. 2012. Investigation on building waste and reclaim in Wenchuan earthquake disaster area. *Resources, Conservation and Recycling,* 61**,** 109-117.

YI, T. 2004. *Experimental investigation and numerical simulation of an unreinforced masonry structure with flexible diaphragms.* Georgia Institute of Technology.

YI, T., MOON, F. L., LEON, R. T. & KAHN, L. F. J. J. O. S. E. 2006. Analyses of a two-story unreinforced masonry building. 132**,** 653-662.

ZHANG, M. & JIN, Y. 2008. Building damage in Dujiangyan during Wenchuan earthquake. *Earthquake Engineering and Engineering Vibration,* 7**,** 263-269.

ZHUGE, Y., THAMBIRATNAM, D. F. A. & CORDEROY, J. 1998. Nonlinear Dynamic Analysis of Unreinforced Masonry. *Journal of Structural Engineering* [Online], 124.

ZUCCHINI, A., LOURENçO, P. B. J. C. & STRUCTURES 2007. Mechanics of masonry in compression: Results from a homogenisation approach. 85**,** 193-204.